ASSESSMENT OF EARTHING SYSTEMS AND ENHANCEMENT OF THEIR PERFORMANCE

AHMED EL MGHAIRBI

BSc, MPhil (Electrical Engineering)

Thesis submitted to Cardiff University in candidature for the degree of PhD

2012

School of Engineering

Cardiff University, Cardiff

ACKNOWLEDGEMENTS

I wish to express my deep gratitude to my supervisors Professor. A. Haddad and Dr. H. Griffiths for the support, guidance, advice and encouragement throughout the duration of this work. I have benefited from their recognised experience and extensive knowledge in this field.

I would especially like to thank Dr. Noureddine Harid for his support and advice.

I would also like to thank all the members of the academic, administration and technical staff.

Thanks to all High Voltage Energy Systems Research Group for their friendship and continuous support through discussion; David Clark, Hazia Abdulhamid, Mohamed Ahmeda, Salah Mousa, Shuaib Braini, Stephen Robson.

Finally I would like to thank my family for their invaluable support.

SUMMARY

This thesis reports on the evaluation of performance and behaviour of earth electrode systems subjected to DC, AC and transient current injections with different rise times and shapes.

The performance of the earth electrode system when injected with currents at the power frequency is now well understood, but the response of the system under high frequency and transient conditions is yet to be fully clarified. This thesis contributes to the better understanding of complex earthing systems such as earth grids and wind turbine earthing system behaviour under high frequency and transient conditions including voltage distributions along the length of the electrode.

The frequency and time domain responses of earth electrodes (vertical and horizontal earth electrodes and earth grids) were quantified for soil resistivity ranged from 10Ωm to 10kΩm. Practical wind turbine earthing system models were developed to account for the additional effects of the above–ground tower structure of the wind turbine and also to consider the benefits of various enhancements to the earthing system. Simulations using 1/5μs and 8/20μs impulse currents were carried out, and a number of parameters were quantified; these include the earth potential rise and the voltage distributions at ground surface level. In particular, the contribution of mitigating techniques, such as rings and rods were derived. The computations allowed determination of touch and step voltages.

The results show that the performance of an earth electrode depends on a number of factors such as soil resistivity and permittivity and electrode dimensions, and it was found that significant inductive effects dominate at high frequency. Thus, the ability of a horizontal earth electrode to reduce the earth potential rise is limited because, beyond a certain length known as the effective length, no further reduction is obtained. The effective length was determined experimentally by incrementally increasing the length of the test electrode. The experimental and simulation results show reasonably close agreement. Furthermore, reasonable prediction of the effective length may be possible using simple empirically derived equations.

The thesis proposes a new method to increase the effective length of in-ground horizontal earth electrodes and the effective area of earth grids. It is proposed that an additional insulated parallel an above ground conductor is bonded to the horizontal electrode at suitable points along its length. Field tests show that the addition to such enhancement reduces inductance effects and helps dissipation of injected currents, so that a greater length of buried earth conductor is utilised, and this contributes to an additional reduction in the earth impedance. Hence, the earth potential rise at the point of current injection is reduced. Enhancing the earthing system in this way results in a significant reduction in the transient potentials developed at the base of the turbine structure. These TEPR reductions produce associated reductions in touch and step voltages.

LIST OF PUBLICATION

Elmghairbi, A.; Haddad, A.; Griffiths, H.; , "Potential rise and safety voltages of wind turbine earthing systems under transient conditions," *Electricity Distribution.20th International Conference and Exhibition on* , vol., no., pp.1-4, 8-11 June 2009

El Mghairbi. N. Harid. N, Griffiths. H, Haddad, A. 'A new method to increase the effective length of horizontal earth electrodes'. 45th International Universities Power Engineering Conference (UPEC), 2010, Cardiff, UK, p. 4.

Elmghairbi, A.; Ahmeda, M.; Harid, N.; Griffiths, H.; Haddad, A.; , " Current and Voltage Distribution in Horizontal Earth Electrodes and A Technique to Increase Effective Length," 17th International Symposium on High Voltage Engineering, Hannover, Germany, August 22-26, 2011.

Elmghairbi, A.; Ahmeda, M.; Harid, N.; Griffiths, H.; Haddad, A.; , "A Technique to Increase the Effective Length of Horizontal Earth Electrodes and its Application to a Practical Earth Electrode System," Lightning (APL), 2011 7th Asia-Pacific International Conference pp.690-693, 1-4 Nov. 2011

El Mghairbi, et al., Technique to increase the effective length of practical earth electrodes: Simulation and field test results, Electr. Power Syst. Res. (2012), http://dx.doi.org/10.1016/j.epsr.2012.04.015 in press (http://www.sciencedirect.com/science/article/pii/S0378779612001253)

Elmghairbi, A.; Haddad, A.; Griffiths, H: "Performance of Wind Turbine Earthing Systems Subjected to Lightning Strikes", 3rd UHVNet Colloquium on Technologies for Future High Voltage Infrastructure, University of Manchester, 19 & 20 January 2010.

Elmghairbi, A.; Haddad, A.; Griffiths, H, : "A New Technique to Enhance the Earthing System by Increasing the Horizontal Earth Electrode Effective Length", Fourth UHVnet Colloquium January 18th – 19th 2011 Winchester, UK

TABLE OF CONTENTS

CHAPTER ONE: INTRODUCTION

CHAPTER TWO: PERFORMANCE OF EARTH ELECTRODES UNDER VARIABLE FREQUENCY AND TRANSIENT CONDITIONS: LITERATURE REVIEW

CHAPTER THREE

PERFORMANCE OF EARTH ELECTRODES UNDER DC, AC AND IMPULSE CONDITIONS

CHAPTER ONE

INTRODUCTION

1.1 Introduction

Earthing systems are used to divert high currents to the earth. Lightning strikes, for example, can subject electrical power systems to transient currents and voltages of high magnitudes and fast rise-times which require dissipation to earth in a controlled manner. Thus, a properly designed earthing system capable of dissipating large currents safely to earth is required, regardless of the fault type. On high voltage transmission and distribution systems, such safety measures must minimise damage to electrical power system equipment and protect human beings from harm. The main factor that determines the effectiveness of these schemes is the soil resistivity of the earth.

In this thesis, the performance of earth electrodes of various shapes, including wind turbine earthing systems, subjected to power surges and impulses is investigated by considering both their high frequency and transient behaviour.

1.2 Earthing System Functions

Earthing systems are designed primarily for power frequency earth fault conditions, and certain items of plant within substations (such as surge arresters) will provide a path to earth for these transient currents. In such cases the relevant standards have recommended the installation of a 'high frequency earth electrode', usually an earth rod [1.1] to dissipate to earth all the high frequency components of the transient. In practice, all the parts of the earthing system are interconnected and may play a role in the dissipation of both power frequency faults and surges. In the case of wind

turbines there will be an earthing termination system especially designed for lightning protection.

.

1.3 Components of Earthing Systems

Generally, substation earthing grids consist of a system of conductors buried in the ground covering an area related to the dimensions of the substation. Additional components may include the metallic sheaths of cables and the earth wires of tower lines and the associated tower footings. These extended earth systems emanate from the substation and are bonded solidly to the earth grid. The performance of these components is difficult to predict because soil has a non-homogeneous resistivity ranging from 10 to 10,000 Ω m [1.2].

1.4 Soil Resistivity

Conduction properties of soil are important, particularly its specific resistivity which is one of the main factors determining the resistance of any earth electrode. Most soils and rocks are poor conductors of electricity when dry. The exceptions to this are certain minerals. However, when soils contain water, their resistivity drops and they may then be considered as moderate conductors although they are very poor when compared with metals. For example, pure copper has a resistivity of 1.6nΩm whilst a quite common value for soil would be 100Ωm. The resistivity is determined by: a) type of soil b) chemical composition of the soil c) concentration of salts dissolved in water d) overall moisture content e) temperature f) grain size and the distribution of grain size [1.2].

1.5 Earth Impedance Measurement

In order to predict the performance of any earthing system, the earth impedance has to be known. The most reliable method for determining the earth impedance of an earthing system is by site measurement, although a preliminary assessment using computation methods is useful to give an indication of expected results [1.3-1.8].

UK and American earthing standards state that, earth impedance measurement of large area earthing systems such as transmission substation earth grids and wind farms should be made by injecting AC currents [1.5-1.8]. The earth impedance should be measured rather than the earth resistance, because the tower line earthing system contains a significant inductive component. However, in measuring the earth impedance of tower lines and transmission substation earthing system, the effect of mutual coupling between test leads should be minimised by selecting suitable test routes [1.8] or by applying correction measures to the values obtained [1.9].

Earth impedance or resistance techniques involve injecting electrical current into the earthing system under test, and this requires an auxiliary current electrode to be placed some distance away from the earthing system being measured. The difference of the voltage potential between the 'potential electrode' and the earthing system is measured, and by dividing the potential by the injected current the impedance or resistance can then be estimated. The same procedure can be applied to measure the transient impedance of the earthing system which is required to predict the protective ability to assess the necessary proper protection measures.

1.6 Standard Lightning Impulse

The lightning impulse is characterised by three parameters, the peak current magnitude (I_P), the time to peak current (T_1) and time to half peak current which is

the time required for the current impulse to decay to half its peak magnitude (T_2). Figure 1.1 shows the standard lightning impulse shape [1.10] with peak current, time to peak current and the time to the half peak current, e.g. 10kA, 5/20μs.

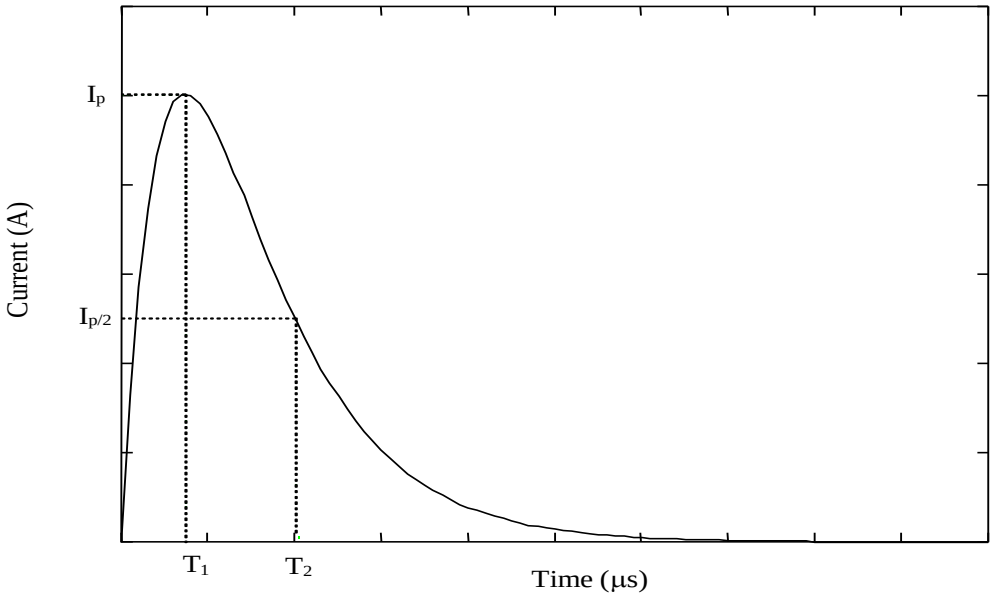

Figure 1.1 Lightning impulse wave shape

1.7 Tolerable Voltage

During an earth fault on a transmission line, a number of towers near the fault are likely to acquire high potential. Potential gradients are also set up in the ground surface, and these may present a hazard to humans and livestock. These hazard voltages are generally referred to as touch and step potentials, which are defined [1.4] as:

a) The touch potential is the difference between the earth potential rise (EPR) and the surface potential at the point where a person is standing, while at the same time having his hand in contact with an earthing structure [1.4].

b) The step potential is the difference in surface potential experienced by a person bridging a distance of 1m with his/her feet without contacting any other earthing object [1.4].

There are limits placed on the allowable EPR of an earthing system as stated in International Telecommunication Union ITU-T [1.12]. These limits are:

- 650V for sites fed from high reliability lines where faults are rare and cleared quickly (200 ms maximum).
- 430V for sites fed from lines having standard protection.

The limits of touch and step potentials are related to the current that can be withstood by a human body before there is a serious risk of fatality [1.4, 1.8, 1.12]. A magnitude in the order of 50mA is sufficient to cause ventricular fibrillation, which will normally result in death [1.13-1.14].

Methods of mitigating the touch and step potential hazards include (i) using a horizontal earth electrode to connect the various parts of the earthing system to reduce the extended earth electrode impedance, (ii) using a potential control ring in the case of tower lines and wind turbine units [1.5] and (iii) redesigning the tower footing to reduce the tower footing resistance in order to meet the limits specified.

1.8 Modelling of Earth Electrode

Field tests and theoretical studies of the impulse response of earth electrodes have been reported since the 1930s [1.15-1.30]. The experimental studies include field and laboratory tests. The majority of tests have been carried out on simple electrodes. The theoretical studies have established useful models using circuit analysis and, more recently, computer codes.

Simple circuit models use lumped parameters and consist of the longitudinal resistance and self-inductance of the earth electrode (r and L, respectively where usually $r << L$. L is at least L 10 times greater than r), and a parallel combination of earth resistance, R, and earth capacitance, C.

The distributed parameter model commonly used for long transmission line analysis can be applied to an earth electrode.

An approach using electromagnetic field theory is considered the most reliable to predict the high frequency and transient behaviours of the earth electrodes [1.29-1.31]. Software based on electromagnetic field theory [1.31] is used throughout this work to simulate the various earth electrodes studied. The transient performance is evaluated by carrying out frequency domain analysis making use of the FFT and inverse FFT.

1.9 Safety Issues of Earthing Systems Subjected to Transient Currents

The design of the earthing system under power frequency conditions is based on satisfying the safety requirements through control of the touch and step potentials **[**1.4 and 1.8]. However, earthing standards contain no basis for determining the transient performance of the earth electrode in terms of safety. This may be due to the lack of data relating to the tolerable thresholds of the human body subjected to impulsive currents [1.11]. IEC 479 [1.11] states thresholds for ventricular fibrillation for power frequency faults but no specific guidelines regarding lightning switching surges are given. IEEE 80 [1.8] states that touch and step voltages for transient or switching types of surges be higher compared to power frequency conditions, and considers that the human body could tolerate higher current magnitudes for lightning discharges than for power frequency currents.

1.10 Earth Electrode Behaviour Under Impulse Conditions

It is well established that the behaviour of earth electrodes subjected to impulse discharges is significantly different from the behaviour expected for power-frequency conditions.

Tests and theoretical studies on earth electrode subjected to fast front impulses, have revealed that the ratio of instantaneous voltage to current (transient impedance) of an earth electrode changes during the passage of a transient current surge [1.19-1.25]. Figure 1.2 shows the initial surge impedance exceeds the power frequency resistance due to the inductance of the earth electrode. After the surge period, the impulse impedance drops to a value below the power frequency resistance. The degree of reduction is larger for higher impulse currents as seen in Figure 1.2.

Many authors have modelled an earth electrode subjected to transient conditions using simple equivalent circuit models [1.18 and 1.24], transmission line approach [1.15, 1.18, 1.21] and electromagnetic approach [1.27-1.31] both of which are used in this thesis.

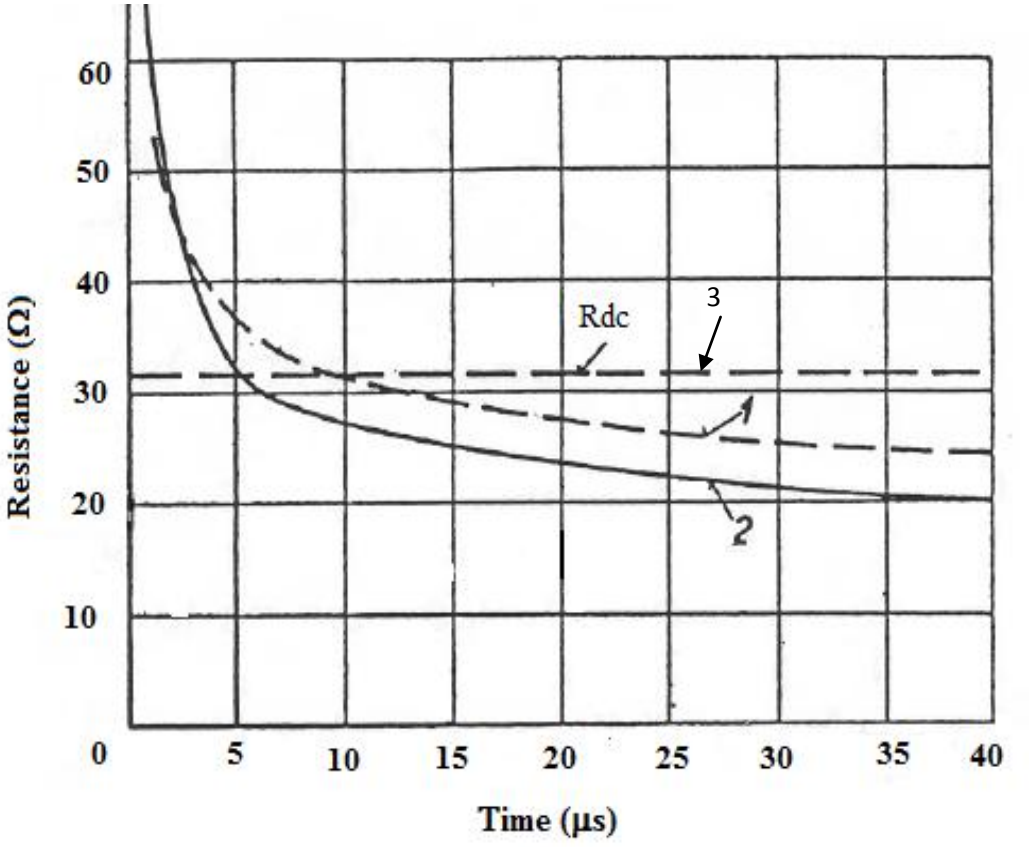

Figure 1.2: The instantaneous voltage divided by instantaneous current for a 110m, horizontal earth electrode 1: surge of 450A 2: surge of 3600A 3: at Power frequency 50Hz [1.19]

1.11 Contribution of Thesis

- Extensive literature review of earthing systems performance under transient conditions with emphasis on wind turbine earthing systems.
- Comprehensive comparative investigation of simple earth electrodes performance under dc, ac and impulse injections. The effect of electrodes parameters (geometry and soil resistivity) were shown to affect their performance through inductive effects and effective length/area
- The current earthing practice for wind turbine application and recommended standards enhancements were assessed under various energisation conditions and their limitations were quantified. The effects of earth electrode parameters, in particular the wind turbine tower, on the predicted safety voltages are quantified for the first time.
- The effective length/area of earth electrode was quantified experimentally and verified using modelling techniques.
- An above ground/insulated conductor new technique is proposed and its benefits to standard electrode was demonstrated experimentally, in addition, its potential benefits for wind turbine earthing were shown through extensive simulations.

1.12 Thesis Layout

The contents of the chapters are summarised as follows:

Chapter two: The literature review includes: Earth electrode behaviour under variable frequency and impulse conditions, a review of published studies of earth electrodes subjected to different current injections including high frequency and transient conditions. These studies were conducted using modelling and site measurement approaches. The effect of earth electrode dimensions on the

performance of the electrode is presented. Wind turbine earthing systems and the difficulties related to this type of earthing are described.

Chapter three: "Performance Of Earth Electrodes Under Dc, Ac And Impulse Conditions". Extensive parametric studies of earthing systems (vertical electrode, horizontal earth electrode and earth grid) are made to characterise earth electrode behaviour under variable frequency and transient conditions. A number of parameters that affect earth electrode performance are examined, such as soil conditions and electrode geometry.

Chapter four: "Safety Performance Evaluation of Wind Turbine Earthing Systems". In this chapter, the effect of the above-ground structure is investigated. Various wind turbine models are examined. The earth potential rise mitigation techniques, including the newly proposed method, are investigated. The safety potentials related to the wind turbine (touch and step) are computed and compared with the different mitigation methods including the new proposed method.

Chapter five: "Effect of Earth Electrode Length/Area on the Performance of the Earthing System: Field Measurements and Simulations". The effect of electrode length is investigated for different frequencies. The analysis is extended to consider the effect of length in different soil conditions and for different impulses. The 'effective length' is quantified in the frequency domain and for transients.

Chapter six: "Enhancing the Earthing System with Increased Effective Length/Area of Horizontal Earth Electrode and Substation Earth Grid". In this chapter a new

method is proposed to enhance earthing systems by reducing earth impedance. Simulation methods are used to investigate this technique: the installation of an additional above ground insulated parallel conductor bonded to the bare underground horizontal electrode at points along its length. This new method is tested using the same experimental setup used to quantify the effective length of the horizontal electrode installed at the university sports field. The same techniques are applied to the earth grid and simulated for various soil resistivities and rise times.

Chapter seven: Conclusions and Suggestions for further Work.

CHAPTER TWO

PERFORMANCE OF EARTH ELECTRODES UNDER VARIABLE FREQUENCY AND IMPULSE CONDITIONS: LITREATURE REVIEW

2.1 Introduction

In this chapter a review of earth resistance and impedance calculation techniques and earth electrode modelling. Analytical methods of calculating the earth impedance of some earth electrode configurations are described, and the performance of earth electrodes under transient conditions is then presented. Furthermore, review of testing and modelling of wind turbine earthing systems under both power frequency and transient conditions is carried out. The effective length and area of earth electrodes are described.

2.2 Calculation of Earth Resistance

A considerable amount of work has been carried out to formulate accurate expressions for earth impedance for a wide range of earth electrodes such as metal cable sheaths and tower line earthing systems associated with tower footings [2.1 – 2.11].

The longitudinal impedance of copper earth electrodes under power frequency is significant only if the electrode is very long, more than several hundred meters. For typical concentrated earth electrodes, the inductive component is negligible, and therefore, such electrodes can be considered to be predominantly resistive at low frequencies.

Dwight [2.1] proposed different formulae to calculate the earth resistance of several configurations of rods; a short horizontal wire, a buried horizontal plate, a horizontal

strip and a ring of wire. The proposed expressions [2.1] are based on the analogous relationship between capacitance and resistance:

$$R = \frac{\rho}{2\pi C} \qquad (2.1)$$

Where R is electrode resistance, ρ is the soil resistivity and C is the capacitance between the electrode and its image above the surface of the earth, and is given by:

$$C = \frac{l}{\ln \frac{2l}{a}} \qquad (2.2)$$

Where l= electrode length and a= electrode radius.

Applying this method leads to a general equation applicable to any form of electrode [2.4]. However, most of the configurations proposed by Dwight such as the three-point star, burial horizontal round plate, and four-point star are not found in practice.

In 1954, Schwarz [2.2] carried out an analytical investigation into the calculation of earth resistance for various electrode configurations. He used an average potential method and modified it to allow for the proximity effects, the influence of one part of the electrode on another. This modification included consideration of a quantity, which he described as the "density" of the number and length of conductors in the area being considered. Here, to make it a dimensionless quantity, the density was taken as the ratio of conductor quantity per linear extension of the area. He compared the results predicted by the expression for earth resistance with the results obtained by measurements made on a scale model, and found good agreement. The expressions proposed by Schwarz are found in practice rather than those developed by Dwight [2.1].

Laurent [2.3] developed the work of Dwight and derived expressions for the calculation of earth electrode resistance for different electrode configurations based on the assumption that the electrode can be divided into small segments, and the current flowing to earth is distributed between these segments. The potential at any point can be calculated as the sum of the potentials resulting from each segment.

Sunde [2.5] independently provided a formula for the calculation of the earth resistance of earth electrodes based on the voltage rise at the electrode midpoint. To find the potential on the surface of the conductor, it is assumed that the longitudinal voltage drop along the conductor can be neglected so the change in potential along the conductor surface can be considered to be zero.

Tagg [2.4] concentrated on the measurement of earth electrode resistance and suggested a formula to determine the resistance to earth of an earth electrode based on expressions originally developed by Dwight [2.1].

Electricity industry earthing standards such as ER/S34 [2.6] provide formulae to determine the resistance of practical earth electrodes based on expressions proposed by Schwarz [2.2], Sunde [2.5] and Tagg [2.4]. Table 1.1 shows the various expressions for the electrical resistance of vertical earth electrodes in a uniform soil as given by Sunde [2.5], Laurent [2.3], Tagg [2.4] and ER/S34 [2.6]. It can be seen that three of the four expressions are identical, only that due to Laurent [2.3] is different.

Table 2.1 Different expressions for calculating the earth resistance of vertical earth electrodes

Tagg[2.4]	$R = \frac{\rho}{2\pi l}\left(\ln\left(\frac{4l}{a}\right)-1\right)$
Sunde [2.5]	$R = \frac{\rho}{2\pi l}\left(\ln\left(\frac{4l}{a}\right)-1\right)$
Laurent [2.3]	$R = 0.366\frac{\rho}{l}\ln\frac{3l}{d}$
ER/S34 [2.6]	$R = \frac{\rho}{2\pi l}\left(\ln\left(\frac{8l}{d}\right)-1\right) = \frac{\rho}{2\pi l}\left(\ln\left(\frac{4l}{a}\right)-1\right)$

Where: ρ is the soil resistivity, l is the electrode length, *a is* radius of the electrode, and d is the diameter of the electrode.

2.3 Earth Electrode Modelling

The earth electrode impedance can be calculated using circuit models or field-theory based techniques. The circuit models comprise lumped or distributed parameters that describe the model as a series resistance and inductance, and shunt conductance and susceptance of the earth electrode. Lumped parameters are used to analyse simple earth electrodes at low frequencies. Studies by [2.12-2.14] have shown that using lumped parameter models to analyse earth electrode at high frequencies can lead to inaccurate estimates of earth impedance magnitudes.

At high frequency, distributed parameter models offer a more accurate estimation of earth electrode performance [2.12- 2.14].

The field theory approach offers advantages over the circuit model approach and can be used to analyse complex and arbitrarily buried earth conductors such as large transmission substations and wind farm earthing systems. Also, it can be used to

calculate the electric and magnetic field in the space around the earth electrode. The validity of these models depends on the type of the earthing system under study [2.15].

Transmission line models have been used [2.12-2.14] to describe simple earth electrode models but, for larger and more complex earthing systems, the electromagnetic field theory model [2.16-2.18] gives more accurate predictions and is easier to use. Grcev and Popov [2.14] conducted a comparison between lumped parameter, distributed parameter and EM (electromagnetic) approaches to the modelling of an earthing rod for a wide range of frequencies with rod lengths of 3m and 30m in soils of resistivity 30Ωm and 300Ωm. The results show significant differences at high frequencies. Their findings are summarised in Figure 2.1. As can be seen, at high frequency the lumped parameter model overestimates the impedance value, compared with EM**F** model which gave much better results [2.14] while the distributed parameter model predicted values closes to those obtained by the EMF model.

2.4 Earth Electrode Under Impulse Condition

Many authors [2.18-2.39] have investigated the behaviour of earth electrodes subjected to high magnitude impulse currents to explore the differences in behaviour compared with 50Hz conditions.

As early as 1928, Towne [2.19] carried out tests on galvanised iron pipes of different lengths up to 6m, and radius 10.65mm, buried in loose gravel soil. Impulse currents of up to 880A were used with rise times between 20μs and 30μs. The impulse resistance of the 6m pipe was 24Ω at 60Hz; however, when an impulse current was injected, the resistance fell to 17Ω, equivalent to a decrease of 19%. The same tests were carried out on different lengths of pipe and in all cases the resistance to an

impulse current was less than for the 60Hz current. Towne [2.19] concluded that the impedance of the earth electrode to an impulse current could be lower than that seen at the power frequency and attributed this to arc sparks that expanded the contact area between the electrode and the soil. Bewley [2.20] carried out impulse tests on counterpoises of different lengths. Impulse currents of 6μs to 12μs rise times with peak currents between 2kA to 8kA were injected. It was found that the transient impedance of the counterpoises was less than for the 60 Hz power frequency. The transient impedance is defined as the ratio of instantaneous voltage to current =V(t)/I(t).

Bellaschi [2.21] also conducted a set of tests with peak currents between 2kA and 8kA and rise times between 6□s and 12□s on vertical earth electrodes. Here, the impulse resistance was taken as the ratio between the peak voltage and the peak current. The findings confirmed Towne's results [2.19] the resistance to the impulse current, was lower than under power frequency condition. Bellaschi attributed this behaviour to a soil ionisation effect suggested by the sharp decrease in voltage immediately after the peak value.

In a subsequent paper Bellaschi [2.22] reported a series of impulse tests on electrodes with a current range between 400A and 15.5kA and using different impulse shapes 20/50, 8/125 and 25/65. It was found that the reduction in the impulse resistance compared to the 60Hz resistance depended on type of soil and earth electrode arrangement, but was independent of impulse rise time. It was also observed that the impulse resistance of an electrode buried in soil of high resistivity had the maximum degree of reduction.

The findings of Towne [2.19], Bewley [2.20] and Bellaschi [2.21-2.22] highlighted the non-linear resistance of an earth electrode under high impulse current, in

particular that resistance under impulse could be less than the power frequency resistance of the same earth electrode.

Berger [2.23] carried out experiments on a spherical electrode, 1.25 cm radius, half buried in a 2.5 m diameter hemispherical pit filled with different soils. The applied peak impulse current ranged from 3.8kA to 11.4kA with rise times between 3μs and 30μs. When the pit was filled with water, the results from the impulse tests showed a constant resistance equal to the power frequency value. However, different values of resistance were obtained for different soils with resistivities between 300Ωm and 57Ωm. The results showed that, when the magnitude of the current was less than a certain threshold value, the V-I characteristic curves showed a linear correspondence to the power frequency resistance. However, when the current exceeded threshold, the characteristic curves showed that the resistance fell below that obtained at 60Hz as shown in Figure 2.2. Berger also carried out tests on a 110m long earth wire of 6mm diameter buried at depths of 20 and 30cm. From these tests with impulse currents, it was found that the resistance decreased to a value below the power frequency resistance.

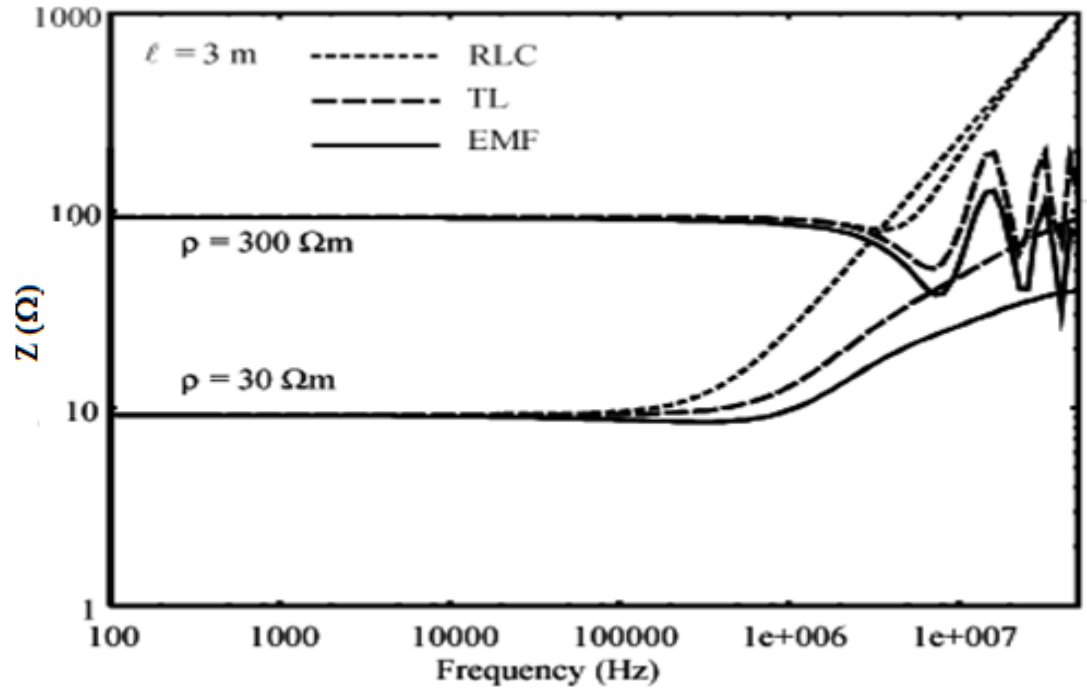

a) L=3m

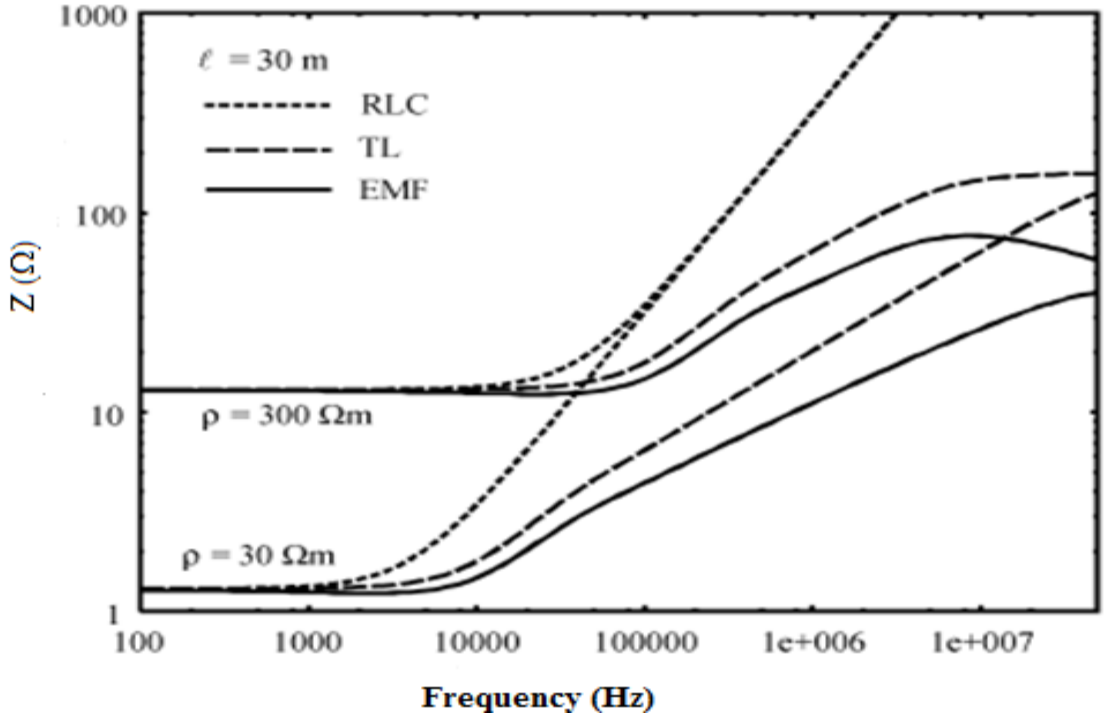

b) **L=30m**

Figure 2.1: Comparison of predicted impedance for two different electrode lengths and two soil resistivity value using transmission line approach, electromagnetic field theory and lumped parameter models [2.14]

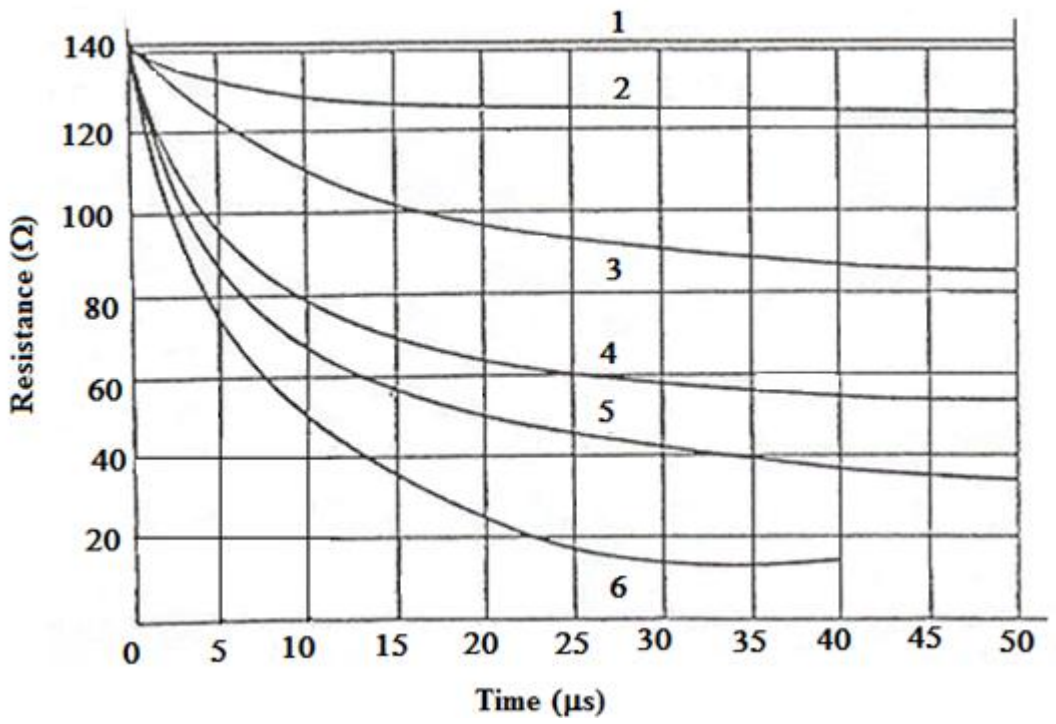

1, i_{max}=250A 2, i_{max}=560A 3, i_{max}=975A

4, i_{max}=1800A 5, i_{max}=2400A 6, i_{max}=5300A

Figure 2.2: Impulse resistance vs. time for mixture of soil at different current magnitudes (Reproduced from reference [2.23]

Petropoulos [2.24] conducted tests using a vertical electrode and electrodes with spikes. He found that the spiked electrodes had lower impedances when subjected to impulse current. This reduction in impedance was attributed to soil break down effects. The results also showed that, as the length of the spikes increased, the impulse resistance decreased.

Liew and Darveniza [2.25] carried out series of tests on vertical electrodes and a hemispherical electrode buried in different types of soils with resistivities ranging from 50□m to 310□m. Impulse current magnitude was varied between 1 and 20kA and rise times ranging from 6μs to 54μs were used. The results showed that the minimum resistance occurred after the time peak of current and that the peak voltage

occurred before the peak current. They proposed a dynamic model to explain the behaviour of earth electrode subjected to high impulse current. Figure 2.3 shows this model which is divided into three stages; stage (a) represents a condition of constant resistivity with increasing current density, stage (c) where the current exceeds the critical current density, decreases the ionisation time when soil breakdown occurs soil resistivity decreases exponentially with a value known as "ionisation time constant". In the third stage, (b) as the current decreases the soil resistivity increases towards the steady state value in an exponential manner according to the "de–ionisation time constant". When the current was increased to 100kA a significant reduction in the resistance value occurred. Also, was found that the level of reduction depended on the soil resistivity and was greater in cases of high resistivity and lower breakdown gradients.

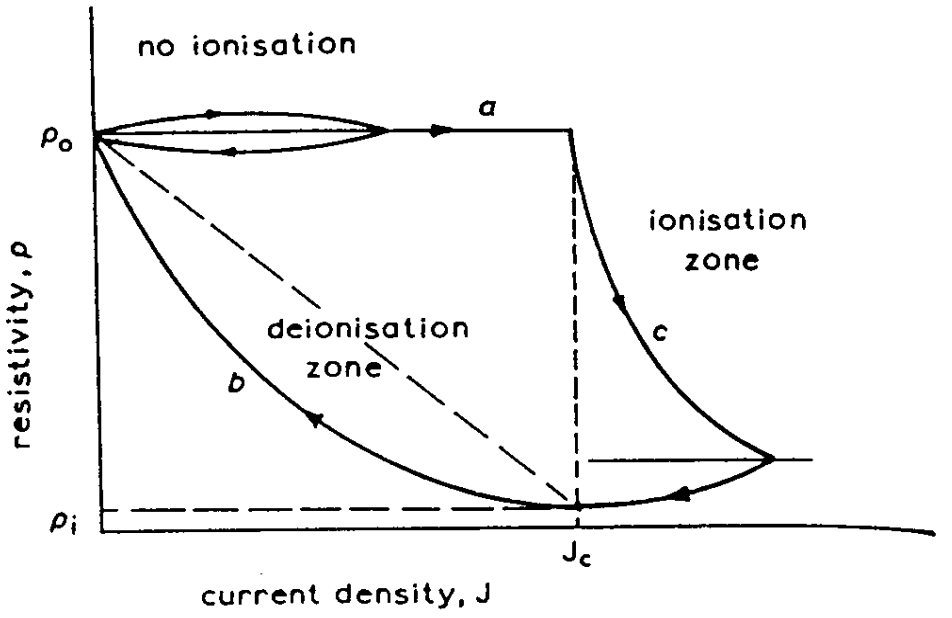

Figure 2.3: Dynamic model for soil ionisation process Reproduced from reference [2.25]

Gupta et. al., [2.26, 2.27] experimentally investigated the effect of impulse currents on square and rectangular earth grids. The impulse resistance was found to be higher than the power frequency impedance. The impulse resistance was defined [2.19] as

the ratio of peak voltage to peak current at the injection point, and it was found that this quantity increased as the soil resistivity increased. It was also found that the impulse resistance was higher for injection at the grid corner rather than at the centre. Laboratory experiments using scale models of square and rectangular grids in soils of different resistivity also confirmed that the impulse resistance was always higher than the DC resistance for all the resistivities tested. Gupta et. al. [2.26, 2.27] concluded that the soil ionisation effect for earth grids was very small and can be ignored, but the impulse impedance decreased as the area of the grid increased until a certain area was reached (referred to as the "effective area" beyond which no further decrease was found. Similar findings have been reported by Ramamoorty, et. al. [2.28] Velazquez and Mukhedkar [2.29] developed a dynamic model of rod electrodes taking into account the soil ionisation process. In this model, the radius of the ionised zone was varied and divided the electrode into a number of segments each having a different current density (a result of the different radii of the ionised zones). It was reported that the capacitance becomes dominant when soil resistivity is more than 1kΩm. The study was extended to include electrodes of lengths ranging from 30m to 150m in soils of resistivity ranging from 1kΩm to 5kΩm. It was found that the transient behaviour of the earth electrode depended on the length of electrode, soil resistivity, permittivity, and the shape of the impulse wave. According to their results, the impulse resistance of the earth electrodes increases to a maximum value equal to the surge impedance then decreases, eventually reaching the DC resistance of the earth electrode.

Kosztaluk et. al. [2.30] carried out tests on four electrodes encased in concrete representing tower footings. Peak currents of up to 26kA were applied with rise time and half peak times of 3μs and 35μs respectively. The results indicated that for low

values of the current, the measured impulse resistance was the same as for 60Hz or DC. As the peak current was increased to 2kA, a decrease in the resistance value was observed. This reduction was attributed to soil ionisation.

Geri et. al. [2.31] conducted high-voltage tests on a 1m long, vertical steel earth rod and a 5m long horizontal steel wire. Impulse currents up to 30kA magnitude and 2.5μs rise-time were applied. The "impulse resistance" was defined as the ratio of the peak current to peak voltage. It was found that over the full range of the current, the impulse resistance for the rod decreased from 18Ω to 6Ω and for the wire from 10Ω to 4Ω. It was observed that the voltage peak preceded the current peak for the vertical rod. The greater inductance of the horizontal wire compared with the vertical rod was considered to be the reason. Almeida et. al. [2.32] carried out tests on an earth electrode buried in sand/ gravel soil, with length 0.61 and radius 0.0075 m. Current of up to 3.5kA with 5μs to 16μs rise time was applied. Figure 2.4, shows that the resistance, defined as V(t)/i(t) is constant until a critical current has been exceeded (1000A) which makes the point at which soil breakdown occurs. Above this value of current, the electrode exhibited a decrease in soil resistivity. The electrode resistance decreased according to an "ionisation time constant", as suggested by Liew and Darveniza [2.25]. As the current decreases from its peak, the soil recovers to reach its initial resistivity value, and the electrode resistance again takes the value of the DC resistance at a rate determined by the "de-ionisation time constant".

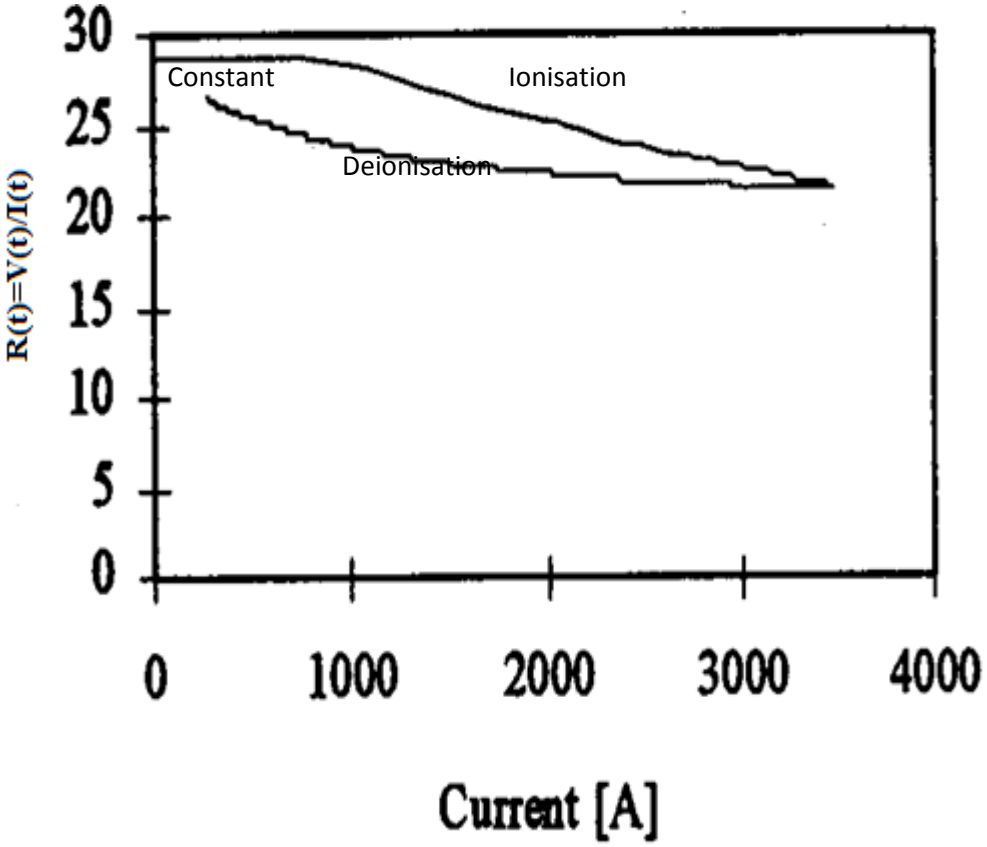

Figure 2.4: Resistance as a function of peak current for dynamic model for soil ionisation process [2.32]

Sekioka et al. [2.33] carried out field tests on three types of earth electrode: i) an 8.1m long buried concrete pole, ii) a 17m long buried earth conductor and iii) a grounding net with dimension of 34mx24.8m. Peaks current of up to 40kA and impulse rise times of a few microseconds rise time were used. In the case of the concrete pole and the buried conductor, the impulse resistance decreases as the current increased as can be seen in Figure 2.5. However, the resistance of the grounding net was found to be current independent, and this was attributed to be due to its large surface area.

.

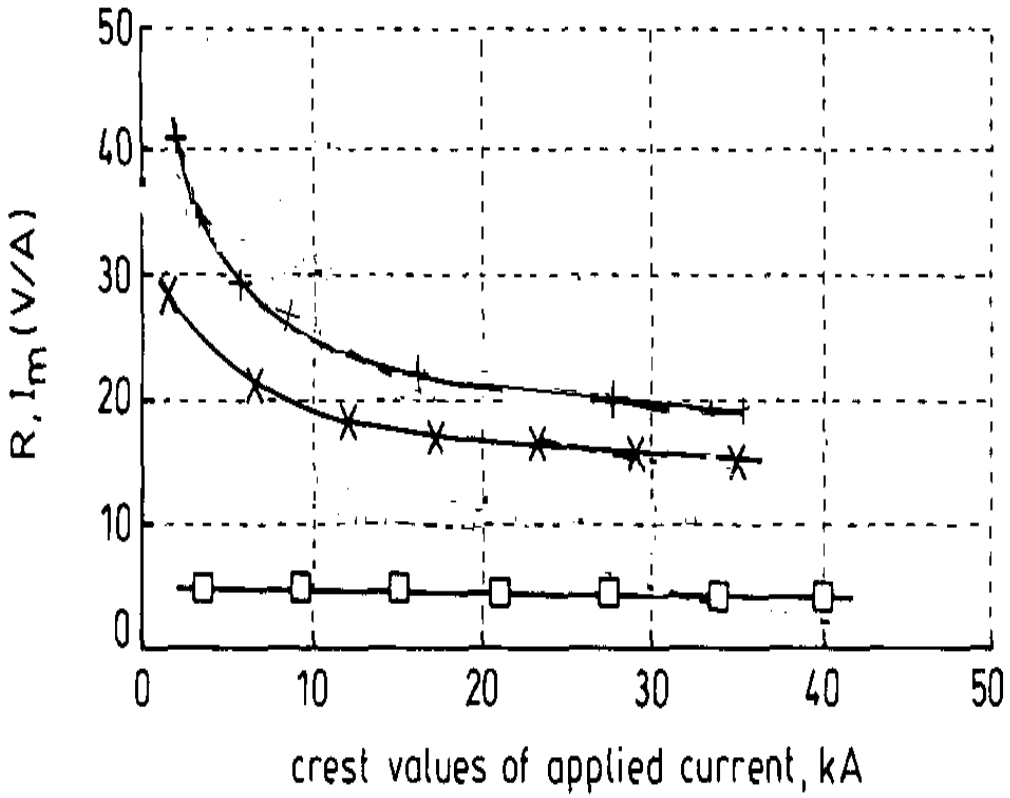

□ Grounding net, + 8.1m buried conductor, X - 17m earth conductor

Figure 2.5: Earthing resistance of three different earth electrode vs. peak (crest) current [2.33]

Similar findings have been reported by Ramamoorty et al. [2.28] and Stojkovic et al. [2.34]; i.e. no ionisation process occurs in the soil when large area earthing systems were subjected to high impulse currents.

Cotton [2.35] used a hemispherical model to describe the process of soil ionisation. Two hemispherical electrodes 2.4cm and 5cm in diameter were placed in a 75cm diameter inverted concrete hemisphere. An impulse generator was used to inject peak currents up to 3.25kA with rise times 4μs and 10μs. With the smaller electrode, the results generally showed a decrease in the impulse resistance of the earthing system as the applied voltage increases, except in the case of the lowest applied voltages which did not appear to cause any ionisation of the soil. The results showed that the impulse resistance was independent of rise time. With the larger electrode

and the same applied voltages, there was no evidence of significant soil ionisation since the electric field levels at the surface of the hemisphere were lower than the critical soil ionisation gradient which was in the order of 4.5kV/cm.

Wang et al. [2.36] proposed a model that is an extension of a dynamic model developed by Liew [2.25], introducing a fourth sparking region.

Characterisation of earth electrodes [2.18-2.41] under transient conditions (including experimental work, laboratory tests and computer simulation) has highlighted that:

- The impulse resistance is lower than the power frequency resistance.
- In soils of high resistivity the reduction in impedance is only slight.
- Inductive effects can be seen in cases of high impulse currents.
- No ionisation phenomena occur for large earthing systems.

2.5 Standards and Guidelines for High Frequency Earthing Requirements

In this section, a brief review is provided of recommendations for earthing systems subjected to transients and lightning surges.

EA TS 41-24 [2.11] (Guidelines for design, testing and maintenance of main earthing system in substations) recommends a low impedance value for the earth grid to disperse high frequency currents safely to the earth. It also recommends that for the impulse condition, the earthing connections from the equipment to the earth should be "as short and as free from changes in directions as is practical". The standard suggests improving the effectiveness and the operation of arresters by connecting high frequency electrodes to, for example, an earth electrode in the immediate vicinity.

IEEE 80 [2.9] (Guide for safety in substation grounding) gives no guidelines for designing earthing systems subjected to lightning surges but considers that the

earthing systems designed for power frequency faults will provide protection against high magnitude transient currents (with respect to human safety).

BS 62305 [2.42] (Protection against lightning) recommends that the earthing system designed for lightning protection should have an earth resistance of less than 10Ω. The same requirement appears in BS 61400-24:2002 [2.43] (Wind turbine generator system - Lightning protection) which also provides some details of earthing system arrangements for individual wind turbines.

2.6 Wind Turbine Earthing Systems

The earthing system of a single wind turbine is normally achieved by placing a ring electrode around the foundation and bonding it to the tower through the foundation structure. In accordance with relevant standards [2.43], the minimum diameter for earth electrodes embedded in concrete is 10mm (solid round steel). Vertical rods or strip electrodes are often used in conjunction with the ring electrode to obtain the 10Ω value of resistance for an individual turbine earthing system [2.42 and 2.43]. The interconnection of earthing systems is often achieved between wind turbines through bonding the sheath of the supply cables. Such interconnection forms an extended earth electrode system occupying a large area, and provides a much lower resistance/impedance.

Different investigators [2.44-2.54] have studied the earthing systems of wind turbines, including interconnected extended electrode under both power frequency and transient conditions.

Jenkins and Vaudin [2.44] conducted site measurements of soil resistivity and resistance of the extended earth electrode system of a wind farm using the slope method [2.45]. The measured values of earth resistance were higher than the

calculated values obtained using a lumped parameter equivalent circuit. This difference was attributed to the backfill of the trenches not being fully compacted. It was also reported that the soil resistivity conditions varied considerably within one site.

Hatziagyrious et al. [2.46] investigated the earthing systems of individual and interconnected wind turbines using EMTP and CDEGS software. An AC energisation of 1kA at 50Hz and a current impulse (30kA 5/75) was simulated for a soil condition of 100Ωm resistivity. The AC earth resistance and the impulse resistance have the same value. A simple model was used in which the inductive component was neglected. The simulations also demonstrated that by connecting a 50m horizontal electrode to the ring electrode, the a.c. resistance and earth potential (EPR) rise was reduced under transient conditions. The influence of inductive component of long horizontal earth electrode was also shown. Figure 2.6 shows the potential developed at the turbine base and the reduction obtained by adding four extra 12.5 electrode lengths and 50m horizontal electrode. From the graph, splitting the 50m horizontal electrode into four 12.5m strips has the benefit to reduce the EPR.

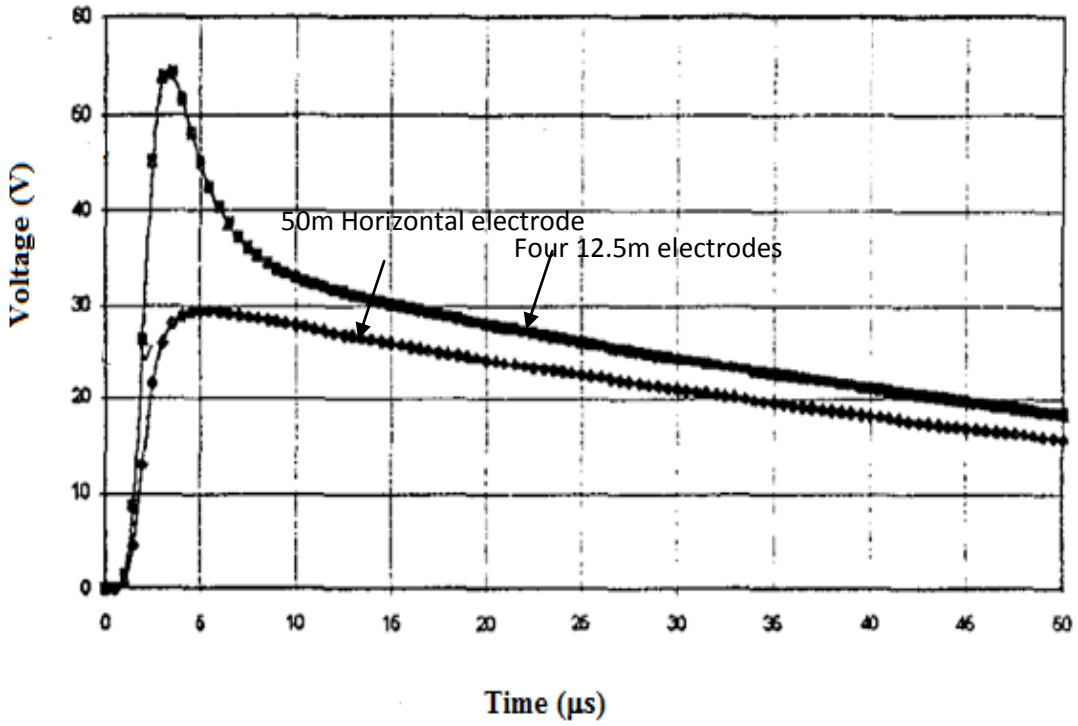

Figure 2.6: Time domain response for wind turbine connected to four 12.5m electrodes and with 50m long earth electrode, subject to lightning voltage rise 30kA 5/75 [2.46]

Cotton [2.47] carried out CDEGS simulations of different arrangements of wind farm earthing systems. The results of AC (50Hz) simulations indicated that there is a little additional benefit in running an extra earth conductor between the wind turbines earthing systems when the earthing system is already interconnected by a cable sheath. Lightning current simulations of (30kA 2.5/20 show a considerable reduction in EPR compared with the case of individual turbine when the wind farm was interconnected via the power cable sheath.

Hatziargyrious et al. [2.48] also conducted computer simulations on wind turbine earthing systems for both power frequency current and fast transient injection. They adopted a simple model for the earthing electrode of a wind turbine which consisted of horizontal electrodes arranged in an octagonal structure of 6.5m radius with 4mm radius copper conductors buried 1.5m deep as shown in Figure. 2.7. The calculated

DC earth resistance of this electrode was 24.8Ω assuming a 500Ωm resistivity homogenous soil.

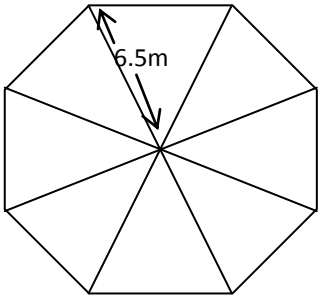

a) Simplified model of wind turbine base earthing system

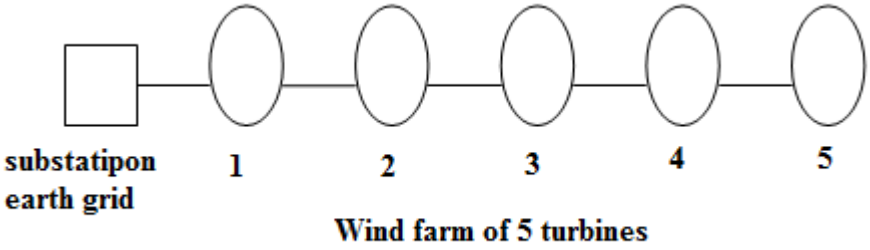

b) Onshore windfarm with 5 wind turbines

Figure 2.7: Illustration of the turbine model and the wind farm arrangement

An impulse current of 9kA, 1.4/1.7 and an AC current of 9kA, 50Hz were each injected into the octagonal model connected to a 300m long horizontal electrode. The results showed that, in the case of 50Hz current the EPR decreased as the length of the horizontal electrode connected to the outer ring of the wind turbine earthing system increased. On the other hand, in the case of the impulse condition, the decrease of the TEPR (Transient Earth Potential Rise) has a limit; there is an effective electrode length above which the impedance remains constant. The effective length at high frequencies was found to be shorter than at 50Hz. The study was extended to include five interconnected wind turbines and substation earth grid.

The distance between two adjacent wind turbines was 400m, the same distance between the substation and the nearest wind turbine.

A lightning current of 30kA, 5.5/ 75μs was injected into the middle wind turbine. The maximum EPR always appears at the injected turbine. The potential rise was reduced when the wind turbine was connected, and no reduction was noticed when an extra electrode was connected in parallel with the power cable.

Lorentzou et al. [2.49] simulated different wind turbine earthing arrangements as shown in Figure 2.8 under 50Hz and impulse currents injection. The results showed that arrangement B gave the lowest resistance. This is due to the area of arrangement B which is larger than other arrangements.

Increasing the burial depth of the earthing system gave no significant reduction in resistance. The results show that the interconnection of the wind turbines has benefit in reducing the EPR significantly in the case of 50Hz injection. For transient injection, however, the reduction of the TEPR was limited by a certain "effective length" which is shorter under transient conditions compared to the power frequency case as can be seen in Figure 2.9.

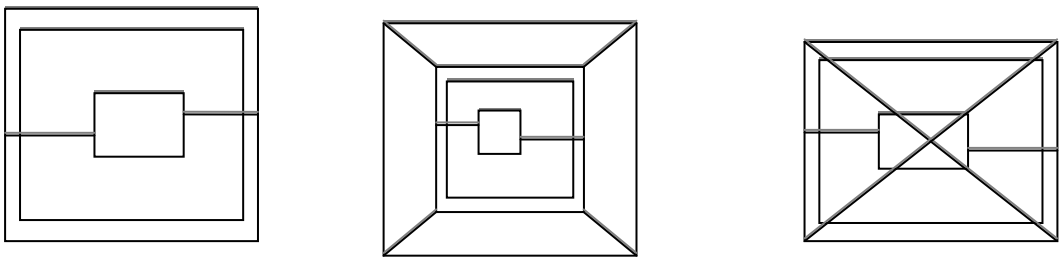

A B C

Figure 2.8: Alternative wind turbine earthing arrangements [2.51]

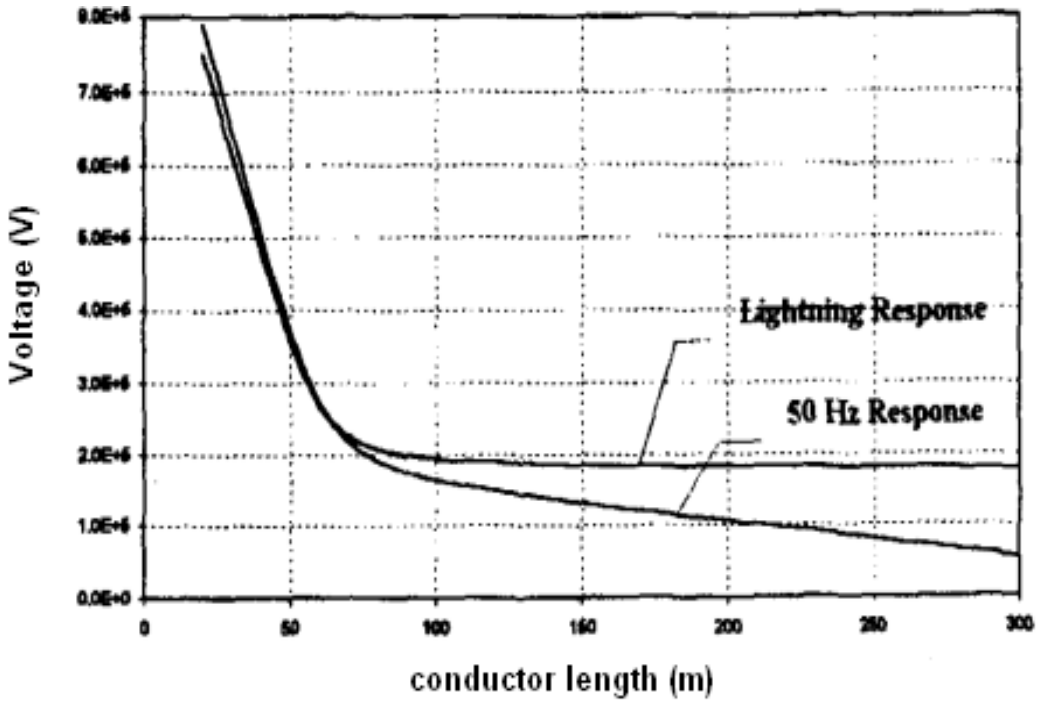

Figure 2.9: Maximum earth potential as a function of conductor length [2.49]

Yasuda et al. [2.50-2.51] conducted transient simulations using power system simulator of wind turbine earthing systems under transient conditions. The simulated system consisted of two (1MW) turbines and a local transformer spaced at 1km intervals, as shown in Figure 2.10. However, the spacing between the turbines seemed to be impractical. A parametric analysis was conducted varying the wind turbine earth resistance from 1Ω to 10Ω, and its inductance from 0μH to 10μH, under an impulse current energisation of 30kA, 2/70. The results showed that the surge magnitude was affected by resistance and inductance of the earthing system. A high inductance produced high potentials around the struck turbine. It was found that the case B in Figure 2.10 gave lower TEPR magnitude compared with the other arrangements.

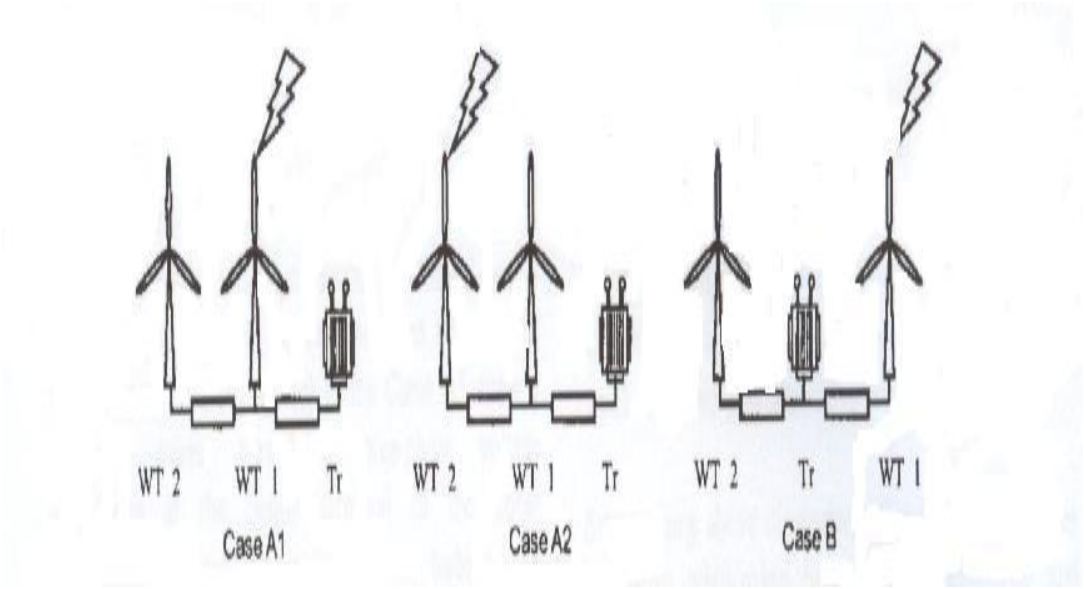

Figure 2.10: Turbines arrangement and lightning struck reproduced from reference [2.50]

Kontargyri et al. [2.52] studied an interconnected wind turbine earthing system using CDEGS up to 1MHz. The investigation accounted for a two layer soil model with a range of soil resistivity values taken for the top and lower layers. The five-interconnected wind turbine arrangement is shown in Figure 2.11. The burial depth of the outer earthing ring of the wind turbine earthing system was 2.5m with radius 6m, the inside ring was 0.9m deep with radius of 1.5m and the outer rectangle was 35x25m buried at a depth of 0.9m. It was shown that when the current was injected into the central wind turbine, the earth impedance was less than when the injection was into a wind turbine at the end of the row.

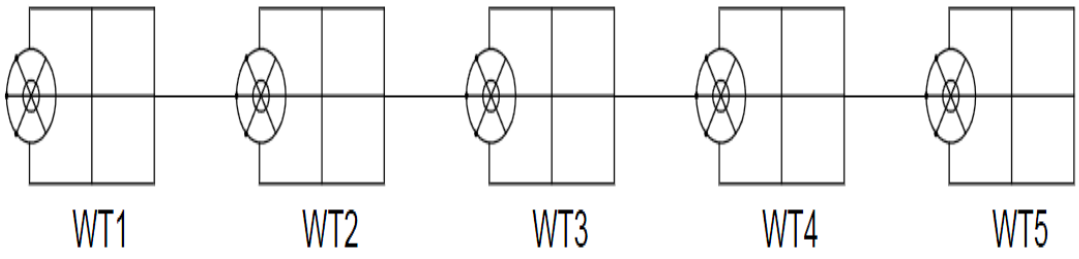

Figure 2.11: Interconnected wind turbine earthing system [2.52]

In a subsequence paper Yasuda et al. [2.53] investigated the recommendation of technical report 61400-24 [2.44] that additional electrodes are required if the radius of the foundation of the wind turbine is less than the minimum radius stated by IEC 62305-3 [2.42].

Computer simulations on the following earth-electrode combinations using the FDTD method were carried out.

i) Four vertical electrodes installed at the corners of the wind turbine foundations.

ii) Four vertical electrodes installed around the ring electrode.

iii) Combinations of i) and ii).

The results showed that arrangements (ii) and (iii) were able to meet the standards recommendations as shown in Figure 2.12. However, they recommended that further work was required in order to obtain an effective design for wind turbine earthing systems.

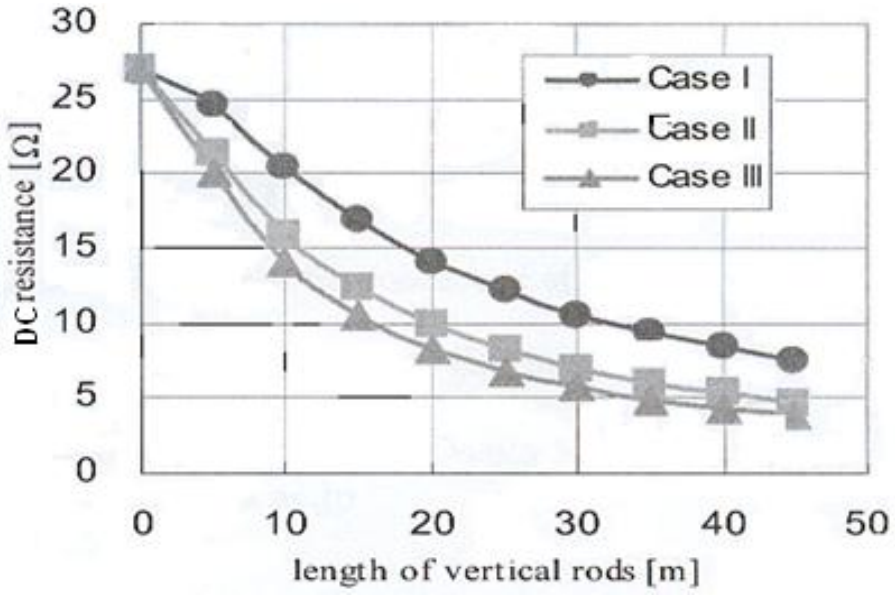

Figure 2.12 Resistance vs. vertical electrode length for various wind turbine electrode configurations [2.53]

Ukar et al. [2.54] noted that, while some standards deal with wind turbine lightning protection, there is no standard for wind turbine and wind farm earthing system design. Moreover, the available standards have not considered the transient behaviour of wind turbine earthing systems. Using the electromagnetic approach, both individual wind turbine and interconnected configurations were modelled as shown in Figure 2.13. The earthing systems were subjected to a peak impulse current of 100A, 1.2/50 with a soil of 1kΩm resistivity. The larger square earth grid was given lower step voltage compared with the ring earth electrode arrangement. It was found that step potential was also reduced by a 30% by increasing the burial depth of the earthing system from 0.5m to 0.8m with limited benefit for greater depth. It was also found that extending the earthing system improved the transient behaviour while interconnection of the wind turbines earthing systems also reduced step potential.

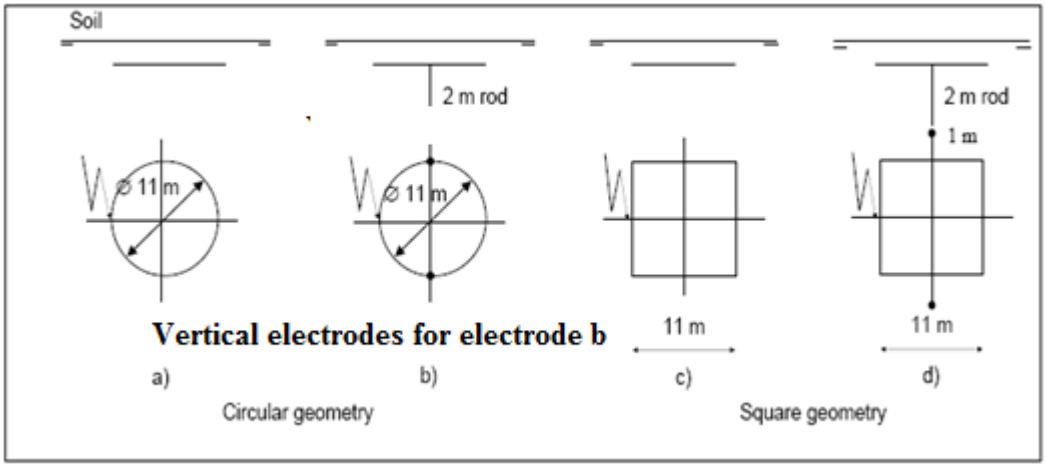

a) Individual wind turbine earthing systems

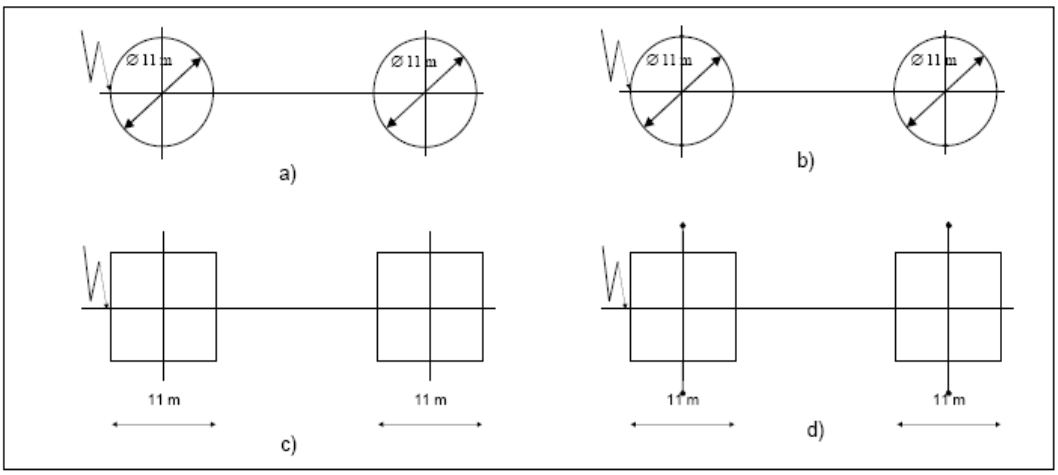

b) Interconnected wind turbine earthing system

Figure 2.13: Different earthing arrangements used by Ukar, et. al. [2.54]

2.7 Effective Length of Horizontal Earth Electrode

Many investigations have been carried out into the effect of an earth electrode [2.55-2.62]. This has led to the identification of a particular length beyond what provides little or no sign of earthing system performance as seen from the point of injection [2.57]. Furthermore, it has been shown that the effective length is affected by energisations characteristics.

Bewley [2.20] observed from tests that a counterpoise, beyond 91.4m in length gave little further reduction of the earth impedance leading to the conclusion that additional parallel conductors would offer improved performance.

Recently Mazzetti et al, [2.55] carried out studies of the horizontal earth electrode using the transmission line model. Their results showed that the voltage drop along the horizontal electrode was significant due to inductance, but only a certain length, the "effective length", contributed to current dissipation. The effective length was shown to increase with increasing soil resistivity.

Gosh and Munshi [2.56] used an analytical model of a horizontal earth electrode based on an equivalent transmission line, and demonstrated that no significant benefit could be achieved by extending the electrode length beyond the effective length.

Farag et al. [2.57] proposed a definition of the effective length as the length at which the voltage reaches 3% of its value at the current injection point. An analytical expression was proposed to calculate the effective length of a horizontal earth electrode based on a formula from earlier work by Gupta and Thaper [2.26]. The expression they proposed is based on work to determine the effective area of the earthing grid with current injected at the centre or the corner. Their expression for calculating the effective length of the horizontal electrode is :

Effective length $L = k(\rho \tau)^{0.5}$ (2.3)

Where L is the conductor effective length in (m), ρ is the soil resistivity (Ωm),

τ is the rise time of the injected current (μs), k = 1.4 when the current is injected into one of the conductor ends and k = 1.55 when the current is injected into the middle of the conductor.

Lorentzou et al. [2.58] simulated the transient response of a horizontal earth conductor using EMTP in order to identify its effective length. An 8/20 current impulse peak magnitude of 31kA was assumed as the source. Figure 2.14 shows that the peak transient voltage per unit of peak injected current decreases as the length of the electrode increases until it reaches a constant value which is referred to as the effective length. It was shown that the effective lengths are shorter for lower values of soil resistivity.

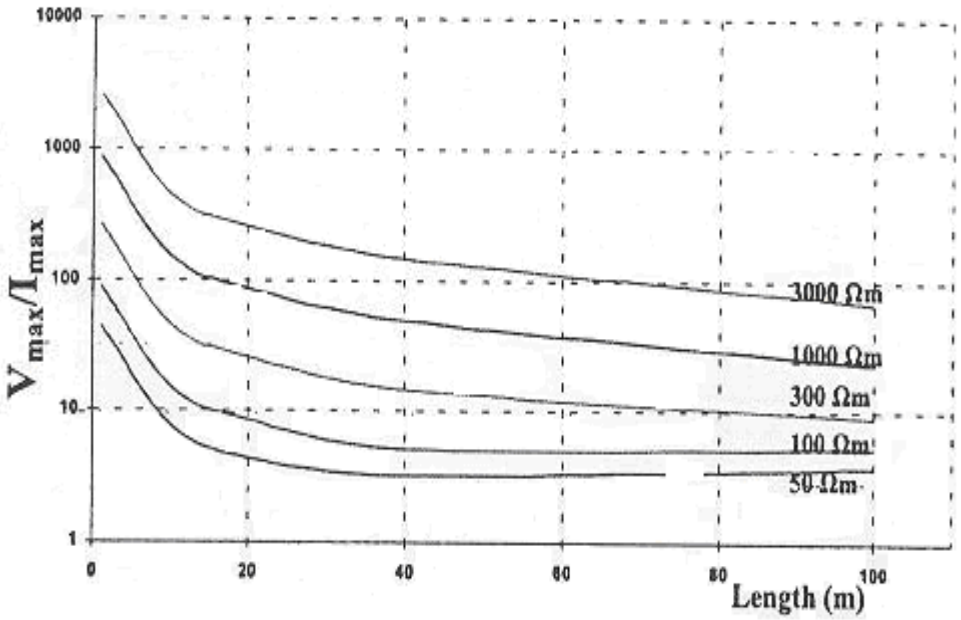

Figure 2.14: Vmax/Imax as a function of a horizontal electrode length [2.62]

Griffiths et al. [2.59] investigated the effective length of rod electrodes over a range of frequencies using a distributed parameter circuit model. It was shown that the electrode earth impedance decreases with electrode length until it reaches the characteristic impedance at the effective length.

Lu et al. [2.60] investigated the effect of length of an extended earth electrode subjected to lightning strikes. Their results showed that the extended electrode has a limited effective length under transient conditions. On the other hand, the performance of the earthing system at power frequency was found to improve beyond the transient effective length of the earthing electrode. Lu et al. [2.60] found the effective length of a conductor increased with soil resistivity and front rise time, due to high frequency content of short rise time as shown in Figure 2.15.

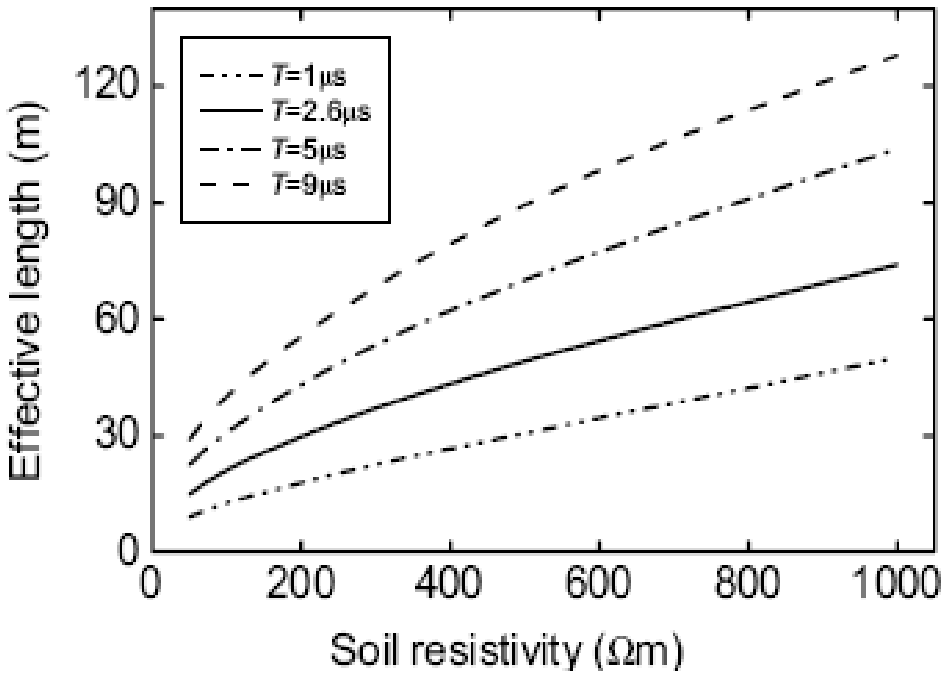

Figure 2.15: Electrode effective length for different soil resistivity and front rise time [2.60]

Liu et al. [2.61] compared the different definitions of the effective length/area of earth electrode using the simulation technique reported in [2.62]. They suggested that when the transient injection has a rise time less than 1μs, the effective length may be overestimated.

2.8 Effective Area of Earth Grid

One of the measures taken to reduce the rise in earth grid potential is to increase the earth grid area. This will reduce the grid earth impedance, but this has a limit after which further increase in the area results in no further reduction in potential. This area is known as the effective area. This section presents a brief review of work concerning this issue.

Gupta and Thapar [2.26] showed that, as the area of the earth grid increased, the impulse impedance decreased until a limiting area was reached, defined as the

"effective area". This is an extension of the principle of effective length for a long horizontal electrode described by Mazzetti and Veca [2.58]. An empirical formula for the effective radius of an earth grid was proposed [2.26],

$$r_e = K(\rho T)^{0.5} \tag{2.4}$$

Where: K = (1.45-0.05s) for centre fed grids, K = (0.6-0.025s) for corner fed grids, ρ is the soil resistivity, T is the impulse rise-time and s is the spacing between grid conductors**.**

The higher effective area for centre fed grids was explained by the higher inductance for the corner injection compared with centre injection.

The effect of injection point on the effective area was investigated. The results showed that the inductance of a corner injected earth grid is higher than a centre injected earth grid. The effective area for the corner fed earth grid is less than for a centre injected grid with the same current injection. This is because of the higher inductance of the corner injection case.

Grcev [2.63] studied the effect of earth grid size on its performance using electromagnetic field theory approach. Different earth grid sizes were considered ranging from 10mx10m to 120mx120m. The results showed that the effective area covered by the earth grid is less than 20mx20m for fast impulse injection. It was concluded that, for high frequency and fast impulse conditions, increasing the grid size does not result in significant impedance reduction.

In a recent paper, Grcev [2.65] reported that the calculation of effective area using an electromagnetic field theory model would give more accurate estimation because the circuit theory model has an upper frequency limit. According to Grcev, the formulae suggested by [2.26 and 2.64] would not be valid for fast front impulses because of the high frequency content. The formula proposed by Grcev is

$$a_{eff} = K.\exp\left[0.84(\rho T)^{0.22}\right] \quad (2.5)$$

Where: K=1 for grid centre injection, K=0.5 for grid corner injection, ρ = soil resistivity and T is the impulse rise-time.

A comparison with the different proposed formulae [2.26 and 2.68] for effective area and this shows that there is a quite large difference in predicted effective area particularly at higher resistivity.

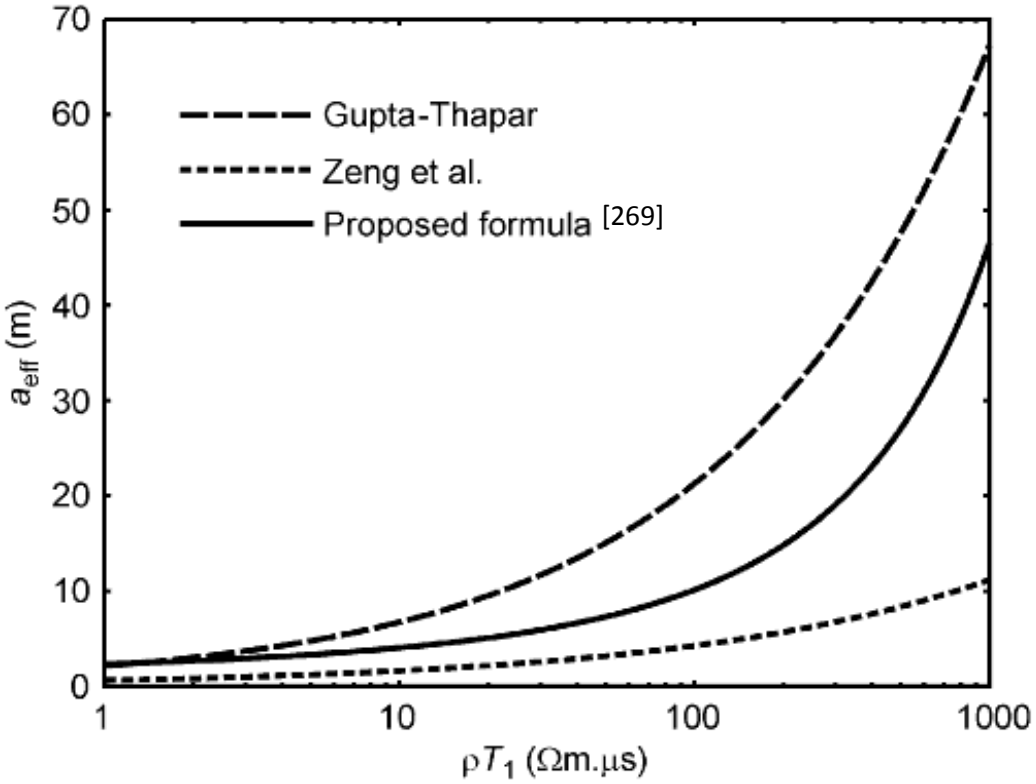

Figure 2.16 Comparison between different methods of estimating square earth grid effective area [2.65]

2.9 Conclusions

A review of literature relating to the high frequency and transient performance of earth electrodes and wind farm earthing systems has been carried out.

Investigators have attempted to characterise the behaviour of earth electrodes using a number of different approaches. Such work has included high-voltage testing both in the laboratory and on earth electrodes installed in the field. Simulation approaches have used circuit models and the electromagnetic models.

The standards dealing with recommendation for earthing systems contain guidelines for design which are primarily for power frequency earth fault conditions. However, it is well established that earthing systems subjected to high impulse currents will behave differently from power frequency faults. In the specific case of wind farms , the earthing systems occupy extensive areas, usually located in areas with high soil resistivity. Such extended earth electrode systems of the wind farms exhibit a significant reactive component and any estimation of EPR based on DC measurements is likely to contain a significant error. The relatively large inductive component of the wind farm earthing impedance system shows that DC resistance measurement techniques should not be used on sites such as wind farms. If the resistance value is used in determining the maximum potential rise during a fault, a hazard to human safety may occur as the earth potential rise would be underestimated.

It has been identified that the length of the earth electrode is an important parameter affecting its performance, and the concept of effective length has been defined. The literature clearly indicates that the ability of a horizontal earth electrode in reducing earth potential rise is limited because no further reduction is obtained by increasing its length beyond a certain amount known as the effective length. A number of

parameter-specific definitions of effective length have been proposed in the literature. It is also well known that the behaviour of earthing systems under transient conditions is different from that under power frequency resulting in shorter effective lengths. The effective length under transient conditions depends on soil resistivity, impulse risetime and electrode geometry. Many researchers have studied the transient performance of the horizontal earth electrode and an empirical formula for calculating the effective length has been proposed. Most of these studies were conducted using simulations and circuit theory methods, and limited experimental work have been reported. Chapter 5 of this thesis investigates the effective length in more detail using an experimental test and simulation techniques.

CHAPTER THREE

PERFORMANCE OF EARTH ELECTRODES UNDER DC, AC AND IMPULSE CONDITIONS

3.1 Introduction

The design and the requirements of the earthing systems for power frequency faults are well established [3.1-3.3]. However, earthing system performance and response to fast-fronted surges caused by e.g. lightning and switching surges are more complicated. Considerable work has been carried out to characterise the performance of the earthing systems under impulse conditions [3.4-3.12], but most of this work was concentrated on simple electrodes such as vertical and horizontal earth electrodes. A few investigators [3.11-3.12] have studied the performance of earth grids under high frequency and impulse conditions, investigating such factors as earth grid size and spacing that were expected to improve the behaviour of the earthing system.

National and international standards give detailed guidelines for earthing system design under power frequency conditions, but only limited recommendations for high frequency and transient conditions are available [3.3-3.4].

In this chapter, a detailed parametric study is performed on the responses of different earthing systems under variable frequency and transient conditions. Different factors such as soil resistivity and soil relative permittivity which affect the performance of the earthing systems are investigated. Also, the effects of electrode length or area for vertical earth electrodes, horizontal earth electrodes and grid earthing systems on performance of earthing systems are considered. Circuit models are compared with computer simulation based on a numerical electromagnetic approach [3.14].

3.2 Modelling Methodology and Model Arrangements

In order to study the generic behaviour of earthing systems, three simple earth electrode model arrangements (vertical earth electrode, horizontal earth electrode and earth grid) were adopted for these studies, see Figure 3.1.

(i) Vertical Earth Rod

A reference copper earth rod is used and assumed to have a radius of 1cm. Different lengths of this type of earth electrode were considered.

(ii) Horizontal Earth Electrode

A 100m horizontal earth electrode of radius 1cm is modelled when buried 0.6m below the ground.

(iii) Earth Grid

The generic earth grid is assumed to have 100mx100m area with mesh size 10m square, and buried at a depth of 1m below the surface of the soil. The grid conductors are also assumed to have a radius of 1cm.

Each earth electrode is simulated with variable frequency and impulse currents energisation for a range of soil conditions likely to be found in practice; soil resistivity between 10Ωm to 10kΩm, and with relative permittivity of 1 to 80 reported by [3.8].

For each electrode under a.c. energisation, the earth impedance is calculated for an injection of 1A current, and unity soil permittivity and permeability were assumed.

The simulations are carried out using CDEGS earthing software [3.13]. In addition, both lumped and distributed parameter circuit models are used in the case of the vertical earth electrode for comparison purposes.

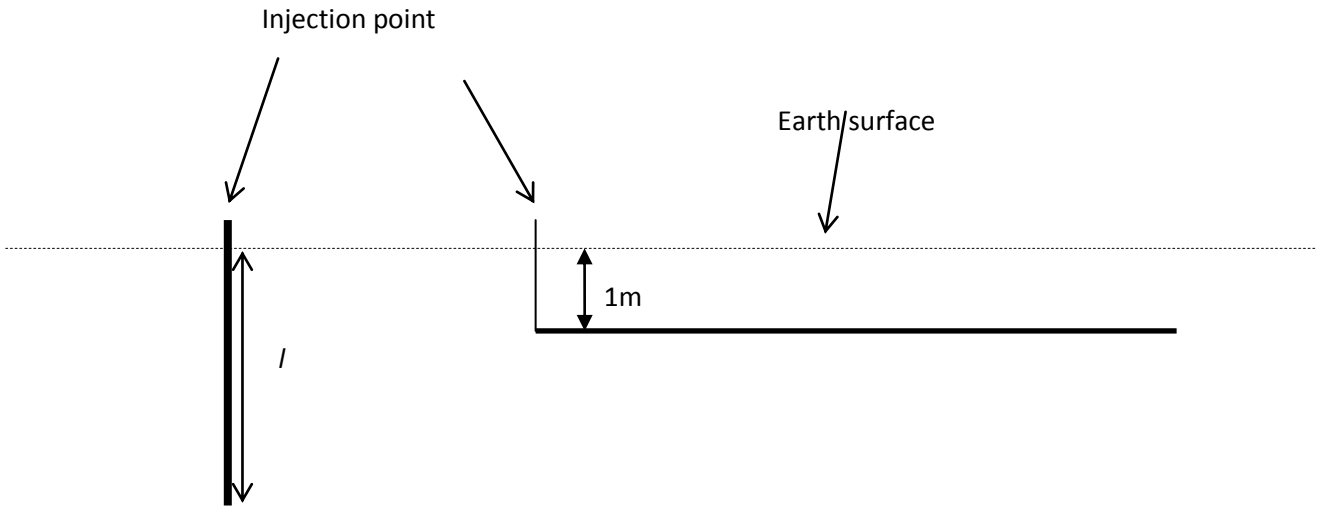

a) Vertical electrode **b) Horizontal electrode**

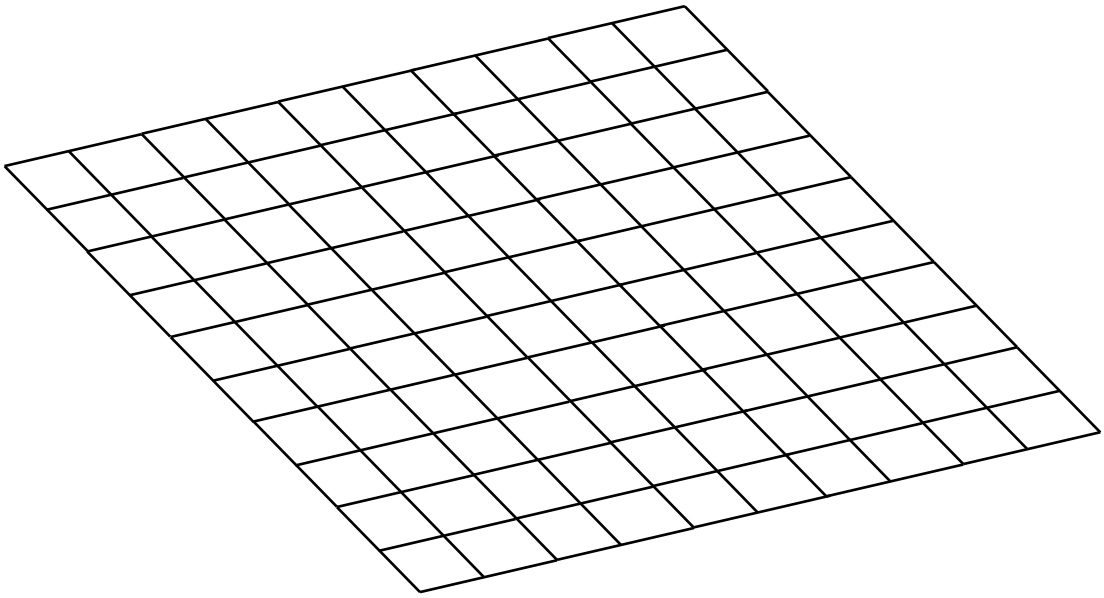

c) Earth grid model used for simulation

Figure 3.1 Simulated earth electrode models

The resistance or impedance of earth electrodes can be calculated by different methods such as field theory based software or equivalent circuit models using analytical expressions for the lumped or uniformly distributed parameters that describe the overall earth impedance as equivalent to a series of resistances and inductances. However, studies by Davies [3.14] have shown that the earth electrode response predicted by the lumped parameter approach can lead to inaccurate estimations of the earth electrode under high frequency or transient conditions. Thus, lumped parameters are commonly used to estimate the behaviour of simple and small dimension earth electrodes at low frequencies. For high frequency studies distributed parameter are more accurately used in the prediction of the behaviour of vertical and horizontal earth electrodes. The field theory approach [3.13] has advantages over the circuit approach, as it can be applied to analyse complex and arbitrarily oriented buried earth electrodes such as transmission substations and wind farm earthing systems. A major disadvantage is the long calculation time required when simulating a complex earthing system such as a large transmission line substation and wind farm containing many wind turbines.

In the following sections, calculations of the earth impedance of simple earth electrodes using circuit models and field theory based software are presented and compared.

3.3 Circuit Model Parameters

The equivalent circuit model for the earth rod was first suggested by Rudenberg [3.15]. It is a simple circuit consisting of the series resistance, r, and series self-inductance, L, of the electrode and a parallel combination of a shunt earth resistance, R, and shunt earth capacitance, C, as shown in Figure 3.2.

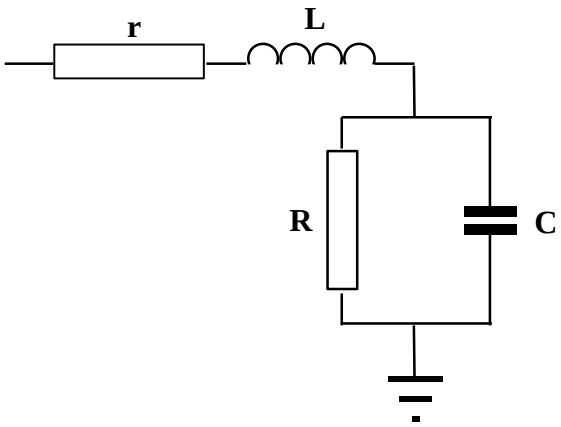

Figure 3.2: Equivalent circuit model for a vertical earth rod

The relevant equations for the circuit model parameters for the vertical electrode as suggested by Rudenberg [3.15] are:

$$\mathrm{R} = \frac{\rho}{2\pi\ell}\left(\ln\left(\frac{2\ell}{\mathrm{a}}\right) - 1\right) \tag{3.1}$$

$$G = \frac{2\pi}{\rho\left[\ln\left(\frac{2\ell}{a}\right)\right]} \tag{3.2}$$

$$C = \frac{2\pi\varepsilon_r\ell}{\ln\left(\frac{2\ell}{a}\right)} \tag{3.3}$$

$$L = \frac{\mu\ell}{2\pi}\left(\ln\frac{2\ell}{a}\right) \tag{3.4}$$

Where: ℓ and a are the length and radius of the rod electrode respectively, μ is the permeability of the soil and ε_r is the relative permittivity of the soil.

Figure 3.3 shows a horizontal earth electrode represented as a series of lumped elements. The relevant equations for the circuit model parameters of horizontal earth electrode as suggested by Sunde [3.2] are shown below.

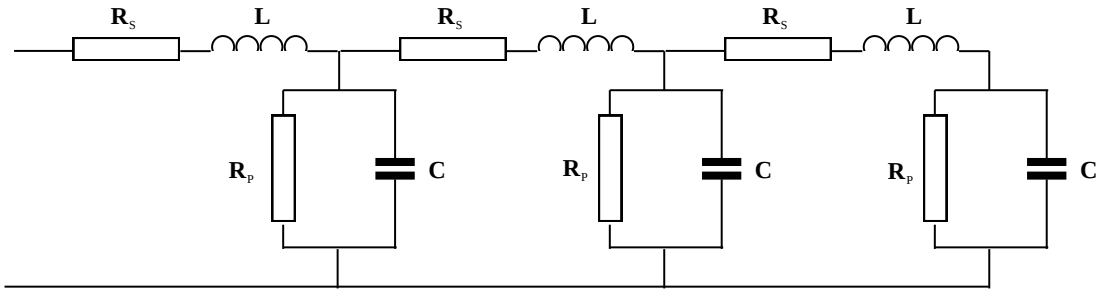

Figure 3.3: Equivalent circuit model for a horizontal earth electrode where each loop corresponds to a one metre length of earthing rod

$$R = \frac{\rho}{2\pi\ell}\left(\ln\left(\frac{2\ell}{\sqrt{2ha}}\right)-1\right) \qquad (3.5)$$

$$C = \frac{2\pi\varepsilon_r\ell}{\left[\ln\left(\frac{2\ell}{\sqrt{2ha}}\right)-1\right]} \qquad (3.7)$$

$$L = \frac{\mu\ell}{2\pi}\left(\ln\left(\frac{2\ell}{\sqrt{2ha}}\right)-1\right) \qquad (3.8)$$

Where: ℓ, a, μ and ε have the same meaning as in Equation (3.7) and h is the burial depth in m.

The distributed parameter model is commonly used for analysis of long transmission lines. Using this approach, the open-circuit impedance of a vertical earth electrode, and horizontal earth electrode Z_{oc}, can be expressed by Equation (3.90 [3.16]

$$Z_{oc} = Z_o \coth(\gamma l) \qquad (3.9)$$

Where Z_o is the characteristic impedance

$$Z_o = \sqrt{(R + j\omega L)(G + j\omega C)} \qquad (3.10)$$

and the γ is Propagation constant

$$\gamma = \sqrt{\frac{R + j\omega L}{G + j\omega C}} \qquad (3.11)$$

Where: ℓ, a, μ and ε_r have the same meaning as in Equation (3.7) and (3.8), ρ is the resistivity of the soil, ε_r is the relative permittivity of the soil and G is the conductance of the soil.

3.4 Frequency Response

In this section, simulations are carried out to investigate the frequency performance of the earth electrode.

3.4.1 Vertical Earth Electrode

The effect of soil resistivity and permittivity and the electrode length were investigated by computer simulation [3.13].

3.4.1.1 Effect of Soil Resistivity and Permittivity

The frequency response of a 5m vertical earth electrode is shown in Figure 3.4. Soil resistivities of 10Ωm, 100Ωm, 1kΩm and 10kΩm and soil relative permittivities of ε_r = 1, 5, 30 and 80. Each curve has a low frequency range at which the impedance magnitude is almost constant. The impedance value depends on the resistivity value. As the resistivity increases, the impedance magnitude also increases. For low soil resistivities (10 to 100Ωm), the impedance increases at high frequencies, which can be explained by the high influence of the inductive component of the earth rod in

which increases the impedance magnitude at high frequency. For high resistivity values (≥1kΩm), the impedance decreases at high frequencies, and this is may be due to capacitance effects.

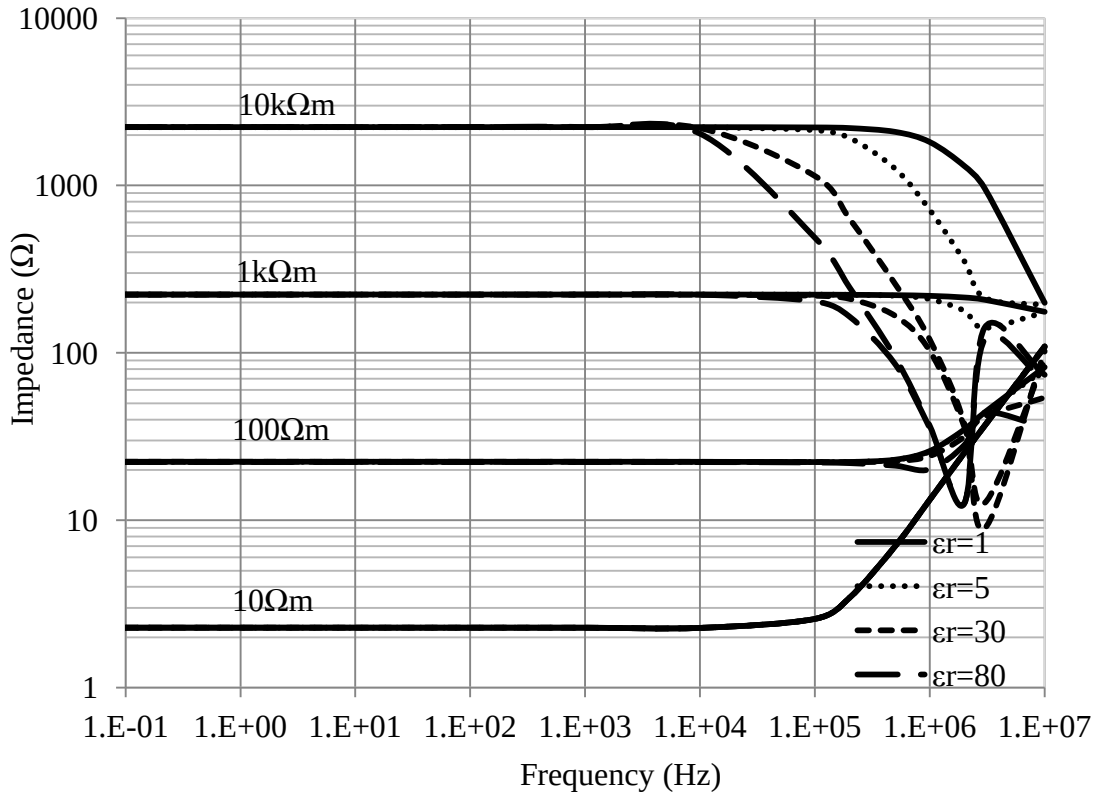

Figure 3.4: Earth impedance vs. frequency for a vertical earth electrode with various values of relative soil permittivity and resistivity

The effect of soil relative permittivity on the vertical earth electrode impedance and impedance phase angle were investigated for a range of soil resistivity (10Ωm, 100Ωm, 1kΩm and 10kΩm) over a frequency range from DC to 10MHz. The assumed value of soil relative permittivity is related to the moisture content in the soil and values as high as $\varepsilon_r = 80$ have been measured [3.8]. In these studies, the soil relative permittivity is assumed to be in the range $1 \leq \varepsilon_r \leq 80$. The results of the simulations are also shown in Figure 3.4. As can be seen, no significant effect is observed on the impedance of the vertical earth electrode under low soil resistivity

conditions. However, for high soil resistivity, the effect of soil relative permittivity is more pronounced, if there is a significant reduction in the earth impedance magnitude. This reduction may be attributed to the enhanced capacitance effects present at higher permittivities.

Figure 3.5 shows the calculated impedance phase angle with frequency. As can be seen in the figure, the phase angle remains at zero up to about 10kHz for all soil resistivities values due to the resistive nature of the impedance at low frequency. The phase angle increases at a particular frequency due to the inductive effect at high soil resistivity for low soil resistivity. For high soil resistivity, greater than about 1kΩm, the impedance phase angle shows a downturn at high frequencies [3.17]. The impedance phase angle decreases by as much as -60^0 at a frequency of 100kHz with soil resistivity of 10kΩm. This can be explained by the capacitive effect is dominant at high frequencies of high resistivity.

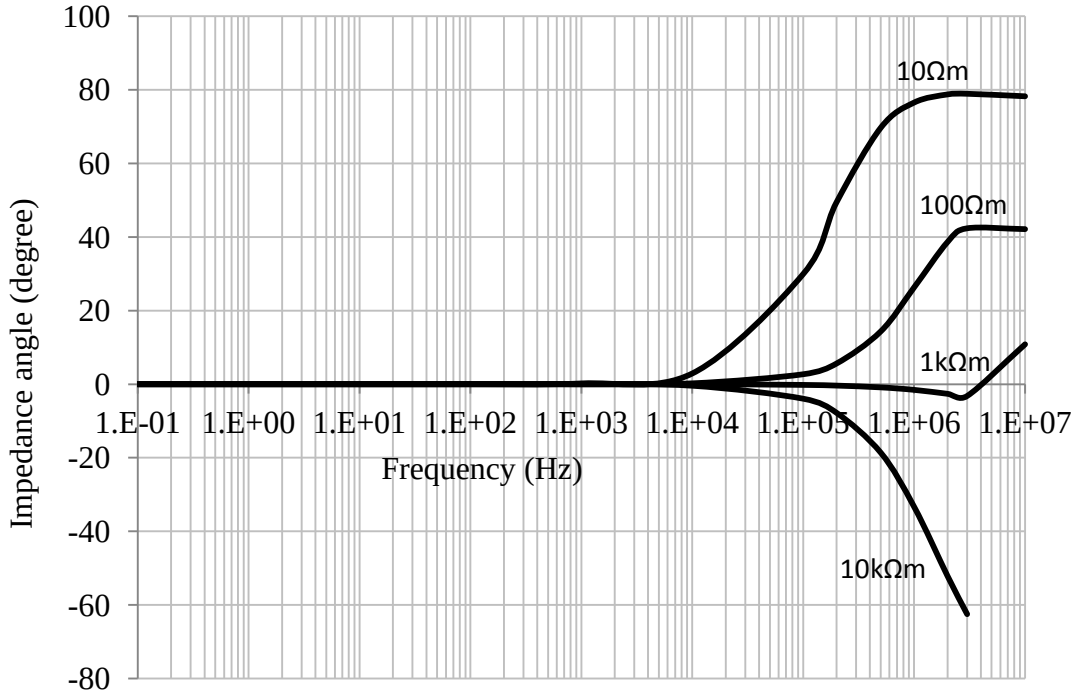

Figure 3.5: Impedance phase angle vs. frequency for a vertical earth electrode with various values of soil resistivity

3.4.1.2 Effect of Electrode Length

To examine the effect of electrode length on the frequency performance of the vertical earth electrode the electrode length was varied from 5m to 20m. The study was performed for a wide range of soil resistivity (10Ωm, 100Ωm, 1kΩm and 10kΩm) over a range of frequencies from DC to 10MHz. The earth impedance was calculated at two selected frequencies, 50Hz and 1 MHz.

Figure 3.6 shows the impedance of a vertical electrode, with length varied between 5m and 20m. From Figure 3.6 a, it can be seen that the impedance magnitude at 50Hz decreases as length increases for all soil resistivities considered. At 100kHz, the impedance is seen to decrease with increase in electrode length for all soil resistivities values (Figure 3.6 b). At this frequency, for the lower resistivities of 10Ωm and 100Ωm, the impedance decreases until it reaches a constant value at a particular length. These results demonstrate that the effective length has been reached. At 10Ωm, the effective length is about 10m.

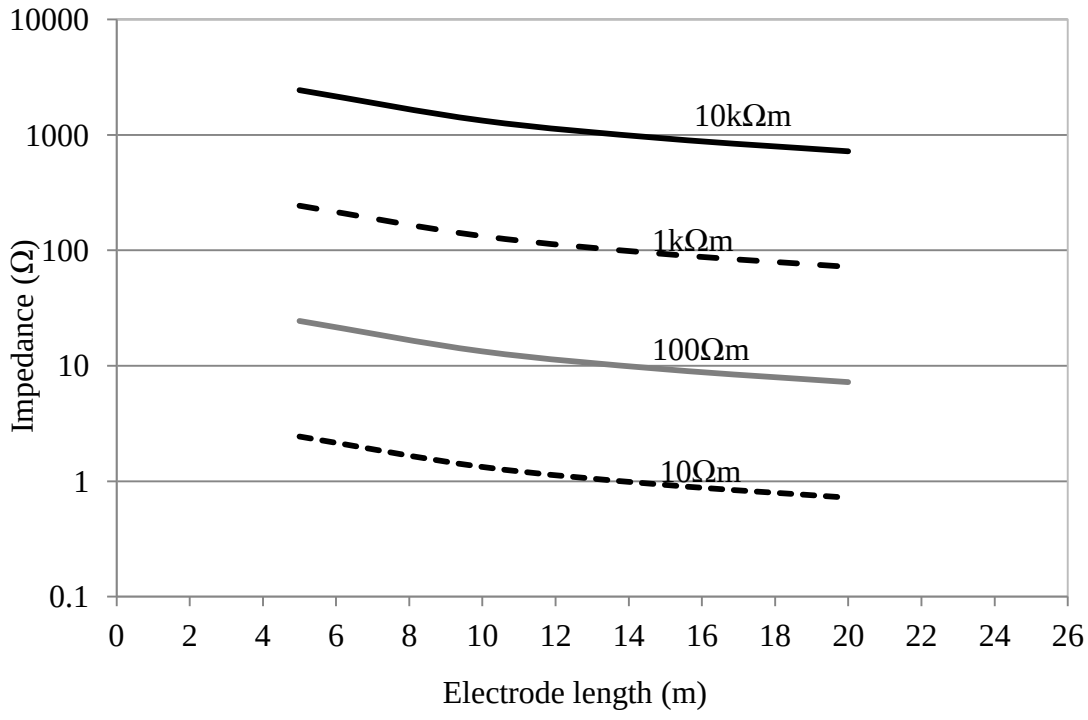

a) 50Hz

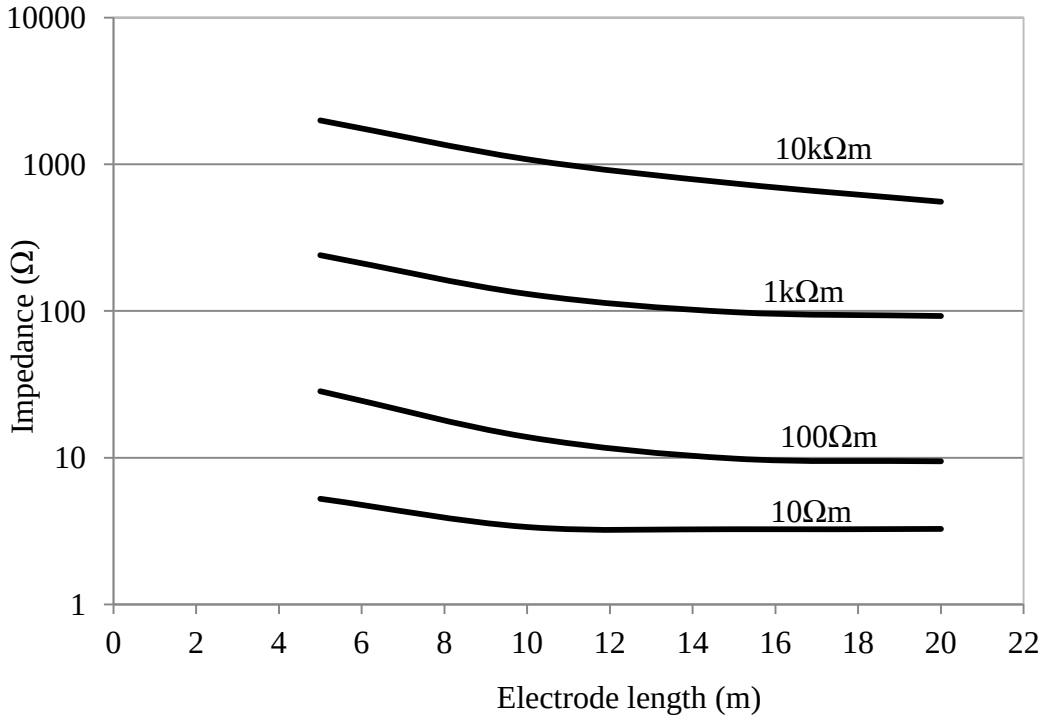

b) 100kHz

Figure 3.6: Effect of length on impedance of vertical electrode at 50Hz and 100kHz for different soil resistivities

3.4.2 Horizontal Earth Electrode

3.4.2.1 Effect of Resistivity and Relative Permittivity

The impedance of a 100m horizontal earth electrode was calculated using the transmission line circuit model and by computer simulation using the HIFREQ software. The calculated earth impedance and the impedance phase angle are shown in Figure 3.7. The results are shown for soil resistivities ranged between 10Ωm and 10kΩm over a range of frequencies from DC to 10MHz. Figure 3.7 shows similar trends to those obtained for the vertical earth electrode, where the impedance is predominantly resistive up to a particular frequency referred to here as upturn frequency which is related to the value of the soil resistivity. Due to the greater length and hence higher longitudinal impedance of the horizontal earth electrode, the

inductive effect becomes apparent at much lower frequencies compared to the vertical earth electrode case.

For the high soil resistivity case (10kΩm), the impedance value starts at a higher magnitude due to the high soil resistivity and remains constant until up to a frequency of 100kHz. Above this frequency, and increasing the permittivity to 80, the impedance starts to decrease which indicates that the capacitive effect is evident with high resistivity.

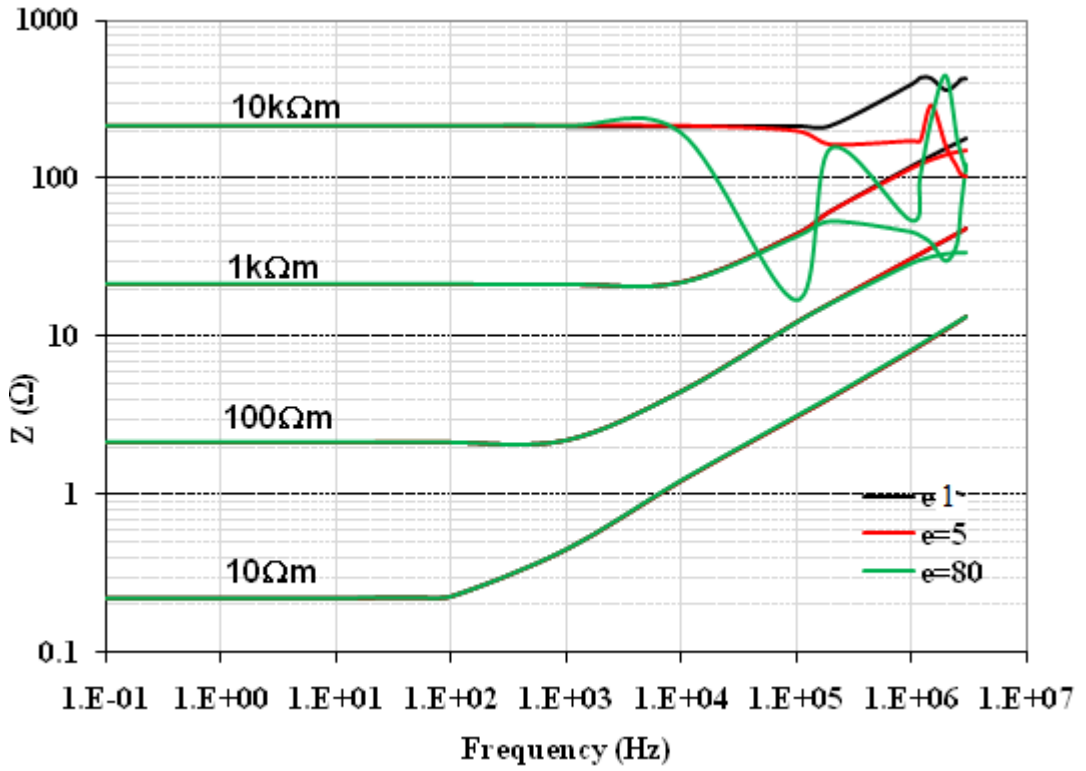

Figure 3.7: Impedance horizontal earth electrode as a function of frequency at different soil resistivities and permittivities

3.4.2.2 Effect of Increasing the Length of Horizontal Earth Electrodes

The impedance magnitude was computed for horizontal earth electrode lengths from 2m to 100m. A 1A magnitude current was injected into one end of the horizontal earth

electrodes for four different soil resistivity values (10Ωm, 100Ωm, 1kΩm and 10kΩm) and for frequencies of 50Hz and 100kHz. The results are shown in Figure 3.8. Figure 3.8(a) shows that at 50Hz, extending the electrode length results in an initial sharp drop of earth impedance followed by a more gradual decrease for all the soil resistivities considered. At 100kHz, Figure 3.8(b) shows that increasing the electrode length causes a significant reduction in earth impedance for high soil resistivities, but for low soil resistivities, there is less reduction. From the figure, it is also clear that the earth impedance of the horizontal electrode reaches a limiting value and further increase in length beyond this will not reduce the impedance of the earth conductor. This limit is known as the effective length; the length at which no further reduction in impedance is observed when increasing electrode length [3.18].

Hence, the higher the frequency is the shorter the effective length will be. For example, in the case of 50Hz injection, the effective length is not reached at 100m.

In contrast, at 100 kHz, and with a soil resistivity of 10Ωm, the effective length is about 15m. Soil resistivity, also plays an important role in characterising the effective length; the lower the resistivity is, the shorter the effective length will be. For example, at 100kHz the effective length is 6m for a soil resistivity of 10Ωm, but it is greater than 100m for a soil resistivity of 10kΩm. Similar results were reported in [3.19]. Experimental tests to determine the effective length of a horizontal electrode under variable frequency injection is investigated in Chapter 5.

The effective length of a horizontal earth electrode for various frequencies over a wide range of soil resistivities is calculated using CDEGS program. The results are shown in Figure 3.9, which indicates that the calculated length required to obtain constant impedance. The results clearly show that for low soil resistivity shorter length required to characterise the impedance of the horizontal earth electrode. For

high soil resistivity case at low frequency great length required for the impedance to reach a asymptotic value. For example, a current of frequency 1kHz has an effective length of more than 1000m in soil of resistivity 10kΩm, but an effective length of only 40m in soil of resistivity 10Ωm. Increasing the frequency reduces the length required to characterise the earth impedance of the horizontal electrode.

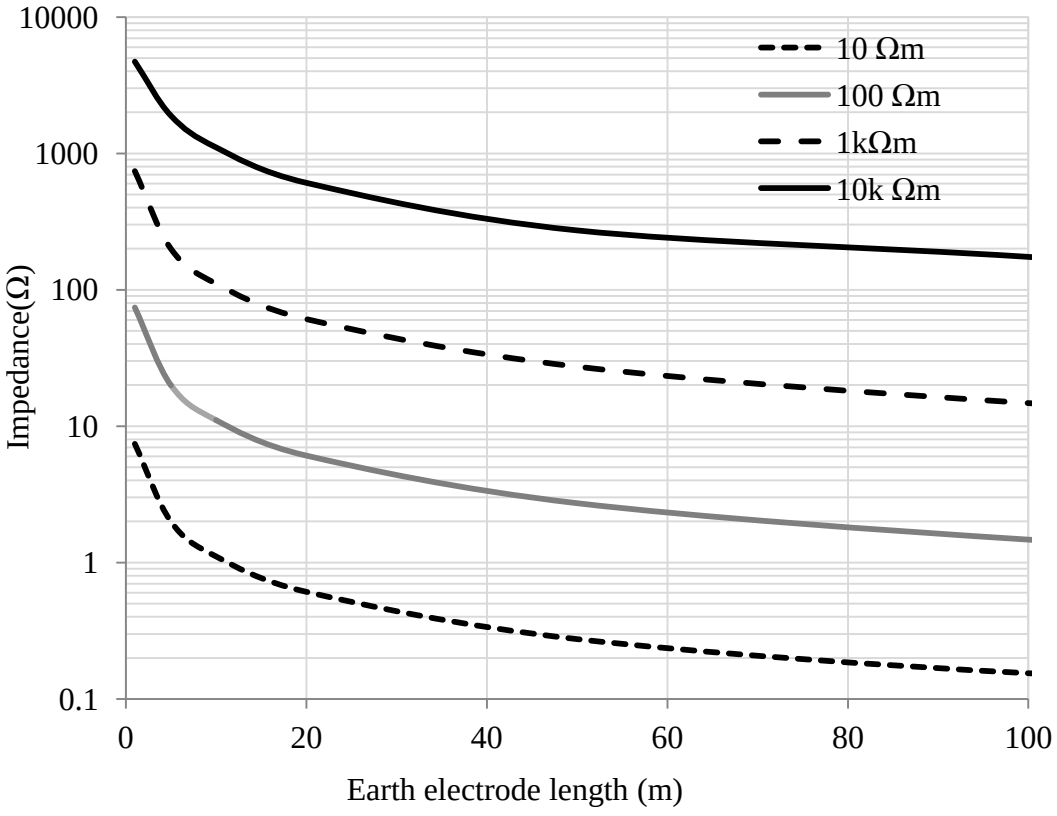

a) 1A injected at 50Hz

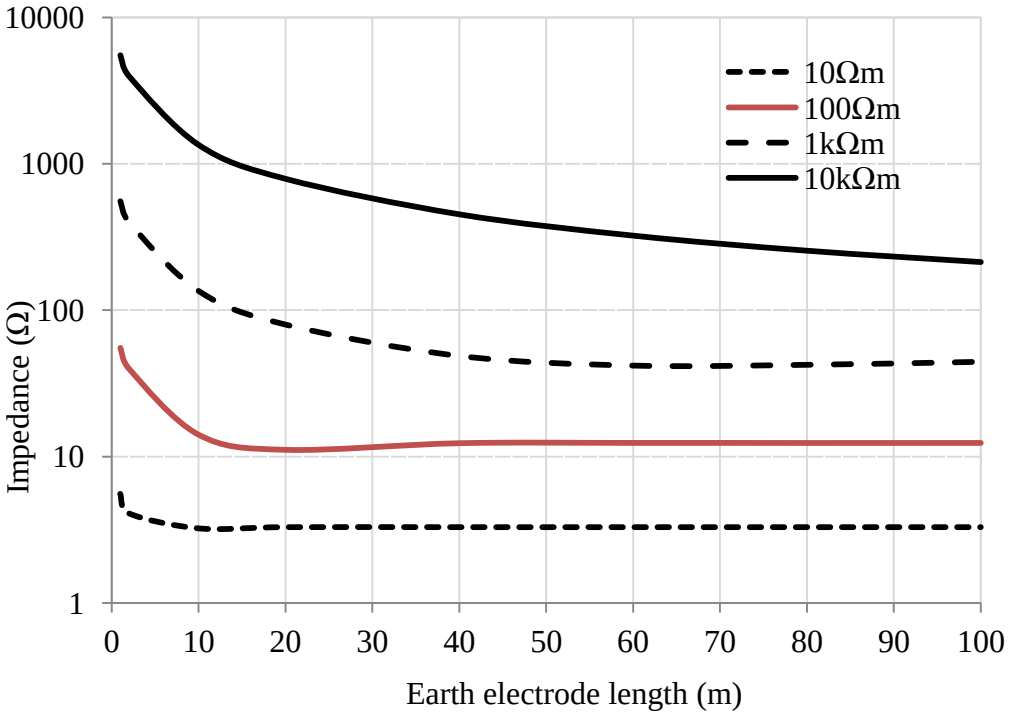

b) 1A injected at 100kHz

Figure 3.8: Effect of horizontal electrode length on earth impedance for different resistivities at selected frequencies

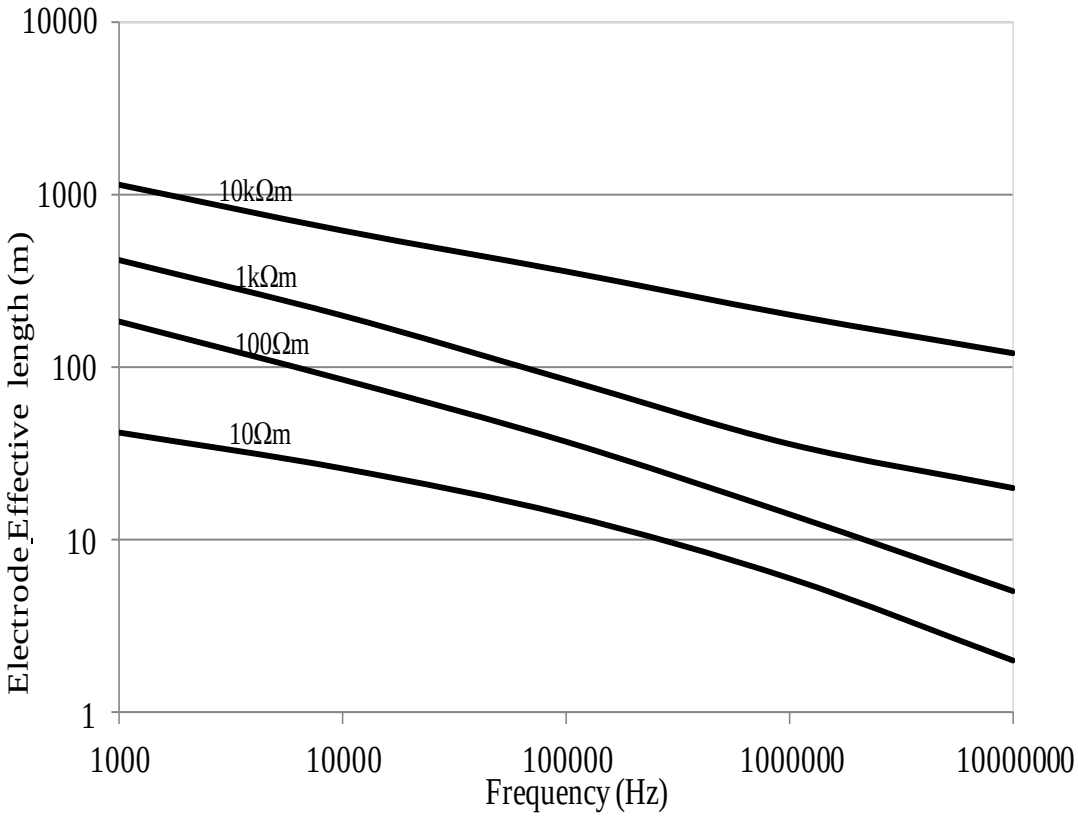

Figure 3.9: Electrode effective length vs. frequency of current

3.5 Comparison of Simulation and Circuit Model Results

A lumped parameter circuit, a distributed parameter representation and a CDEGS model were used to calculate the impedance of a 5m vertical earth electrode in 100Ωm and 1kΩm soil. The frequency responses obtained by all three models are shown in Figure 3.10. For each model, the impedance magnitude is constant at about 20Ω at a soil of resistivity 100Ωm and 223Ω for a soil resistivity of 1kΩm up to a frequency of around 100kHz. There is a good agreement between the results predicted by CDEGS and the distributed parameter circuit model. However, higher impedance magnitudes were obtained by using lumped parameter at frequencies above the upturn frequency. This suggests that prediction of earth electrode behaviour at high frequency is better carried out using the distributed parameter model or CDEGS software. The small discrepancy over the low frequency range 10Hz to 100kHz between the values predicted by the circuit models and CDEGS can be explained by the simplified circuit equations which for example do not taken to account conductor burial depth.

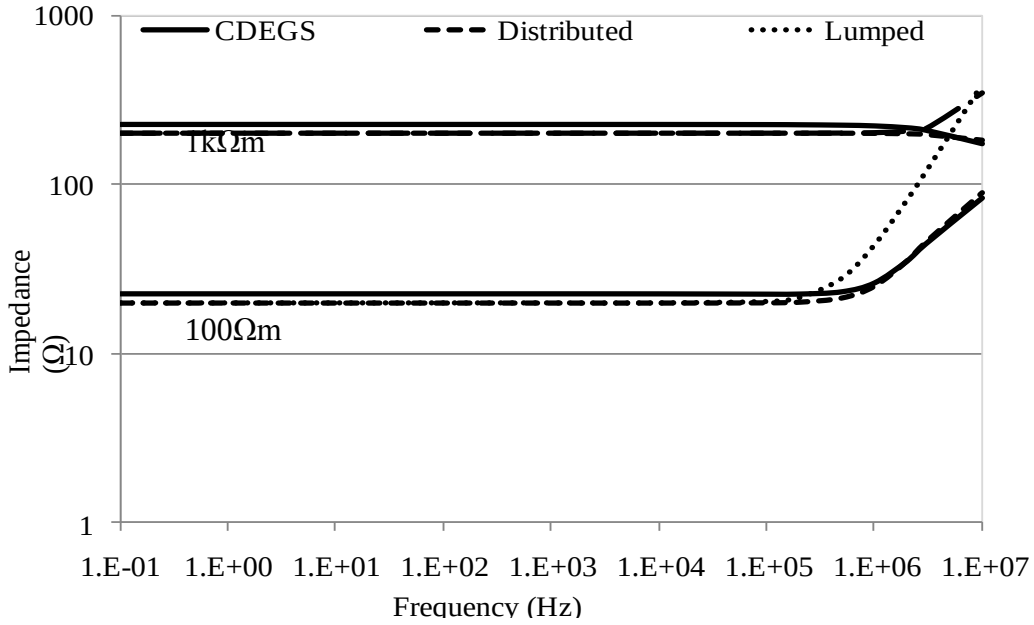

Figure 3.10: Frequency response of 5m vertical electrode using CDEGS, lumped circuit and distributed circuit models

3.6 Earth Grid Frequency Response

3.6.1 Effect of Soil Resistivity and Relative Permittivity

In this section, the simulations are extended to a 100x100m earth grid. CDEGS earthing software [3.13] was used to calculate the earth grid impedance for a range of frequencies from DC to 10MH and soil resistivity ranging from 10Ωm to 10kΩm. A 1A current was injected into the centre of the earth grid and the earth impedance at the point of injection was calculated. Figure 3.11 shows the frequency response. It can be seen that the earth grid shows similar trends to those of the horizontal earth electrode. Each curve has a lower frequency range over which the impedance is almost constant and equal to the earth resistance. There is then an upturn frequency, and this occurs at lower frequency for lower values of soil resistivity. This increase can be attributed to the inductive component of the earth grid at these frequencies. For higher soil resistivities, 1kΩm, and frequencies above 1MHz the impedance shows an oscillatory behaviour [3.17]. These oscillations may be explained by the interaction between the inductive and capacitive components.

Figure 3.12 shows the change in impedance phase angle with frequency, and the curves exhibit similar trends to those obtained by Grcev and Heimbach [3.20]. For a 10Ωm soil resistivity, the impedance phase angle starts to increase at a frequency of about 100Hz and a smaller increase is seen at lower frequencies for the 100Ωm and 1kΩm conditions. For a soil resistivity of 10kΩm, there is a small decrease in impedance phase angle at about 100kHz after which it increases.

The effect of permittivity on the performance of the earth impedance of the earth grid is similar to that seen for the horizontal earth electrode, as shown in Figure 3.11.

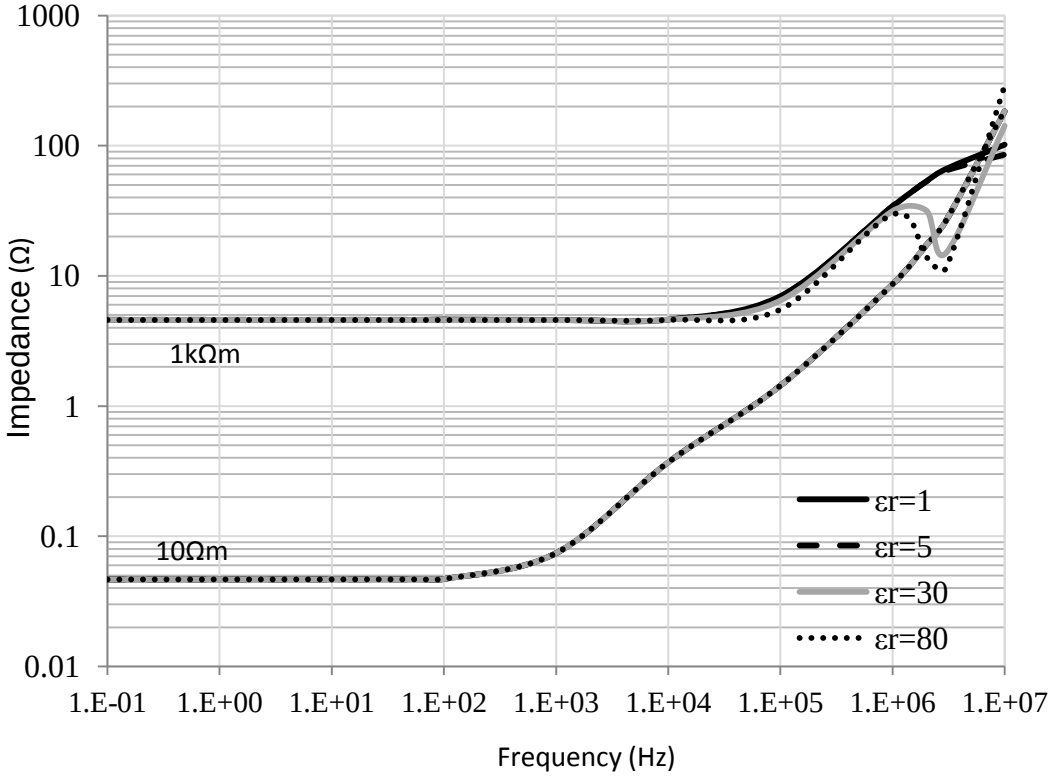

a) Soil resistivities 10Ωm and 1kΩm

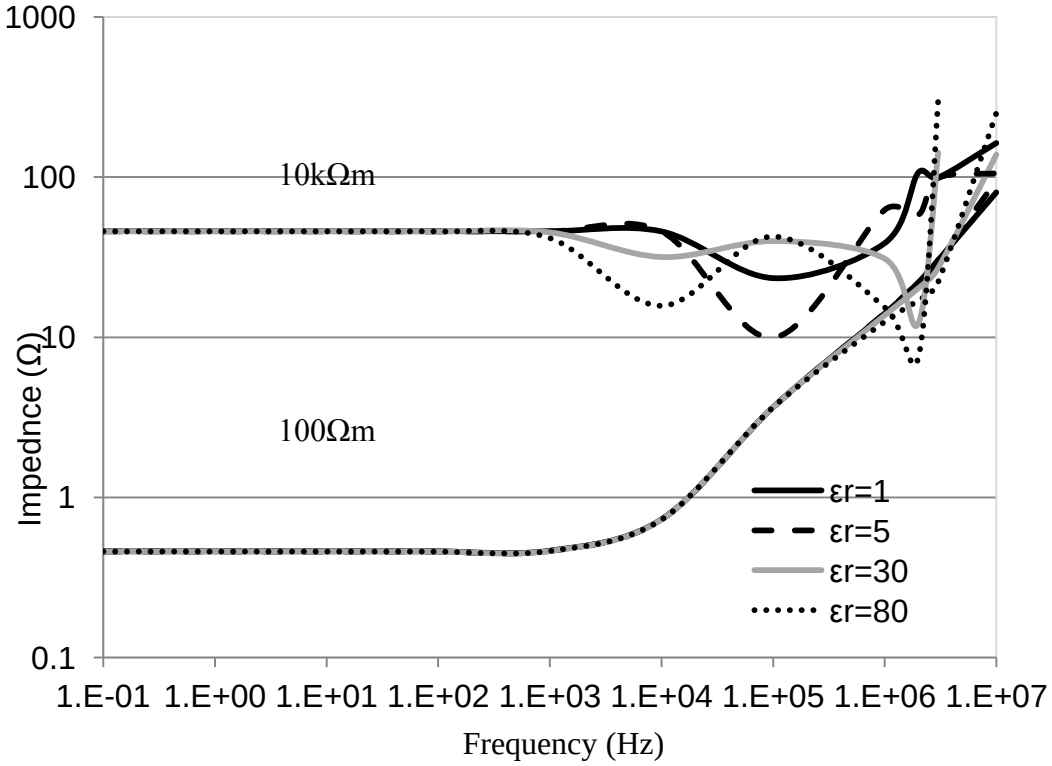

b) Soil resistivities 100Ωm and 10kΩm

Figure 3.11: Calculated earth grid impedance vs. frequency for soil resistivities of 10Ωm, 100Ωm 1kΩm and 10kΩm, for four different soil permittivities (ε_r = 1, 5, 30 and 80)

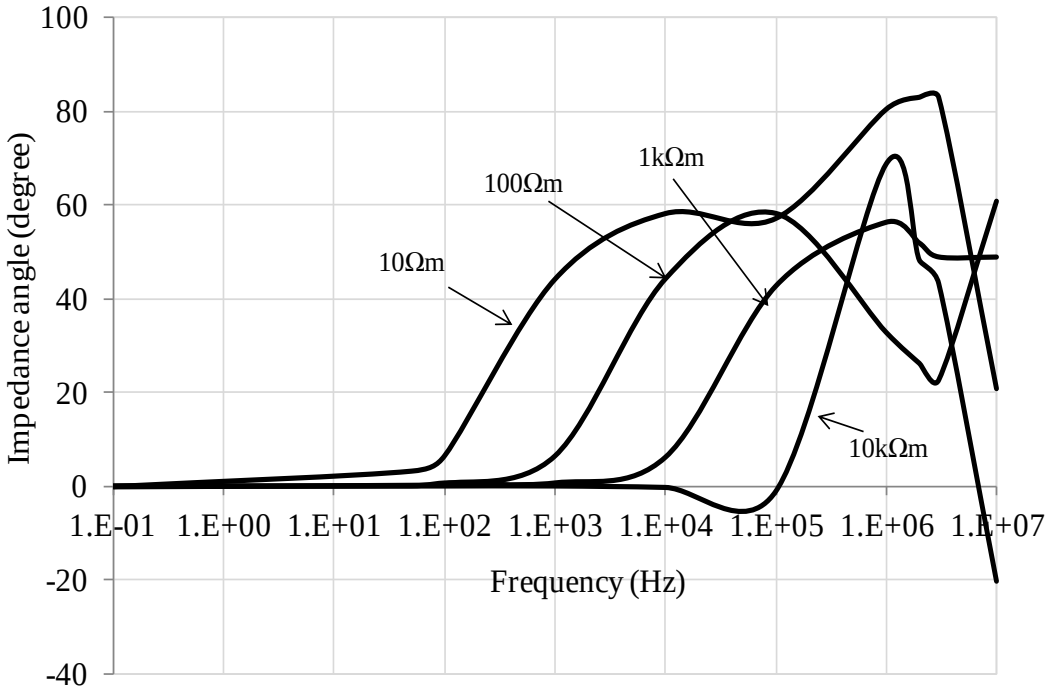

Figure 3.12: Impedance phase angle vs. frequency for soil resistivity values 10Ωm 100Ωm, 1kΩm and 10kΩm.

3.6.2 Effect of Grid Size

The frequency response of earth grids of different sizes ranging from 10mx10m to 120mx120m while maintaining the same mesh size 10mx10m is investigated.

The results, expressed in the form of impedance as a function of side length and shown in Figure 3.13., which demonstrate that, at the low frequency of 50Hz, the earth grid impedance decreases significantly with size of grid for both values of soil resistivity. At 100kHz, and with a soil resistivity of 100Ωm, the impedance decreases slightly as the grid size increased before reaching a constant value. At 1MHz and 100Ωm soil resistivity, the impedance in unaffected for grid sizes beyond10mx10m. Similar trends are seen at higher soil resistivity. General observation was noticed at 100kHz small oscillations in the curve just before it reaches the effective which is area similar to observation reported by [3.17].

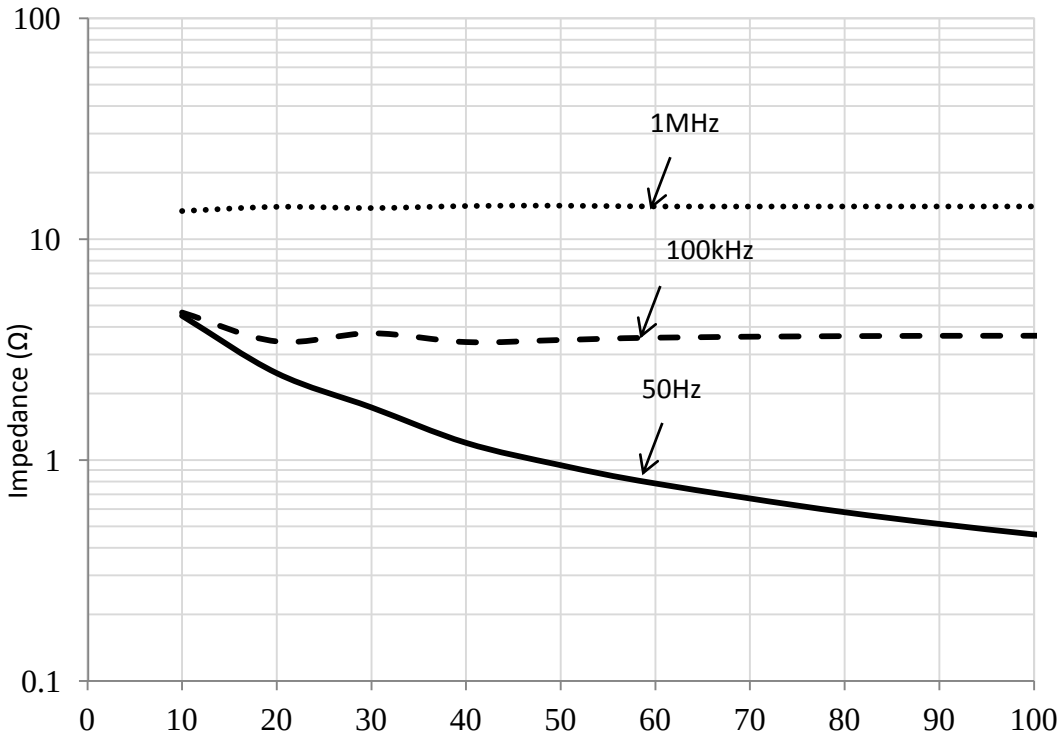

a) 100Ωm soil resistivity

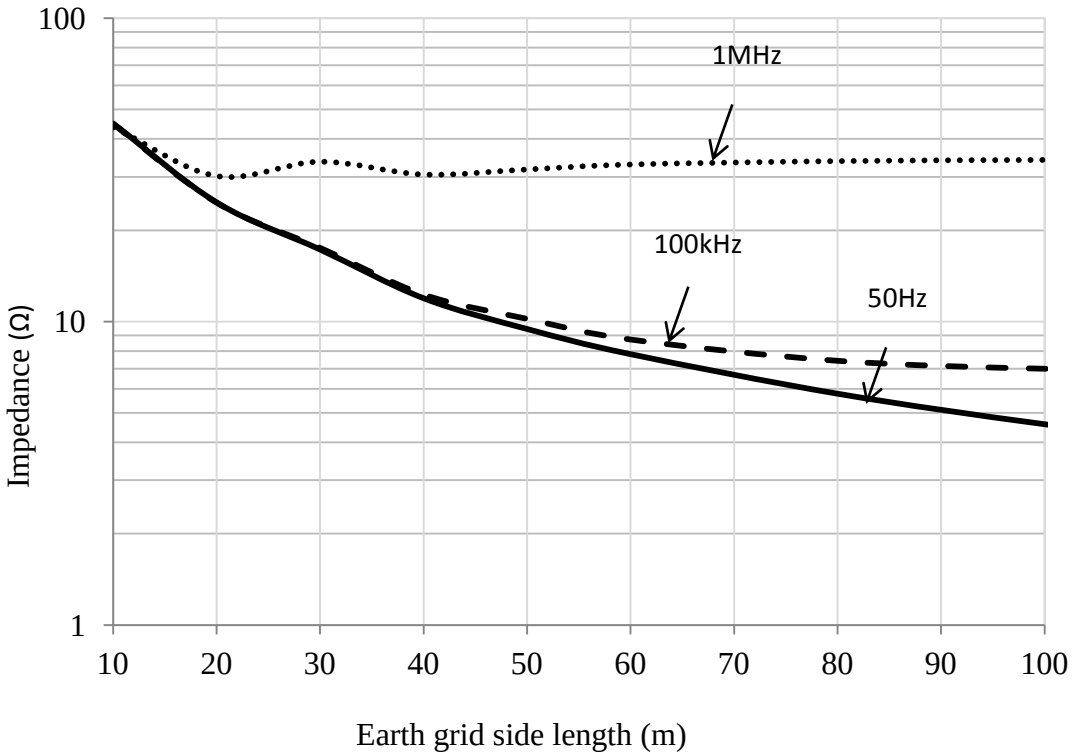

b) 1kΩm soil resistivity

Figure 3.13: Effect of size on earth grid impedance

3.6.3 Effect of Injection Point

The effect of injection point on the performance of the earth grid is examined for frequencies ranging from DC to 10MHz in low and high resistivity soil. A 100mx100m earth grid having 4 meshes was considered with 1A current injected at a corner and at the centre point.

Figure 3.14 shows the calculated earth impedance values obtained from corner and central injections. At high frequency, the corner injected grid shows higher impedance magnitude compared with the centrally injected earth grid. For example, at 3MHz, for 1kΩm soil resistivity, the earth impedance magnitude is about 66.1Ω for central injection and 83.6Ω for corner injection, equivalent to an increase of about 26%. Similar results are reported by [3.11-3.12].

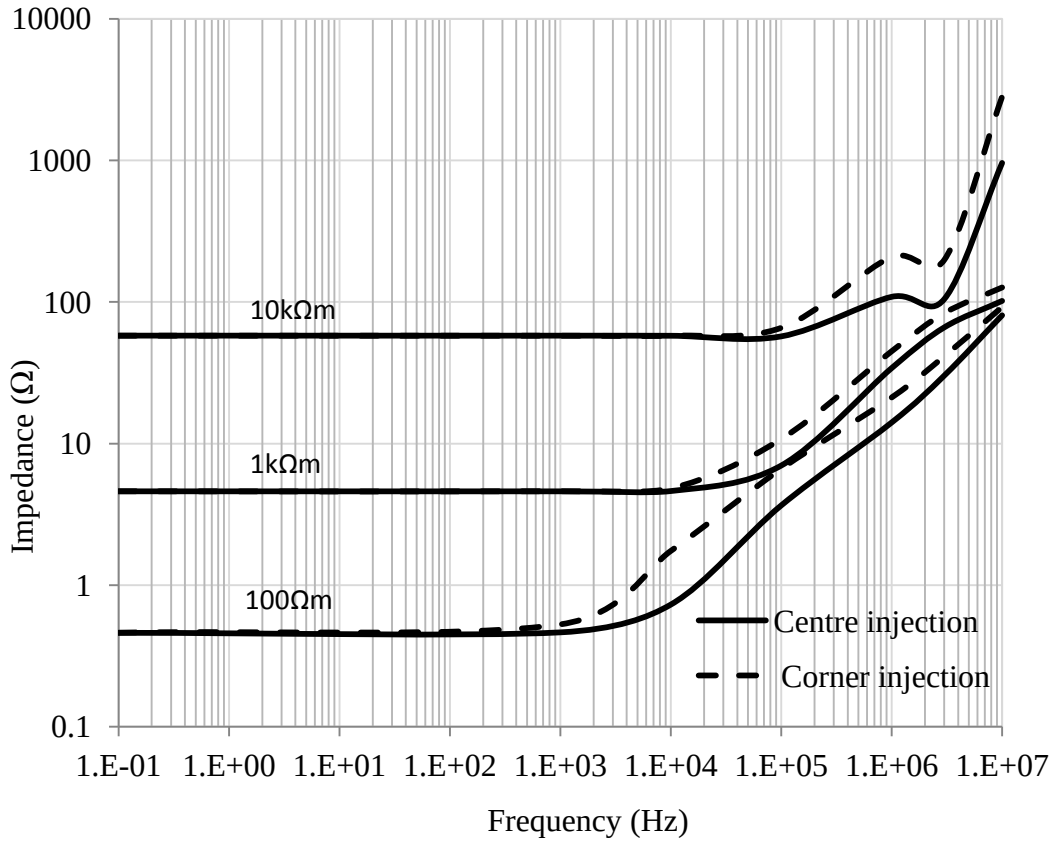

Figure 3.14: Earth grid frequency response for corner and central injection points for soil resistivities 100Ωm, 1kΩm and 10kΩm

3.7 Impulse Energisations

Lightning and switching surges are the main sources of earth transients. These impulse currents have rapid rise times, are of short duration and may be described by a double exponential wave [3.21],

$$I(t) = A(e^{-Bt} - e^{-Ct}) \qquad (3.12)$$

Where I(t) is the impulse current as a function of time, and A, B and C are coefficients which determine the shape of the impulse.

Impulse currents are usually described by their peak current (or voltage) and by T_1 (time for current to reach peak value) and T_2 (time for current to fall to half its peak value); written as T_1/T_2 in microseconds, e.g. a 10kA, 1/5.

At present, only little gaudiness is made in earthing standards [3.4-3.31-3.32] for local enhancement of the earth grid to disperse "high-frequency" and transient currents.

In this section, comprehensive simulations are conducted to contribute to better understanding of the behaviour of earth electrodes under transient conditions. The simulations were carried out using CDEGS [3.13] (field theory based software) for 8/20 and 1/5 standard impulses. In order to analyse the impulse behaviour of earth electodes, the following approach was used with the simulation software:

(a) The routine FFTSES, is used for the calculation of Fourier Transforms (using Fast Fourier Transforms (FFTs)) and Inverse Fourier Transforms (IFTs), and

(b) HIFREQ, routine is used for the calculation of the earth electrode system response of at specific frequencies.

3.7.1 Simulation Techniques and Methodology

Time-domain calculations using simulation software such as CDEGS [3.13] requires a minimum of three operations: (i) taking the FFT of the current impulse waveform (using FFTSES), (ii) calculating the response of the earth electrode system at each frequency (using HIFREQ) and, finally, (iii) calculating the IFT (using FFTSES).

The earth electrode system was implemented in CDEGS as an interconnected network of long thin cylindrical conductors. The geometry of each conductor and its burial depth and orientation with respect to the air-soil interface was specified and the properties of the air and multilayer soil were selected for each study.

For each earth electrode configuration, the transient earth potential rise (TEPR) was calculated at the midpoint of the energised segment. To further quantify the behaviour, the TEPR peak magnitude and rise time for different conditions were compared. The TEPR peak magnitude indicates the highest potential that the earth electrode system will reach. The TEPR rise time, is a simple measure of the impulse shape.

3.7.2 Earth Electrode Configurations

The same earth electrodes used in the previous section, (rod, horizontal electrode and grid) were adopted for this study. The response to the two standard impulses are compared over a wide range of soil resistivity with different relative soil permittivities.

3.7.3 Vertical and Horizontal Earth Electrodes

3.7.3.1 Effect of Resistivity

The transient response of a 10m vertical rod and a 100m horizontal earth electrode to an injected standard 1A, 8/20 impulse current is shown in Figure 3.15. Figure 3.15 a) shows this impulse current and the resultant TEPR for soil with 100Ωm resistivity and unity relative soil permittivity at the injection point for a horizontal electrode.

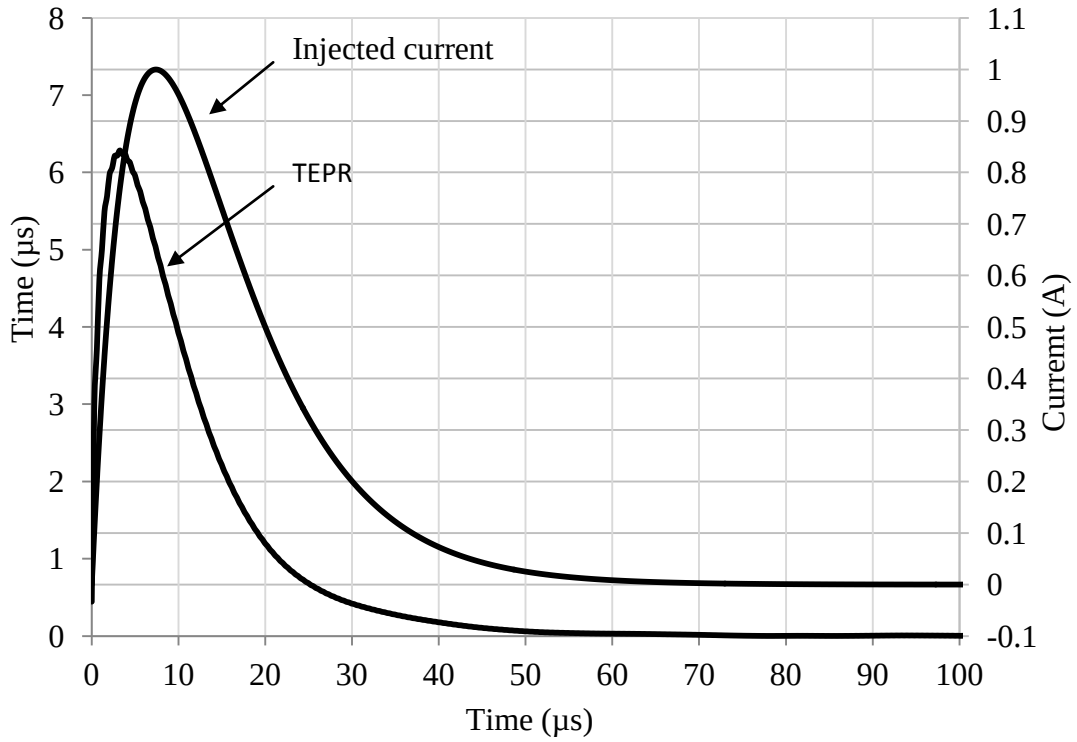

a) 100m horizontal earth electrode

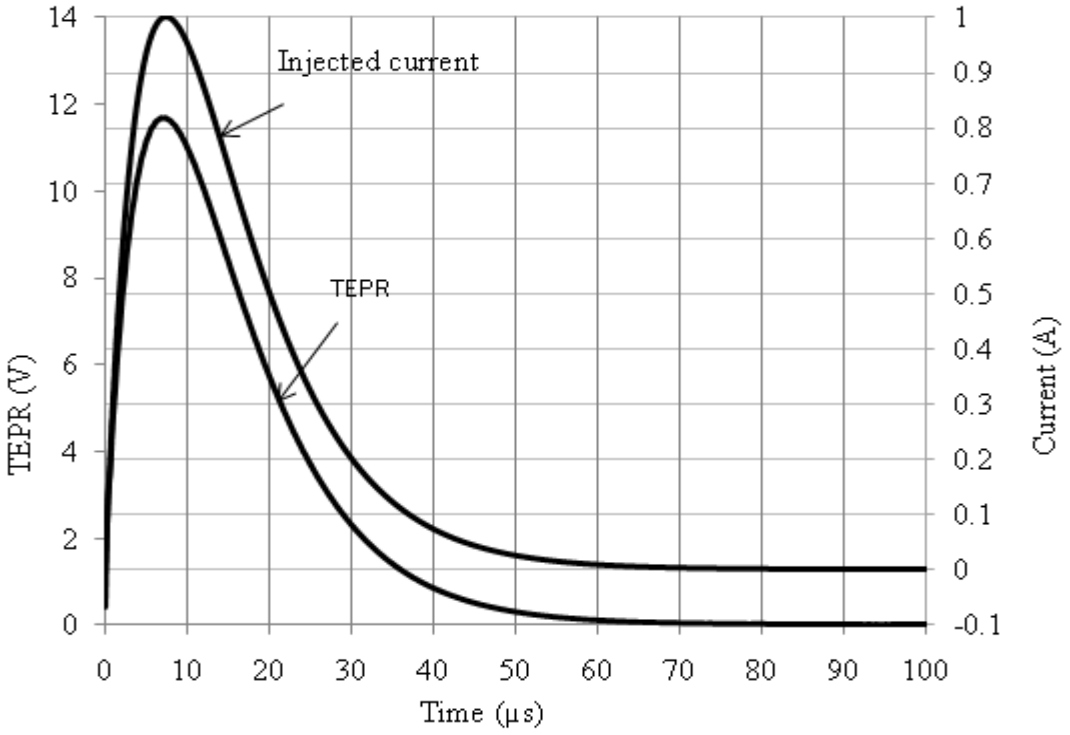

b) 10m vertical earth electrode

Figure 3.15: Transient earth potential rise for an 8/20 impulse current with soil resistivity of 100Ωm and unity permittivity

It can be seen from Figures 3.15.a and 3.15.b, the TEPR reaches its peak before the injected impulse current for both electrodes but much more quickly in the case of the horizontal electrode. This highlights the effect of inductive component which is greater for the longer electrode. Figures 3.16.a and 3.16.b illustrate the peak TEPR at the injection point as a function of soil resistivity for both rod and horizontal electrodes. As expected, the TEPR increases as the resistivity increases, confirming that the inductive effect is present for both the horizontal and vertical earth electrodes. In each case, the peak TEPR occurs before the peak current due to the inductive effect and the high frequency content of the impulse current. It can also be seen that the peak TEPR rise time increases as the soil resistivity increases. The little oscillation in the voltage for low soil resistivity is explained by the higher inductance at low resistivity which affect the voltage at the decay region. Similar results were

reported by Nixon [3.27] when an earth rod buried in 100Ωm and 1kΩm soils was injected with two types of current impulses.

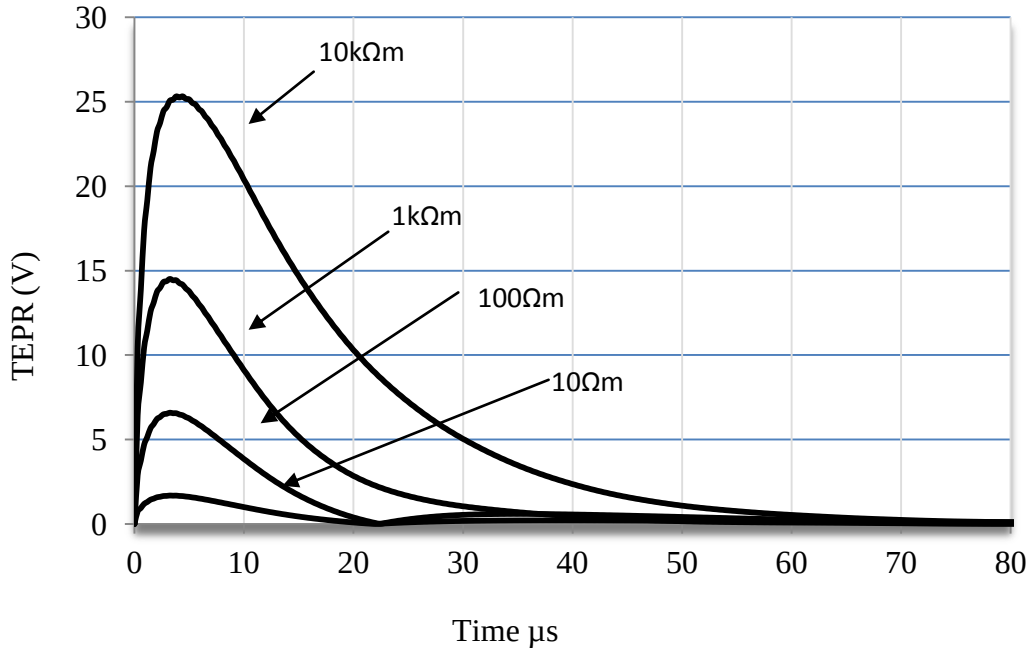

a) 100m horizontal electrode

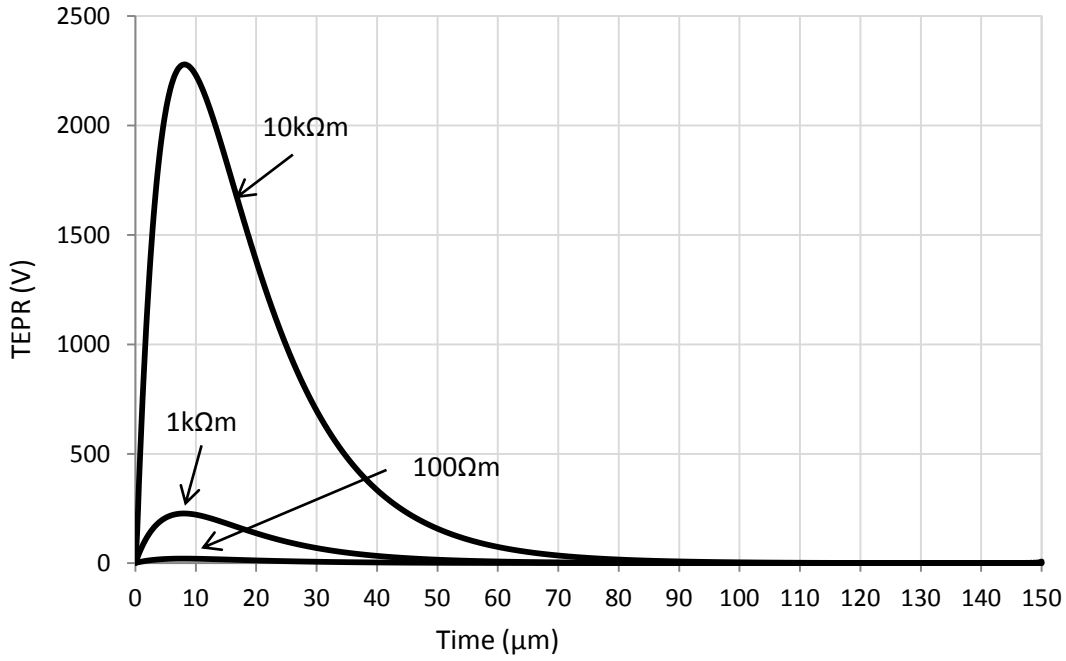

b) 10m vertical electrode

Figure 3.16: Effect of soil resistivity on value of transient earth potential rise of earth electrode

Figure 3.17 presents the results of a comparison of the transient behaviour of a vertical and horizontal earth electrode, both of 5m length and buried in soil with resistivity of 100Ωm. As can be seen, the TEPR for the horizontal earth electrode is higher than that for the vertical earth electrode. For 100Ωm, soil resistivity the horizontal earth electrode peak TEPR was about 10% higher than that for the vertical electrode.

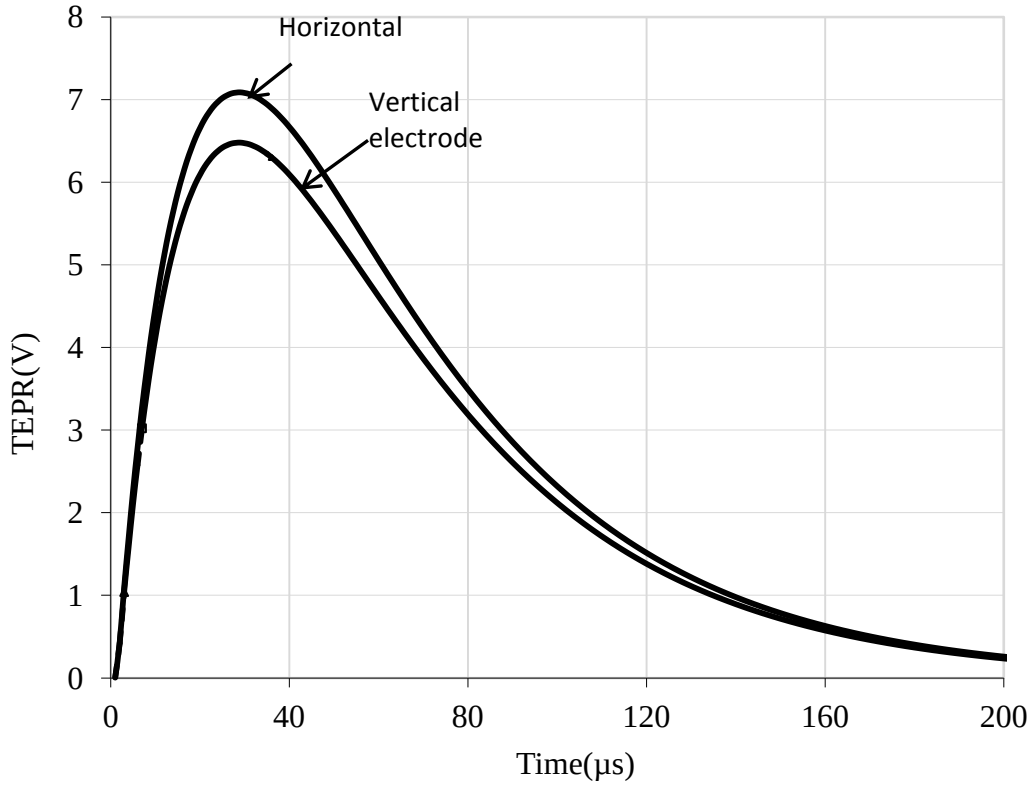

Figure 3.17: Comparison of transient earth potential rise for a 5m vertical electrode and a 5m horizontal electrode

3.7.3.2 Effect of Permittivity

A 5m long vertical earth electrode and a 100m counterpoise with 50mm^2 cross section area (8mm diameter) buried at a depth of 1m was used for this study. A 1A, 8/20 impulse was injected into the electrodes, and the transient potential at the

injection point was calculated. The study was carried out for soil resistivity ranging from 10Ωm to 10kΩm and soil relative permittivity values of 1, 5, 30 and 80.

The calculated TEPR as a function of time is shown in Figure 3.18. It is clear from the figure that the relative permittivity has no major effect on the TEPR for low soil resistivity (below 1kΩm). However, for a resistivity of 10kΩm, it can be seen that increasing the permittivity reduces the peak value of the TEPR but increases the rise time, making the shape of the curve less "spiky".

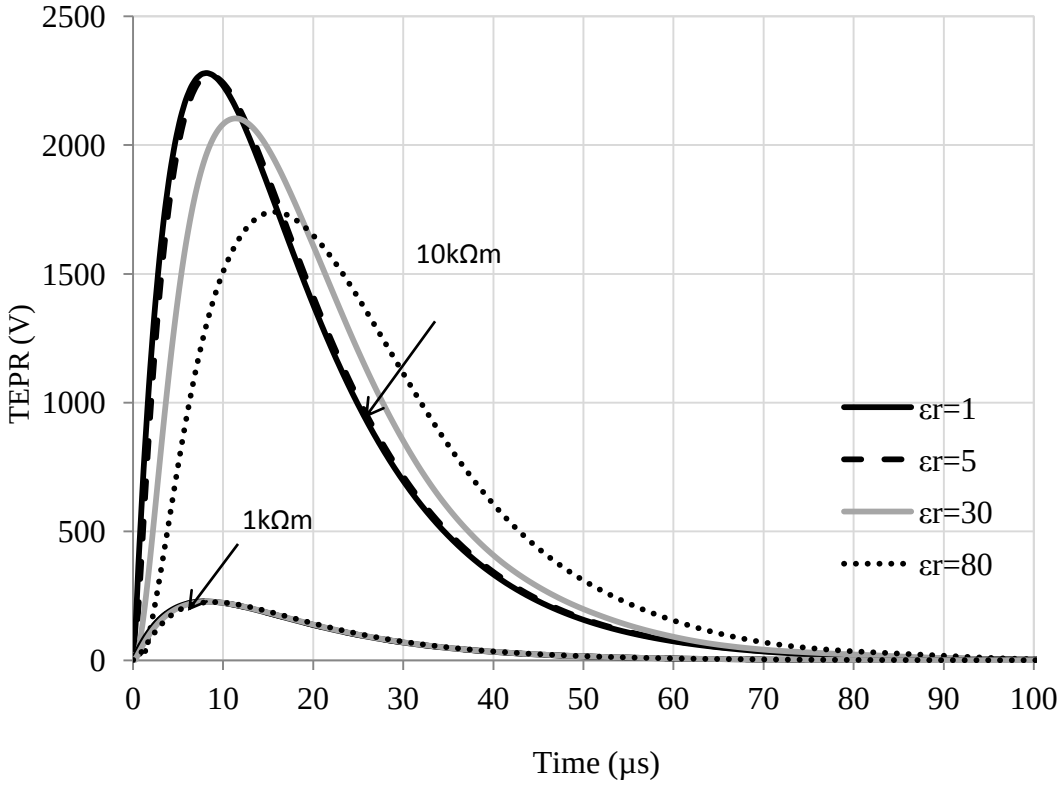

a) 5m vertical electrode

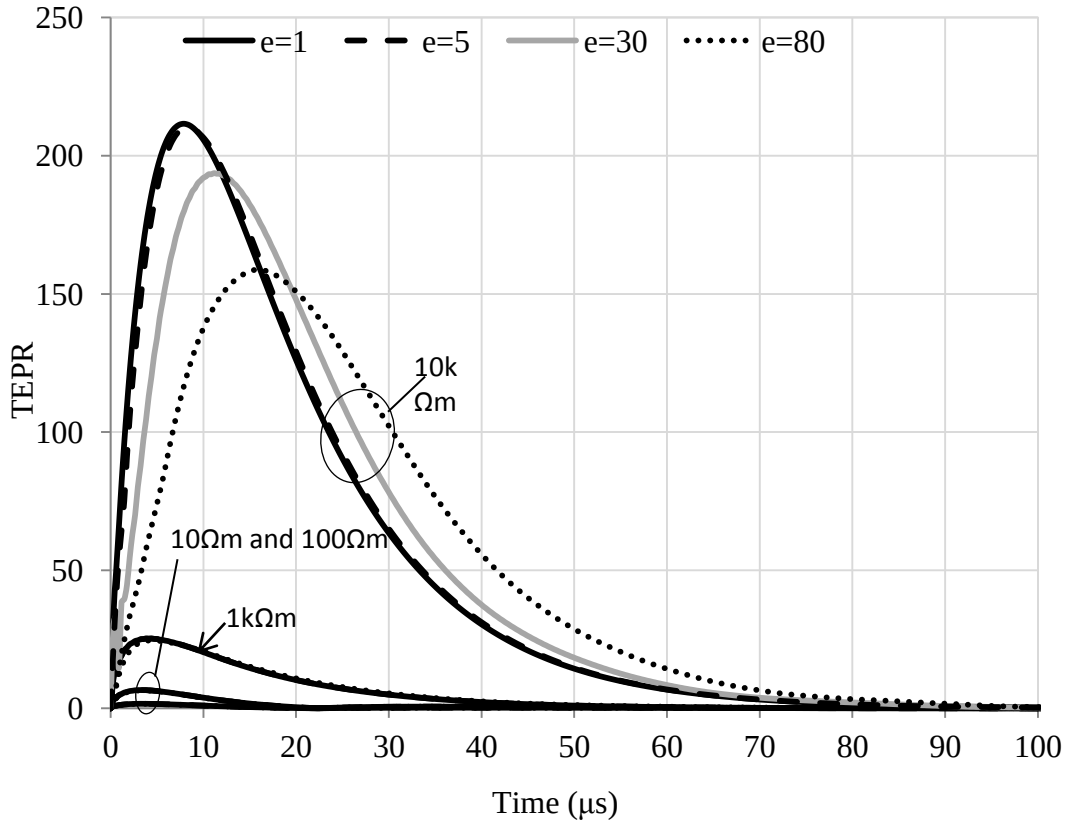

b) 100m horizontal electrode

Figure 3.18: Effect of soil permittivity on transient earth potential rise of earth electrode

3.7.3.3 Effect of Current Impulse Type

In this section, the effect of current impulse shape on the time domain response of the earth electrode is presented. A 100m horizontal electrode was subjected to two current impulses: i) 1A, 8/20 and ii) 1A, 1/5. The simulations were conducted using CDEGS software for soil resistivity values between 10Ωm and 10kΩm. Injection was made into one end of the horizontal earth electrode, and peak TEPR was calculated at the injection point. Figure 3.19 shows that peak TEPR increases as the soil resistivity increases. The 1/5 impulse produces higher peak TEPR values computed with 8/20 impulse because of its higher frequency content. This is due to 1/5 impulse contains higher frequency component. The increase in TEPR peak

values with soil resistivity is reasonably linear for the 8/20 impulse, but this is not the case under fast impulse conditions.

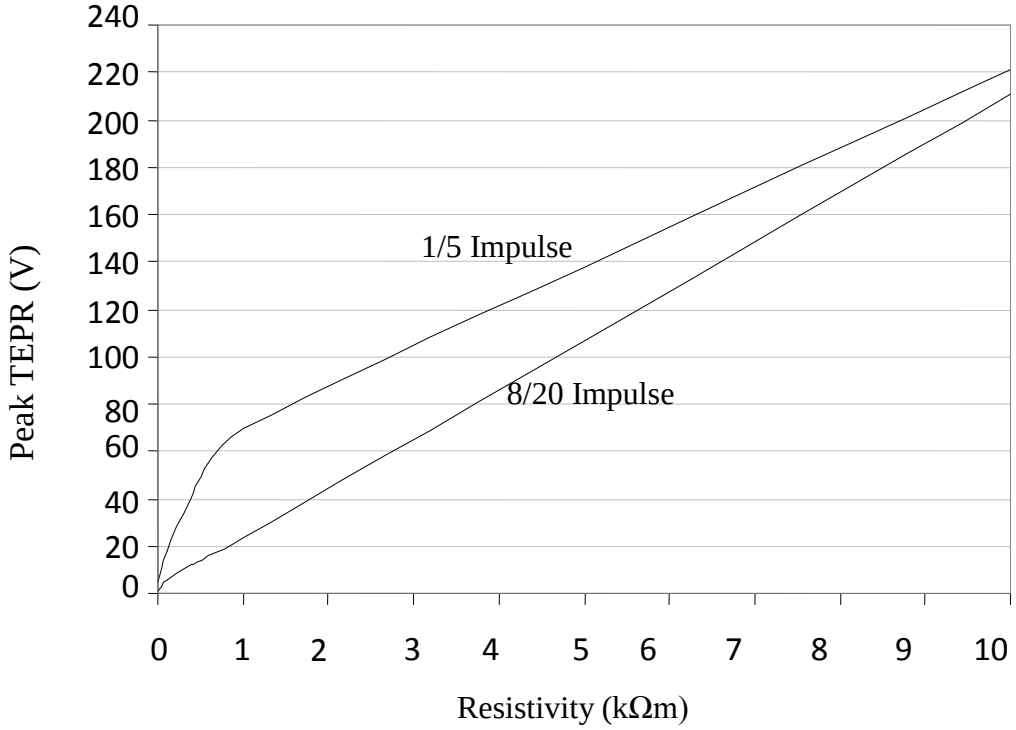

Figure 3.19: Effect of impulse wave shape on peak transient earth potential rise for different soil resistivity values for a 100m horizontal electrode.

3.7.3.4 Effect of Electrode Length

The frequency responses of the earth electrodes described in the previous sections have shown that the electrode length has a significant effect on the electrode performance. In this section, the transient responses of vertical earth electrodes of lengths 5m, 10m, 15m and 20m, and of horizontal earth electrodes of lengths 10m, 20m, 40m and 50m are presented. The copper electrodes are assumed to be buried at a depth of 1m and injected at one end with 1A, magnitude 8/20 impulse current. The results are shown in Figure 3.20 with TEPR as a function of time.

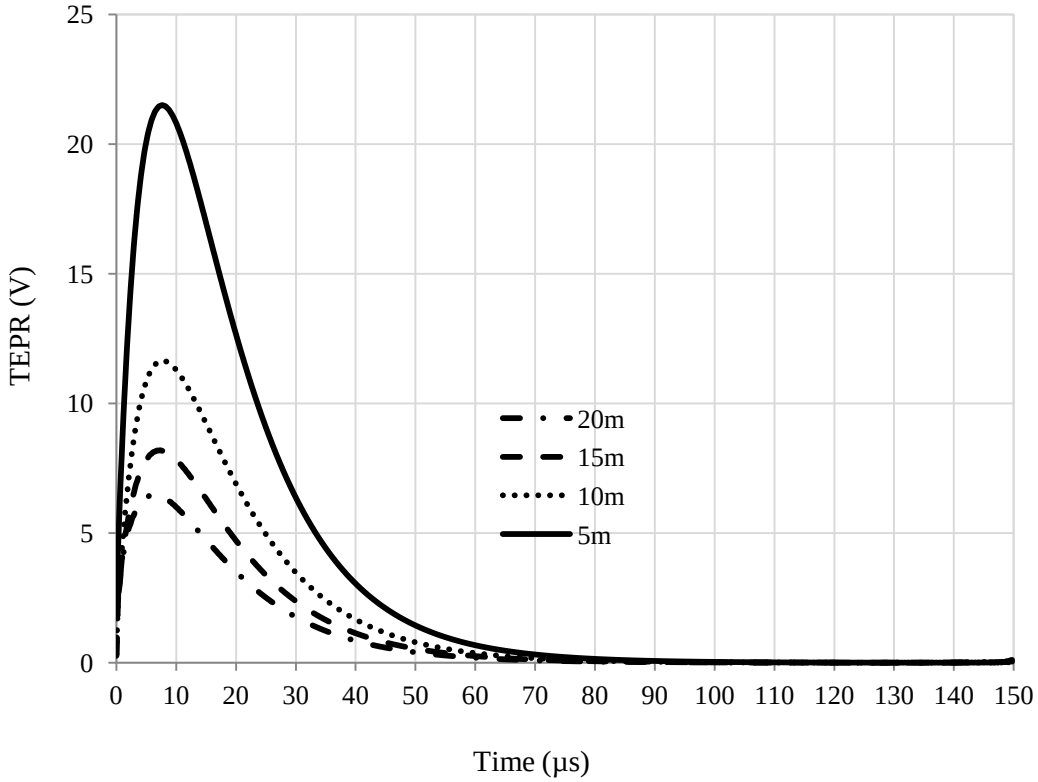

a) Vertical earth electrode

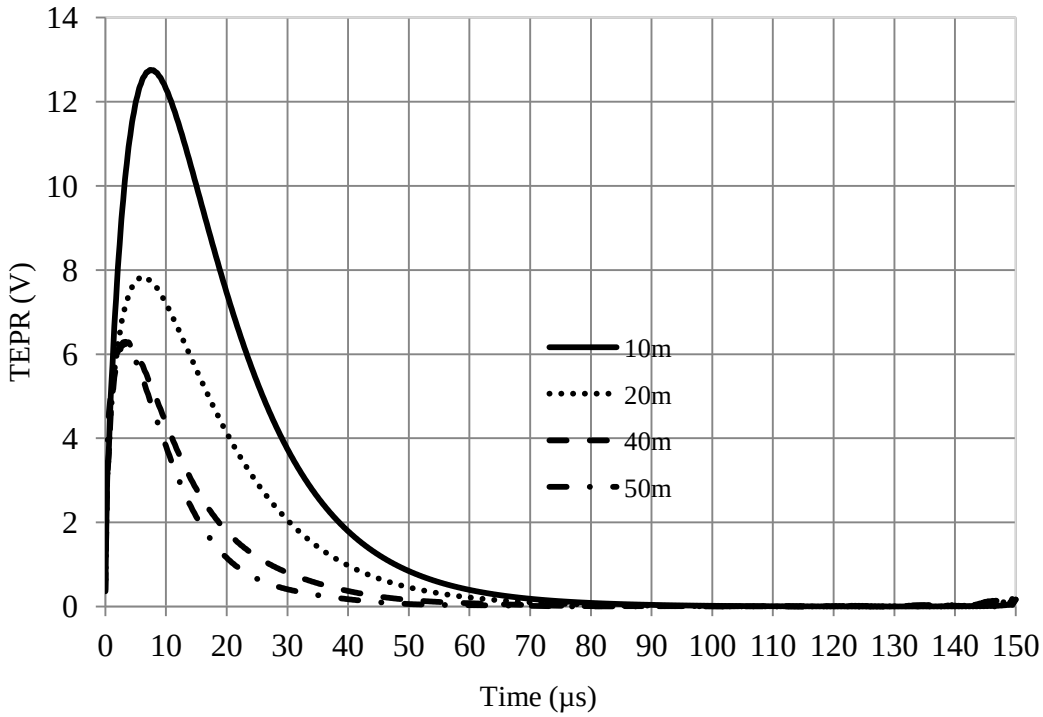

b) Horizontal earth electrode

c)

Figure 3.20 Effect of length on the performance of vertical and horizontal earth electrodes

Figure 3.20.a shows that the TEPR decreases as the electrode length increases. For example, the TEPR at the injection point is 21.5V, 11.6V, 8.2V and 6.4V for vertical electrode lengths 5m, 10m, 15m and 20m respectively. It is clear that the length has a significant effect on the TEPR with a reduction of about 70% when the vertical earth electrode length was increased from 5m to 20m. Similar trends are obtained for the horizontal electrode with lengths varied between 10m and 50m. As can be seen from Figures 3.20.b increasing the length of the horizontal electrode decreases the TEPR. However, in the case of the horizontal electrode, it is clear that the effective length of the electrode has been reached at 40m as no further decrease in TEPR is obtained beyond this length [3.18].

3.8 Earth Grid under Impulse Condition

The frequency response of the earth grid was studied earlier in this chapter for different soil resistivities, soil relative permittivities and earth grid areas. In this section, the transient response of the earth grid subjected to different impulses is investigated.

3.8.1 Effect of Resistivity

The performance of a square earth grid of (100mx100m) buried at a depth of 1m, was centrally injected with a 1A magnitude 8/20 impulse current. The time domain response of the grid is presented in Figure 3.21. As expected, and similar to the horizontal and vertical earth electrodes, the TEPR peak magnitude for the earth grid increases as the soil resistivity increases. Moreover, the TEPR rise time increases with increasing soil resistivity.

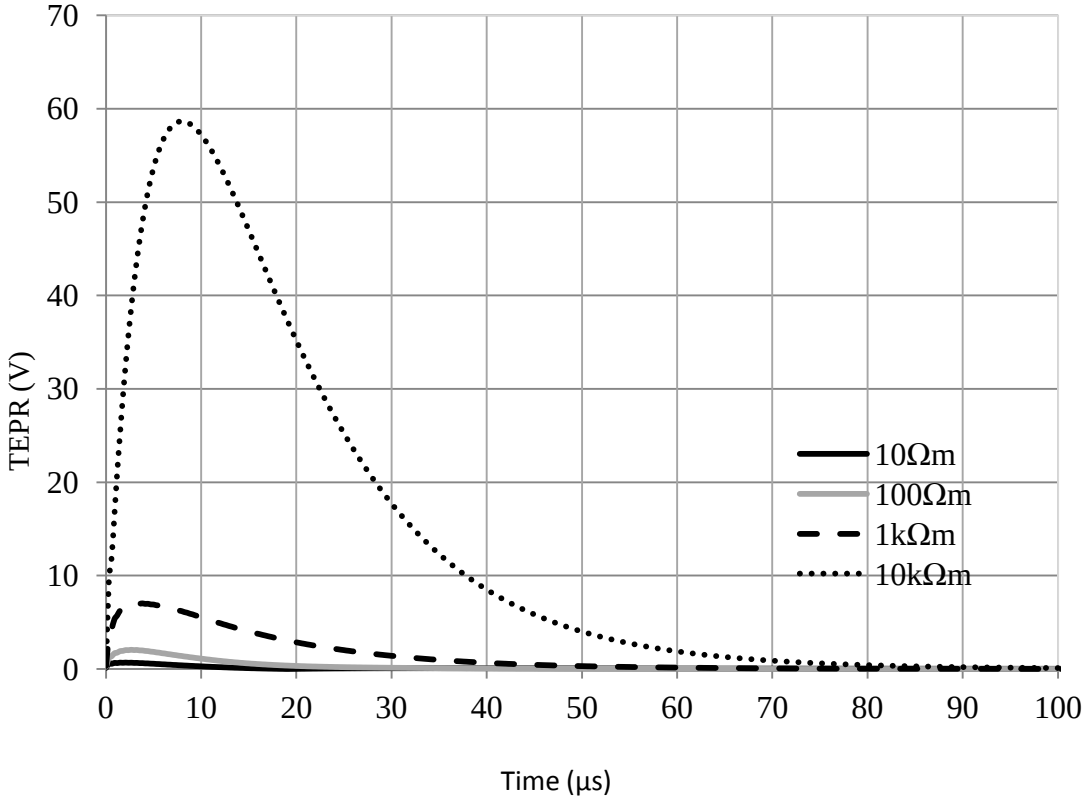

Figure 3.21: Effect of soil resistivity on TEPR of 100mx100m earth grid (injected impulse current 1A 8/20µs)

3.8.2 Effect of Permittivity

The TEPR was simulated for a soil resistivity ranging from 100Ωm to 10kΩm and soil relative permittivities of 1, 5, 30 and 80. Figure 3.22 shows that for a given current impulse, the resultant TEPR at the injection point is independent of soil relative permittivity for low soil resistivity (100Ωm). For the 8/20 impulse, a permittivity effect is observed only at high resistivity. However, for the 1/5 impulse, a significant permittivity effect on the TEPR is observed, the larger ε_r is the lower the TEPR will be. For example, with the faster impulse 1/5, it is clear that the change in permittivity has a considerable effect, and the peak TEPR drops from 62V at ε_r=1, to 23V at ε_r=80, suggesting that a capacitive effect is influential under these conditions.

The rise time of the TEPR is plotted as a function of soil resistivity, in Figure 3.23. Similar results were reported by [3.30-3.35]. The figure clearly shows that, in soil of low resistivity (100Ωm), the soil permittivity has little effect on the resultant TEPR rise time for either current impulse. However, for a soil of high resistivity (10kΩm), a change in permittivity from ε_r=1 to ε_r=80 has a considerable effect on TEPR rise time for both impulses: from 7.60μs at ε_r=1 to 15.30μs at ε_r=80 for the 8/20 impulse, from 0.2μs at ε_r=1 to 5.8μs at ε_r=80 for the 1/5 impulse.

These results indicate that for both impulses inductive effects dominate and the TEPR voltage rise time is shorter than that of the impulse current for soil with a resistivity below 100Ωm. Figure 3.23 also shows that when the soil resistivity was 10kΩm and the relative permittivity was greater than 30, the TEPR rise time for both impulses was longer than that of the injected current impulse due to capacitive effects.

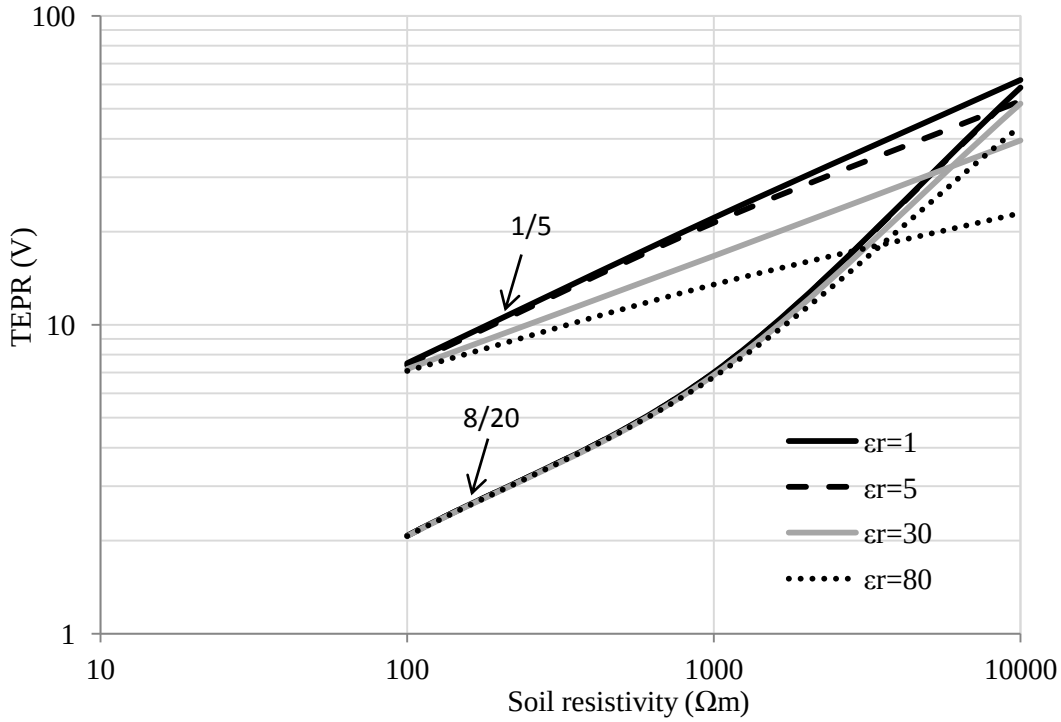

Figure 3.22: TEPR Peak values for 100mx100m earth grid injected with current impulses 1A 8/20μs and 1A 1/5μs for soil of different resistivities with relative permittivity 1, 5, 30 and 80

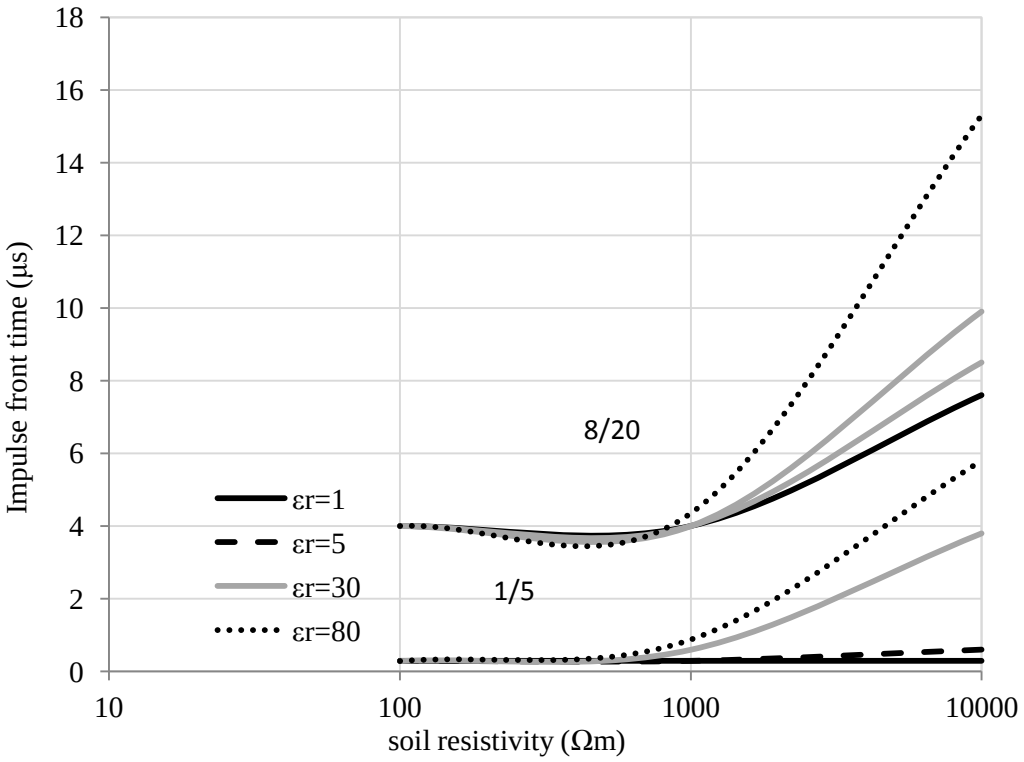

Figure 3.23: TEPR rise time vs. soil resistivity injected with current impulses 1A 8/20 and 1A 1/5 for relative permittivities 1, 5, 30 and 80,

3.8.3 Effect of Earth Grid Size

The frequency response of different sizes of earth grid was presented in section 3.6. In this section, the transient response calculated for square earth grids of sizes from 10mx10m to 100mx100m. The simulations were carried out by injecting a standard 1A, 8/20 impulse into the centre of the earth grid.

The results are summarised in Figure 3.24, showing the peak TEPR as a function of the grid side length for resistivities 10Ωm, 100Ωm, 1kΩm to 10kΩm. As can be seen, at low soil resistivity, there is little change in observed peak TEPR with an increase in size of grid; only an 8% decrease in moving from a 10mx10m to a 100mx100m earth grid. However, at the higher resistivity investigated (10kΩm), the results demonstrate that the area of the earth grid area has a pronounced effect on the peak value of the TEPR. Increasing the earth grid size from 10mx10m to

100mx100m results in a reduction in peak TEPR of about 85%, from over 400V to less than 60V.

The overall observation is that the earth grid does have an effective area beyond which further increases in grid size have little or no effect in reducing the impedance or the TEPR [3.10]. The higher the soil resistivity is the greater is the effective area, but the higher the TEPR will be. The transient effective area is different from that obtained for single frequencies as illustrated above. Similar results have been reported by [3.10-3.12]. Chapter 5 addresses effective electrode area and length in more detail.

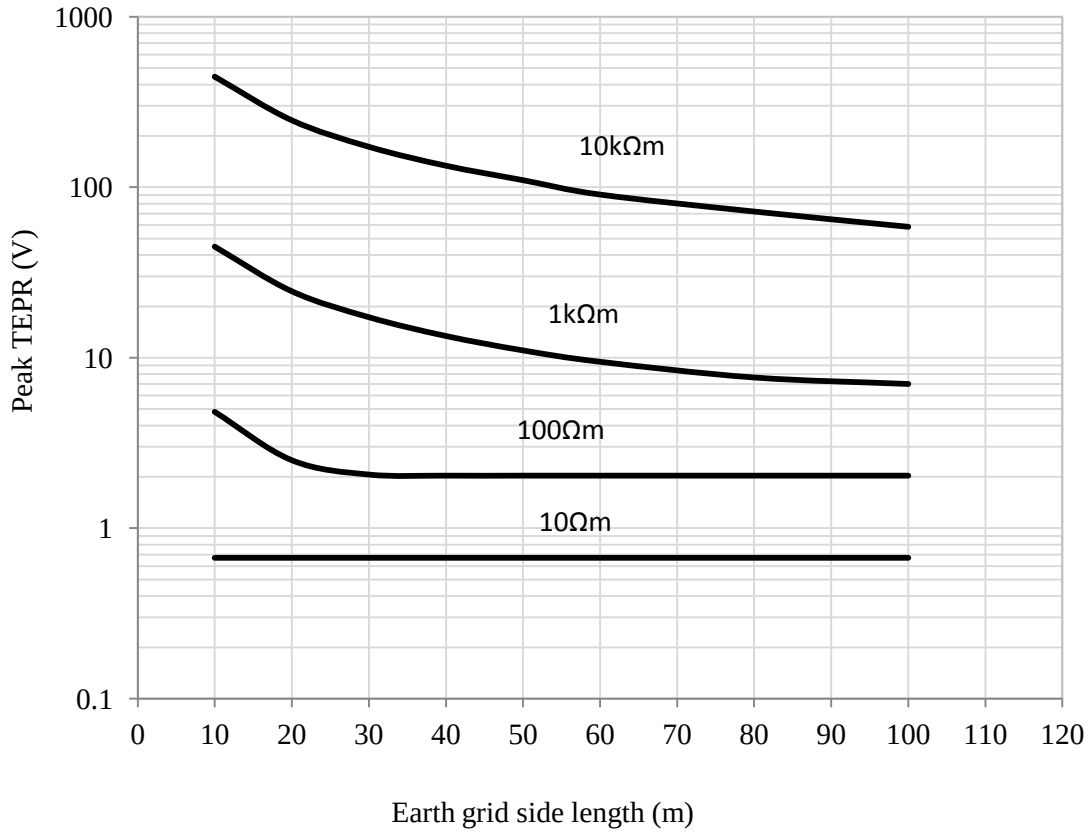

Figure 3.24: Effect of earth grid area on TEPR peak magnitude injected with 1A 8/20 μs impulse current

3.9 Conclusions

Different models of simple earth electrodes for various frequencies and different soil resistivities have been used to calculate the response of such electrodes under variable frequency and transient conditions. Parametric studies were carried out for vertical and horizontal electrodes and an earthing grid. The results confirm the limitations of the lumped parameter circuit model in predicting the performance of the earth electrode at high frequencies. For large earthing systems, computer simulations allow prediction of earth electrode performance for more complex electrode systems.

In general, the results indicate that inductive effects become significant for most earth electrodes above a particular frequency for a given soil resistivity, increasing significantly the magnitude of the earth impedance. For soils of high resistivity, the earth impedance of an earth electrode e.g. for the short rod, the impedance is lower at higher frequencies due to capacitive effects.

The electrode length or area was investigated in detail by varying the length of the horizontal earth electrode and the earth grid size. It is clear that the earth impedance magnitude decreases as the length or the grid size increases up to a limit beyond which further increase in length or area has no beneficial effect. This length or area at which no further reduction is achieved is known as the effective length or area.

The impulse response of different electrode configurations was studied. Two different standard wave shapes and a wide range of soil resistivities were considered. The results show that the transient earth impedance and peak TEPR of all electrode configurations increases with resistivity. The TEPR and the impedance decrease significantly with the increase of the relative permittivity in soils of high resistivity. The effective length /area was also demonstrated under impulse condition.

CHAPTER FOUR

SAFETY PERFORMANCE EVALUATION OF WIND TURBINE EARTHING SYSTEMS

4.1 Introduction

The increase in the number of wind farms and the physical size of individual wind turbine units has greatly increased the probability of lightning strikes of turbine structures. As a result, the provision of protection to human beings, livestock and equipment in the vicinity of such structures is becoming increasingly important. Wind farm earthing systems have different features and requirements than conventional earthing systems for electrical installations such as substations. Due to the nature of their particular physical layout, wind farm earthing systems comprise concentrated electrode systems at the individual turbine locations, and these are normally interconnected to form an earthing system that may extend over several kilometres. Moreover, due to the location of onshore wind turbine on high rocky terrain, soil resistivity can be relatively high, and this contributes to the development of very high transient potentials on the earthing system under lightning strike conditions. It is important that the earthing system is designed to dissipate high magnitude transient currents safely to ground. Previous studies [4.1-4.4] used models based on various geometric arrangements of the wind turbine earthing system. However, a shortfall of these models is that they neglect the tower structure and model the in-ground electrodes as a number of simple horizontal electrodes arranged in square or ring shapes. These models may accurately predict the performance of the wind turbine earthing system at low frequency injection, but for high frequency or transient conditions, the tower structure should be included to take into account inductive effects and travelling wave phenomena.

In the previous chapters, the frequency response and the transient performance of generic earthing systems including the substation earth grid were described. In this chapter the frequency response and the transient performance, including earth potential rise and related safety voltages (touch and step potentials) of wind turbine earthing systems under transient conditions, are investigated. The special case of offshore wind turbine earthing system performance is also presented.

4.2 Onshore Wind Turbine Earthing System

A typical earthing system of an individual wind turbine consists of a ring electrode installed around the foundation and bonded to the metal tower through the concrete foundations, as can be seen in Figure 4.1. Each individual turbine earthing system is required to have an earth resistance of 10Ω or less, as specified in IEC 61024 – 1998 and TR61400-24, 2002 [4.5, 4.6]. Vertical rods and additional horizontal electrodes are often used in conjunction with the ring electrode to achieve this value of earth resistance. Some alternative earthing arrangements are shown in Figure 4.2 [4.1-4.4].

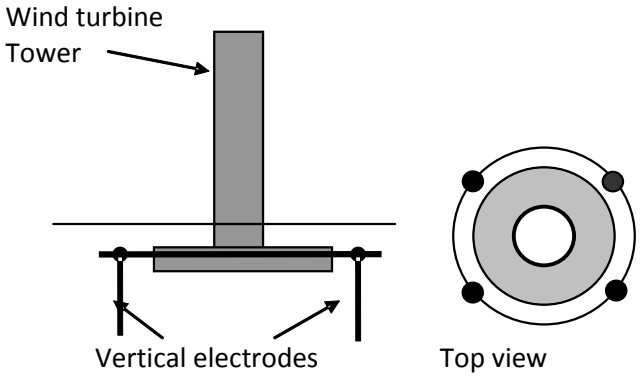

Figure 4.1: Typical wind turbine earthing layout [4.6]

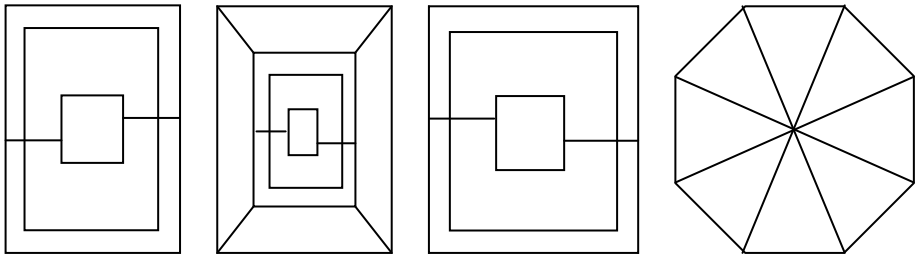

a) **b)** **c)** **d)**

Figure 4.2: Alternative earthing arrangements [4.1-4.4] of wind turbine earthing systems

4.3 Modelling Methodology

Based on an actual 1.5MW wind turbine unit, the in-ground part of an onshore wind turbine earthing system was modelled, and the frequency responses computed using software based on the electromagnetic field theory [4.7]. Examples of models used in the simulations are shown in Figure 4.3. Figure 4.3.a shows an arrangement consisting of an octagonal-shaped turbine earthing system bonded to the reinforcing grid metalwork of the turbine foundation at a depth of 2.65m. Figure 4.3.b shows this basic earthing system with a ring electrode placed around the earth electrode. For both models shown in Figure 4.3, the current injection is achieved through a short single vertical lead connected to the centre of the grid.

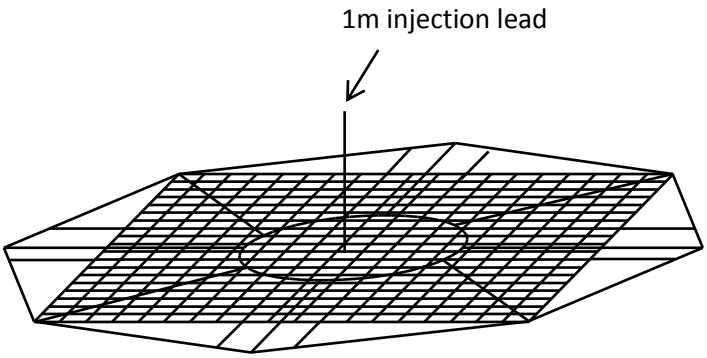

a) Basic wind turbine earthing system

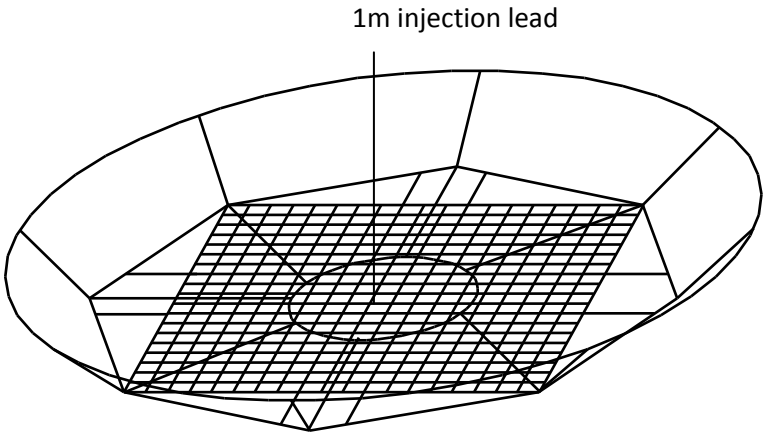

b) Basic wind turbine earthing system with ring electrode

Figure 4.3: Basic on shore wind turbine earthing models used for the simulation

4.4 Frequency Response

Normally, a ring electrode is placed around the wind turbine foundation and bonded to the reinforced steel and then to the wind turbine tower. In the published literature, the available models of wind turbines represent only in-ground part and do not include the above ground part, i.e. the tower structure [4.1-4.4]. In this section, the simulation carried out using CDEGS software is of the earth electrode and the ring electrode ignoring the steel tower. The effect of the steel tower on the TEPR and safety voltages is discussed later in chapter 6. For each simulation model, a current of 1A was injected over the frequency range DC to 3MHz and the EPR computed at the injection point, assuming a soil resistivity of 400Ωm. From the computed values of voltage and current, the impedance magnitudes seen from the injection point were determined, and the results are shown in Figure 4.4. As can be seen in the figure, and similar the frequency response of the generic electrodes, each curve shows a low frequency range over which the earth impedance is almost constant and the earth electrode is predominantly resistive. The upturn frequency occurs above 100kHz at

which the impedance magnitude (and EPR) increases suddenly indicating that the inductive characteristics of the electrodes have become important. The same general behaviour is observed for the basic earthing system and also when the ring electrode is added, despite that in the latter case, there is about a 14% reduction in earth impedance at low frequencies compared to the basic wind turbine earthing system. Similar results are reported by [4.8-4.9].

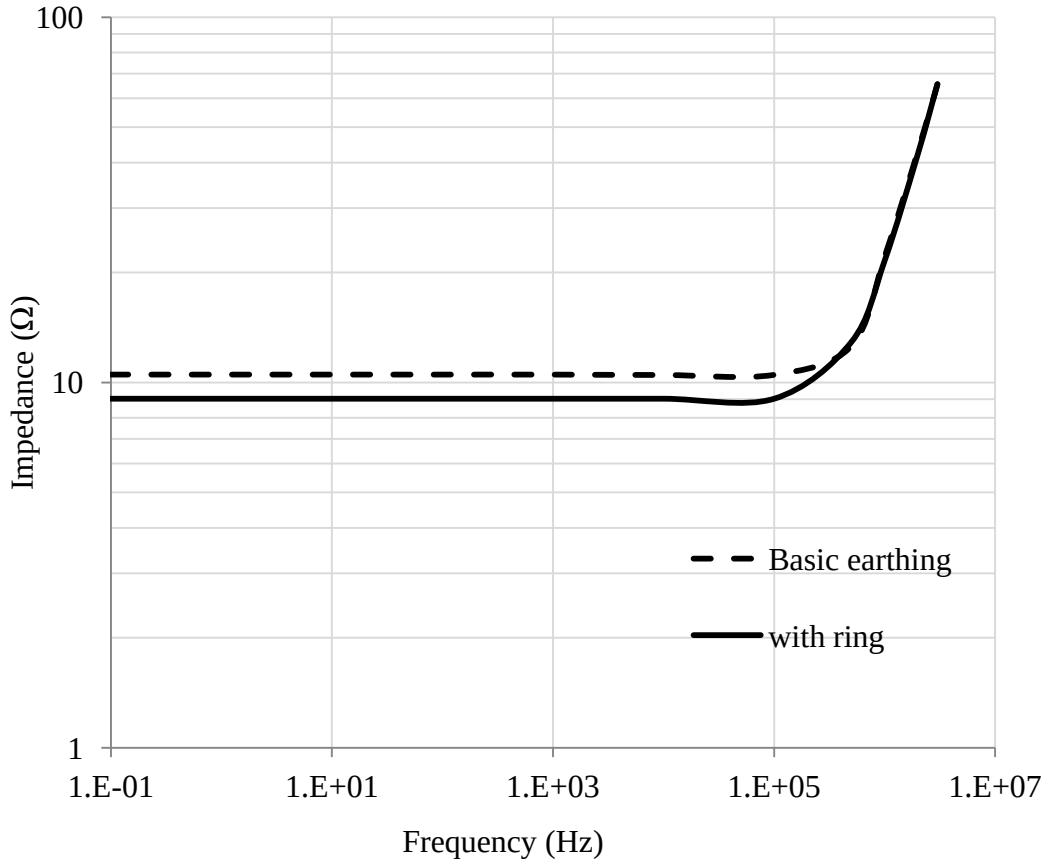

Figure 4.4: Frequency response of on shore turbine earthing system (soil resistivity 400Ωm)

4.4.1 Effect of Soil Resistivity

The frequency response of the basic wind turbine earthing system was studied for different soil resistivities. The impedance magnitude and the impedance phase angle were calculated for different soils with resistivity 100Ωm, 1kΩm and 10kΩm for a relative permittivity of 1. Figure 4.5 shows the computed wind turbine earth impedance over a frequency range from DC to 3MHz for the three values of soil resistivity. The trends found are similar to those for the earth rod models simulated in chapter 3. It is clear that the curves for resistivities up to 1kΩm have a low frequency range in which the impedance is almost constant. At higher frequencies, the impedance magnitude increases sharply above a particular frequency related to the magnitude of the soil resistivity. For high soil resistivity (10kΩm), the impedance of the wind turbine earth electrode decreases starting from a frequency of about 500kHz. Due to the locations of onshore wind turbines, high soil resistivity is frequently encountered.

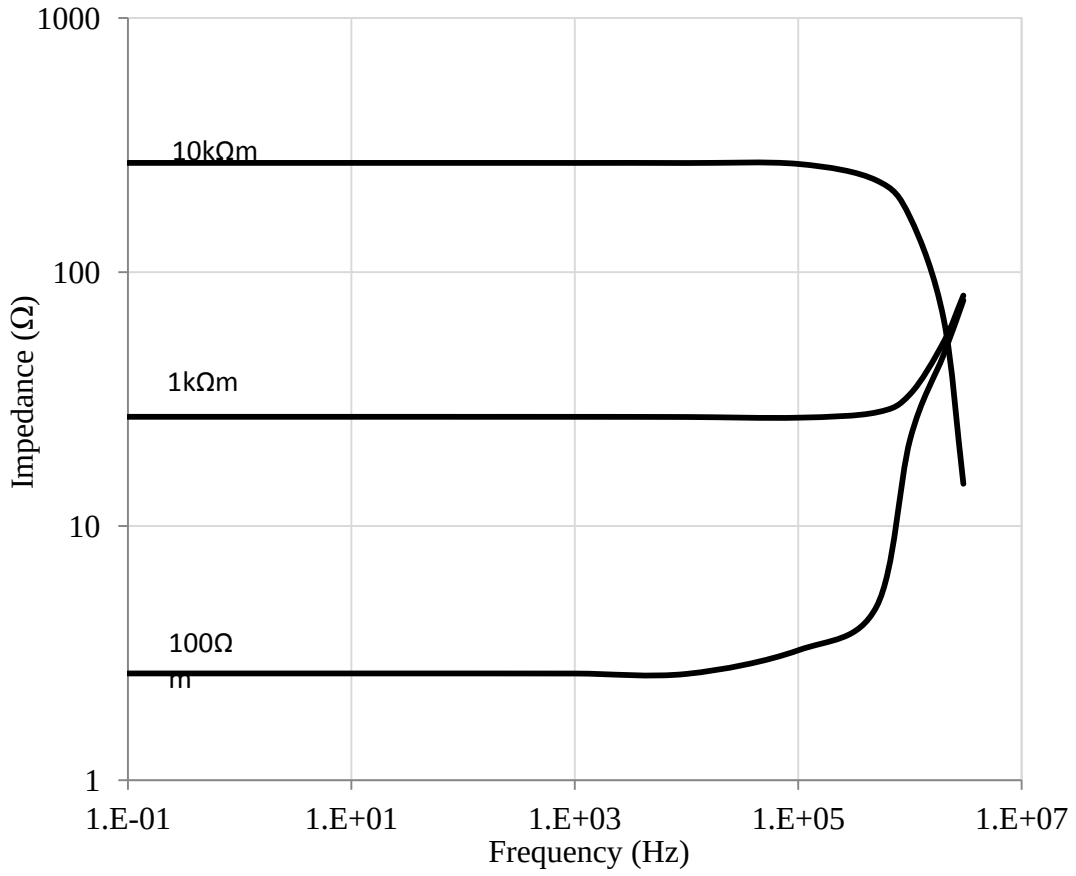

Figure 4.5: Impedance magnitude vs. frequency for soils of three resistivity values

4.4.2 Effect of Soil Relative Permittivity

The basic wind turbine earthing system shown in Figure 4.3.a was simulated for different soil permittivity. The computed trends were very similar to those obtained for the rod electrode examined in section 3.7.

4.5 Extended Earth Electrode

Wind turbines are connected to form a wind farm, and they are electrically interconnected. Also, in practice, the various earthing systems are connected to each

other to form an extended earth electrode covering a large area. Connecting wind turbines with horizontal electrodes or by insulating cable sheaths has the benefit of reducing the overall earth impedance. In this section, the effect of the interconnection of the wind turbine earthing systems on the overall earth impedance is investigated. To calculate the resistance/impedance of the interconnected wind farm, a model of a wind farm earthing system was constructed, based on an approximation of the physical wind turbine earthing electrode geometry, as described chapter 2. A single horizontal electrode of 250m length buried at a depth of 1m was assumed as the conductor interconnecting the wind turbines. Up to 15 interconnected wind turbines were examined and carried out with soil resistivity values of 10Ωm, 100Ωm and 400Ωm. A 1A current was injected into one of the turbine bases as shown in Figure 4.6, and the EPR at the injection point was computed. AC simulations were carried out ranging from DC to 3MHz.

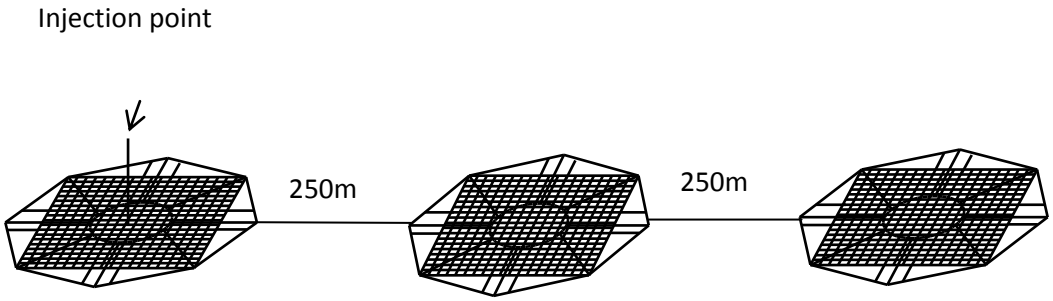

Figure 4.6: Extended earth electrode model

4.5.1 DC Resistance

The calculated values of the DC resistance of the wind farm earth electrode as a function of the number of interconnected wind turbines are shown in Figure 4.7. As expected, the earth resistance magnitude falls as the number of the interconnected

wind turbines increases. An initial rapid decrease is followed by a more gradual decrease which depends on the resistivity of the soil. For each soil resistivity, the earth resistance approaches a constant value as the interconnected number of turbines increases. This is explained using the concept of effective length. As can be seen in the figure, for very low soil resistivity (10Ωm), the effective length is reached very quickly, with only three or four turbines connected. For higher soil resistivity, a larger number of wind turbine units are required to reach the resistance asymptotic value; for soil resistivity of 400Ωm, this value is not reached with more than 15 turbines.

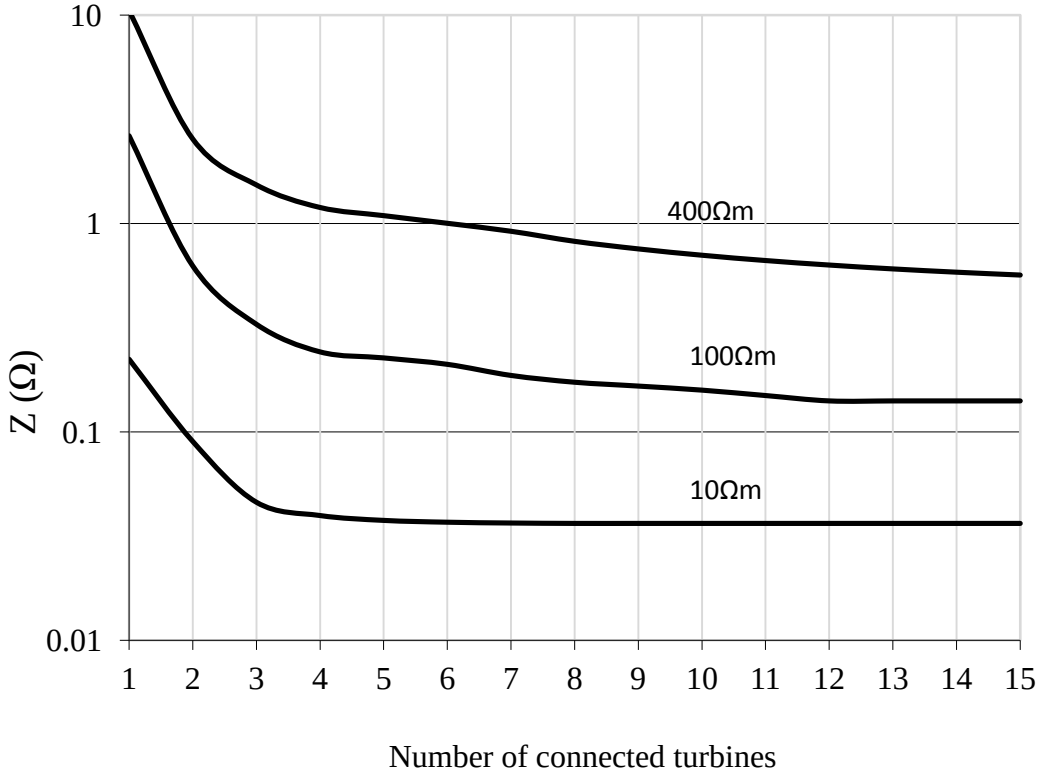

Figure 4.7: Connected wind turbines vs. resistance

4.5.2 50Hz Impedance

Similar computations were carried out for a frequency of 50Hz. The wind farm earth impedance as a function of the number of interconnected wind turbines is shown in Figure 4.8. As can be observed, a similar trend to the DC case was obtained. However, the 50Hz, AC earth impedance reaches a constant value for fewer interconnected wind turbines than for the DC, i.e. the effective length of the line is shorter AC because of the effect of the inductive component of the series impedance of the horizontal electrode. For the higher resistivity soils (100Ωm and 400Ωm), the effective length is less than 15 turbines.

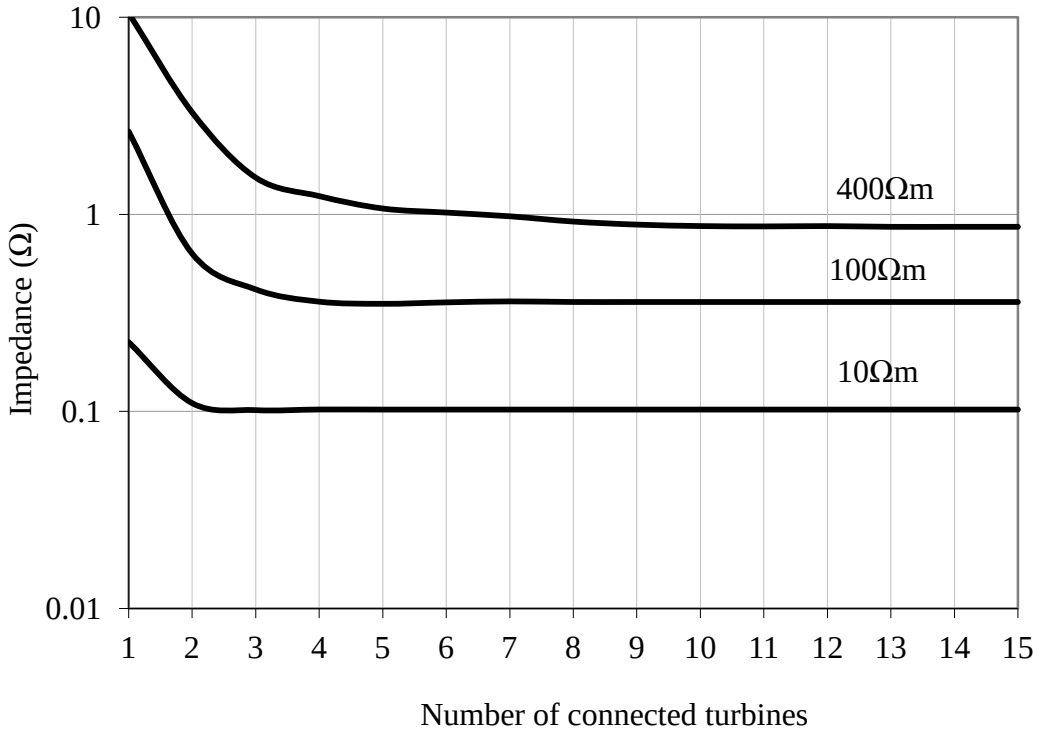

Figure 4.8: 50 Hz Impedance vs. number of connected wind turbines

4.5.3 Effect of Frequency

Computations were carried out for frequencies up to 3MHz and soil resistivity up to 400Ωm for ten inter-connected turbines. Assuming a 1A current injected at one of the turbine bases, the computed EPR at the point of injection was divided by the current injected to calculate the wind turbine earth impedance. The results are shown in Figures 4.9. From Figure 4.9, it can be seen that the wind farm earth impedance increases with frequency until it reaches a maximum at 1MHz due to a significant inductive component. The shape of the curve is, however, different from that of electrodes studied in Chapter 3 in that there is no flat region at low frequency. For frequencies higher than 1MHz, the impedance value decreases, and this is due to capacitive effects becoming more important.

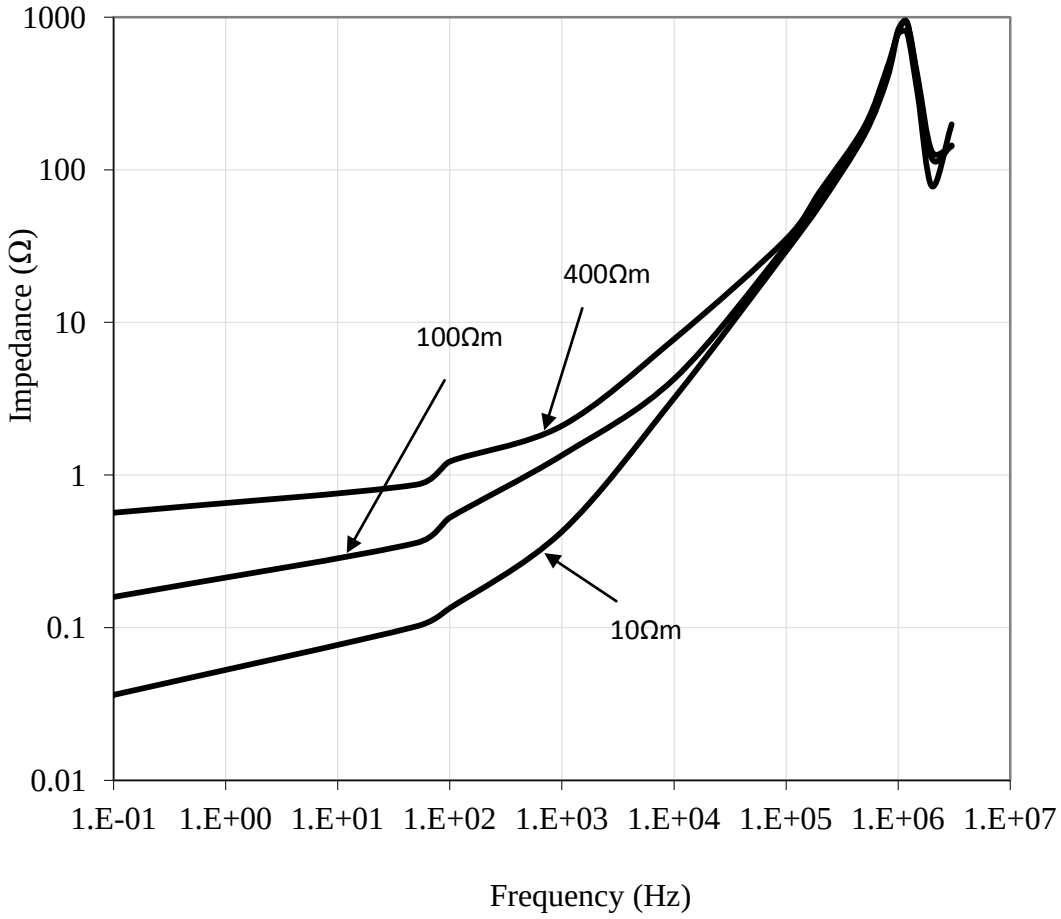

Figure 4.9: Effect of frequency on wind farm earth impedance

4.6 Transient Response of Onshore Wind Turbine Earthing System

In this section, the transient response of the wind turbine earthing system and the potential distribution around the wind turbine are considered. The effect of the wind turbine steel tower on the transient voltage and frequency performance is investigated. Simulations were carried out with two impulses; i) 10kA, 8/20 and, ii) 10kA, 1/5 injected at the top of the turbine model for soil resistivities of 10Ωm, 400Ωm and 10kΩm.

4.6.1 Modelling Methodology

Wind turbine earthing systems based on an actual 1.5MW unit were modelled, and the frequency response was computed using field theory based software [4.7]. The transient response of onshore wind turbine earthing systems to current impulses, as well as the distribution of the transient ground surface potential in the vicinity of the turbine, was determined. The models used in the simulations are shown in Figure 4.10. Figure 4.10.a shows an arrangement consisting of an octagonal-shaped turbine earthing system bonded to the reinforcing grid metalwork of the turbine foundation which extends to a depth of 2.65m into the ground. Current injection is through a short single vertical lead connected to the centre of the grid.

Figure 4.10.b shows the same basic earthing system, with the addition of a 3.65m tower section of which 1m of the tower section is above ground. For this model, the current is injected at one point on the perimeter at the top of the tower. Figure 4.10.c illustrates an enhanced model which includes a full tower structure represented by a series of interconnected vertical electrodes arranged in a cylindrical form.

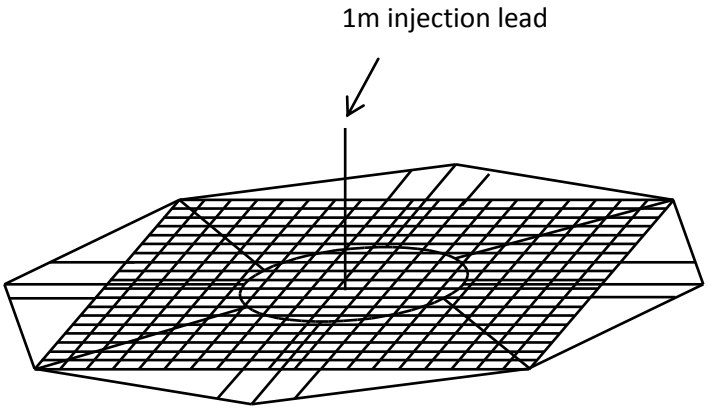

(a) Basic wind turbine earthing system

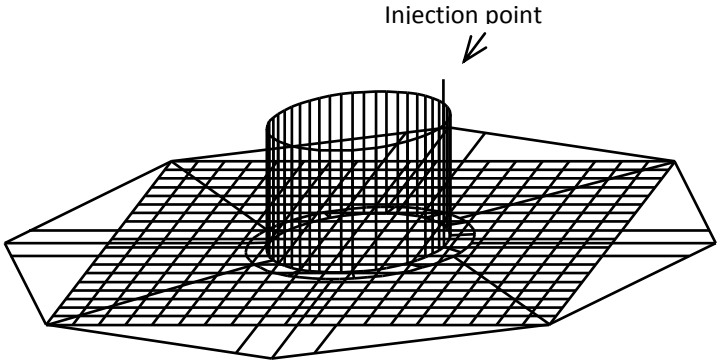

(b) Wind turbine earthing system with 3.65m long tower section, 1m above ground

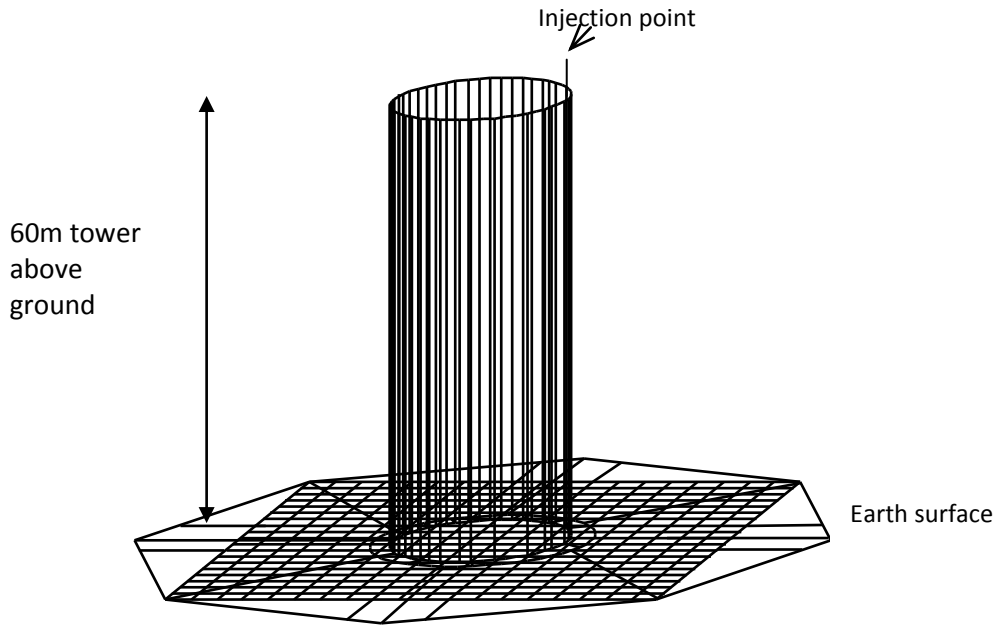

c) Wind turbine earthing system with full tower

Figure 4.10: Wind turbine earthing system models used in computer simulation

4.6.2 Transient Earth Potential

4.6.2.1 Effect of Tower Structure

To quantify the effect of the above-ground turbine structure, the transient responses of the wind turbine earthing models shown in Figures 4.10.a, b and c were determined using two current impulses, 10kA, 8/20μs and 10kA, 1/5μs. For these simulations, the transient earth potential rise TEPR was calculated at the point of

injection and at a point located at a distance 1m away from the tower on the ground surface, as seen in Figure 4.11.

Figures 4.12 and 4.13 show the calculated TEPR at the injection and ground observation points for a soil resistivity of 400Ωm. From Figure 4.12.a it is clear that including the tower as part of the earthing system affects significantly the TEPR, giving a very high magnitude at the injection point for the 8/20 impulse. The fast rise time and the high peak TEPR magnitude of the model c can be explained by the significant additional inductance of the above-ground structure. The voltage signal shows oscillations due to the reflection of TEPR from the bottom of the wind turbine. Considering the observation point on the surface of the ground, it was found that, including the tower affects the ground surface potential and that the TEPR has a high peak value.

The peak transient potentials at the injection point for the models subjected to a 10kA, 1/5 impulse are shown in Figure 4.13,a. In this case and accounting for the tower in the model, a significantly higher TEPR. Figure 4.13 (b) shows that, with fast rise time impulses, the earth surface potential at 1m from the base is almost three times higher for 4.11.b which includes the tower compared with the model of the earthing base shown in Figure 4.11.a. These results emphasise the significant effect when, accounting for the above-ground structure for the prediction of voltages developed at the turbine base.

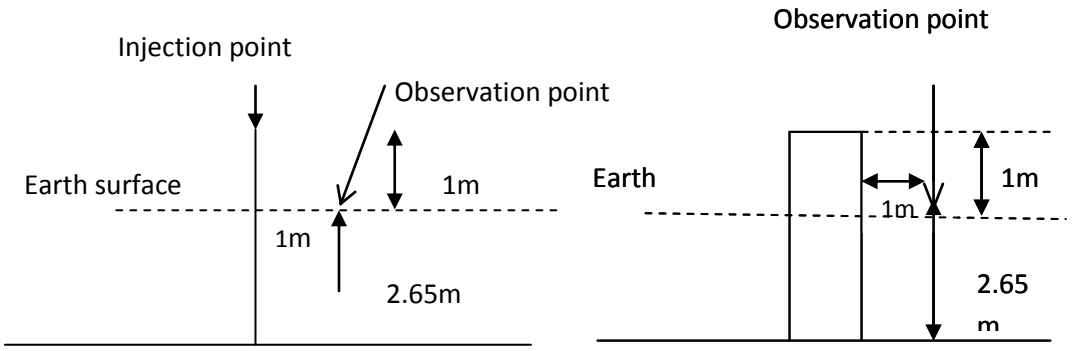

a) Plan elevation of model **b) Plan elevation of model**

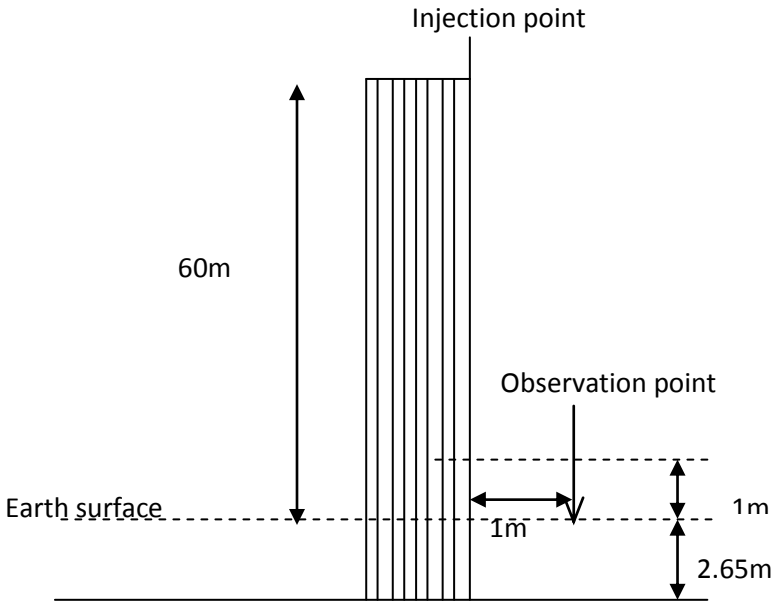

c) Plan elevation of full tower model

Figure 4.11: Illustration of potential injection and observation points on earth surface

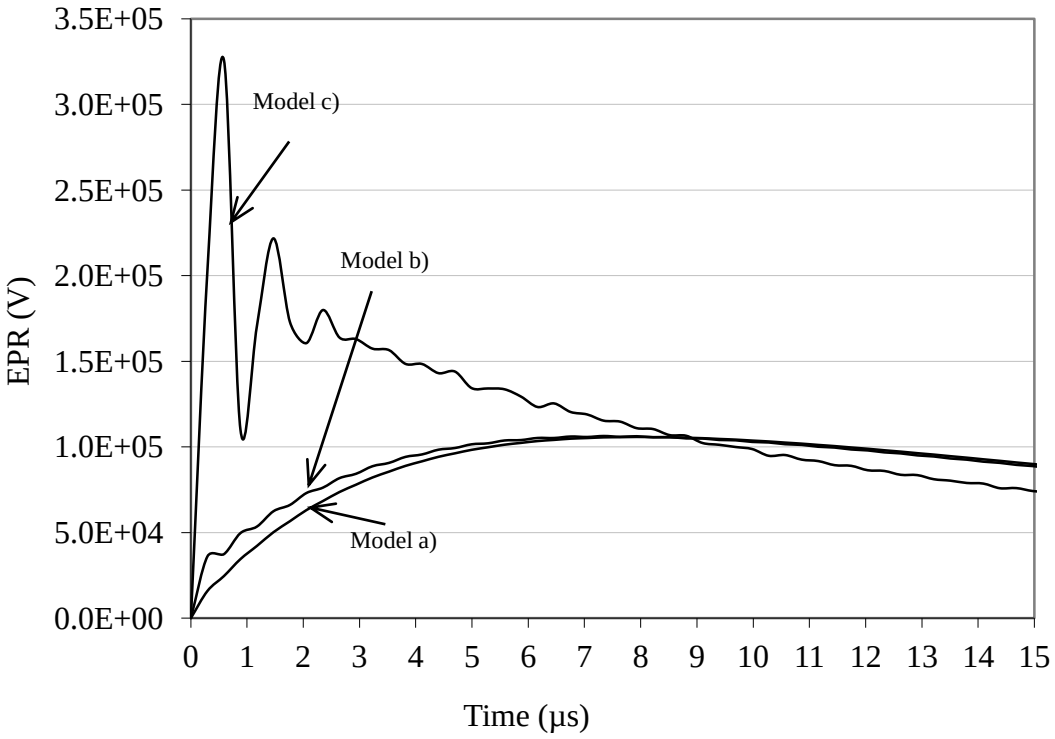

a) EPR at injection point

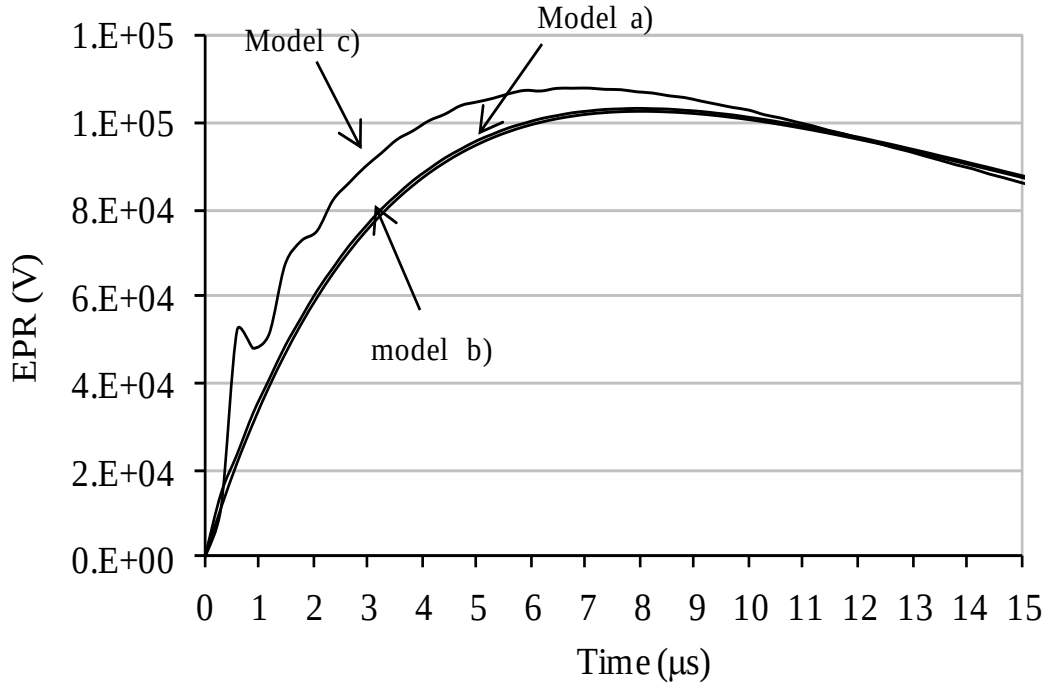

b) Earth surface potential 1m from the turbine base

Figure 4.12: Turbine transient earth potential: effect of including tower structure in model, current impulse 10kA 8/20, soil resistivity400Ωm

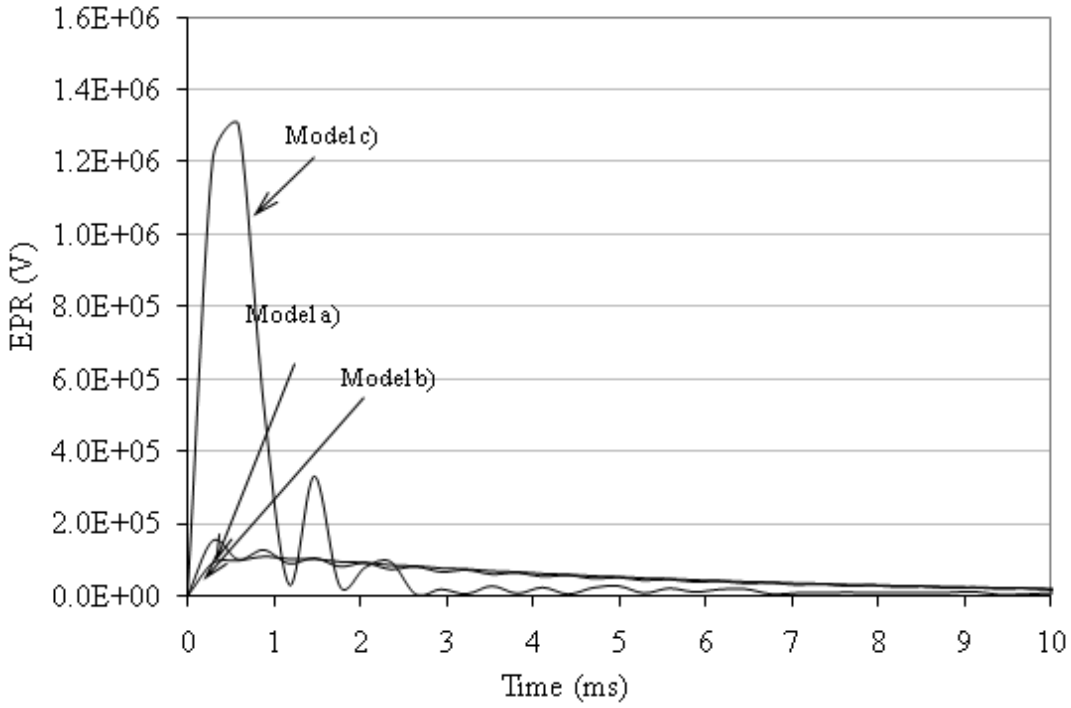

(a) EPR at injection point

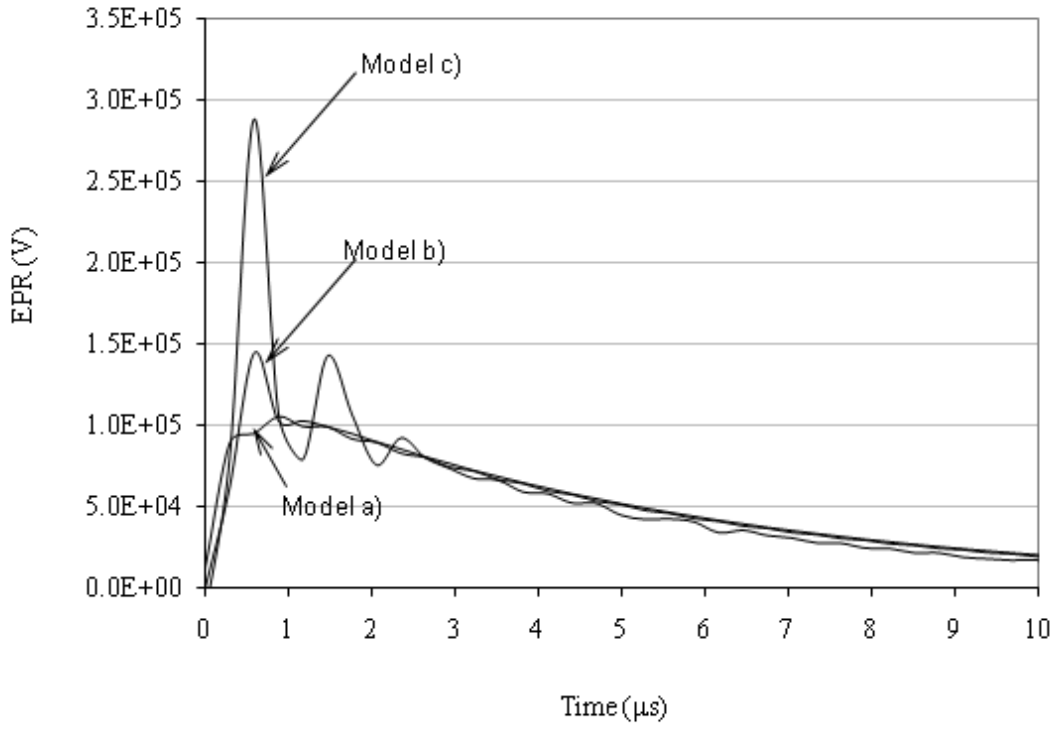

(b) Earth surface potential 1m from turbine base

Figure 4.13: Turbine transient earth potential: effect of including tower structure in model, current impulse 10kA 1/5, soil resistivity400Ωm

4.6.3 Voltage Distribution Along Profile From Turbine Base

The potentials at the ground surface along a 200m radial profile from the turbine base were computed for 10kA, 8/20 and 1/5 impulses. Figure 4.14 shows results for the 8/20 impulse; these illustrate that the potential falls with distance along the profile away from the turbine base**.** The rate of change of potential is highest nearest to the tower base and for high resistivity conditions.

A similar behaviour is seen for the 1/5 impulse where potentials are higher and decay more rapidly.

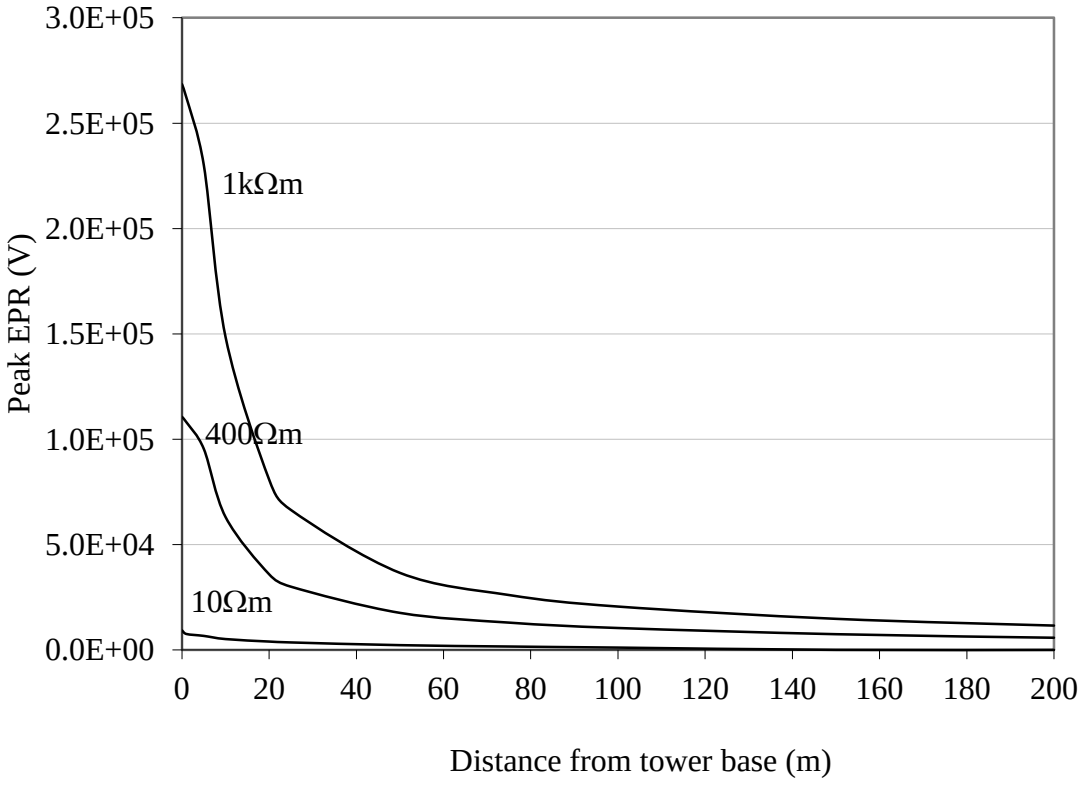

Figure 4.14: Transient earth along surface profile (8/20μs impulse)

4.6.4 Wind Turbine Earthing System-Local Enhancement Extended Earth electrode

The wind turbines are normally interconnected to form an earthing system often extending over several kilometres. This contributes to reduce the overall earth impedance at power frequency [4.3]. However, the response of the wind farm to rapid transient injections is quite different from power frequency injection as illustrated in the earlier sections of this chapter. In the case of impulse injection, TEPR value is very high due to the inductance of the system and the fast current rise time. Moreover, the contribution of the interconnection of the earthing systems of turbines in the wind farm imposes a limit on reduction of TEPR attainable due to the effective length phenomenon [4.3]. Therefore, a wind farm model was constructed using 3 turbines only and arranged in a line and separated 200m apart and interconnected with a 200m bare horizontal electrode**.** Due to the very long time required for simulation analysis, only one soil type was examined (ρ=400Ωm, ε_r=1). An impulse current (1A, 8/20) was injected into the first and middle wind turbines. The injected current and TEPR at the injection point are plotted in Figure 4.15, which shows that the TEPR rise time is shorter than that of the injected current. This is attributed to inductive effects. The TEPR impulse decays more rapidly than the injected impulse current. Similar observations were reported in [4.20, 4.21]. The results show that injecting the current impulse into the middle turbine generates less potential than for injection into an end turbine, about 20% reduction of the TEPR is obtained. Injection into an end interconnected turbine gives a peak TEPR about 35% less than for an unconnected single turbine.

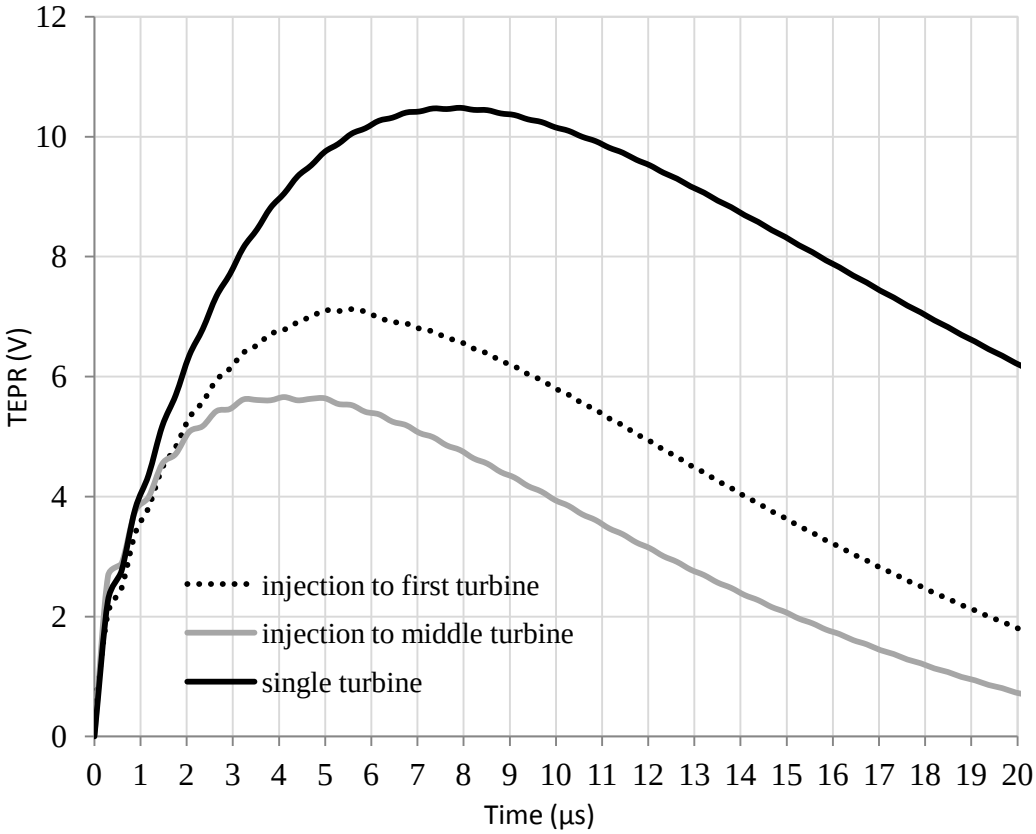

Figure 4.15: Wind farm transient performance for different injection locations

4.7 Offshore Wind Turbines

The first offshore wind turbine was installed in Sweden in 1991, only 250m from land at a water depth of 6m. The turbine was rated at 210kW [4.11]. Wind turbines are now becoming more widely used offshore because, unobstructed, the wind can blow strongly and larger turbines can be installed. Large offshore areas with shallow water are particularly suitable. In this section, the frequency response and transient performance of offshore wind turbine earthing systems are investigated.

4.7.1 Offshore Wind Turbine Foundation

Gravity foundations have been used predominantly in shallow water applications, typically, less than 10 meters depth [4.13]. At greater water depths, monopile structures generally become more economically attractive [4.13].

In this section, simulations using CDEGS [4.7] are carried out to investigate the response of the earthing system of offshore wind turbines subjected to power frequency and transient faults.

4.7.2 Offshore Wind Turbine Earthing System

The offshore wind turbine earthing system has significantly different features from onshore installations. The foundations of the offshore turbine are considered to be its earthing system, either monopile or metal reinforced concrete. According to IEC 61400-24 “Lightning Protection of Wind Turbines” [4.6], no further measures such as a ring electrode etc. are required in the case of offshore wind turbines as the resistivity of seawater is considerably lower than most soils. Only the interconnection of the offshore foundations by the interconnection of the power system cable sheaths is generally required. A metal monopile foundation is, by its nature, a large earth electrode and is modelled here as the primary earth electrode. The same situation applies for the concrete foundation; its reinforced steel may be considered as an earth electrode and the concrete assumed to have the same resistivity of the surrounding soil [4.3]. In this section, simulations are carried out to contribute to better understanding of offshore earthing system behaviour under power frequency and transient conditions.

4.7.3 Modelling Methodology

Offshore wind turbine earthing systems based on an actual 2.5MW unit were modelled, and the frequency responses computed using electromagnetic field theory based software [4.7]. The basic arrangement consists of a cylindrical-shaped turbine tower with a bottom of radius up to 4m depending on the offshore wind turbine size.

Figure 4.16 shows the two types of structure used to support offshore wind turbine: concrete foundation and the monopile. The concrete structure shown in Figure 4.16(a) is an earthing system located in two media, the metal turbine tower and the upper layer of the concrete tower will be in air, and the lower part the concrete tower and the base will be submerged in sea water. The earthing arrangement consists of a cylindrical-shaped turbine tower bonded to the reinforcing grid metalwork of the reinforced concrete. For the monopile structure, the steel tower does not end on the sea bed but continues into the sea bed for up to 25m.

The earthing systems were simulated under transient current injection with different rise times (100kA 8/20 and 100kA 1.2/50). The current injection is achieved through a short single vertical lead connected to the top of the tower. A two-layer soil model for the two types of foundations was used. To represent sea water, the resistivity was taken as 0.2Ωm with a relative permittivity of 80. The lower layer representing the sea bed, assumed to have a resistivity of 100Ωm and a relative permittivity of 80.

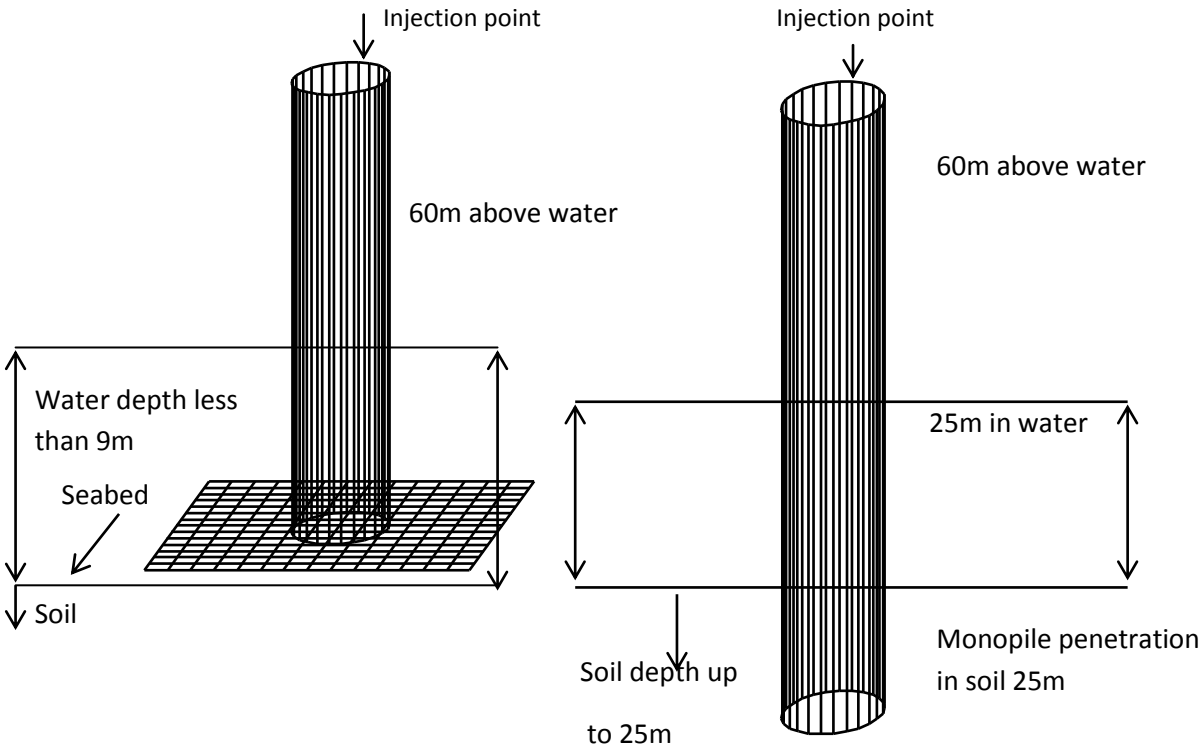

a) Reinforced concrete foundation model **b) Monopile foundation model**

Figure 4.16: Earthing system model for offshore wind turbine

4.7.4 DC and 50Hz Current Injection

1A, DC and 50Hz currents were injected into the top of the steel tower of the turbine with different arrangements to determine the resistance of a single turbine and also an interconnected wind farm. The impedance/resistance was obtained by dividing the EPR at the injection point by the injected current.

The calculated values of the resistance and impedance for the concrete foundation model, as a function of the number of turbines connected, are shown in Figure 4.17. The 50Hz impedance as seen from the point of injection is constant and independent of the number of interconnected turbines. DC resistance is lower for increasing number of interconnected turbines but, beyond two turbines, there is no additional benefit.

The AC effective length of the offshore earthing system is, therefore, limited to a length less than the inter-turbine spacing.

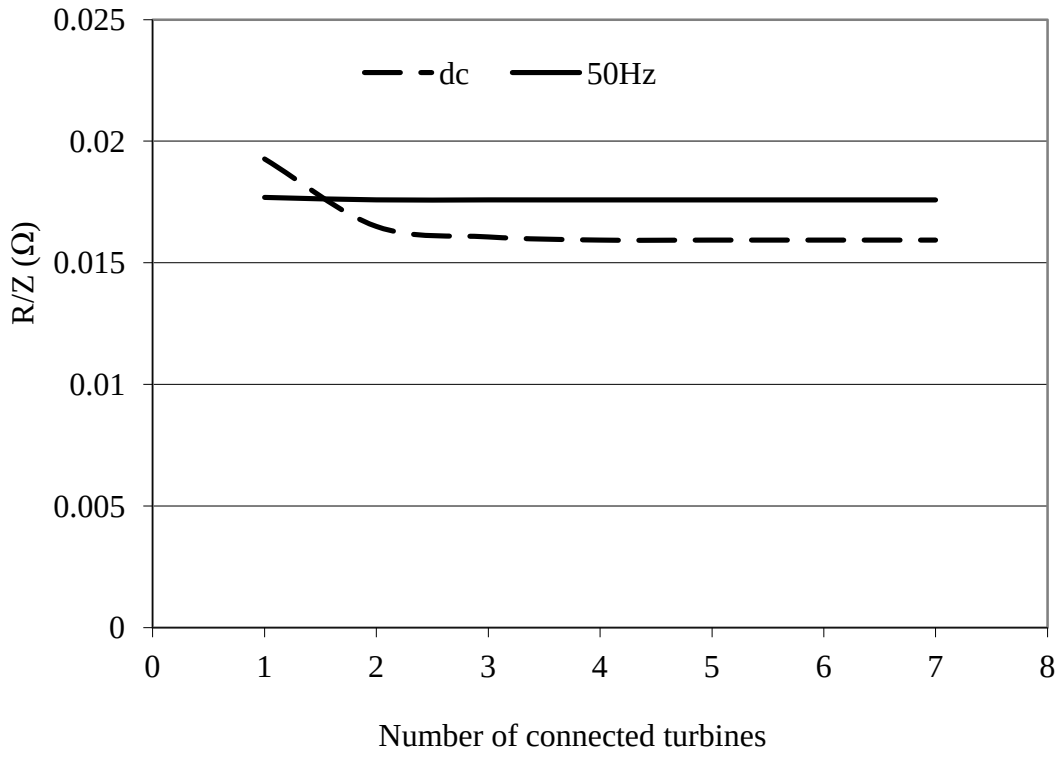

Figure 4.17: Resistance and impedance vs. number of turbines connected (earthing system concrete foundation model)

Figure 4.18 shows the results obtained for the monopile earthing system. As can be seen for DC, the resistance is significantly lower than that for the concrete earthing system. This can be explained by the fact that in deeper water the monopile is used which means greater area of contact with the low resistivity value medium compared with the case of the concrete foundation.

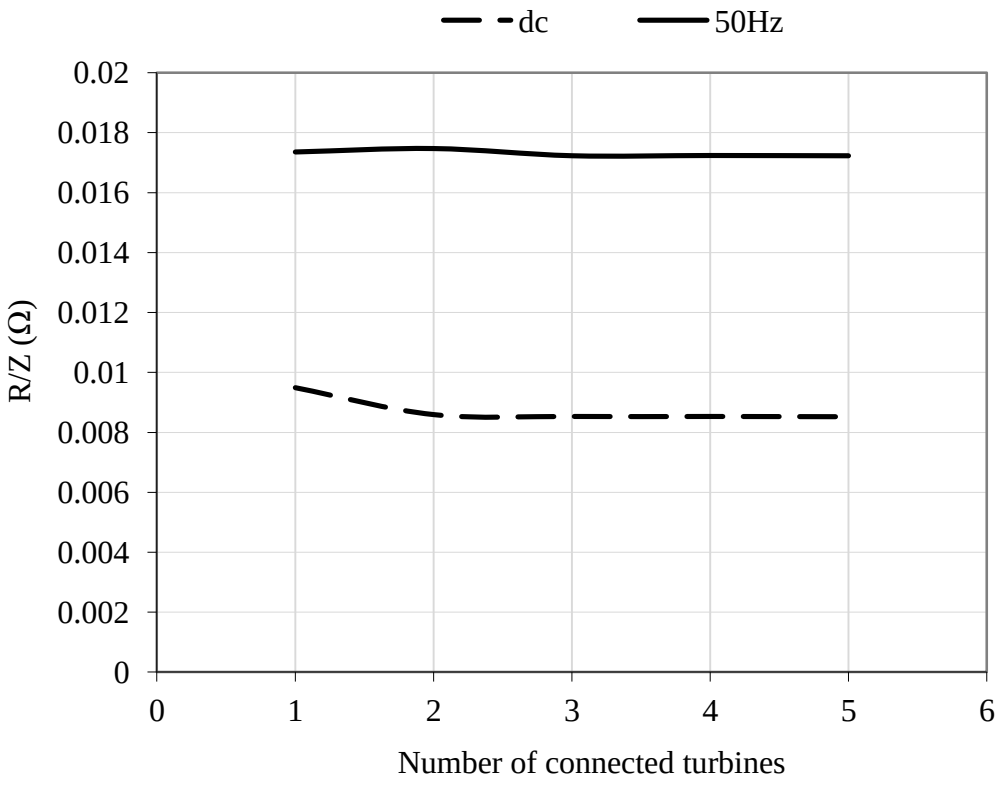

Figure 4.18: Resistance and impedance vs. number of turbines connected (earthing system monopile foundation model)

4.8 Transient Response of Offshore Wind Turbine

A 100kA current with 8/20 impulse was injected to the top of the offshore wind turbine steel tower and the TEPR were calculated along the steel tower. The results are shown in Figure 4.19. As can be seen in the figure that the TEPR falls as going along the injection point. Sharp decrease of the TEPR was observed particularly in

the parts near from the sea water. This decrease can be explained by the very low resistivity of the sea water which makes the earth resistance very low enables large amount of fault current to be dissipated.

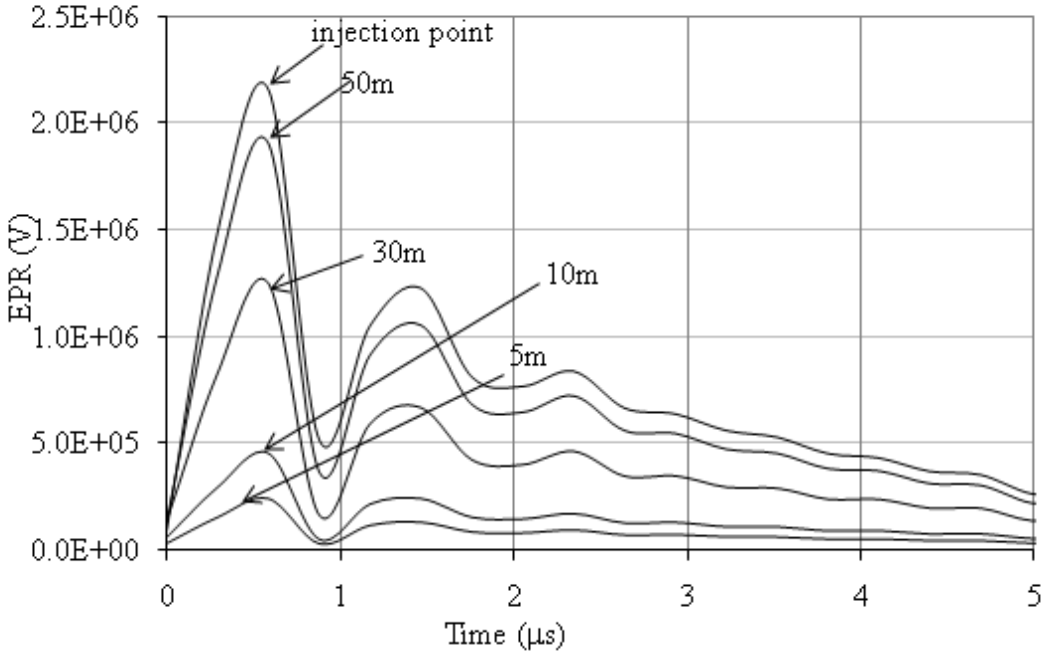

Figure 4.19: Calculated TEPR along offshore steel tower (100kA, 8/20 impulse current)

4.9 Conclusions

This chapter has investigated the effect of soil resistivity and soil relative permittivity on wind turbine earthing system performance under variable frequency and transient conditions. The results have shown that the inductive component of the wind turbine earthing system becomes significant above a particular frequency for a given soil resistivity, resulting in an increase in wind turbine earth impedance for both onshore and offshore wind turbines. Under a high resistivity, e.g. 10kΩm, the earth impedance magnitude falls under high frequencies range which suggests a

capacitive effect at these frequencies, similar to that seen with individual earth rods. It was found that interconnection of adjacent on-shore wind turbines has benefit in reduction of EPR and TEPR.

The lowest potential magnitudes were found in the middle turbine, and the effective length is limited to about three sections of wind turbines. In the case of offshore wind turbine earthing systems, the benefits of interconnection are less significant due to the very low water resistivity condition limiting the effective length to less than the interconnection length.

It was established that, for high frequency and transient currents, the magnitude of a wind turbine earth impedance seen from the point of injection is significantly higher when the above-ground turbine structure is taken into account. Also the calculated transient earth potential rise at the tower base ground surface is higher when the model includes the above-ground structure.

In this chapter, it was demonstrated that as the permittivity increases, the potential decreases. This also, depends on soil resistivity values. This reduction is attributed to the increase of the capacitive effect as the permittivity increases.

CHAPTER FIVE

EFFECT OF EARTH ELECTRODE LENGTH/AREA ON THE PERFORMANCE OF THE EARTHING SYSTEM: FIELD MEASUREMENTS AND SIMULATIONS

5.1 Introduction

Assessment of an earthing system requires the earth impedance to be known. So the best way to assess the performance of the earthing system is by direct measurement. Computer simulations and analytical equations can provide estimates of earthing systems performances under both power frequency and transient conditions, and require knowledge of soil resistivity values and detailed description of conductor geometry.

Validation of such computations and assessment of model limitations can be highlighted. In this chapter, a programme of field tests on generic type earthing systems installed at the University test site are reported, and the results obtained are compared with those obtained by computations.

Field tests were conducted on a purposely installed 88m long horizontal earth electrode under different energisations (DC, variable AC frequencies and transients of different shapes). Prior to the installation of the 88m horizontal electrode, soil resistivity measurements were made along the route of the cable at two different times of year in order to characterise the local soil conditions.

5.2 Test Site

A plan view of the University earthing test facility at Llanrumney fields is shown in Figure 5.1. On the figure, the route of the sectionalised 88m length horizontal earth electrode is shown.

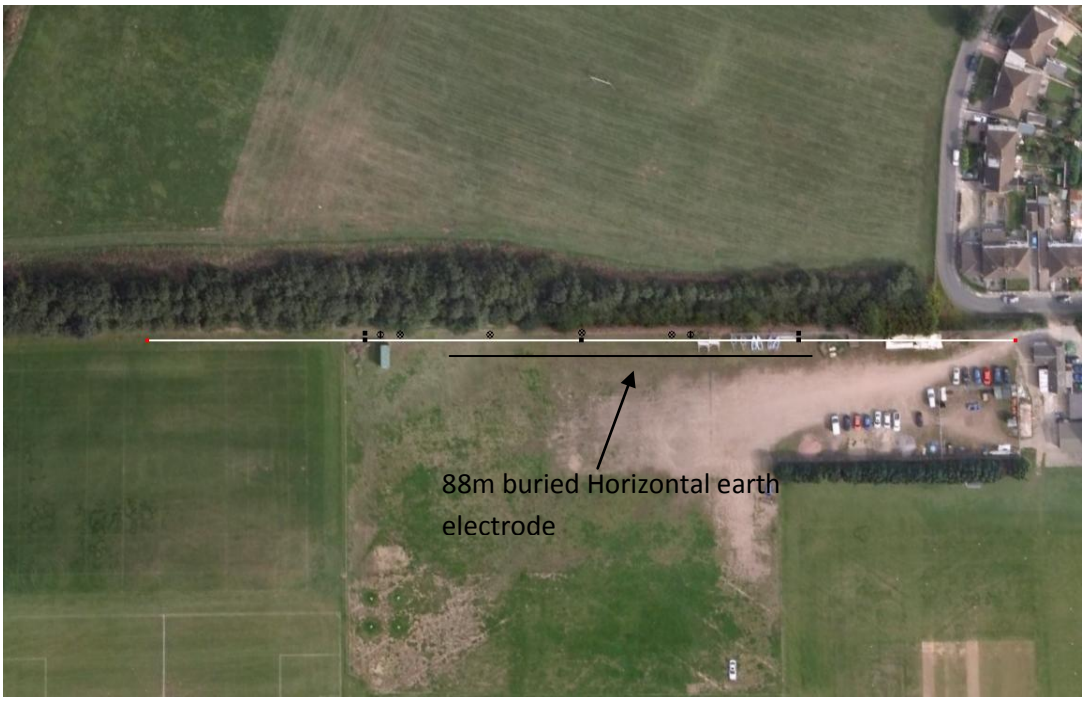

Figure 5.1 University earthing test facility - Llanrumney fields

5.3 Soil Resistivity Measurements

Soil resistivity measurements were carried on 23/01/2009 and 01/04/2009 respectively along the proposed line of installation of the horizontal electrode. ABEM Terrameter SAS 1000 [5.1] and associated LUND imaging system earth tester were used. A two-dimensional resistivity inversion software [5.2] was used to interpret the measured data. Application of the test equipment and post test analysis enables a 2-D picture of the subsurface soil resistivity to be obtained.

The ABEM tester is capable of injecting a DC current of up to 1A between any two current electrodes, and it has an open circuit output voltage of 400V.

The ABEM tester was used in conjunction with the Lund electric imaging system for automatic multi-electrode resistivity profiling [5.3]. The Lund system consists of an electronic switching unit (the electrode selector), and multiple electrodes. The system has a built-in microprocessor which enables automatic measurement, processing and data storage. For the sets of measurements carried out at Llanrumney, minimum and maximum electrode spacings were chosen as 3m and 72m respectively. A total of 61 electrodes were used along a line of 240m. For each survey set, 276 voltage and current readings at various positions and spacing were taken using Wenner configuration. Wenner soil resistivity measurement method involve a current *I* is circulated through the earth between two outer electrodes (C_1, C_2) and the voltage difference (V) is measured between two inner electrodes (P_1 and $P_{2)}$ then the apparent resistivity can be calculated by

$$\rho_a = 2\pi aR \qquad (5.1)$$

Where *a* is the electrode separation and assuming that $a>>r$, where *r* is the electrode radius. This is known as the Wenner configuration as shown in Figure 5.2. The depth investigated is related to the spacing. Therefore, deeper soil information can be obtained with larger inter electrodes spacing [5.4] for each individual reading. The ratio of voltage and current yields an apparent resistance and then the apparent resistivity can be calculated for each spacing. The layout of the cables and the measuring system is shown in Figure 5.3.

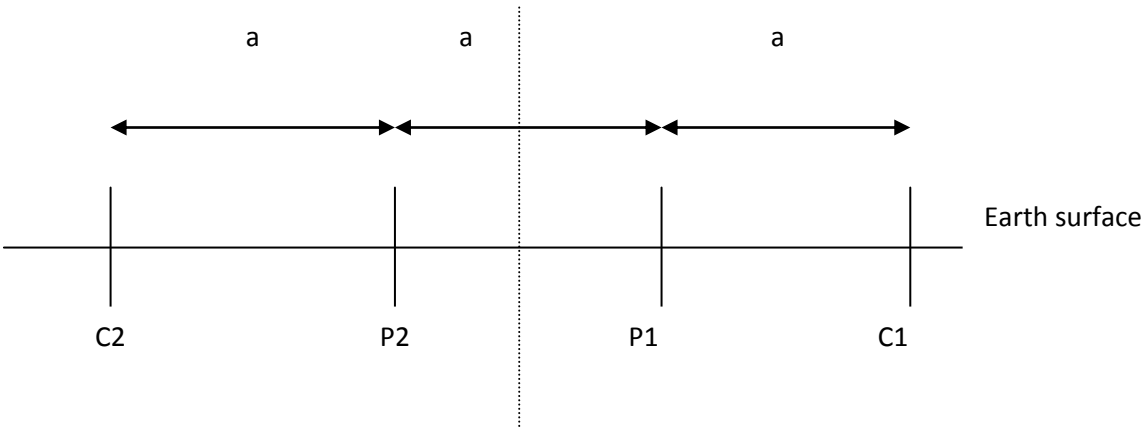

Figure 5.2: Wenner configuration

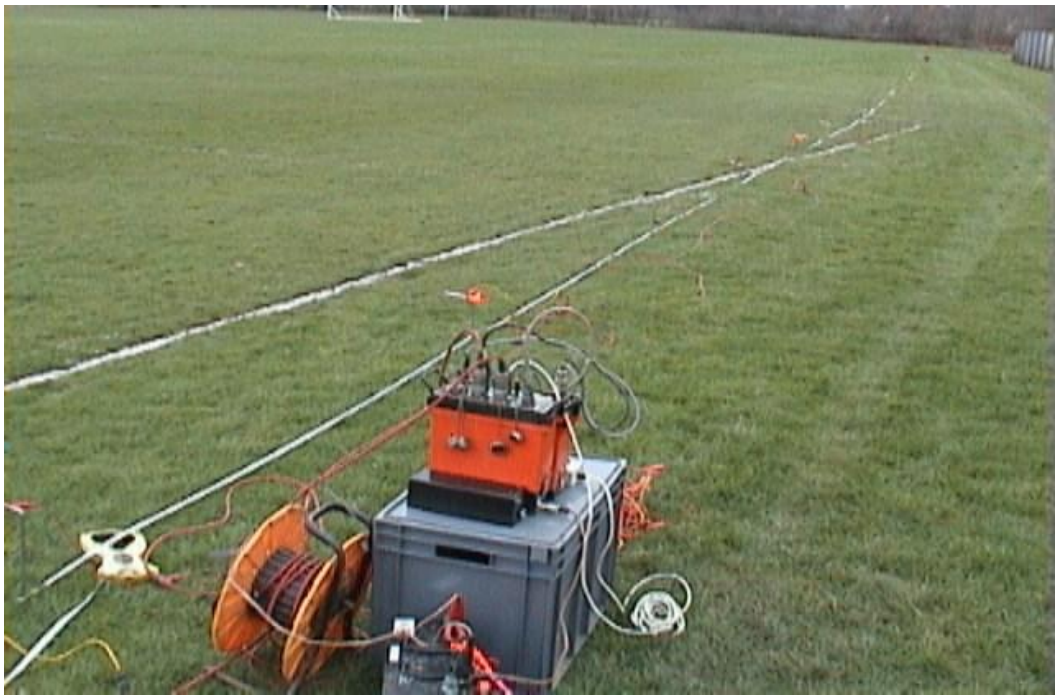

Figure 5.3: Test set-up for the ABEM/LUND imaging system

5.3.1 Resistivity Measurement Results

Figure 5.4 shows the apparent resistivity readings obtained along the route before the installation for all spacing combinations. The results from the figure indicate that there is a considerable lateral variation in the soil resistivity.

Lateral variations were recorded for 3m spacings ranging between 24Ωm and 288Ωm for the line measured on 23/01/09 and between 14.6Ωm and 303Ωm for the

line measured on 01/04/09. As the spacing increased, the variations decreased. For 72m spacing, a range of variation between 73Ωm and 146Ωm was recorded. The minimum readings of soil resistivity recorded were 14.6 Ωm and 24 Ωm for the two lines respectively. The average value of all soil resistivity readings measured on 23/01/09 was 131.3Ωm and 130.8Ωm measured on 01/04/09.

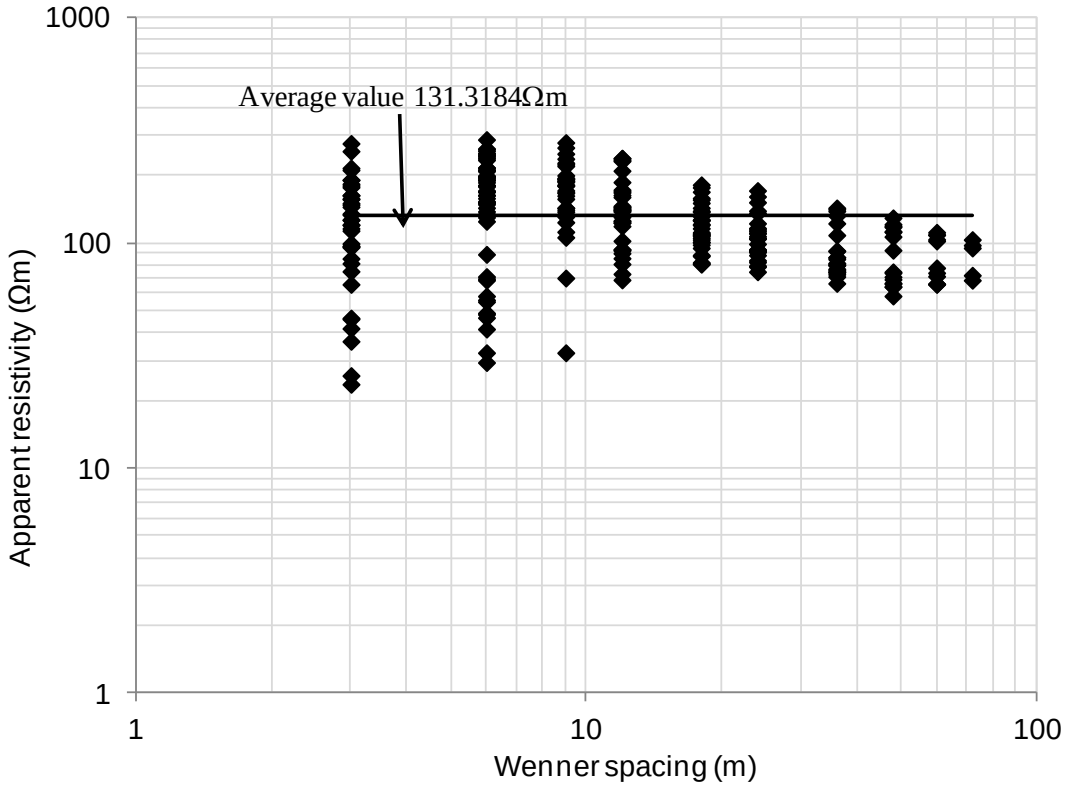

a) Apparent resistivity measured on 23/01/2009

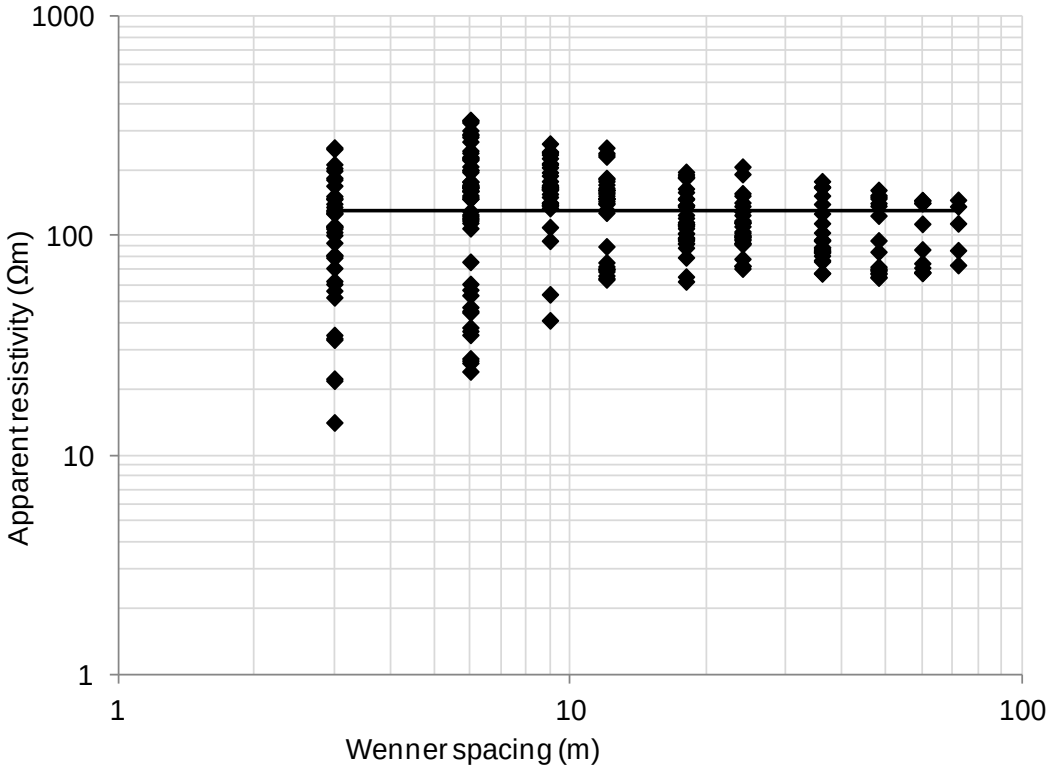

b) Apparent resistivity measured on 01/04/2009

Figure 5.4: Apparent resistivity distribution measured prior to the installation of 88m horizontal electrode

Figure 5.5 shows the average apparent resistivity for both sets of measurements plotted as a function of the Wenner electrode spacing. The apparent resistivity curves shown in Figure 5.4 indicate higher resistivity for shorter spacing (up to 10m) and a gradual fall up to 72m spacing. Such curves indicate the potential to apply a simplified 2-layer soil model. The same results obtained were analysed using RES2DINV software [5.2] to obtain a 2-D distribution of the subsurface soil resistivity.

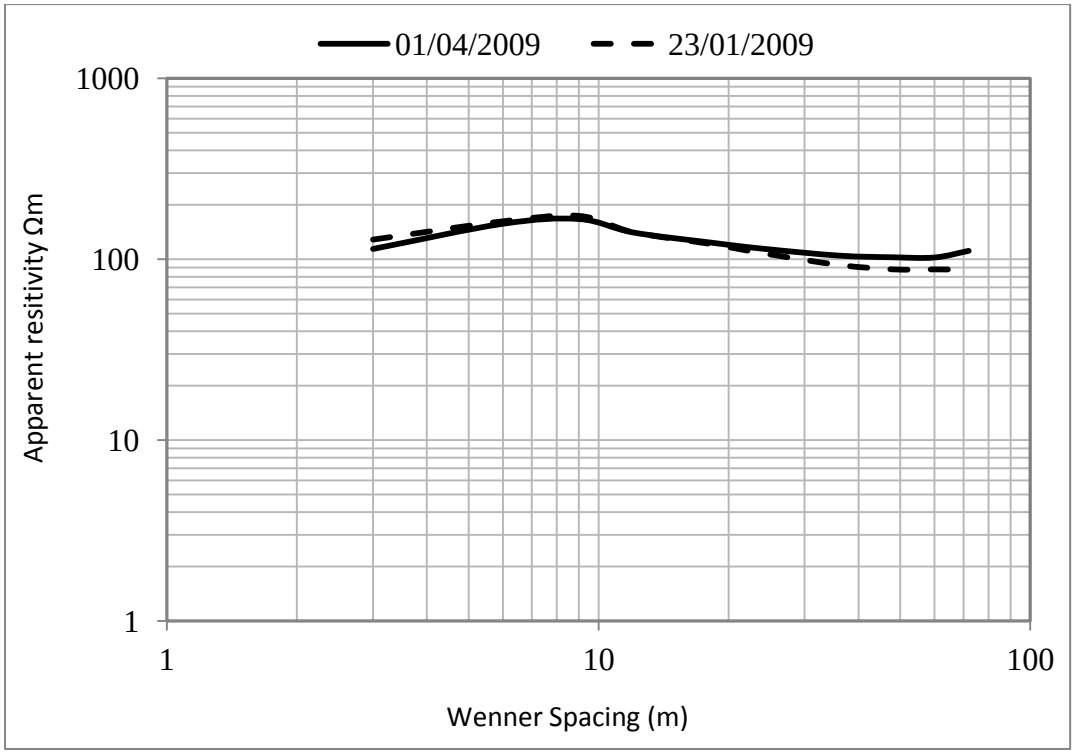

Figure 5.5: Average soil resistivity curves obtained for both lines

The inversion software adopted first plots the data using the pseudo-section method, which consists of plotting the measured calculated apparent resistivity at points located mid-way between the electrodes and at a depth equal to half the spacing [5.7]. Then, the subsurface is divided into a large number of rectangles. Based on the measured apparent resistivity, the program calculates the resistivity of each rectangular section using a finite element method. The final picture is produced by best fit between the measured and calculated values.

Figure 5.6 shows the 2-D inversion models obtained for the data measured on 23/01/2009. The figure has three parts, i) the top part of measured apparent resistivity, ii) the middle part giving the calculated resistivity and iii) the bottom part showing the model obtained by means of the best fit between the measured and calculated resistivity. The figure shows a complete picture with significant lateral

variations in the top layer clearly identifiable from the figure. The distribution of the soil resistivity of the subsurface shows regions having different resistivity with values ranging from 23Ωm to 300Ωm. In general, however, the soil resistivity values tend to be between 130Ωm to 200Ωm except at those areas identified above. A similar observation can be made for the model based on data collected on 01/04/2009. Based on these measurements, a soil model was proposed; with a resistivity of 180Ωm for the top layer having a depth of 9m and 70Ωm for the bottom layer having infinite depth.

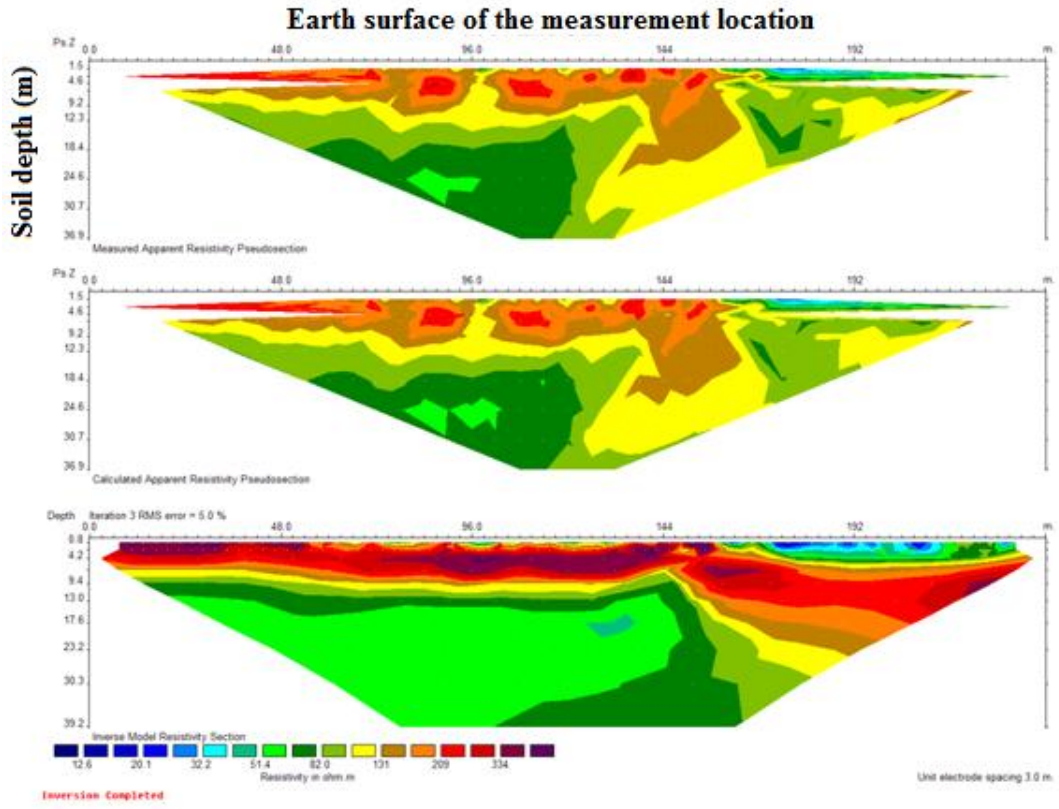

Figure 5.6: Inversion model for soil resistivity measured on 0/04/2009

5.4 Experimental Setup

Figure 5.7 shows a schematic diagram of the experimental setup installed at the Cardiff University earthing test facility. With reference to Figure 5.1, the copper test electrode is 88m long, had a cross-sectional area of 50mm^2, and is buried at a depth of 30cm. The electrode is divided into 13 sections of graded lengths such that the inter-sectional spacing is smallest nearest to the injection point and increases with distance along the electrode. Test junction boxes are installed above each intersection, to enable voltage and current measurements to be made for the different electrode lengths. Each section has a test pit and can be connected to or disconnected from the other sections to vary the electrode length and enable measurement of current distribution. Current was injected at one end of the electrode, as shown in Figure 5.7, and a nearby transmission line tower base was used as the auxiliary electrode current return. A reference potential electrode was placed 100m away from the injection point and its lead is laid perpendicular to the test electrode to minimise mutual coupling effects. A low-voltage recurrent surge generator was used as source for the impulse tests. DC resistance tests were carried out using a composite earth tester (Megger DET2/2) [5.8] and the frequency response of the electrode was measured using a variable frequency test instrument IMS [5.9]. Tests were carried out by injecting an impulse current with different rise times to identify effective length and to compare with DC results. Using an IMS test instrument [5.18], the impedance was measured at different frequencies.

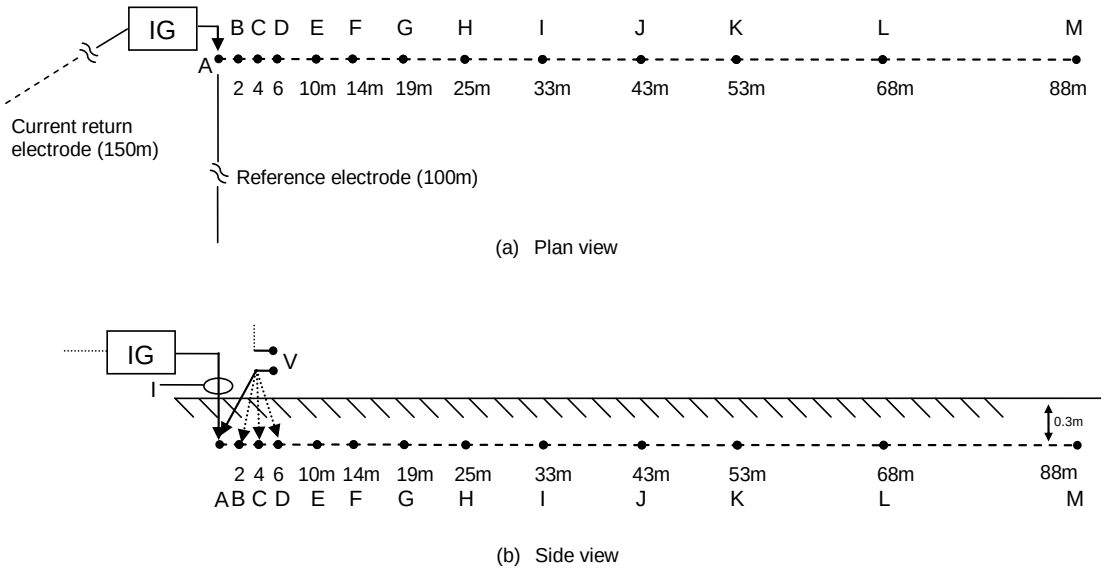

Figure 5.7: Test setup of 88m long conductor divided into 13 sections of increasing length

5.5 Horizontal Earth Electrode

As a described previously horizontal, earth electrodes are commonly used to enhance earthing systems located in areas with high soil resistivity, to reduce overall earth impedance; for example, to interconnect adjacent earthing grids or the individual earthing systems of turbines on wind farms [5.10]. As described in Chapters 3 and 4, the ability of a horizontal earth electrode to reduce earth potential rise is limited, because no further reduction is obtained by increasing its length beyond the effective length [5.11-5.13].

In this chapter, results from experimental tests to investigate the effective length of the horizontal earth electrode under different energisations are presented.

5.5.1 DC measurements

Figure 5.8 shows the measured DC earth resistance for different lengths of the horizontal electrode using two commercial DC earth resistance test meters [5.3, 5.8]. The results show that the DC earth resistance decreases as the length of conductor is increased. Also, as the conductor length increases, the rate of fall in resistance decreases. From the results, it can be seen that, under DC energisation, the resistance curve does not reach an asymptotic value. The effective length can, therefore, be greater than 88m.

Simulations were carried out using CDEGS-HIFREQ software [5.19] based on the actual geometry of the test electrode and the equivalent two-layer soil model is described in section 5.3.1(top layer 180Ωm and bottom layer 70 Ωm). The results are also shown in Figure 5.8. From the figure, it can be seen that there is a good agreement between measured and simulated DC resistance values. Some discrepancies between the simulation and measured values are expected due to the use of a simplified soil model.

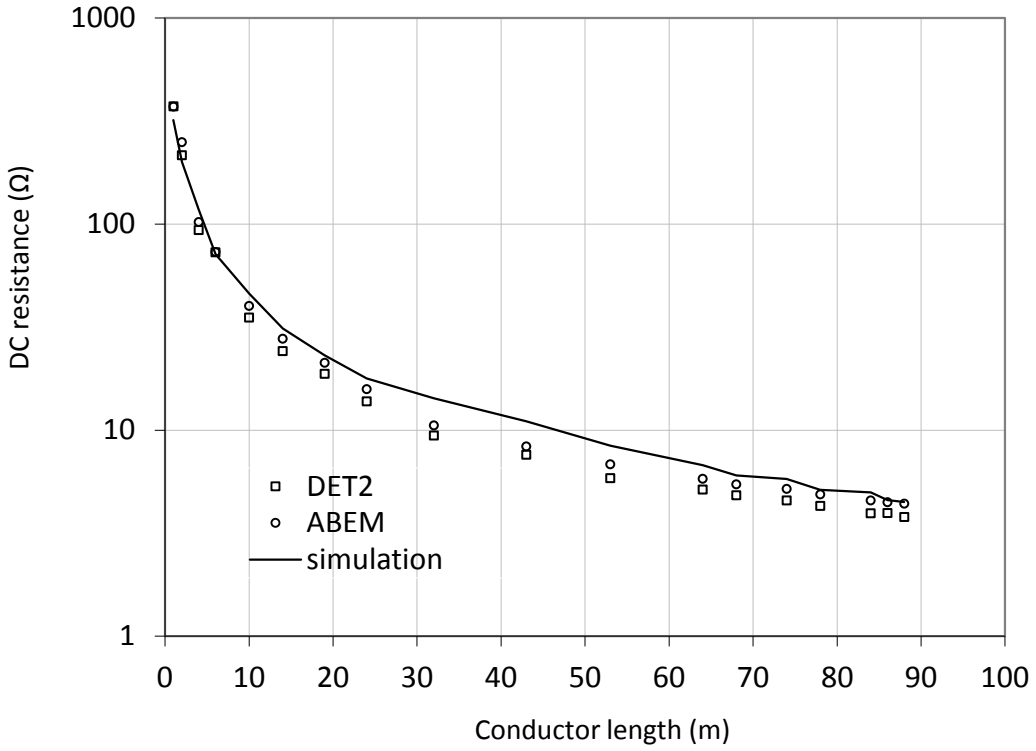

Figure 5.8: Comparison of computed resistance and measured resistance using two different test instruments

5.5.2 Resistance measurements on different days

In order to investigate seasonal effects, i.e. the differences between resistance and impedance readings on different days, further sets of measurements were taken on 14/09/09, 13/10/09, 21/10/09 and 09/11/09. Figure 5.9 shows the measured resistance of the horizontal electrode and, as can be seen, the measured DC resistance follows the same trend but differences are observed between the measurements made on different days. These differences are attributed to variation in soil moisture content.

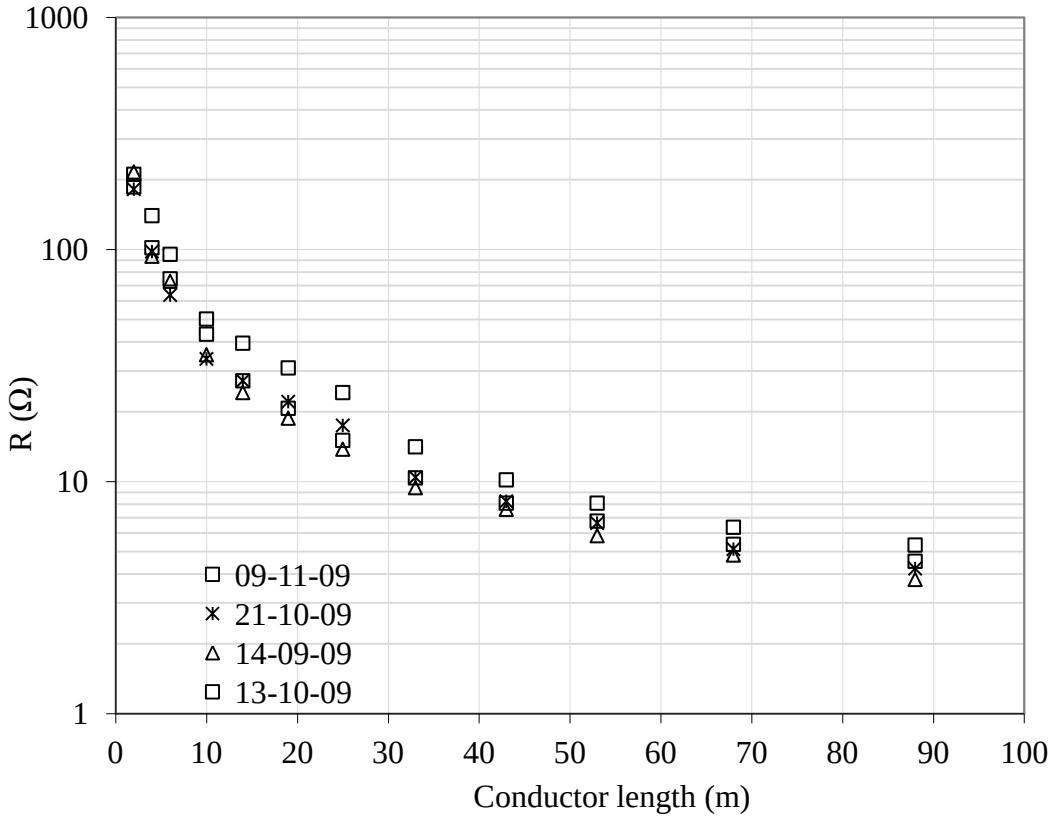

Figure 5.9: Comparison of DC resistance measured on four days in the autumn of 2009

5.5.3 Frequency response of earth impedance

The same test set up shown in Figure 5.7 is used for the impedance measurement using the variable frequency test instrument IMS Impedance Measuring System developed at Cardiff University [5.18]. The impedance of the soil was measured as a function of frequency of the current input. A differential probe with a ratio of 20:1 attenuation provides the voltage signal, and the current is measured by means of a current probe having a sensitivity of 100mV/A.

The current was injected into one end of the conductor with frequencies ranging from 20Hz to 120kHz. The results obtained are shown in Figure 5.10. For short lengths of the earth electrode, the frequency of the current had no significant effect

on the measured impedance because there are no significant inductive effects at these lengths and frequencies. Above 33m, the inductive component of impedance is present at higher frequencies and then at lower frequencies as conductor length is further increased. The upturn frequency, at which the magnitude of the impedance significantly increases, is clearly seen for lengths greater than 33m.

The earth impedance values for two particular frequencies (52Hz and 120kHz) are plotted in Figure 5.11 as a function of conductor length, and the results show that the effective length of the horizontal conductor is reached at the higher frequencies by the clearly defined asymptote. 52Hz was selected to avoid 50Hz interference. Simulations at the same frequencies show very good agreement with the test results. The differences may possibly be due the simplified soil model.

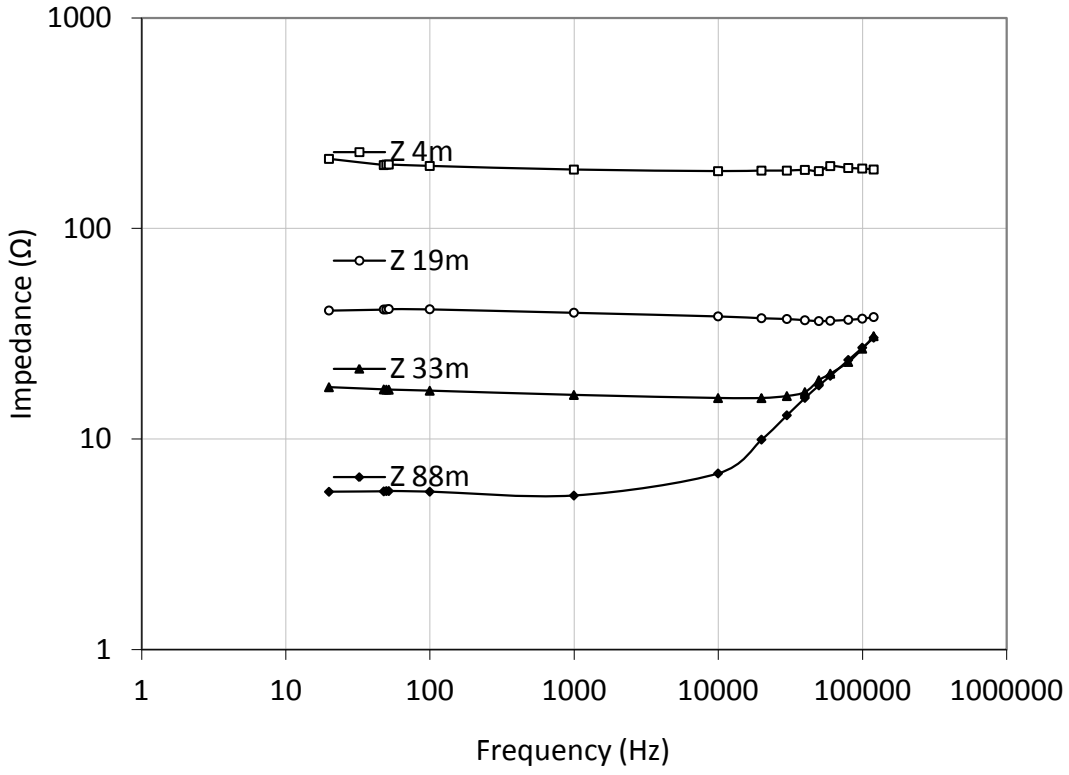

Figure 5.10: Impedance vs. frequency for different lengths obtained by IMS

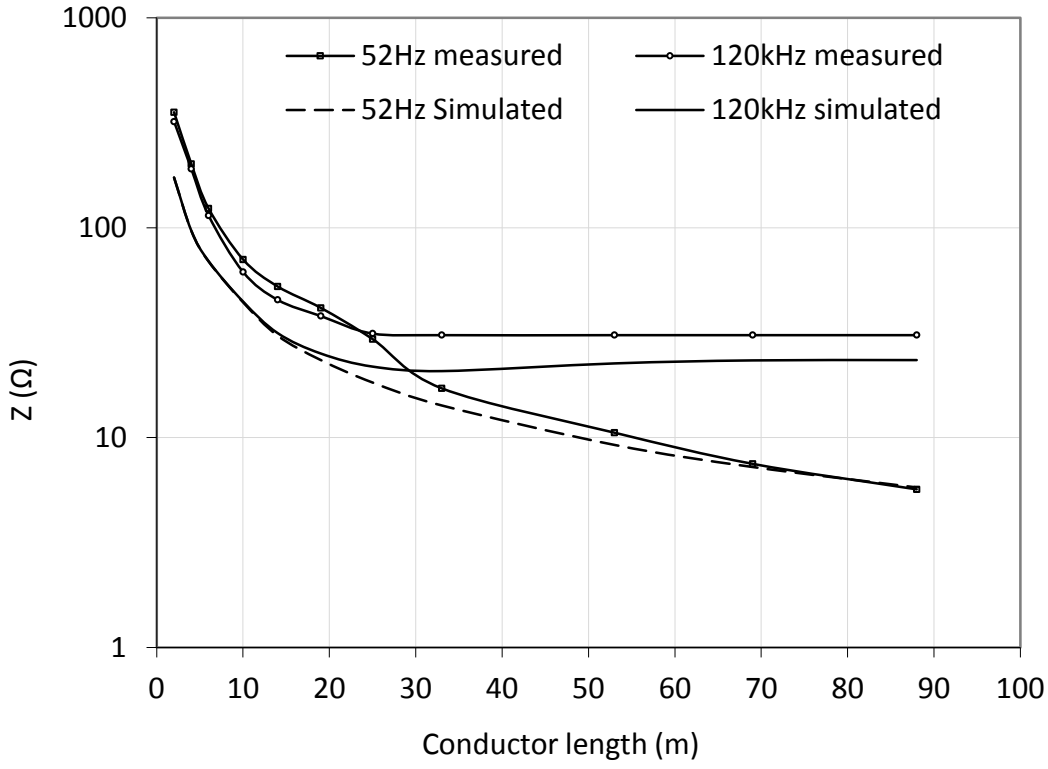

Figure 5.11: AC impedance vs. length

5.5.4 Transient Measurement

Impulse currents of different shapes and magnitude were applied to the 88m counterpoise shown in Figure 5.7. An example of experimental voltage and current at the point of injection are shown in Figure 5.12. From the figure, it can be seen that the transient EPR leads the current which indicates the presence of a significant inductive effect.

In the following sections, results from a series of transient experimental studies are presented which explore (i) current distribution along the electrode (ii) the effect of electrode length and (iii) the effect of impulse rise time.

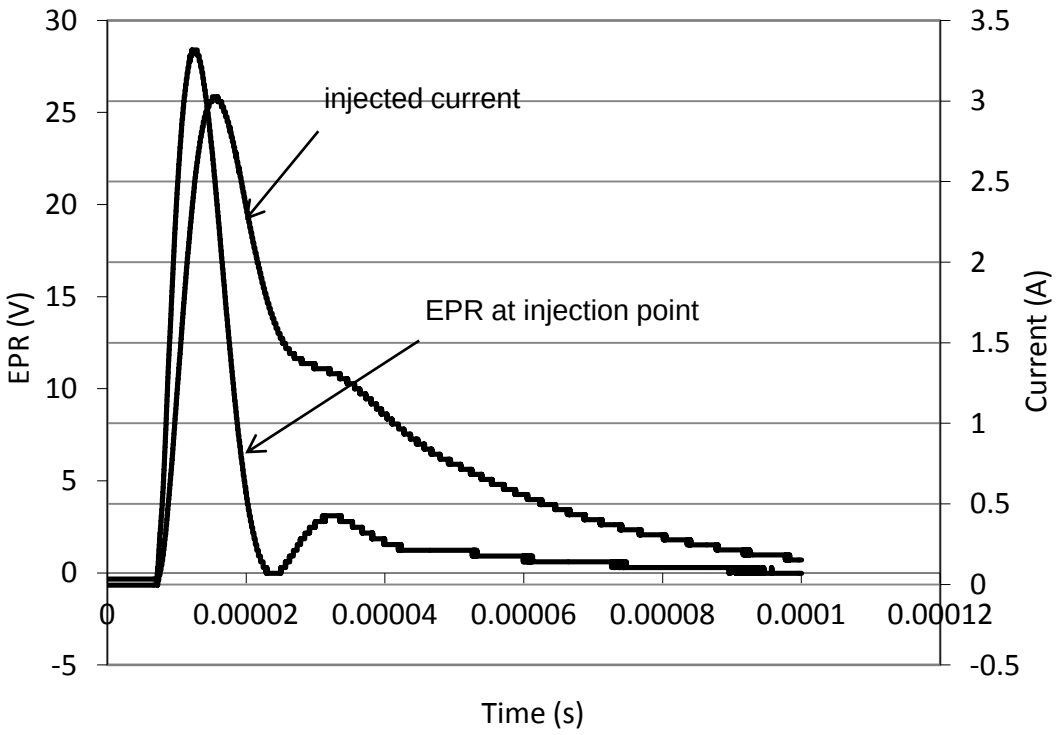

Figure 5.12: Voltage and current at injection point (conductor length 88m)

5.5.5 Current Distribution along the Electrode

Figure 5.13 shows the measured current along the electrode for an injected impulse current of 3A, 4.85μs rise time and 24μs half magnitude time. As the distance from the injection point increases, the magnitude of the impulse current decreases. Also, a time delay due to the propagation of the current along the horizontal electrode is evident.

Figure 5.14 shows the distribution of peak values of the current measured by current transformer (CT) along different lengths of the electrode as a percentage of the peak impulse current (3A) at the injection point. The reduction in current is fairly linear.

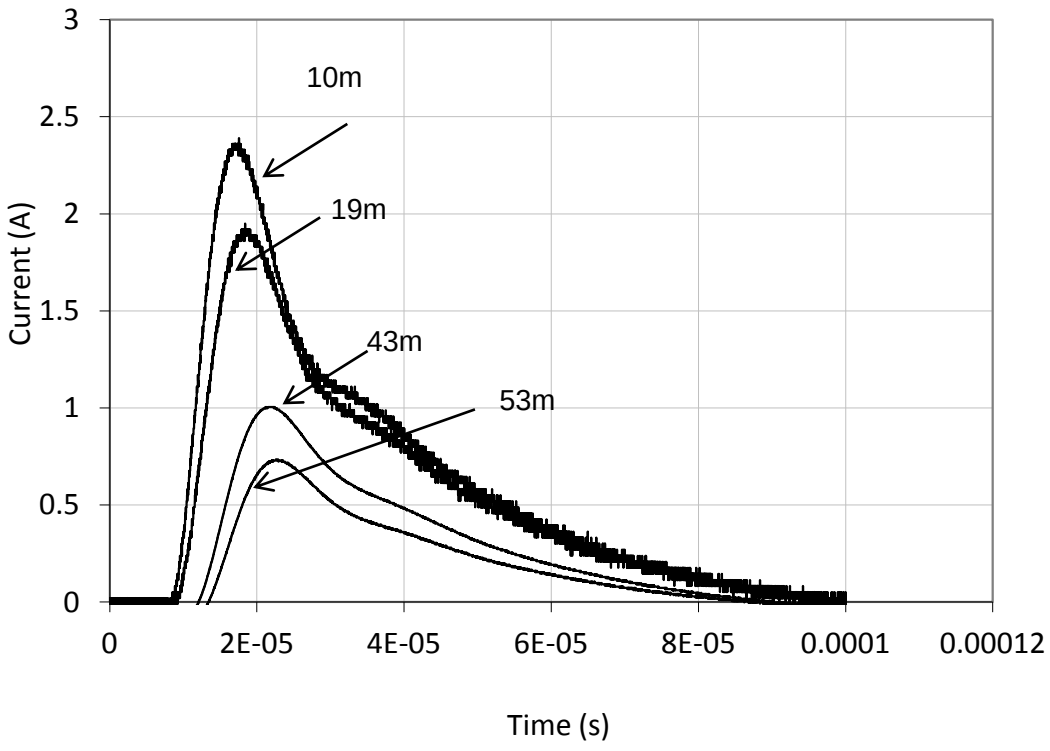

Figure 5.13: Current magnitudes along counterpoise at different points

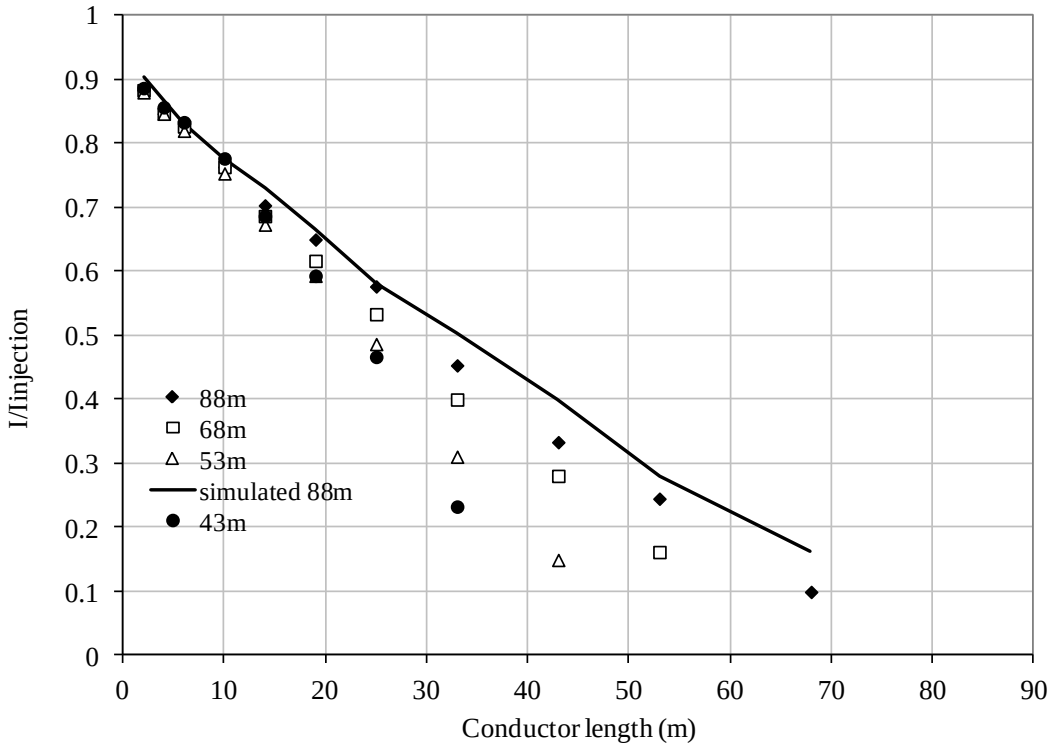

Figure 5.14: Percentage of peak current distribution along conductor length

5.5.6 Effect of Electrode Length and Rise Time

In this section a different impulse current shapes 2μs, 2.5μs and 4.85μs are injected to the 88m horizontal electrode of various lengths. A sample of resulting waveforms shown in Figure 5.14 which reports the impulse applied to different conductor lengths and resulting TEPR. The resulted waveforms of 4.85 μs rise time impulse current of 3A injected to electrode lengths of (14m, 25m and 88m) are clearly show the effect of the length on peak TEPR. From the figure increasing the electrode length decreases the peak TEPR. For example peak TEPR magnitudes of measured at the injection point were (62.4, 36.5 and 26.5) for lengths (14m, 25m and 88m) respectively. Moreover, the results clearly show that the peak TEPR occurs before the peak injected current which is confirms the present of the inductive effect.

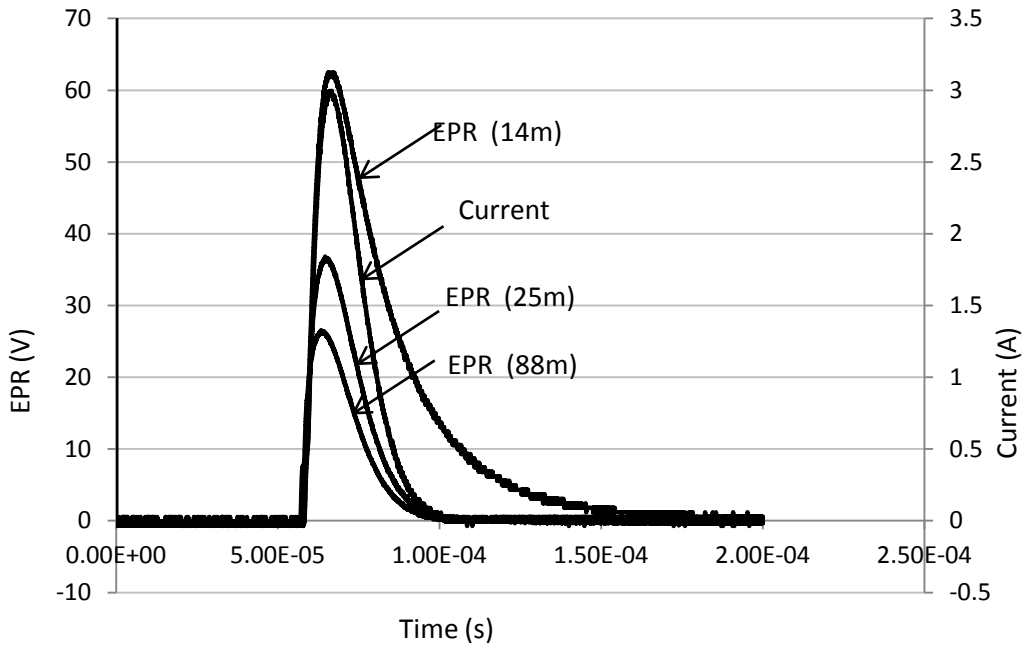

Figure 5.15: Voltage and current at injection point

The impulse resistance was calculated for each length and for the three impulse shapes, and the results are shown in Figure 5.16. From the figure, it can be seen that the impulse resistance decreases as the electrode length increases, reaching its asymptotic value at a particular length which is dependent on the impulse rise time. The faster the rise time is the shorter the effective length of the electrode will be.

The impulse impedance as a function of electrode length was also calculated using the CDEGS program [5.19] for a 4.85μs impulse rise time with an equivalent two-layer soil model derived from data obtained using a detailed soil resistivity Wenner survey carried out along the line of the electrode and prior to its installation. As can be seen from Figure 5.16, the simulated values are reasonably close to those measured at the corresponding rise time.

The results show that a faster rise time will have a higher TEPR at the injection point compared to a slower rise time because the faster rise time contains higher frequency components. As shown in Figure 5.16, higher impedance magnitudes are observed for faster rise times. For faster rise times, the current distribution reaches a constant rate of dissipation in the sections nearest to the injection point. For the same current magnitude, the current is dissipated faster for faster rise time compared with slower impulses.

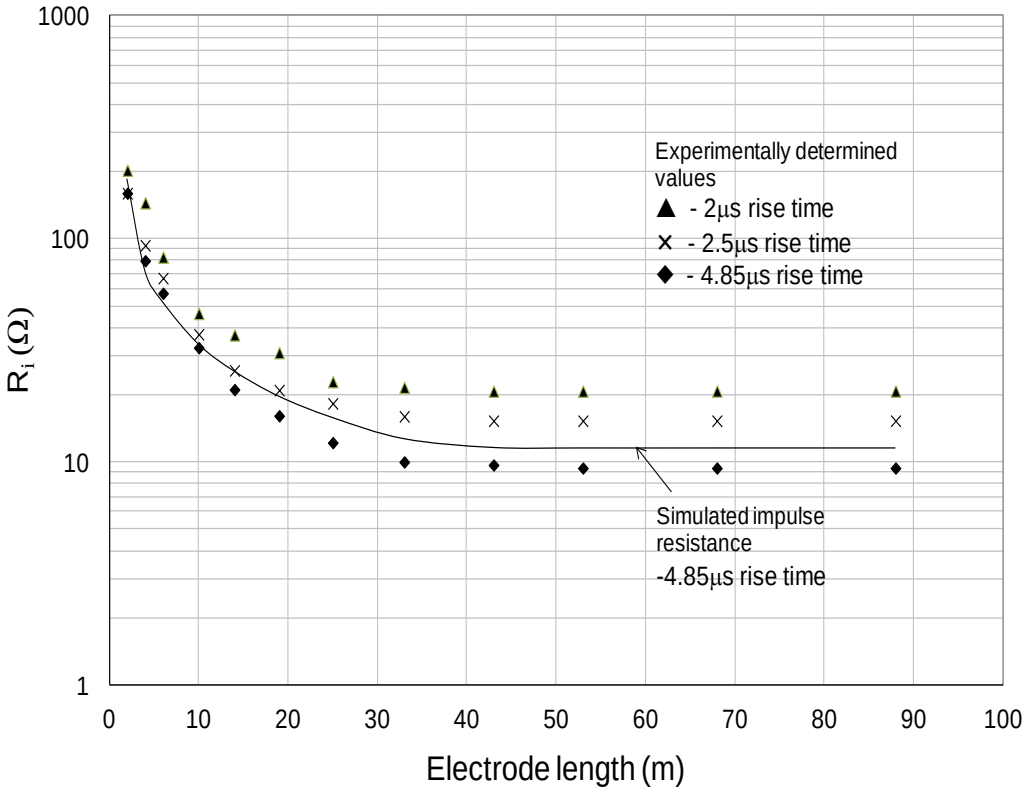

Figure 5.16: Impulse resistance vs. length for different rise times

5.6 Measurement of Effective Length

This section reports practical measurements for the tests using the 88m horizontal earth electrode in Llanrumney fields as seen in Figure 5.7. The same test setup was

used as for the transient measurements. Impulse current with rise times between 2μs and 7μs were injected into the earth electrode. The measured results are shown in Figure 5.17 which reports the effective lengths determined using (a) computer simulations, (b) a published empirical formula [5.11] and (c) the measured values from the experiments. An approximate two-layer soil model was used; an upper layer of resistivity ρ=180Ωm and 9m depth over a lower layer of resistivity ρ=70Ωm and infinite depth for the simulation for empirical formula [5.11]. An average soil resistivity value of 130Ωm was used. Unity relative permittivity was assumed. The results in Figure 5.17 show reasonably close agreement with those obtained from the CDEGS simulation; the effective length obtained by measurement, simulation and using the simplified formula all show reasonable agreement.

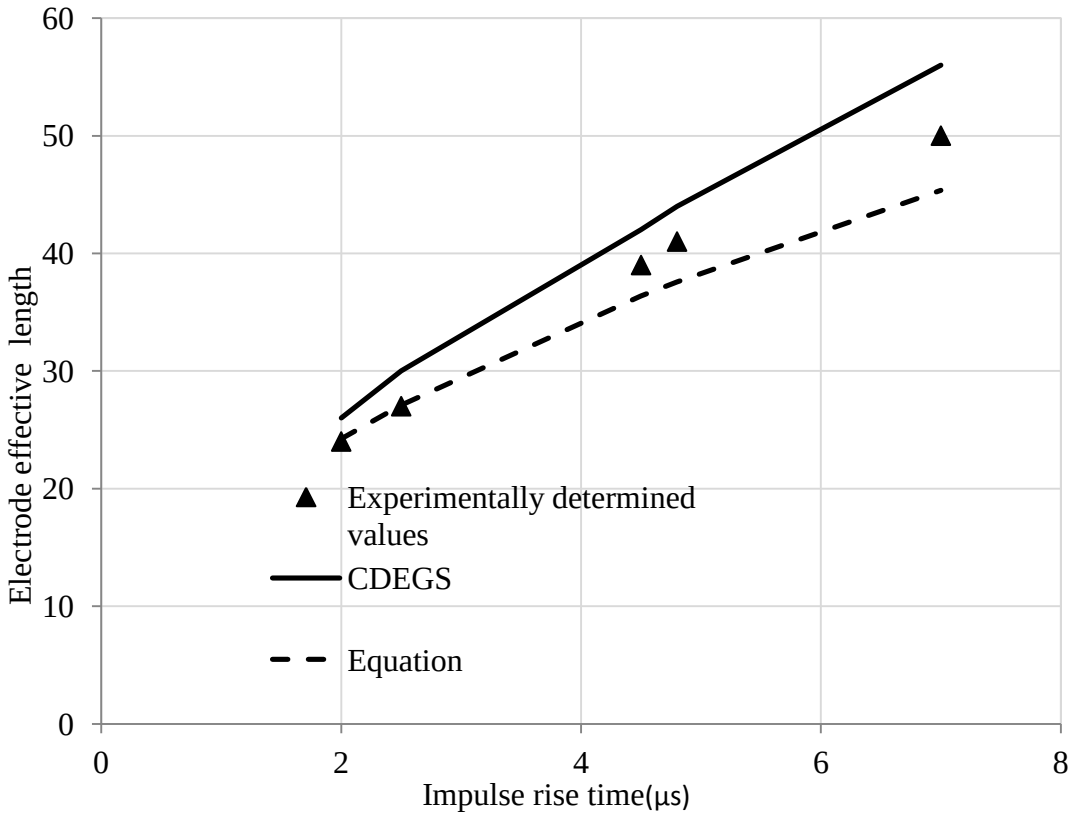

Figure 5.17: Effective length of a horizontal earth electrode

5.7 Earth Grid Effective Area

In this section, the effective area concept of the earth grid is investigated. A number of parameter-specific definitions of effective area have been proposed in the literature [5.21-5.23]. Gupta et al. [5.21] defined the earth grid effective area as the area of the earthing grid at which the transient impedance at the injection point has decreased to a value within 3% of the final impedance. Grecv [5.22] has defined the effective area of earthing grid as the area of the earth grid beyond which the maximum voltage at the injection point remains constant.

In this section, the effective area is defined as the area at which the constant value of impulse impedance is practically reached. The effective area depends on soil resistivity, impulse rise time and electrode geometry. The transient simulations were carried out on earth grids size ranged from (10mx10m) square meters to (140mx140m) square meters for soil resistivities of 100Ωm and 1kΩm. Different impulses were considered.

Figure 5.18 shows the earth impedance as a function of grid-side length. It is clear from the figure that for soils of high resistivity (1kΩm), the earth impedance initially decreases as the grid side length increases and then levels off. The reduction in impulse resistance depends on the point of injection. For example, for corner injection of grid buried in soil of 1kΩ, the TEPR of a 10mx10m grid is about 60V and reaches a constant value of 46.5V as the grid size changed to 20mx20m. For central injection, the TEPR of the 10mx10m grid is 44.5V and decreased until the grid was 40mx40m when the earth grid TEPR reached its asymptotic value of 17.5V. Thus, the effective area of the earth grid excited by a current impulse of 1A, 0.1/5μs buried in soil of 1kΩm is a (40mx40m) square meters for central injection but only 20mx20m for corner injection.

For soils of lower resistivity (100Ωm), the earth impedance has a constant value because the size of the smallest grid (10mx10m) is sufficient to characterise the earth impedance and effective area for a current impulse of 1A 0.1/5μs for either corner or centre injection, though the TEPR had a greater magnitude for corner injection.

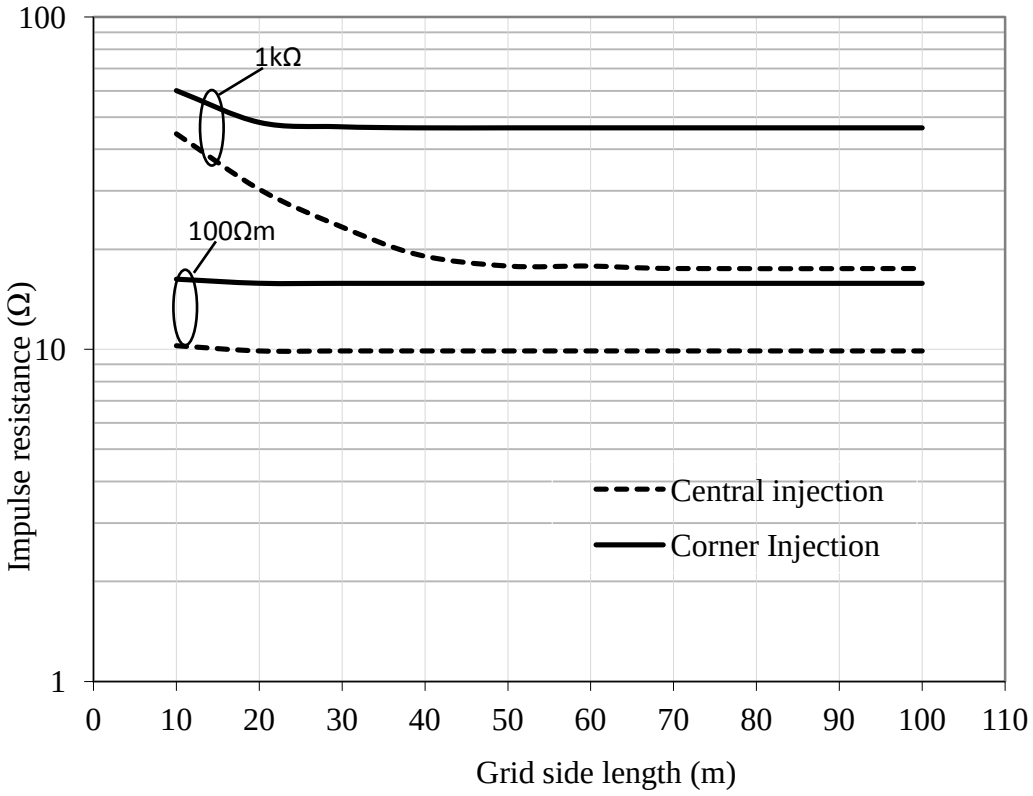

Figure 5.18: Input resistance for corner and central injection of earth grids

5.8 Conclusions

An approximate model of the subsurface resistivity distribution can be obtained by conducting a resistivity sounding in the vicinity of the earthing system under test. Soil resistivity measurements using a two-dimensional method are presented. A two layer soil resistivity model was derived from soil resistivity measurements and used when comparing the simulations with field measurements. An 88m horizontal earth electrode was installed with 13 junction boxes to allow changes to the measured length as required to test for an effective length. Experimental tests to investigate current and voltage distributions along a buried horizontal electrode under impulse currents are reported. The results show that the DC earth resistance decreases with the length of conductor, and as the length of conductor increases, the rate of decrease in resistance decreases. The results from the tests show that a large proportion of the injected impulse current is dissipated into the ground along a length close to the injection point. The effective length of the electrode was determined from the impulse impedance, and was found to be comparable to that predicted by a simplified empirical expression and computer simulation. This effective length is dependent upon the soil properties and the impulse shape. It was found that more current was dissipated over shorter distances along the horizontal electrode into the ground for fast impulses compared with the slow impulse. The earth grid response under variable frequency and transient conditions was investigated.

The effective area of an earth grid subjected to transient conditions are studied. The effective area was found to be dependent on soil resistivity and point of injection. A larger effective area is obtained for a high soil resistivity. The effective area for the corner injection is less than for central injection. This is explained by the difference in the inductive component between central and corner fed-points.

CHAPTER SIX

ENHANCING THE EARTHING SYSTEM WITH INCREASED EFFECTIVE LENGTH/AREA OF HORIZONTAL EARTH ELECTRODE AND SUBSTATION EARTH GRID

6.1 Introduction

Horizontal earth electrodes are commonly used to enhance earthing systems in order to reduce overall earth impedance [6.1]. However, as demonstrated in previous chapters, the ability of a horizontal earth electrode to reduce earth potential rise is limited because no further reduction is obtained by increasing its length beyond the effective length [6.2]. The same concept applies in terms of area to substation earth grids. The effective length of a conductor and the effective area of an earth grid at high frequency or under fast transient conditions are limited particularly in the case of earthing systems buried in soil of low resistivity.

In this chapter, a new method is proposed to enhance earthing systems to reduce earth impedance by installing an additional above ground or insulated parallel conductor which is bonded to the bare underground horizontal electrode at points along its length. This technique aims to increase the effective length of the horizontal electrode and the earth grid area, and to reduce the impedance of the earth electrode as seen from the point of energisation. This method aims to reduce the inductance of the buried bare conductor in order to utilize longer length to contribute in reducing the electrode earth impedance.

A preliminary investigation of this technique was carried out by simulations to establish its benefits. This was followed up with an experimental investigation of the technique using the experimental test setup as described in Chapter 5.

6.2 Earthing System Enhancement

In previous chapters, the effective length of a simple earth electrode and the effective area of an earth grid have been quantified, and the limits they impose on the improvement of earthing system performance have been described.

In this proposed method, an above ground insulated conductor is connected with down leads to a buried conductor. Frequency performance and transient behaviour of a horizontal electrode and an earth grid with above ground enhancement are investigated.

6.3 Simulation Arrangements

To examine the effect of above ground enhancement, two types of earth electrode were adopted for this study (horizontal earth electrode and earth grid). Figure 6.1 shows these electrode configurations:

i) A 100m long copper conductor with radius of 4mm buried at a depth of 0.5m, enhanced with an identical parallel conductor (20cm above ground and insulated and bonded to the bare underground horizontal electrode at points along its length.

ii) A 100mx100m square earth grid buried 1m below ground. This earth grid is enhanced with an identical insulated earth grid 6cm above ground and connected to the buried grid by downleads.

Each of the above earth electrodes were simulated under three different soil resistivities; 100Ωm 1kΩm and 10kΩm. The impedance at the injection point was calculated for an injection current of 1A. The simulations were performed using the CDEGS software.

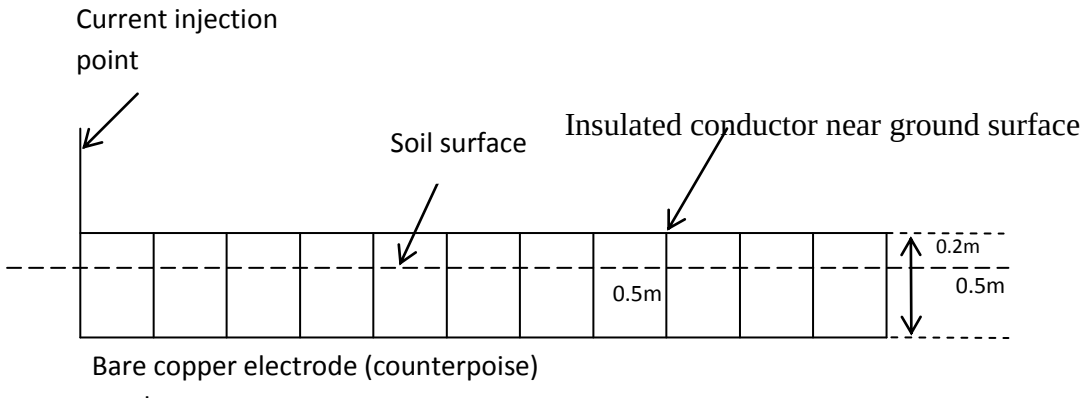

a) 100m conductor with additional insulated conductor above ground

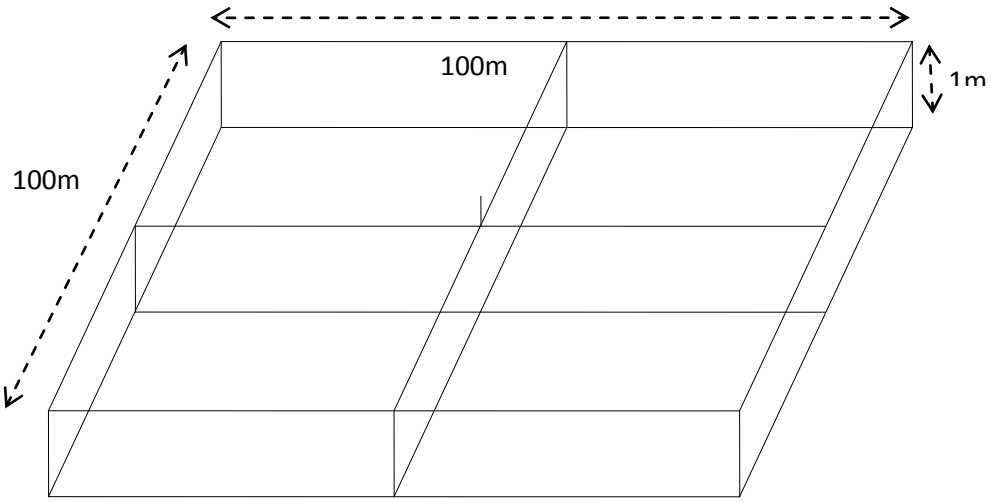

b) 100mx100m earth grid, with four meshes and additional insulated earth grid 6cm above ground

Figure 6.1: Earth electrode enhancement models

6.4 Frequency Response of Electrodes with Enhancements

6.4.1 Horizontal electrode

The frequency response of the 100m long horizontal electrode with and without the above ground enhancement is shown in Figure 6.2 for different values of soil resistivity over a wide range of frequency. The results in Figure 6.2 demonstrate that there is no significant benefit at low frequency obtained by adding the additional conductor. However, beyond the upturn frequency, the earth impedance is significantly lower for all soil resistivity conditions considered. For example at 10MHz and 10kΩm, a reduction of 38% in earth impedance is obtained by adding the parallel insulated conductor.

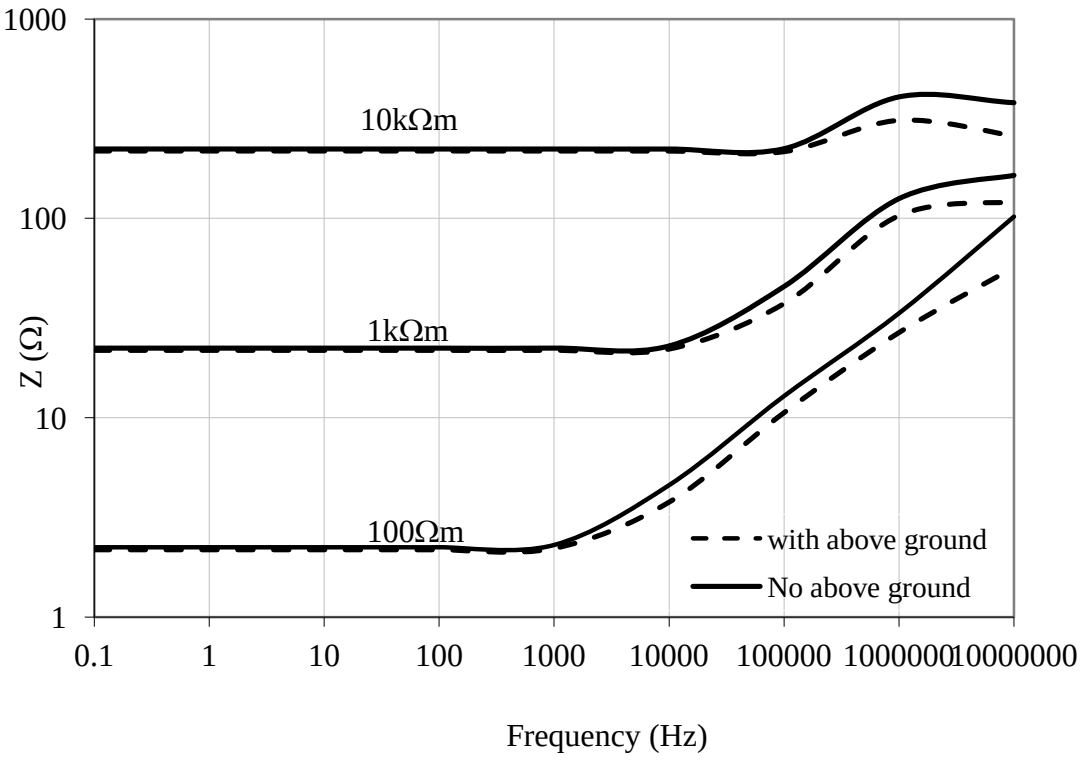

Figure 6.2: Horizontal earth electrode with and without above ground enhancement; impedance vs. frequency for soil resistivities 100Ωm, 1kΩm and 10kΩm

6.4.2 Earth grid

Similar studies were carried out based on the 100mx100m earth gird. The earth impedance at the centre injection point was calculated, and the results are shown in Figure 6.3. As can be seen from the figure at low frequencies, there is no change in impedance when the above ground insulated earth grid is added. At these low frequencies and for all three soil resistivities, the impedance of the earth grid with and without enhancement is the same. Above the upturn frequency, a reduction in the impedance is observed when the above ground earth grid is added. For a soil resistivity of 100Ωm, 27% and 65% reductions in the impedance are obtained at 1MHz and 10MHz respectively with the above ground earth grid. Similar reductions can be seen for other values of soil resistivity.

The results clearly demonstrated that the above ground enhancement play a beneficial role in reducing the earth grid impedance, thus improving the performance of an earthing system. However, it is impractical to implement an above ground system in a substation due to plant arrangement. To overcome this problem, it is proposed that instead of above ground an identical insulated grid is buried below ground. This arrangement makes it possible to bury the entire earthing system below the surface of the ground.

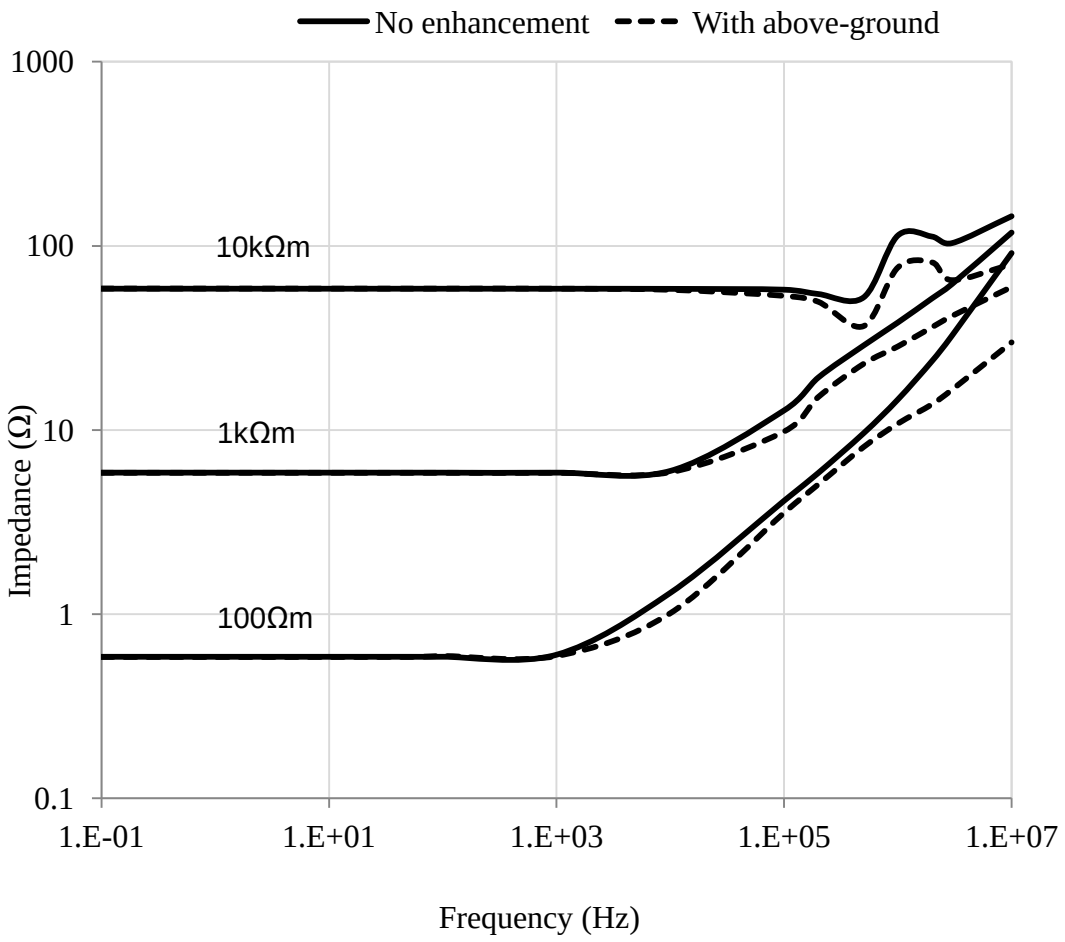

Figure 6.3: Earth grid with and without above ground enhancement impedance vs. frequency for soil resistivities 100Ωm, 1kΩm and 10kΩm

6.5 Transients Simulation Results

In this section, the time domain performance of the enhanced system is described. The earth electrode systems under study were injected with a transient impulse current 1A, 8/20.

Figure 6.4 shows the calculated peak TEPR for three different soil resistivity values; 100Ωm, 1kΩm and 10kΩm. The peak TEPR decreases when the horizontal earth electrode is equipped with the additional above ground insulated conductor. The reduction in TEPR increases with increase in soil resistivity. For example, the peak TEPR of the buried earth electrode with and without enhancement was 6Ω and 7.9Ω respectively for a soil resistivity of 1kΩm. For a soil resistivity of 10kΩm there was

a reduction of about 29% (58.6Ω to 41.3Ω) when the buried horizontal earth electrode was equipped with the above-ground enhancement. At 100Ωm, there was a reduction of about 24% (2.25Ω to 1.7Ω) in adding the above ground electrode.

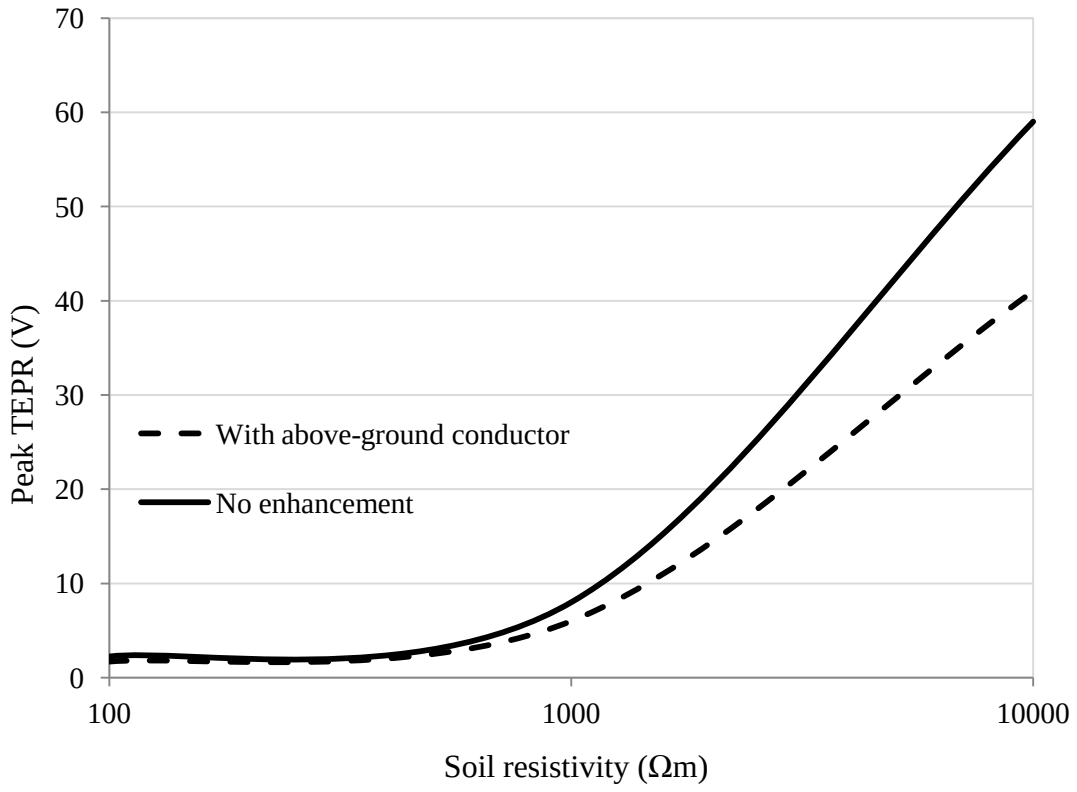

Figure 6.4: Effect of horizontal electrode enhancement under transient (8/20)

Figure 6.5 shows similar results for the 100mx100m buried earth grid. The results show that the TEPR magnitudes decrease when the above ground technique is used, particularly for the high soil resistivity conditions.

For the low soil resistivity of 100Ωm a reduction of about 21% is obtained when the above-ground technique is used a reduction in the resistance value from 6.6Ω to 5.18Ω. At 10kΩm the reduction is about 22% (from 218Ω to 170Ω) when the earth grid was enhanced with the addition of the identical insulated above ground earth grid.

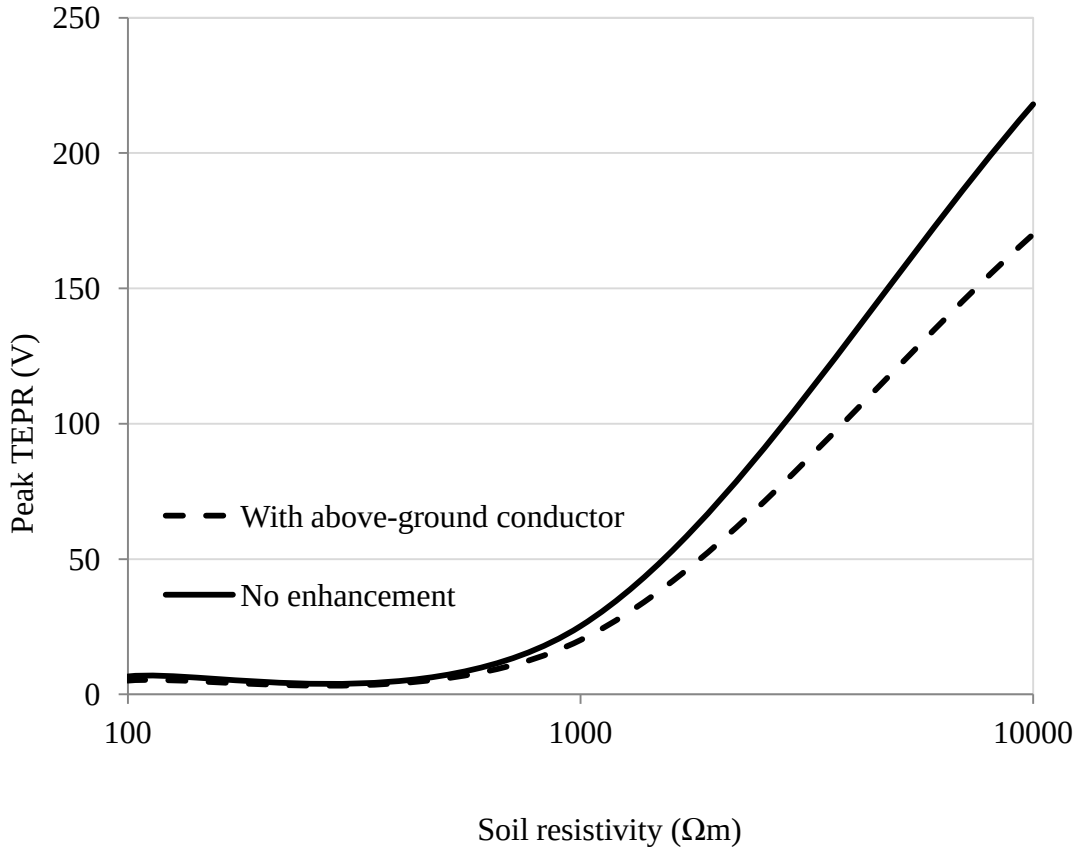

Figure 6.5: Effect of earth grid enhancement under transient (8/20)

6.6 Application of Above Ground Technique to Enhance Effective Length/Area

In this section, the effective length of the horizontal earth electrode and the effective area of the earth grid are calculated over a wide range of frequency and resistivity. The approach adopted was to carry out simulations at a given frequency and resistivity and to increase the dimensions (length and area) until the minimum impedance is obtained. A similar investigation was carried out on the earth grid shown in Figure 6.1 with a centre injection

6.6.1 Horizontal Electrode

6.6.1.1 Effect of Variable Frequency

The identified minimum impedance describes both the effective length and the corresponding impedance at effective length for a particular pair of frequency and resistivity values. Repeating this procedure over a range of frequency and resistivity values allows the effective length and impedance at effective length to be characterized for a given electrode type. The simulations were then repeated for the electrodes (horizontal and grid) with the parallel insulated conductors added. This allows the contribution of the enhancement to be quantified.

Figure 6.6 shows the effective of the horizontal electrode as a function of frequency for three resistivity conditions. As can be seen from the figure, there is a significant reduction in effective length with frequency and resistivity. The addition of the insulated parallel conductor has the effect of increasing slightly the effective length of the electrode system. However, as can be seen in Figure 6.7, the addition of the insulated parallel conductor has a very remarkable effect by reducing the impedance at the effective length. This effect is more pronounced for higher frequency injections and high resistivity soils. At 10kΩm soil resistivity a reduction of 22% and 39% at 1MHz and 10MHz respectively when the above ground grid is installed.

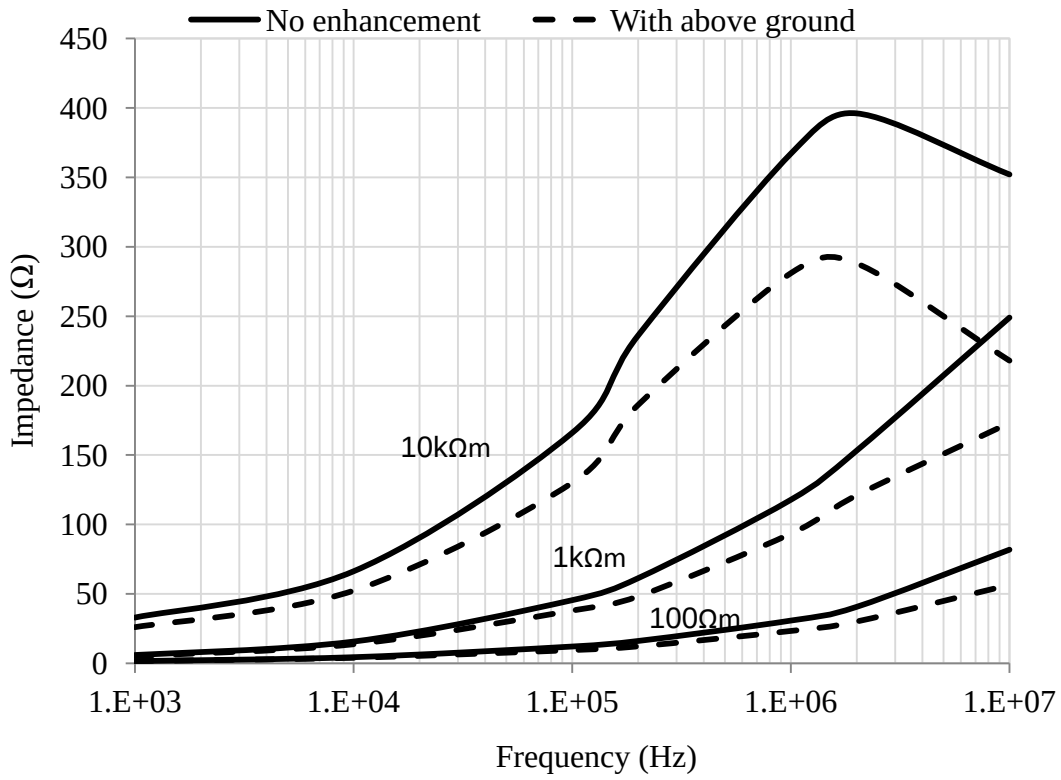

Figure 6.6: Impedance at effective length: effect of additional parallel insulated conductor

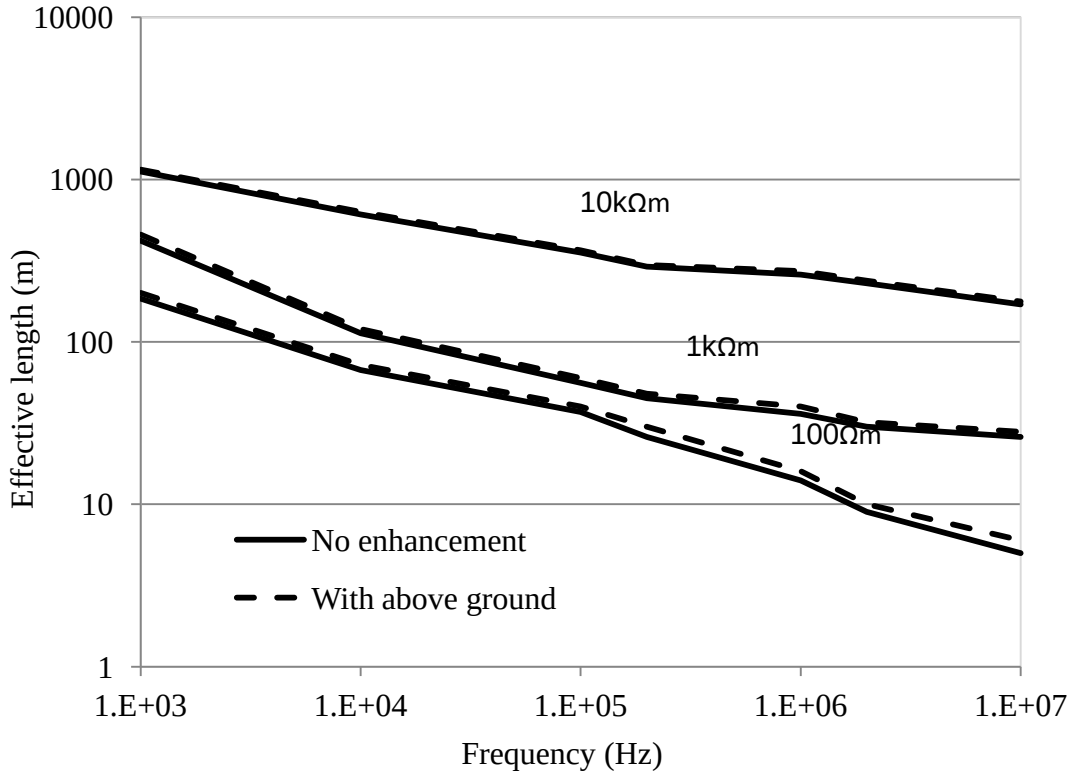

Figure 6.7: Effective length of horizontal earth electrode

6.6.2 Earth Grid

6.6.2.1 Effective Area of Earth Grid

A 1A current was injected into the earth grid with and without the above ground arrangement. Due to the long simulation time required, the injection calculation was limited to only two soil resistivity values, 100Ωm and 1kΩm for the frequency range from 1kHz to 10MHz. Figure 6.8 shows the earth grid effective area as a function of frequency for the earth grid with and without the above ground enhancement. It is clear from the results that that effective area is increased when the above ground grid is employed. Figure 6.8 illustrates the impedance at effective area of the earth grid for the two arrangements. It is clear from the results that the addition of the above ground insulated earth grid has a significant effect in reducing the earth grid impedance at the effective area. For 100Ωm at 10MHz, the impedance values are about 31Ω without the above ground earth insulated grid and 17Ω with the above ground grid respectively. This represents a 45% reduction in impedance. Under low soil resistivity the effect of the above ground grid is significant at frequencies greater than 1MHz.

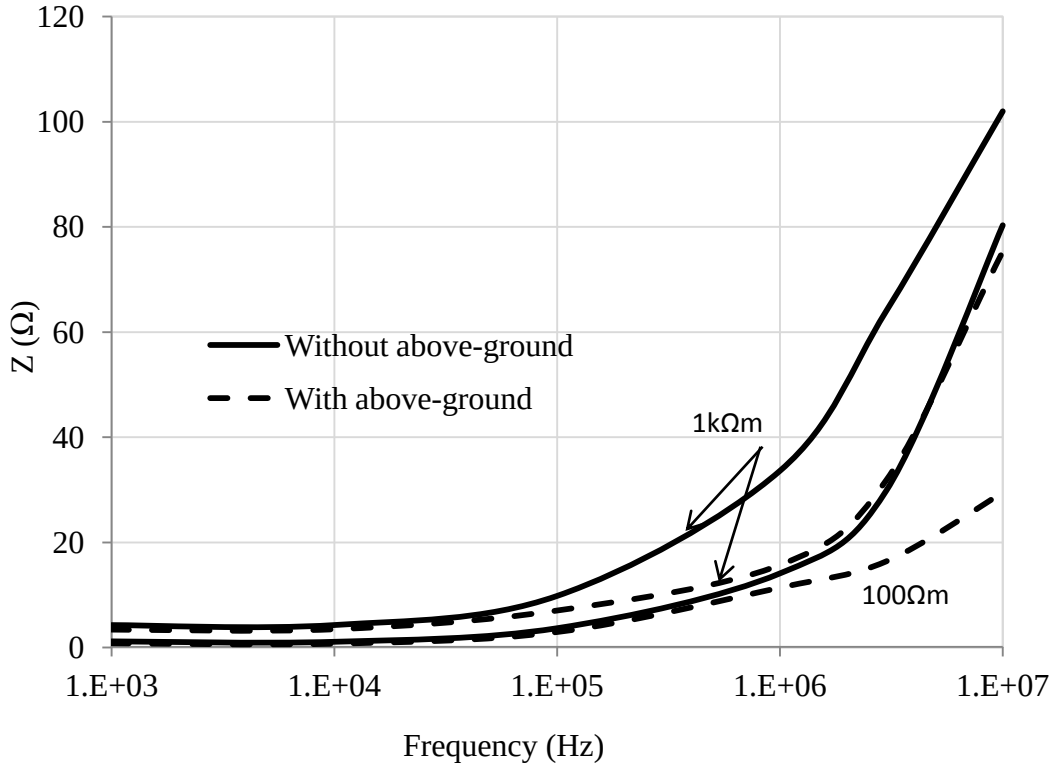

Figure 6.8: Impedance vs. frequency for earth grid effective area at soil resistivities 100Ωm and 1kΩm with and without addition of an insulated above ground conductor

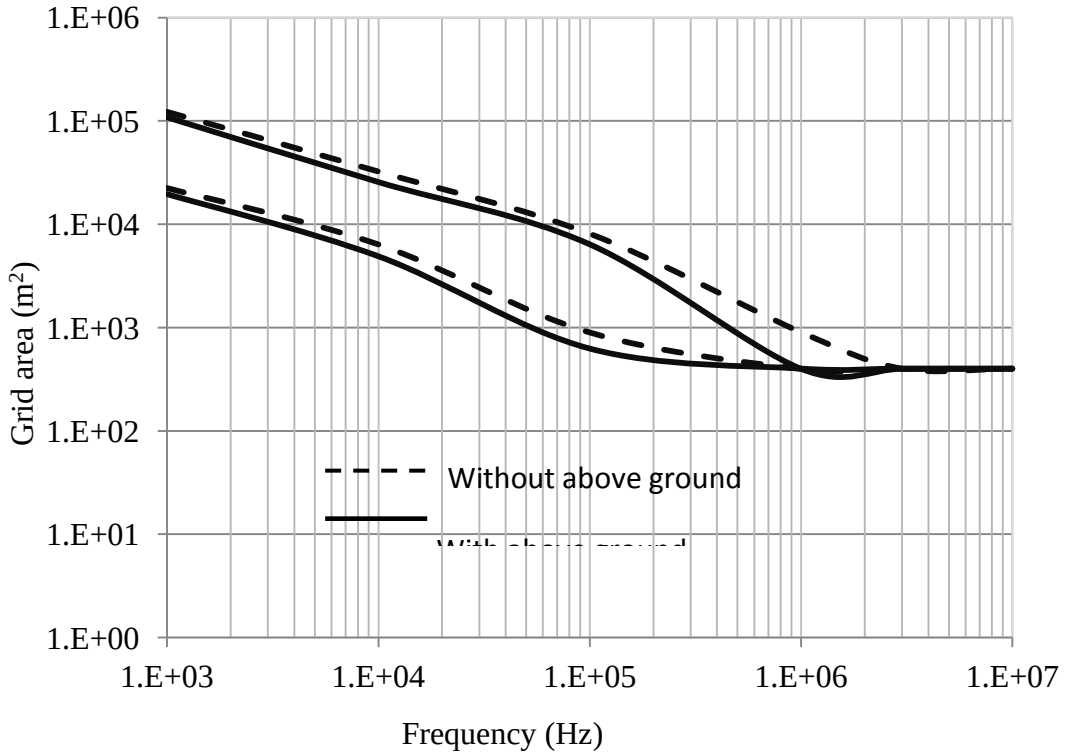

Figure 6.9: Effective area of earth grid

6.7 Effective Length under Transient Conditions

This section reports simulations and experimental investigations to quantify the benefit of adding the above ground insulated earth electrode under transient conditions.

6.7.1 Simulation Input Details

Simulations of the horizontal electrode and earth grid equipped with above ground insulated electrodes were subjected to different impulse shapes over a range of soil resistivities.

A 1A impulse current was injected into at one end of the horizontal electrode and into the centre of the earth grid. A series of simulations were carried out for various conductor lengths and different earth grid sizes over a range of soil resistivity values to determine effective length and impulse resistance.

6.7.2 Horizontal Earth Electrode Enhancement

The horizontal earth electrode shown in Figure 6.1 was subjected to a lightning impulse having 1A current peak value with different rise times.

Figure 6.10 shows the calculated peak TEPR at the injection point for the buried bare counterpoise alone and also with the additional insulated above ground conductor. The results show that the addition of the above ground insulated conductor has a significant effect in reducing the peak TEPR and also in extending the effective length. The TEPR for the 5/20 current impulse is reduced by 20% and by 24% for the 0.1/5 current impulse.

The addition of the above ground electrode also increases the effective length. For example, the effective length of the horizontal earth electrode for the 0.1/5 current

impulse is about 7m. The addition of the above ground conductor increases this to about 10m. The corresponding impedances are 29.3Ω and 22.2Ω.

For slower impulses, a higher percentage reduction and longer effective length were obtained. A 29% reduction in impedance was obtained when the 5/20 current impulse is injected into the horizontal electrode with the above ground conductor compared to the horizontal in-ground electrode only. Moreover, the effective length increased from about 29m to about 34m.

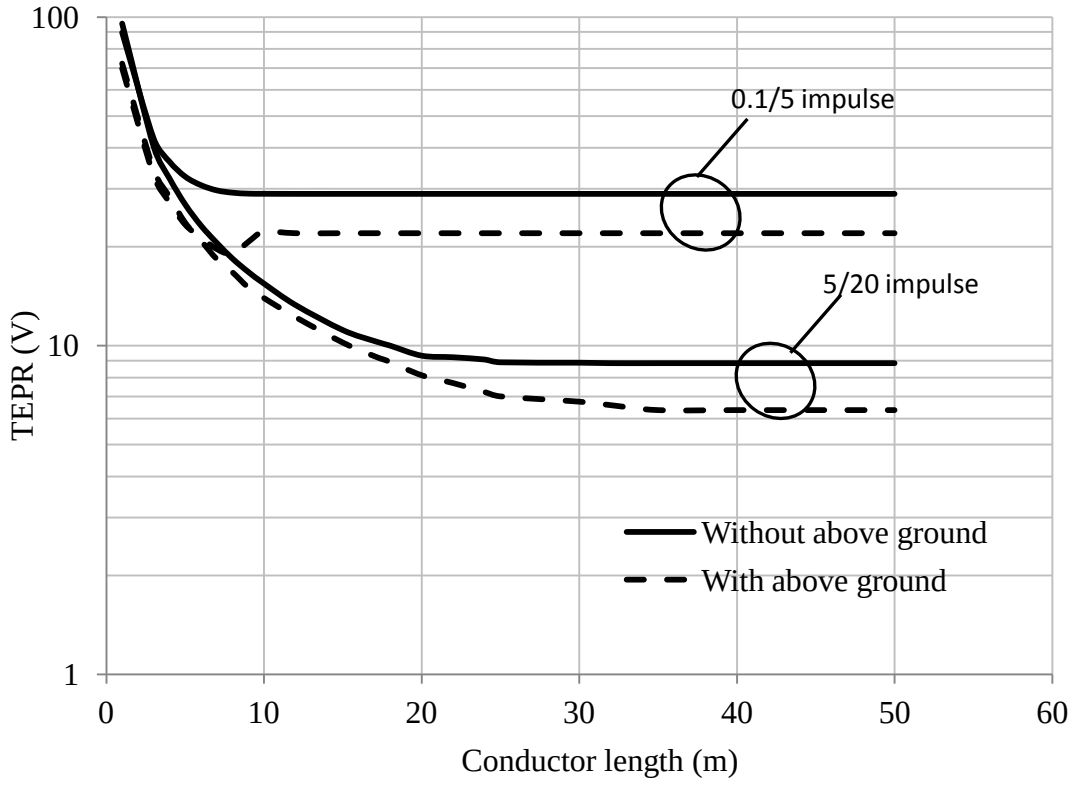

Figure 6.10 Peak TEPR vs. conductor length with and without addition of an insulated above ground conductor (100Ωm soil resistivity)

Figure 6.11 shows the results corresponding to a 1kΩm soil resistivity for the same two impulses (0.1/5 and 5/20). The benefit of adding the insulated parallel conductor is confirmed also for the higher resistivity condition.

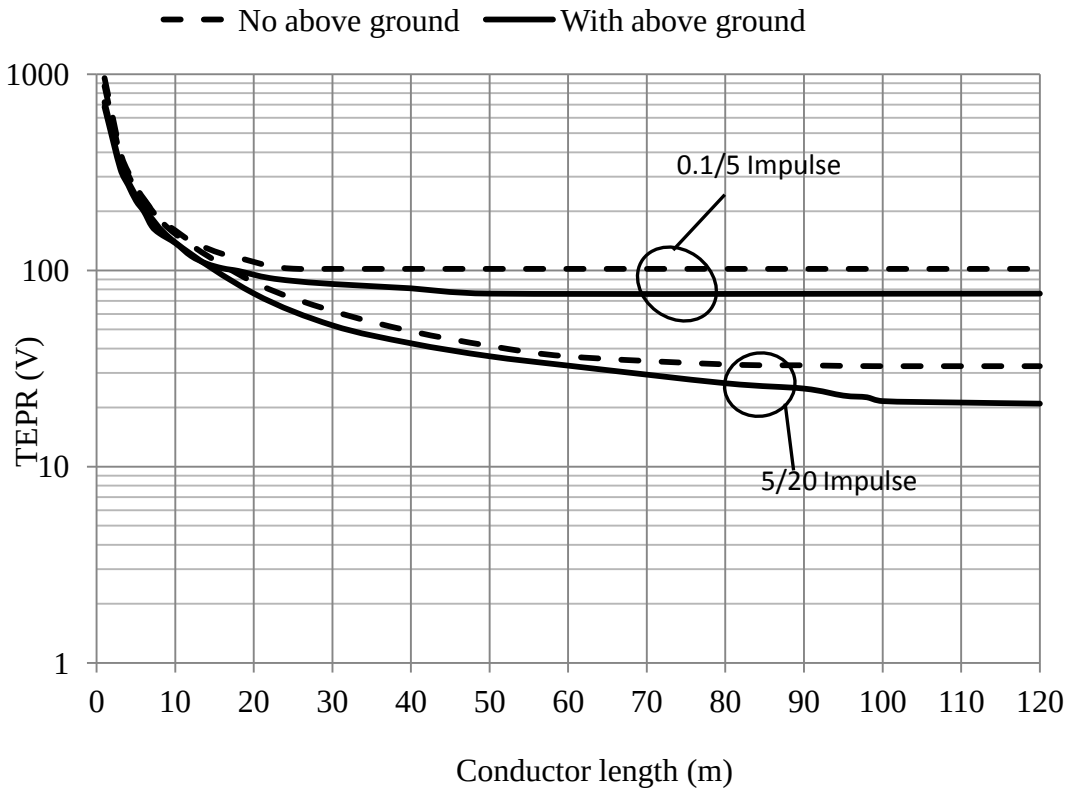

Figure 6.11: Peak TEPR vs. conductor length with and without addition of an insulated above ground conductor (1kΩm soil resistivity)

Figure 6.12, shows the calculated impulse impedance as a function of electrode length. From the figure, it can be seen that the insulated conductor has an effect on reducing the earth impulse resistance. However, the reduction is more significant when the earth electrode is buried in soil of high resistivity and excited with a fast impulse.

Table 1 shows the effective length and the impulse resistance at effective length for various rise times for (i) the in-ground counterpoise only, and (ii) the in-ground

counterpoise combined with the above ground conductor. From the table, it is clear that the above ground insulated conductor increases the effective length significantly and reduces the impulse impedance.

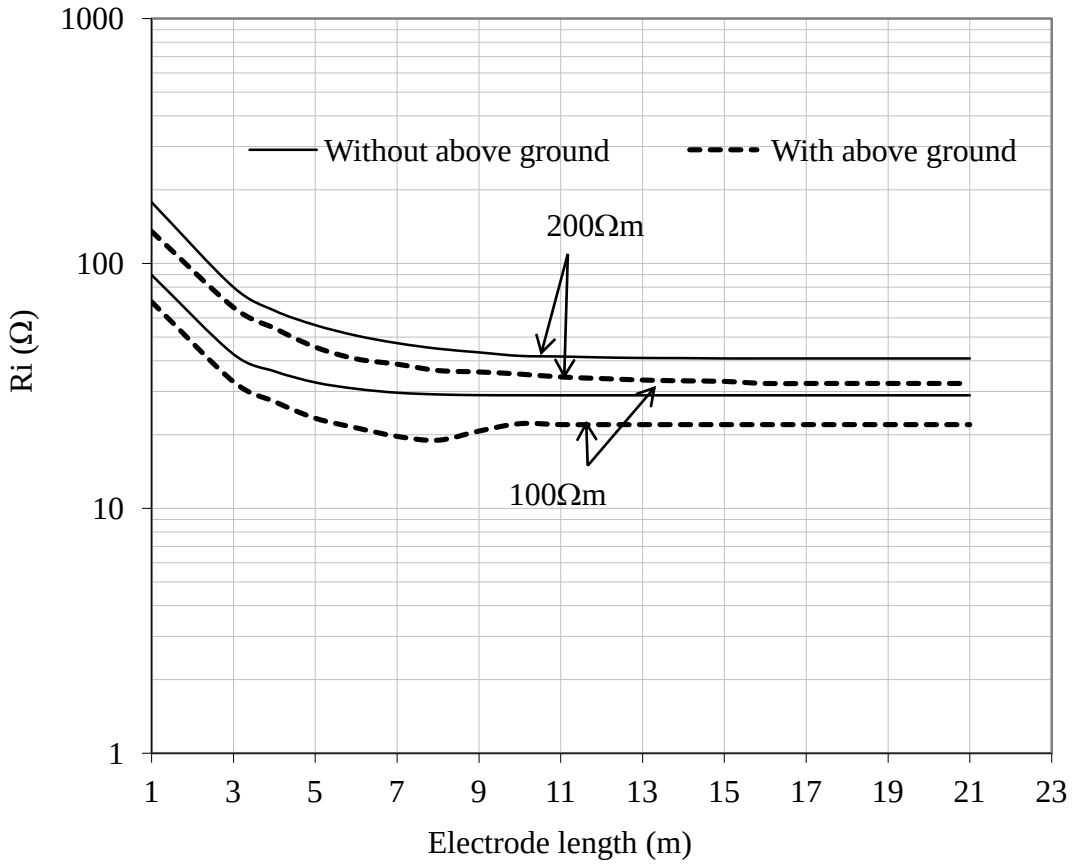

Figure 6.12: Impulse resistance vs. length conductor length with and without addition of an insulated above ground conductor (100Ωm and 200Ωm soil resistivity)

Table 1: Effective length and the impulse resistance at effective length

Impulse rise time (μs)	Effective length		Impulse resistance at effective length	
	Counterpoise	Counterpoise with above	Counterpoise	Counterpoise with above

	only	ground electrode	only	ground electrode
0.1	7m	10m	29.3Ω	22.2Ω
1	12m	16m	21.4Ω	15.5Ω
5	29m	35m	8.9Ω	6.4Ω
10	47m	60m	6.2Ω	4.9Ω

6.7.3 Earth Grid Enhancement

Figure 6.13 shows the impulse resistance of the earth grid as a function of grid area. The earth grid was assumed to be buried in 100Ωm soil and a constant mesh 5m x5m size was injected. From Figure 6.13, it is clear that the presence of the above ground insulated grid reduces the impulse resistance significantly. When the impulse is injected at the centre of the grid, there is a reduction in impedance of about 22% compared with the in-ground conductor alone when the above ground conductor is added.

The same general conclusions is reached for corner injection, where the addition of an above ground conductor reduces the impedance by about 20% compared to the in-ground conductor alone.

For higher soil resistivity (1kΩm), adding the above ground conductor reduces the corner injection impedance by 21% and the centre injection impedance by 22% (see Figure 6.14).

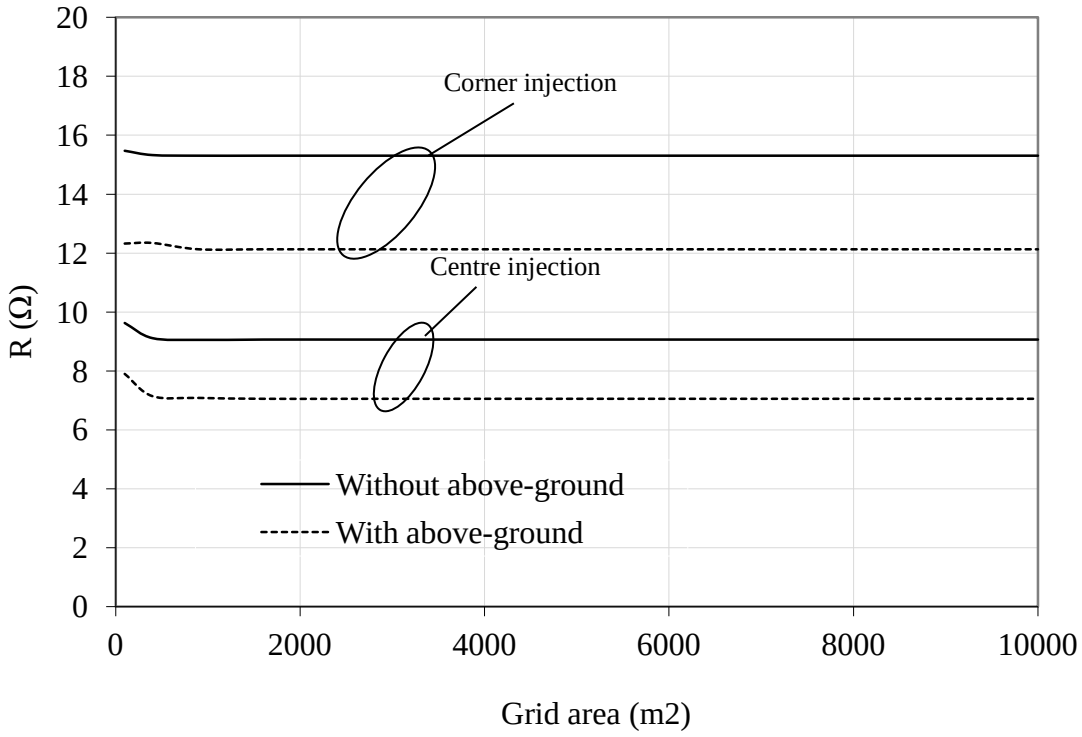

Figure 6.13: Impulse resistance as a function of grid area (0.1/5, 100Ωm)

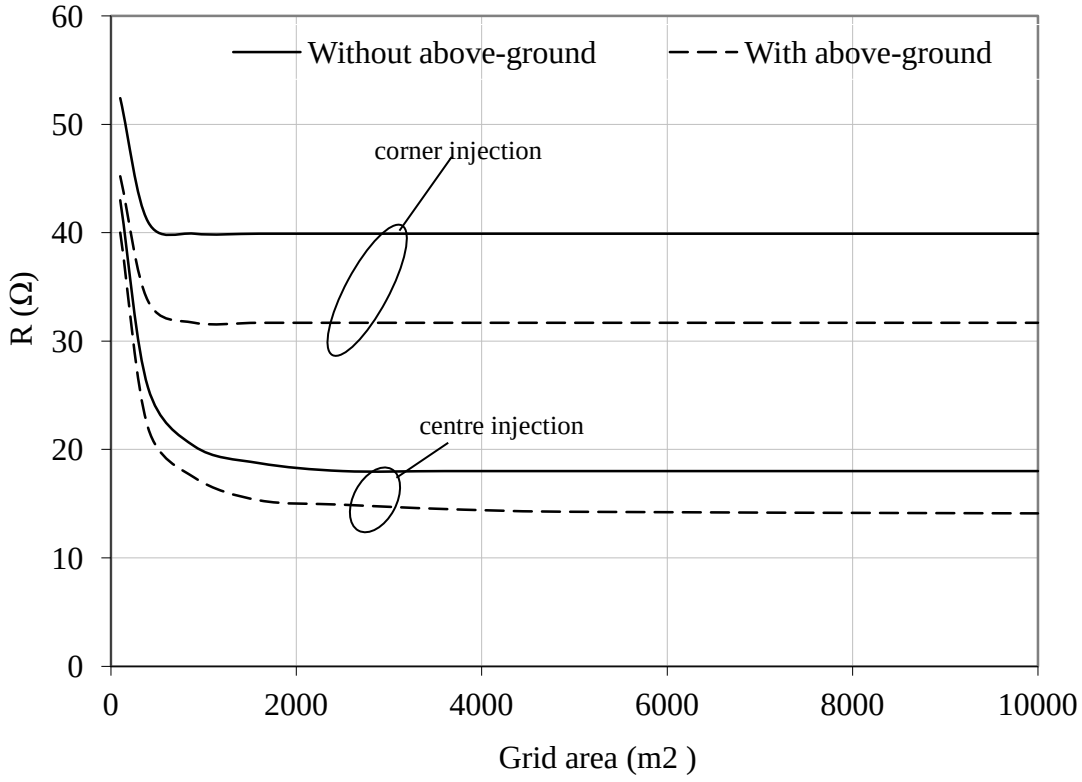

Figure 6.14: Impulse resistance as a function of grid area (0.1/5, 1kΩm)

Further simulations were carried out for slower front impulse rise times and soil resistivities of 100Ωm and 1kΩm. Figure 6.15 shows the impulse resistance at effective length as a function of front rise time. From the figure, it can be seen that the degree of reduction of the resistance for faster rise times and higher soil resistivity. For example, for 1kΩ soil resistivity, the earth impedance value for the in-ground grid only and with the above ground insulated earth grid is 18.9Ω and 13.8Ω respectively when the impulse front is 0.1μs (a reduction of about 28%). For the same condition with the rise time increased to 10μs, the impedances for the two cases 6.5Ω and 4.9Ω respectively corresponding to a reduction of about 23%. For soil of resistivity of 100Ωm with the same range of reduction percentage, the results clearly show that the above ground technique is very useful in soils of high resistivity with a larger percentage reduction when excited by a current impulse with as fast rise time.

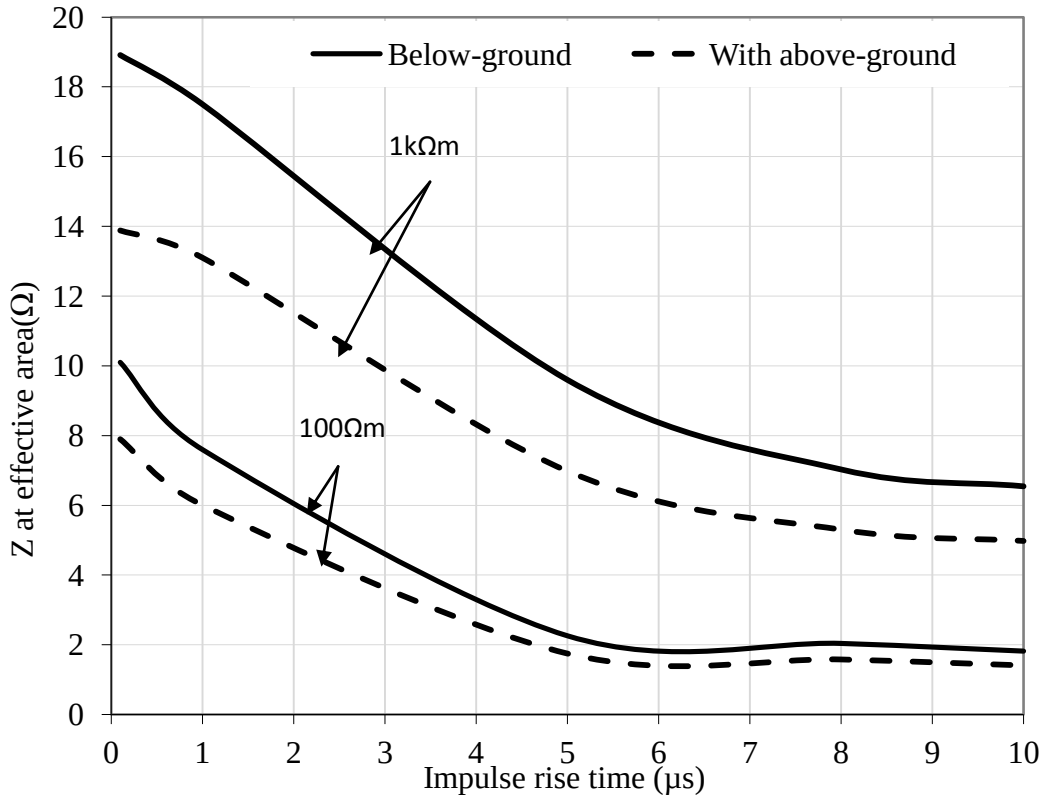

Figure 6.15: Impedance asymptotic value vs. impulse front time

6.8 Experimental Tests to Investigate the Benefits of Additional Parallel Insulated Conductor

The proposed technique was subjected to field tests using a horizontal in-ground earth electrode with a PVC insulated copper conductor of 50mm^2 cross-sectional area running parallel with the buried electrode above ground. The insulated conductor, was in sections of the same lengths as the bare buried electrode. It was bonded to the bare underground horizontal electrode at the sections points along its length, as can be seen in Figure 6.16.

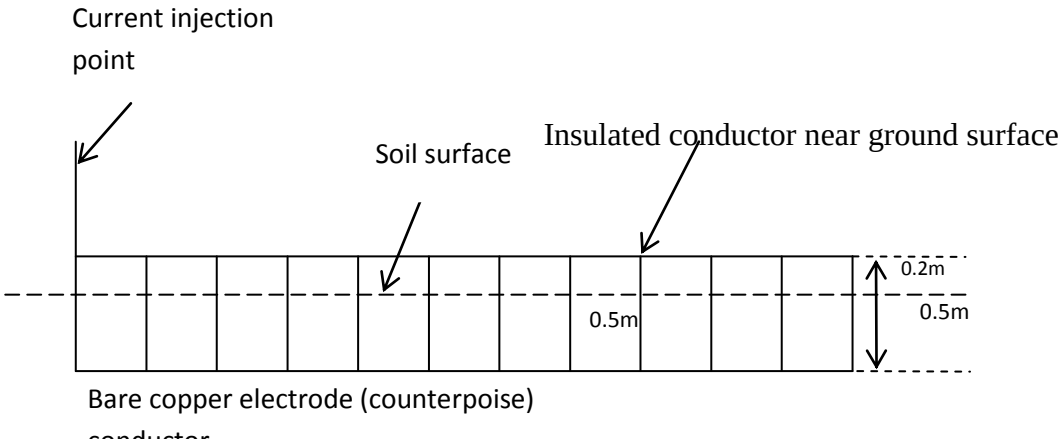

Figure 6.16: Proposed method for increasing the electrode effective length

Impulse tests were carried out for increasing lengths of electrode both with and without the additional above ground conductor. An impulse current having a 2.5μs rise time was injected at one end of the horizontal electrode. Figure 6.17 shows the calculated impulse resistance obtained from the transient voltage and current recordings for different electrode lengths. The higher impulse impedance values compared with those shown in Chapter 5 are attributed to seasonal variations in soil resistivity.

As can be seen from Figure 6.17, preliminary field tests using the proposed enhancement technique indicate that, by adding a parallel insulated conductor the impulse impedance is reduced by 22%, confirming the findings of the computer simulations. The simulations and experimental tests with the above ground insulated conductor demonstrate that the effective length of the electrode system can be increased, which contributes to the reduction of the earth impedance or the earth potential rise**.**

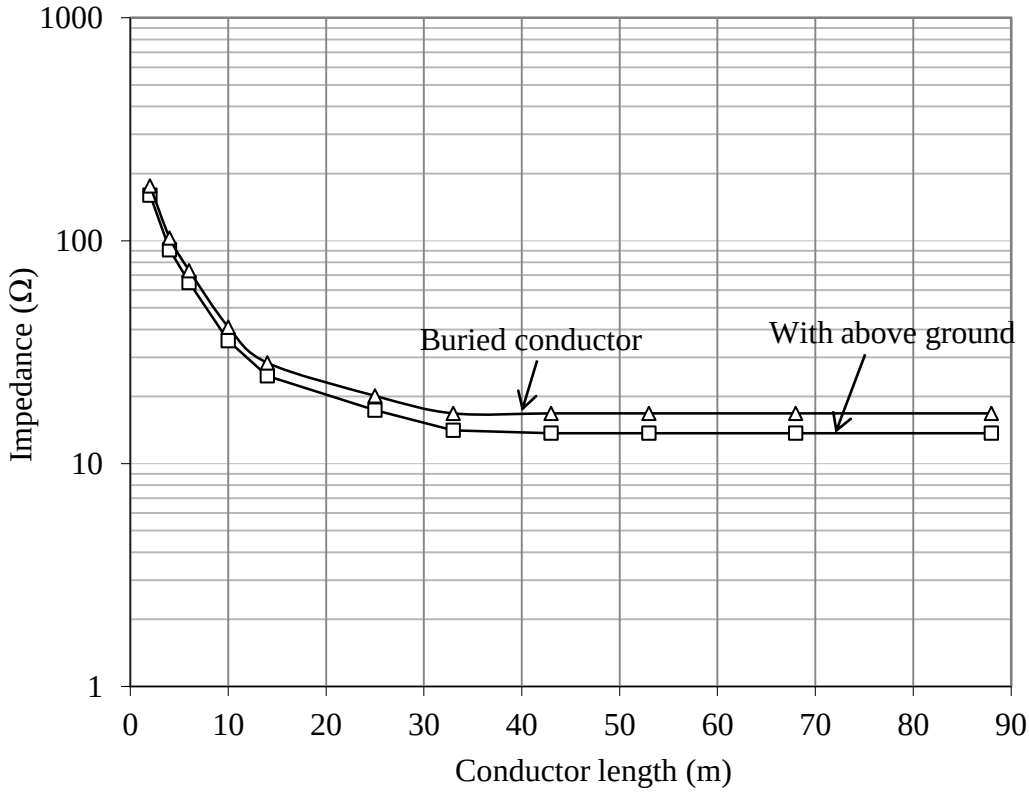

Figure 6.17: Effect of additional insulated conductor on impulse resistance as a function of horizontal earth electrode length (2.5μs)

Further tests were carried out for different rise times. Figure 6.18 shows the impulse resistance as a function of line length for a (7μs) rise time impulse. From the figure it is clear that the above ground insulated conductor has contributed to the reduction of the resistance. The impulse resistance as a function of electrode length was also calculated using the CDEGS program [6.10] for a 7μs impulse risetime and an equivalent two-layer. As can be seen from Fig.6.18, the simulated values are reasonably close to those measured at the corresponding risetime.

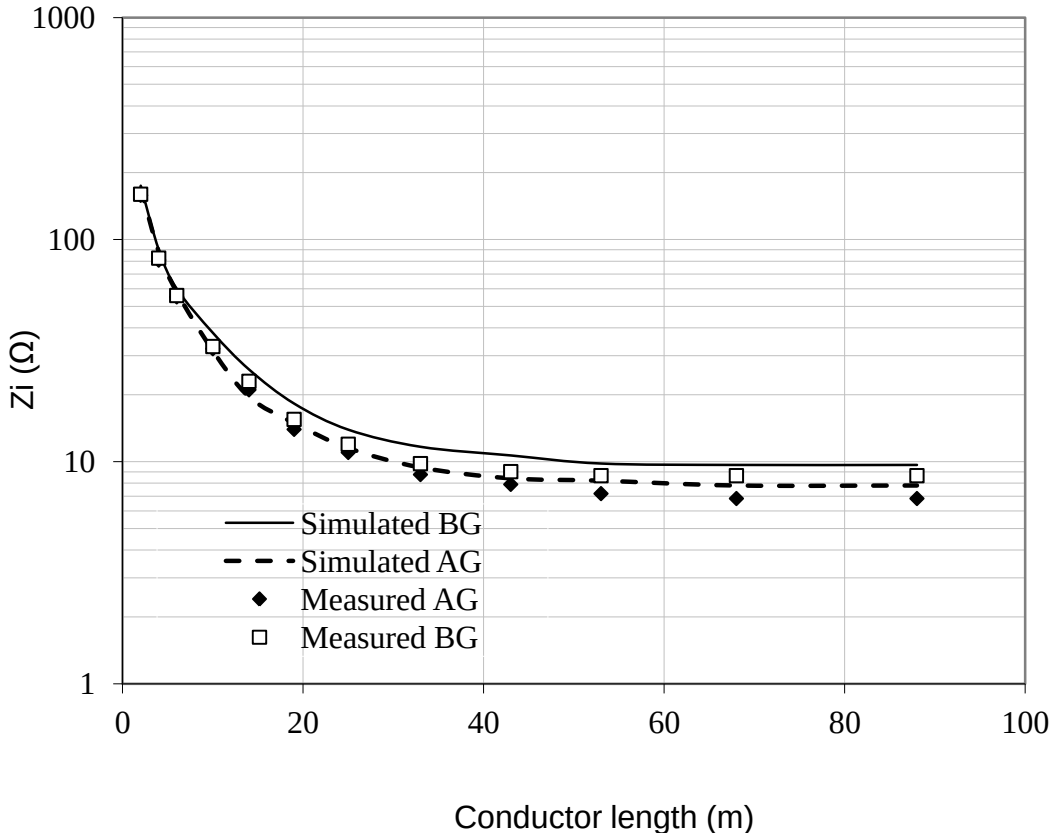

Figure 6.18: Transient impedance vs. length simulation and measurement for rise time of 7μs (AG – above ground, BG – in-ground)

6.9 Application of New Technique to Wind Turbine Earthing System

Safety requires the earthing system of wind turbines to have low impedance but, in general, onshore wind turbines are installed in high rocky terrain with high soil resistivities. Additional earth electrodes may be used in order to meet the requirements of standards [6.12-6.13]. Selected standard mitigation techniques [6.12-6.13], to reduce the wind turbine earth impedance, have been simulated in this work. These include: (i) a 20m diameter ring electrode around the tower base foundation, (ii) the ring supplemented by 4 additional vertical electrodes distributed with equal spacing (see Figure 4.1), and (iii) further enhancement by four additional radial 12.5m horizontal conductors buried at a depth of 1m and connected to the ring.

Furthermore, a new earthing arrangement (iv) is proposed and investigated in this work. This proposes to add insulated counterpoise conductors on the ground-surface directly above and connected to the buried horizontal conductors, as shown in Figure 6.19. Such an arrangement offers the benefit of enhancement without increasing the area covered by the earthing system. Variants of this arrangement involve adding additional interconnections between the insulated and buried bare horizontal conductors along their length. The insulated conductors extend the effective length of the buried horizontal earth electrodes.

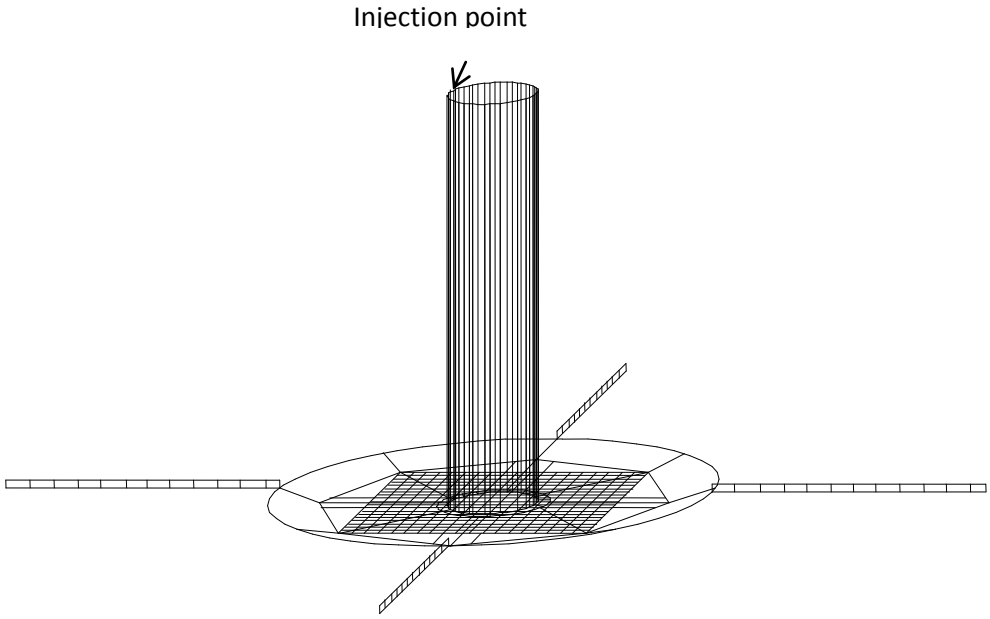

Figure 6.19: Wind turbine earthing system enhanced with proposed insulated horizontal conductors in parallel with counterpoises.

Simulations of the turbine earthing system with the above enhancement were carried out with a 10kA, 8/20 impulse current injection, assuming a 400Ωm soil resistivity and using field theory software [6.10]. The calculated values of peak voltage at the turbine base are shown in Figure 6.20. From this figure, it can be seen that adding the ring achieves a 14% reduction in transient earth potential compared with the

basic earthing arrangement. However, the addition of four vertical rods to the ring produces no substantial further reductions in transient earth potential. Arrangement (iii) with 4 horizontal conductors achieves a 25% reduction in peak transient earth potential while introducing the insulated conductors produces a further significant reduction, up to about 40% of peak transient earth potential when the system has 12 interconnecting leads. Similar trends are seen with different soil resistivities and for fast rise-time impulses. In high resistivity soil and for fast impulse (1/5) conditions, the peak transient earth potential can be reduced by up to 60% compared with the voltages developed with the basic turbine earthing system as seen in Figure 6.21.

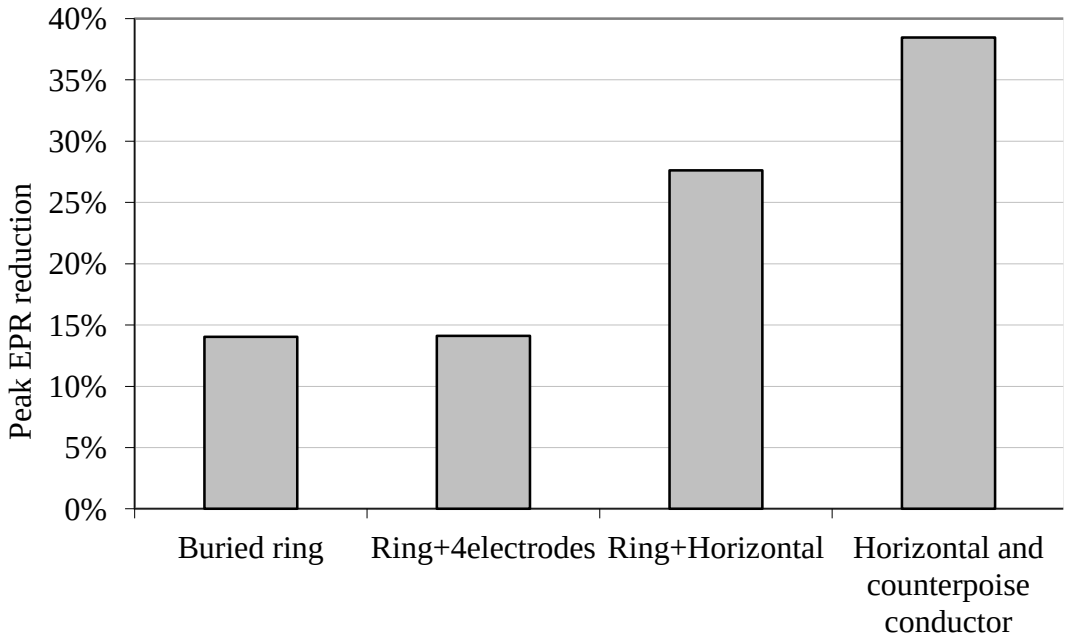

Figure 6.20: Reduction in earth surface potential rise reduction with enhanced earth systems (400Ωm and 8/20μs current impulse)

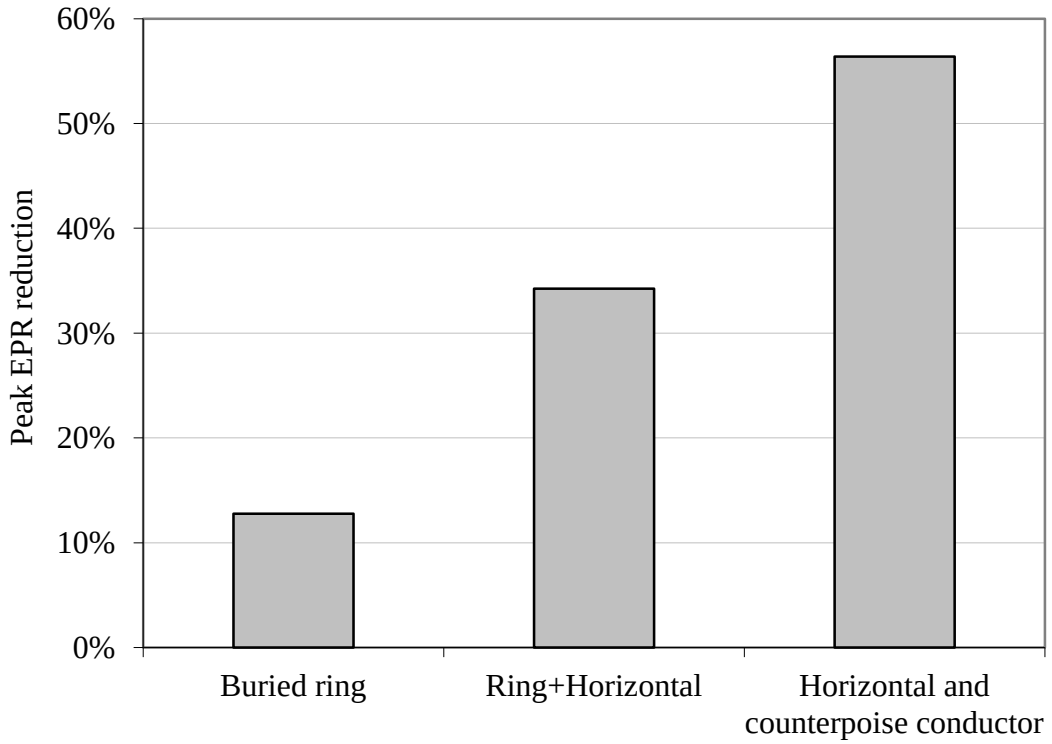

Figure 6.21: Reduction in earth surface potential rise with enhanced earth systems (400Ωm and 1/5μs current impulse)

6.10 Safety considerations in the Vicinity of Wind Turbines

In this section, current injections of 10kA 8/20 and 10kA 1/5 into the turbine earthing system were simulated. In order to compare the results, different mitigation techniques used to reduce the step and touch potentials which include; ring, 4 buried horizontal electrodes and the above ground technique - horizontal and counterpoise conductor. Three different values of soil resistivity were considered. Step and touch potentials were then calculated and the results compared.

6.10.1 Step Potential

The previous section indicates that it is necessary to allow for the above-ground structure for more accurate prediction of voltages developed at the turbine base. In this section, step voltages at a number of observation points are calculated. The results, obtained using different models are compared.

To calculate the step potential around the wind turbine, a number of observation points are placed on the earthing system and around it. These points are in the form of a profile at the base of the turbine. The step potential developed by the transient injection is calculated for each arrangement. For 400Ωm, the wind turbine was injected with 10kA, 8/20 impulse current; the step potential was calculated for two points at 1m and 5m away from the tower base. Figure 6.22 shows the reduction percentage obtained by the different mitigation techniques. As can be seen in the figure, the highest reduction percentage is achieved when the above-ground insulated conductor is connected, which is about 60% of reduction achieved by the addition of the above-ground counterpoise. The percentage of reduction depends on soil resistivity and rise time. In the case of 1/5 impulse current, the same conclusion can be drawn with the higher reduction percentage achieved by the new method as can be seen in Figure 6.23. Similar results were obtained for high soil resistivity with higher step potential magnitudes. In general, the lowest step potential values are calculated when the above-ground insulated conductor is connected.

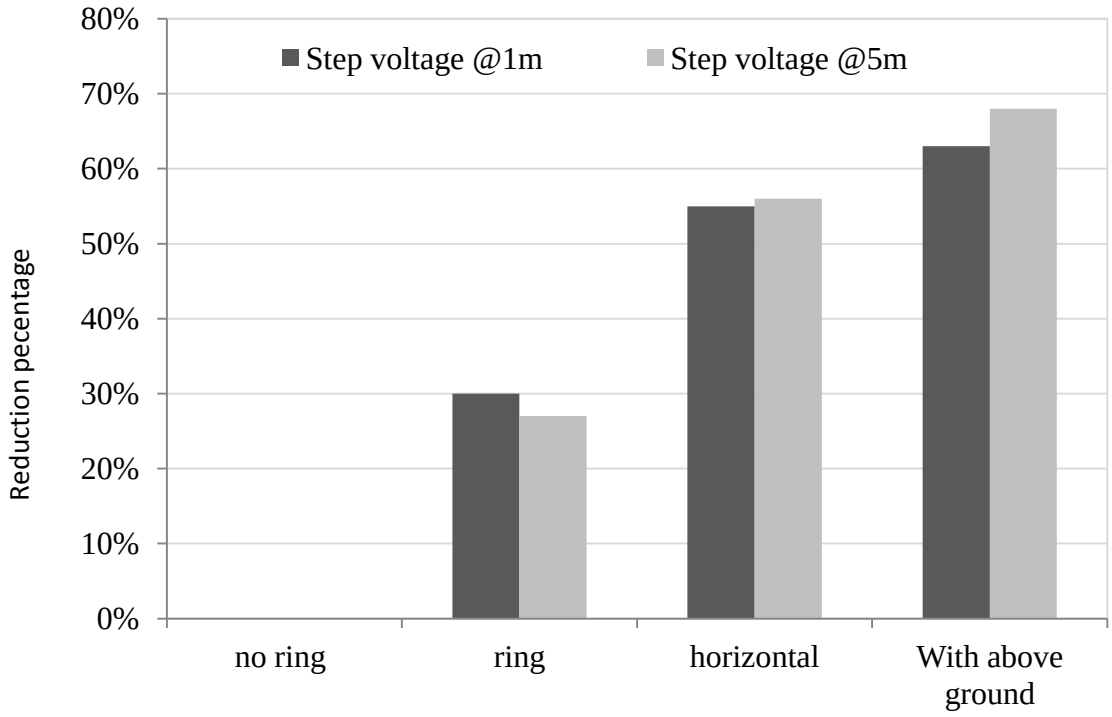

Figure 6.22: Step potential reduction 1m and 5m away from the tower with enhanced earthing systems: (10kA, 8/20 impulse and 400Ωm soil resistivity)

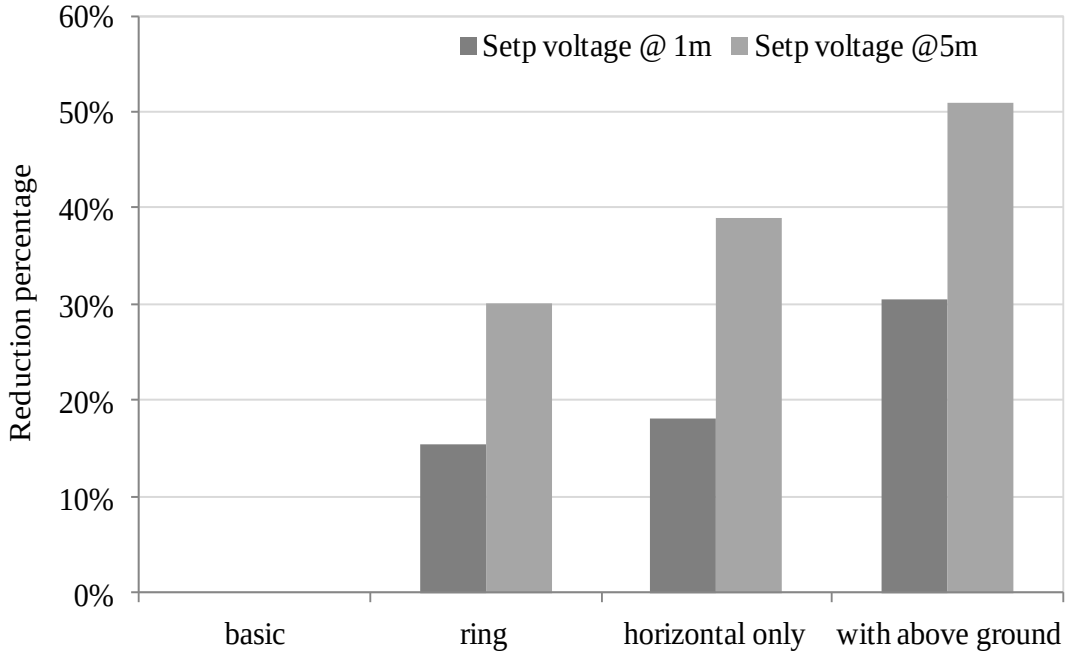

Figure 6.23: Step potential reduction 1m and 5m away from the tower with enhanced earthing systems: (10kA, 1/5 impulse and 400Ωm soil resistivity)

6.10.2 Touch Potential

In this section, the calculated touch potentials for various wind turbine earthing systems arrangements are presented. The touch potential may be defined as the difference between the TEPR and the surface potential at the point where a person is standing, while at the same time having his/her hand in contact with a ground structure [6.14]. The touch potential generated by the transient injection of 10kA impulse current into the top of the wind turbine earthing system is calculated 1m from the turbine base for all arrangements considered in this study. Figure 6.24 summarises the calculated values of touch voltages for 400Ωm soil resistivity and for the two standard current impulses. For the 8/20 impulse, it is clear from the figure that about 13% reduction in touch potential is achieved when the ring electrode is placed around the basic earthing system of the wind turbine. There is a further reduction when the horizontal electrode is connected to the earthing system and this represents approximately a 36% reduction. The maximum touch potential reduction, about 44%, is for the case of an above-ground insulated conductor connected to the wind turbine earthing system.

In the case of the 1/5 rise time, the introduction of connecting ring electrode, horizontal electrode and the above-ground enhancement are 9%, 16% and 26% respectively, as can be seen in Figure 6.24. The same conclusion is drawn in the case of higher soil resistivity with higher touch potential values for both impulses. Using these mitigation techniques offers substantial reductions in touch voltage as a result of earthing system enhancements, and these are mainly due to the reduction in overall TEPR. This further reduction in transient touch voltage obtained with the installation of a near surface potential grading ring 1m outside the perimeter of the

turbine base. As seen, the above-ground insulated conductor helps to distribute the transient currents more effectively to areas further away from the turbine base.

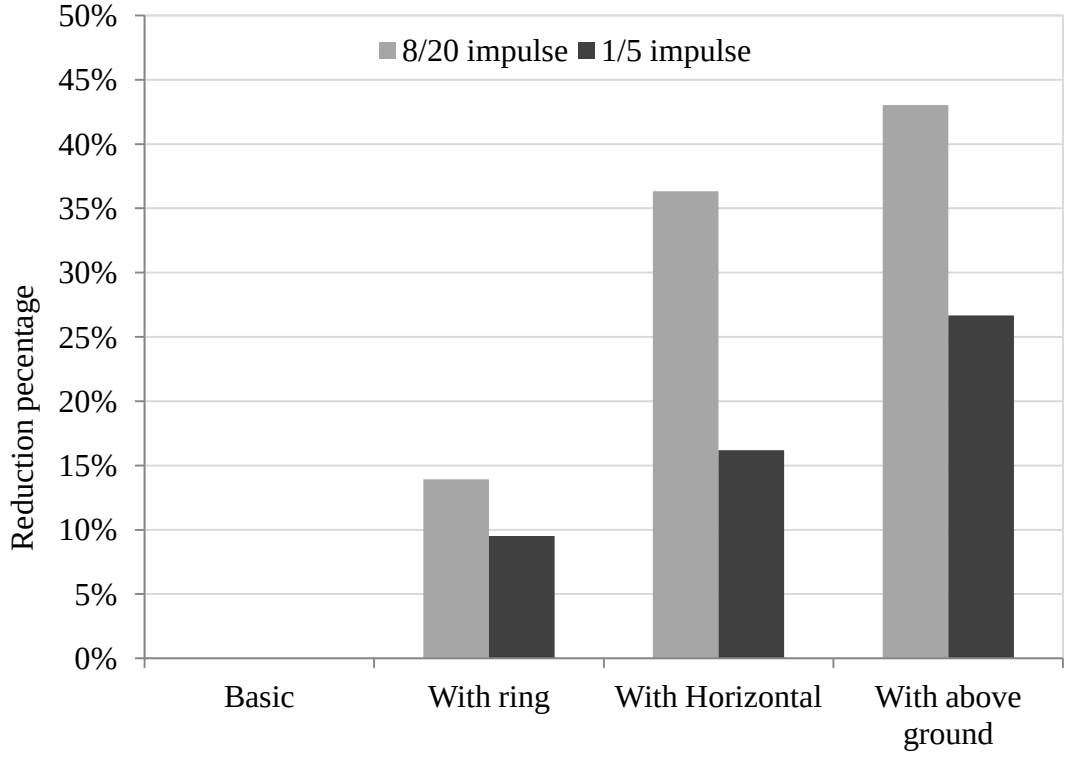

Figure 6.24: Touch potential produced by two different impulses (10kA 8/20 and 10kA 1/5 with 400Ωm)

6.11Conclusions

A new method to enhance earth electrode performance under high frequency and transient conditions has been investigated. An above ground insulated conductor can play an important role in reducing the earth impedance of both horizontal and grid earth electrodes above a particular frequency related to the soil resistivity.

In the low frequency range, no significant reduction was observed. For high frequencies, the reduction of the earth impedance is noticeable and can be explained by a reduction in the inductance of the earth electrode due to the additional parallel paths.

At high frequencies, only a small part of the earthing system contributes to reducing the earth impedance because of the effective length/area limitation. The proposed above ground insulated conductor method acts to increase the earth electrode dimension, which contributes to increasing the effective dimension beyond that for the in-ground conductor alone.

For earth electrodes fitted with the above ground insulated electrode, under impulse conditions the results show that current and voltage distributions are changed such that a greater length of buried conductor is utilised, and this contributes to the reduction in earth impedance magnitude. Hence, this reduces the developed earth potential rise at the point of current injection.

The proposed technique was applied in field tests to a horizontal earth electrode by installing an additional PVC insulated copper conductor of $50mm^2$ cross-sectional area running in parallel with the buried electrode. The results confirm the predictions of the computer simulations.

Enhancing the earthing system with the proposed above-ground insulated conductor results in a substantial reduction in the developed transient potentials at the base of the turbine structure, and this reduction is more significant than with only the buried bare horizontal conductor. The transient touch and step potentials have been examined around the turbine and along profile under fast transient conditions (8/20 and 1/5). These TEPR reductions produce associated reductions in touch and step voltages. Although it is not possible to quantify what is acceptably safe, due to the absence of recognised transient voltage safety thresholds for the human body, the proposed earthing system enhancement has the advantage of improving earthing system performance, and possibly safer earthing system.

CHAPTER SEVEN

GENERAL CONCLUSIONS AND SUGGESTED FURTHER WORK

7.1 Conclusion of the Literature Survey

A review of literature relating to the high frequency and transient performance of earth electrodes and wind farm earthing systems was carried out. The calculation of simple earth electrode impedance was described.

The open literature describes comprehensive studies on simple electrodes subjected to transient and power frequency currents. Published works clearly indicate that the earth electrode subjected to transients would behave differently from the expected power frequency behaviour, and indicate that the earth electrode impulse resistance is different from the power frequency resistance. The impulse resistance depends on a number of factors such as soil parameters, electrode geometry and impulse current rise time and magnitude. High current magnitudes with fast rise times can cause soil ionisation around the electrode and reduce the earth resistance. Soil ionisation is more likely to occur in high soil resistivity, but not with large earthing systems due to lower current density.

Investigators have attempted to characterise the behaviour of earth electrodes using a number of different approaches involving high-voltage testing both in the laboratory and on earth electrodes installed in the field. In particular, the literature has clearly identified the difficulties of measuring and testing the earthing systems of the wind turbines and the extended earth electrodes of wind farms.

The standards dealing with the recommendations for earthing systems contain guidelines for design of the earthing system, where the earthing system is designed primarily for power frequency earth fault conditions. However, limited guidance is given in the standards for transient conditions.

Different earthing arrangements for wind turbines are presented and reviewed and the limitations of measurement procedures have been highlighted. Due the fact that wind farm earthing system contains a large amount of inductive component, the DC measurements is likely to be different from AC response. Therefore, AC tests should always be employed on such systems.

Published work has identified the length of an earth electrode as being an important parameter affecting its performance. Many researchers have studied the transient performance of the horizontal earth electrode and an empirical formula for calculating the effective length has been proposed. Most of these studies have used simulation and circuit theory methods and limited experimental work has been reported.

The models presented in the available literature simulate a simple electrode and the tower of the wind turbine was not taken into account, but the tower may contain inductive elements which must be taken into account for accurate modelling of the wind turbine.

7.2 General Conclusion of Generic Earth Electrode

The response of the earth electrode under variable frequency and for different soil resistivities is described. Parametric studies were carried out for simple electrodes such as vertical and horizontal earth electrodes. Further investigations were carried out to include complicated earthing systems such as a large substation earthing grid. The earthing system performance mainly depends on the soil resistivity, soil permittivity, and the dimensions of the earthing system and the location of the injection point. The frequency is an important factor that affects the performance of the earthing system. The results have demonstrated the limitation of the circuit

model in predicting the performance of the earth electrode at high frequency. For large earthing systems, computer models and simulation techniques may produce more reliable predictions of earth electrode performance than the circuit model.

The investigations have shown that the inductive effects become significant for all earth electrode systems above a threshold frequency for a given soil resistivity. The frequency is an important factor that affects the performance of the earthing system. The impedance of earth electrodes increases remarkably at high frequency due to the inductive effect of the earth electrode, particularly at low soil resistivity. The earthing system impedance increases with the soil resistivity. The earth grid under variable frequency is presented and similar results to those of the horizontal earth electrode are noticed.

a) The simulations results have revealed that the impedance magnitude decreases with increasing electrode length up to a certain length when the electrode reaches its effective length, beyond which increasing the length no longer affects the earth impedance magnitude, b) The capacitive effect becomes evident at high frequencies for high soil resistivity, especially with high permittivity, c) The earth impedance of the earth electrode increases with the increase of soil resistivity.

The same concept of the effective length of the horizontal electrode has been confirmed to be applicable to the earth grid effective area. Increasing the grid area has significant effect in reducing the earth grid impedance until it reaches its effective area after which increasing the grid size results in no reduction of the earth grid impedance.

The effect of the injection point location has been studied, it was found that the injection point location has no effect on the earth impedance at low frequencies due to the resistive behaviour of the earth grid. A centrally injected earth grid has lower

impedance magnitude than corner injected earth grid for high frequencies. This may be explained by the corner injection having higher inductance than the centrally injected grid.

The impulse response of different electrode configurations was studied. Two different standard wave shapes and a wide range of soil resistivities were considered. The results clearly show that the transient earth impedance and TEPR peaks of all electrode configurations increase with resistivity. The TEPR and the impedance significantly decrease with the increase of the relative permittivity in soils of high resistivity.

7.3 Wind Turbine Earthing System

The effects of soil resistivity, soil relative permittivity and above-ground structure of the wind turbine under variable frequency and transient conditions are investigated. The results have shown that the inductive component become significant for wind turbine earthing system above a particular frequency for a given soil resistivity, resulting in an increase in wind turbine earth impedance for both onshore and offshore wind turbines. For high soil resistivity (10kΩm) and at high frequency the earth impedance magnitude tends to drop with increase in frequency which may suggest a capacitive effect. It is found that interconnection of adjacent on-shore wind turbines has benefit in reduction of EPR and TEPR.

It was established that, for high frequency and transient currents, the magnitude of wind turbine earth impedance seen from the point of injection is significantly higher when the above-ground turbine structure is taken into account. Also, the calculated transient earth potential rise at the tower base ground surface is higher when the model includes the above-ground structure.

7.4 Effect of Electrode Dimension

A two layer soil resistivity model was derived from the soil resistivity measurements and used in the simulations when conducting a comparison between simulation and field measurements. An 88m long horizontal electrode was installed with 13 junction boxes in order to vary the measured length as required, to allow quantification of the effective length. The results show that the DC earth resistance decreases with the length of the conductor. A large proportion of the injected impulse current is dissipated into the ground along a length close to the injection point. The effective length of the electrode was determined from the impulse impedance, and was found to be comparable to that predicted by a simplified empirical expression and computer simulations.

A large proportion of the injected impulse current is dissipated into the ground along the earth conductor but within a length close to the injection point.

7.5 New proposed method and its application to wind turbine

A new proposed method to enhance the earth electrode performance under variable frequency and transient conditions has been investigated. The above-ground insulated conductor method plays an important role in reducing the earth impedance for both horizontal and grid earth electrodes. In the low frequency range no significant reduction was observed due to the resistive behaviour of the soil at low frequencies. For high frequencies the reduction is more noticeable. At high frequencies, only a small part of the earthing system contributes to reducing the earth impedance due to the effective length/area limitation. The above-ground method may act to increase the earth electrode dimension able to contribute to further reduction beyond the effective dimension.

The time domain of the in-ground earth electrodes fitted with an above ground insulated electrode was studied. The results show that the current and voltage distribution are changed such that a greater length of buried conductor is utilised and that this contributes to an additional reduction in the earth impedance and, hence, the developed earth potential rises at the point of current injection.

The proposed technique was applied in field tests to the horizontal earth electrode by installing an additional PVC insulated copper conductor of 50mm^2 cross-sectional area running in parallel with the buried electrode. The results confirm the findings of the computer simulations.

Enhancing the wind turbine earthing system with the proposed above-ground insulated conductor results in a substantial reduction in the developed transient potentials at the base of the turbine structure, and this reduction is more significant than with only the buried bare horizontal conductor. The transient touch and step potentials have been examined around the turbine and along the radial profile under fast transient conditions (8/20μs and 1/5μs impulse currents). These TEPR reductions produce associated reductions in touch and step voltages.

7.6 Further Work

Further simulations are necessary to quantify the performance of the wind turbine earthing system in terms of safety potentials to yield guidelines for design.

The followings are suggested to provide a better understanding of wind turbine earthing system behaviour:

(a) DC, AC and impulse measurements of resistance/ impedance of an isolated wind turbine.

(b) DC, AC and impulse measurement of resistance/ impedance of the wind turbine used in (a) above when part of an interconnected wind farm.

(c) Field measurement of safety voltages (step and touch voltages) around an isolated wind turbine.

(d) Field measurements of safety voltages (step and touch voltages) around the same wind turbine when its earthing system is bonded connected to the wind farm earthing network.

The new proposed method using the above ground/insulated conductor requires further examination under various conditions particularly field measurements on the 88m long bare earth conductor installed at the university test field. The measurements should include safety potentials and current distribution when the above ground insulated conductor is connected.

REFERENCES

Chapter One

[1.1] Bell, H.: 'Protection of a.c Systems', Journal of IEE, 6, Vol.70, pp. 571-575

[1.2] Say, M. G.: 'Electrical Earthing and Accident Prevention' (Gorge Newnes Limited, London, 1954)

[1.3] Tagg, G. F.: 'Earth Resistance.' Gorge Newnes Limited. (London), 1964.

[1.4] IEEE guide for safety in AC substation grounding., ANS/IEEE standard 80,2000.

[1.5] Electricity Association: 'Engineering Recommendation S.34: A guide for assessing the rise of earth potential at substation sites.' Engineering Management Conference, May 1986.

[1.6] IEEE: 'IEEE Std 81-1983, IEEE Guide for Measuring Earth Resistivity, Ground Impedance, and Earth Surface Potential of Ground System', IEEE, New York, 1983.

[1.7] IEEE: 'IEEE Std 81.2-1991, IEEE Guide for measurement of Impedance and Safety Characteristics of Large, Extended of Interconnected Grounding Systems', IEEE, New York, 1991.

[1.8] Technical Specification 41-24, Guidelines for the Design, Testing and Maintenance of Main Earthing Systems in Substations, Electricity Association, 1992.

[1.9] Rogers E.J., and White J.F: 'Mutual Coupling Between Finite Lengths of Parallel or Angled Horizontal Earth Return Conductors.' IEEE Transactions on Power Delivery, January, Vol. 4, No. 1, pp. 103-113, 1989.

[1.5] Golde R.H. (Editor), Lightning Vol.1: Physics of Lightning, Academic Press,

London, ISBN 0-12-287801-9, 1977.

[1.11] IEC 479-2, 'Guide to effects of current passing through the human body Part 2: Special Aspects', BSi Standards, 1987.

[1.12] ITU-T (International Telecommunication Union): 'Calculating Induced Voltage and Currents in Practical Cases.' Volume II, 1999

[1.13] International Electro-technical Commission IEC Report 479-1: 'Effects of current passing through the human body', IEC, 1984.

[1.14] Dalziel, C.F., and Lagen, J.B: 'Electric Shock', AIEE Transactions, Vol. 60. pp. 1073-1079, 1941.

[1.15] Bewley, L.V: 'Theory and tests of the counterpoise', AIEE Transactions on Electrical Engineering, 12632, pp. 1163 – 1172, 1934.

[1.16] Bellaschi, P.L: 'Impulse and 60-cycle characteristics of driven grounds', AIEE Transactions on Electrical Engineering, March, Vol. 60, pp. 123 – 128, 1941.

[1.17] Bellaschi, P.L., Armington, R,E., and Snowden, A.E: 'Impulse and 60-cycle characteristics of driven gounds –II', AIEE Transactions on Electrical Engineering, Vol. 61, pp. 349 – 363, 1942.

[1.18] Bellaschi, P.L., and Armington, R.E: 'Impulse and 60-cycle characteristics of driven gounds -III: Effect of lead in ground installation', AIEE Transactions on Electrical Engineering, Vol. 62, pp. 335 – 345, 1943.

[1.19] Berger, K: 'The behaviour of earth connections under high intensity impulse currents', Cigre Paper No. 215, 1946

[1.20] Petropoulos, G.M: ‘The high-voltage characteristics of earth resistances’, Journal of the IEE, Vol. 95, pp. 59 – 70, 1948.

[1.21] Kosztaluk, R., Loboda, M., and Mukhedkar, D: ‘Experimental study of transient ground impedances.’, IEEE Transaction on Power Apparatus and Systems, Vol. PAS-100, No. 11, pp. 4653 – 4660, 1981.

[1.22] Velazquez, R., and Mukhedkar, D: ‘Analytical modelling of grounding electrodes transient behaviour.’, IEEE Transaction on Power Apparatus and Systems, Vol. Pas 103, No. 3, pp. 1314 – 1322, 1984.

[1.23] 'Aguado, M., Hermoso, B., Senosiain, V., and Martinez-Cid, P:

‘Lightning: earthing electrodes harmonic response’, 11th ISH, London, 23 - 27 August, pp. 2.262.S15 - 2.266.S15, 1999.

[1.24] Mohammed Nor, N., Srisakot, S., Griffiths, H., and Haddad, A: ‘Characterisation of soil ionisation under fast impulses’, 25rd ICLP, Rhodes, Greece, pp. 417 – 422, 18-22 September, 2000.

[1.25] Sonoda, T, Takesue, H., and Sekioka, S: ‘Measurements on surge characteristics of grounding resistance of counterpoise for impulse currents’, 23rd ICLP, Rhodes, Greece, pp. 411 – 416, 18-22 September, 2000.

[1.26] Meliopoulos, A.P., Moharam, M.G: ‘Transient analysis of grounding systems’, IEEE Transaction on Power Apparatus and Systems, Vol. 102, No. 2, pp. 389 – 399, 1983

[1.27] Grcev, L.D: 'Computer analysis of transient voltages in large grounding systems', IEEE Transactions on Power Delivery, Vol. 11, No. 2, April, pp. 815 – 823, 1996.

[1.28] Grcev, L.D., and Menter, F.E: 'Transient electromagnetic fields near large earthing systems', IEEE Transactions on Magnetics, Vol. 32, No. 3, pp. 1525 – 1528, 1996

[1.29] Davies, A.M: 'High Frequency and Transient Performance of Earthing Systems', PhD thesis, Cardiff University 1999.

[1.30] Grcev, L.D., and Popov. M: 'On High-Frequency Circuit Equivalents of a Vertical Ground Rod' IEEE Transactions on Power Delivery, Vol. 20, No. 2, April 2005.

[1.31] CDEGS, HIFREQ Module, Safe Engineering Services, Montreal Canada, 2010.

Chapter Two

[2.1] Dwight H.B.: 'Calculation of resistance to ground.' Electrical Engineering, , pp 1319 – 1328, December 1936.

[2.2] Schwarz S.J.: 'Analytical expressions for the resistance of grounding system.' July 1951, pp368-402 (Translated from the original French in IEEE guide for safety in AC substation grounding., ANSI/IEEE standard 80,1986).

[2.3] Laurent P.: 'Les bases générales de la technique des mises à la terre dans les installations électriques.' Le bulletin de la Société Française des Electriciens,

1967(Translated from the original French in IEEE guide for safety in AC substation grounding, ANSI/IEEE standard 80,1986.

[2.4] Tagg G.F.: 'Earth Resistance.' (George Newnes Ltd, England, 1964)

[2.5] Sunde E. D., Earth conduction Effects in Transmission line Systems, Dover Publications Inc., 1968.

[2.6] ENA ER/S.34, 'A guide for assessing the rise of earth potential at substation sites', Energy Network Association, Issue 1, 1986.

[2.7] Edison Electric Institute. 'EHV Transmission Line Reference Book.' USA(1968) .

[2.8] Endrenyi. J, Analysis of Transmission Tower Potentials During Ground Faults, IEEE Transactions on Power Apparatus and Systems, Vol.PAS-86, No.10, p.1274, October 1967.

[2.9] IEEE Guide for Safety in AC Substation Grounding. (2000) ANSI/IEEE Standard 80.

[2.10] BS 7354:1990: 'Code of practice for the design of high-voltage open terminal stations.' British Standards Institution, HMSO, London.

[2.11] Electricity Association Technical Specification 41-24. (1992) 'Guidelines for the design, installation, testing and maintenance of main earthing systems in substations.' Electricity Association, London.

[2.12] Davies. A.M: 'High Frequency and Transient Performance of Earthing Systems', PhD thesis, Cardiff University, 1999.

[2.13] Griffiths. H: 'Aspects of Earthing System under Variable and Impulse Conditions', PhD thesis, Cardiff University, 2008.

[2.14] Grcev, L. D; Popov, M.; , "On high-frequency circuit equivalents of a vertical ground rod," IEEE Transactions on , Vol.20, No.2, pp. 1598- 1603, Power Delivery, April 2005

[2.15] Grcev, L.D., and Arnautovski, V: 'Comparison Between Simulation and Measurement of Frequency Dependent and Transient Characteristics of Power Transmission Line Grounding', 24th Int. Conf. on Lightning Protection ICLP-98, Birmingham UK, pp 524-529.

[2.16] Grcev, L.D.,, Computer Analysis of Transient Voltages in Large Grounding Systems, IEEE Transactions on Power Delivery, Vol.11, No.2,p p.815-819, April 1996.

[2.17] Grcev, L.D., F.Dawalibi, An electromagnetic Model for Transients in Grounding Systems, IEEE Transactions on Power Delivery, Vol.5, No.4, p.1773, November 1990.

[2.18] Grcev, L.D., M.Heimbach, Frequency Dependant and Transient Characteristics of Substation Grounding Sytems, IEEE Transactions on Power Delivery, Vol.-12, No.1, Jan 1997.

[2.19] H.M.Towne, Impulse Characteristics of Driven Grounds, General Electric Review, Vol.31, No.11, p.605, November, 1928.

[2.20] Bewley. L.V, Theory and Tests of the Counterpoise, Electrical Engineering, No.53, p 1163, August 1934.

[2.21] Bellaschi, P.L. Impulse and 60-Cycle Characteristics of Driven Grounds, AIEE Transactions, Vol.60, p.123, March 1941.

[2.3] Bellaschi, P.L. Armington R.E., Snowden. A.E: Impulse and 60-Cycle Characteristics of Driven Grounds -II, AIEE Transactions, Vol.61, p.349, 1942.

[2.23] Berger. K:'The Behaviour of Earth Connections Under High Intensity Impulse Currents', CIGRE Paper No.215, 1946.

2.24] Petropoulos G.M., The High-Voltage Characteristics of Earth Resistances, Journal of the IEE, Vol.95, p59, 1948.

[2.25] Liew. A.C, Darveniza. M: Dynamic Model of Impulse Characteristics of Concentrated Earths, Proc IEE, Vol.121, No.2, p.122, February 1973.

[2.26] Gupta. B.R, Thapar. B: Impulse Impedance of Grounding Grids, IEEE Transactions on Power Apparatus and Systems, Vol.PAS-99, No.6, p.2357 Nov/Dec 1980.

[2.27] Gupta. B. R, V.K.Singh V. K: Impulse Impedance of Rectangular Grounding Grid, IEEE Transactions on Power Delivery, Vol.7, No.1, p.214, January 1991.

[2.28] Ramamoorty. M, Babu. M, Narayanan. M, Parameswaran. S, Mukhedkar. D, Transient Performance of Grounding Grids, IEEE Transactions on Power Delivery, Vol.4, No.4, p.2053, October 1989.

[2.29] Velazquez. R, Mukhedkar. D: Analytical Modelling of Grounding Electrodes Transient Behaviour, IEEE Transactions on Power Apparatus and Systems, Vol.PAS-103, No.6, p.1314, June 1984.

[2.30] R.Kosztaluk. P, Loboda. M, Mukhedkar. D: Experimental Study of Transient Ground Impedances, IEEE Transactions on Power Apparatus and Systems, Vol.PAS-100, No.11, p.4653, November 1981.

[2.31] Geri. A, Veca. M. G, Garbagnati. E,Sartorio. G: Non-linear Behaviour of Ground Electrodes Under Lightning Surge Currents: Computer Modelling and Comparison with Experimental Results, IEEE Transactions on Magnetics, Vol.28, No.2, March, 1992.

[2.32] Almeida. M. E, Correia de Barros. M.T: "accurate modelling of Rod Driven Tower Footing Resistance", IEEE Transaction on Power Delivery, Vol.11, No.3, pp.1606-1609., July 1996

[2.33] Skioka. S, Hayashida. H, T. Hara, Ametani. A: 'Measurement of Grounding Resistance for High Impulse Currents', IEE proceedings Generation, Transmission and Distribution, Vol. 145, pp. 693-699, 1998.

[2.34] Stojkovic, M.S. Savic, J.M. Naham, D. Salamon, B. Bukorovic, 'Sensitivity Analysis of Experimental Determined Grounding Grid Impulse Characteristics', IEEE Transaction on Power Apparatus and Systems, Vol. PAS 13, No. 4, pp 1136-1141, October 1998.

[2.35] Cotton. I, "the Ionisation Process', ERA Conference 2000, pp. 4.4.1-4.4.11, 2000.

[2.36] J. Wang. J, Liew. A. C, Darveniza. M: 'Extension of Dynamic Model of Impulse Behaviour of Concentrated Ground at High Currents', IEEE Transaction on Power Delivery, Vol.20, No.3, pp.2160-2165., July 2005.

[2.37] Mousa. A.M, The Soil Ionisation Gradient Associated With Discharge of High Currents Into Concentrated Earths, IEEE Transactions on Power Delivery, Vol.9, No.3, p.1669, July 1994.

[2.38] Grcev. L.D, Menter F.E: Transient Electromagnetic Fields Near Large Earthing Systems, IEEE Transactions on Magnetics, Vol.32, No.3, p.1525, May 1996.

[2.39] Grcev. L.D, Arnautovski V: 'Grounding and Transient: Some Fundamental Considerations', IEEE Bologna PowerTech conference, Italy, June 23-26, 2003

[2.40] Chen. Y and Chowdhuri. P: "Correlation between laboratory and field tests on the impulse impedance of rod-type ground electrodes," *Proc. Inst.Elect. Eng. Generation Transm. Distrib.*, vol. 150, no. 4, pp. 420–426, Jul. 2003.

[2.41] Nor. N.M., 'Review: Soil Electrical Characteristics Under High Impulse Currents', IEEE Transaction on Electromagnetic Compatibility, Vol.48, No.4, pp.826-829., November 2006.

[2.42] BSEN 62305:2006 ' Protection Against Lightning', Parts 1-4, British Standard 2006.

[2.43] IEC Technical Report, "Wind Turbine Generation System -24: Lightning Protection", TR61400-24, 2002.

[2.44] Jenkins. N, Vaudin. A: "Earthing of Wind farms" Renewable Energy, 17-19 November 1993, Conference Publication No. 385 IEE 1993.

[2.45] Tagg G.F.: 'Measurement of the resistance of physical large earth-electrode systems.' IEE Proceedings, 1970, 117 (11) pp.2185-2189.

[2.46] Hatziargyrious. N, Lorentzou. M, Cotton. I, Jenkins. N: "Windfarm Earthing" The Institution of Electrical Engineers, IEE, Savoy Place, London, 1997

[2.47] Cotton. I: "Windfarm Earthing" in Proc International Symposium on High Voltage Engineering, Vol.2, pp. 288-291, London, UK, 1999.

[2.48] Hatziargyrious. N, Lorentzou. M, Cotton. I, Jenkins. N: "Transferred Overvoltages by Windfarm Grounding Systems" Proceedings of ICHQP conference, 14-16 October 1998, Athens, Greece.

[2.49] Lorentzou, M., Hatziargyrious, N., Papadias, B. (2000) "Analysis of Wind Turbine Grounding System", Proc 10th Mediterranean Eletrotechnical Conference (MELECON 2000, pp. 936-939, Vol.3).

[2.50] Yasuda. Y, Fnabashi. T: "Transient Analysis on Wind Farm Suffered from Lightning" Proceeding of 39th International Universities Power Engineering Conference, pp.202-206, 2004.

[2.51] Yasuda. Y, Fnabashi. T: "Lightning Analysis on Windfarm-Sensitivity Analysis on Earthing" Proceedings of the 27th International Conference on Lightning Protection, Sep 2004.

[2.52] Kontargyri V. T, Gonos. I. F, Stathopulos. I. A: 'Frequency Response of Grounding System of Wind Turbine Generators', Proceedings of the XIVth International Symposium on High Voltage Engineering, Tsinghua University, Beijing, China, August 25-29, 2005

[2.53] Yasuda. Y, Toshiaki F: "How Does Earth Electrode Effect on Wind Turbine" Proceeding of 42nd International Universities Power

Engineering Conference, pp.796-799, 2007.

[2.54] Ukar. O, I. Zamora. I: 'Wind farm grounding system design for transient currents', Renewable Energy, Vol 36, Issue 7, July 2011, pp. 2004-2010, 2011

[2.55] Mazetti. C and Veca. G. M: 'Impulse behavior of .grounding electrodes', IEEE Trans. Power App. Syst., Vol 102, no. PAS-9, 3148-3154, 1983.

[2.56] Ghosh. S, Munshi. S, Biswas. J. R: "Computer aided analysis of surge behaviour of an earthing counterpoise discharging impulse current to ground," Journal of the Institution of Engineers India, vol. 77, pp. 128-132, November 1996.

[2.57] Farag. A. S, Cheng. T. C, Penn. D: "Grounding terminations of lightning protective systems", IEEE Trans. Dielectrics Elect. Insul. 5 (6) 869–877, 1998.

[2.58] Lorentzou. M. I, Hatziargyriou. N. D: 'Effective Dimensioning of Extended Grounding Systems For Lightning Protection', Proceedings of the 25th International Conference On Lightning Protection, Greece, p.435-439 September 2000.

[2.59] Griffiths. H, Davies. M: 'Effective Length of earth electrodes under high Frequency and Transient Conditions', Intrnational Conference on Lightning Protection, Vol. 1, Rhodos Greece, pp 536-540, 2000.

[2.60] Chonghui Lu, Jinliang He , Yanqing Gao, Rong Zeng, Jun Zou, 'Effective length of extended earthing electrode under lightning impulse' XIII International Symposium on High Voltage Engineering, Netherlands 2003

[2.61] Liu. Y, Theethayi. N, Thottappillil. R: “Investigating the validity of existing definitions and empirical equations of effective length/area of grounding wire/grid for transient studies,” J. Electrostat., vol. 65, pp. 329–335, 2007.

[2.62] Liu. Y, Theethayi. N, Thottappillil. R: “An Engineering Model for Transient Analysis of Grounding System under Lightning Strikes: Non Uniform Transmission-Line Approach," *Power Delivery, IEEE Transactions on* , vol.20, no.2, pp. 722- 730, April 2005

[2.63] Grcev. L. D, Heimbach. M: “Frequency Dependant and Transient Characteristics of Substation Grounding Sytems", IEEE Transactions on Power Delivery, Vol.-12, No.1, Jan 1997.

[2.64] Zeng. R, Gong.X, He J, Zang. B, and. Gao. Y, “Lightning impulse performances of grounding grids for substations considering soil ionization,”IEEE Trans. Power Del., vol. 23, no. 2, pp. 667–675, Apr.2008.

[2.65] Grcev. L. D: "Lightning Surge Efficiency of Grounding Grids," Power Delivery, IEEE Transactions on , vol.26, no.3, pp.1692-1699, July 2011

Chapter Three

[3.1] Tagg G.F.: ‘Earth Resistance.’ (George Newnes Ltd, England, 1964)

[3.2] Sunde E. D., Earth conduction Effects in Transmission line Systems, Dover Publications Inc., 1968.

[3.3] IEEE guide for safety in AC substation grounding., ANSI/IEEE standard 80,2000

[3.4] BS 7354:1990: 'Code of practice for the design of high-voltage open terminal stations.' British Standards Institution, 1990.

[3.5] Towne. H. M: "Impulse Characteristics of Driven Grounds, General Electric Review", Vol.31, No.11, pp. 605-609, November, 1928.

[3.6] Liew. A. C,.Darveniza. M: "Dynamic Model of Impulse Characteristics of Concentrated Earths", Proc IEE, Vol.121, No.2, pp.123-135, 1974.

[3.7] Mousa. A. M: "The Soil Ionisation Gradient Associated With Discharge of High Currents Into Concentrated Earths", IEEE Transactions on Power Delivery, Vol.9, No.3, pp.1669-1677, July 1994.

[3.8] Mazetti. C and Veca. G. M: "Impulse Behaviour of Ground Electrodes", IEEE Transactions on Power Apparatus and Systems, Vol.PAS-102, No.9, pp.3148-3158, Sept 1983.

[3.9] Velazquez. R, Mukhedkar. M: "Analytical Modelling of Grounding Electrodes Transient Behaviour", IEEE Transactions on Power Apparatus and Systems, Vol.PAS-103, No.6, pp.1314-1322, June 1984.

[3.10] Gupta. R. B, Thapar. B: "Impulse Impedance of Grounding Grids", IEEE Transactions on Power Apparatus and Systems, Vol.PAS-99, No.6, pp.2357-2362, 1980.

[3.11] Gupta. R. B, Singh. V. K: "Impulse Impedance of Rectangular Grounding Grid", IEEE Transactions on Power Delivery, Vol.7, No.1, pp.214-218, January 1991.

[3.12] Grcev. L. D, F.E.Menter, Transient Electromagnetic Fields Near Large Earthing Systems, IEEE Transactions on Magnetics, Vol.32, No.3, p.1525-1528, May 1996.

[3.13] CDEGS, HIFREQ Module, Safe Engineering Services, Montreal Canada, 2010.

[3.14] Davies. A.M.: 'High Frequency and Transient Performance of Earthing Systems', PhD thesis, Cardiff University 1999.

[3.15] Rudenberg. R, Electrical Shock Waves in Power Systems – Travelling Waves in Lumped and Distributed Circuit Elements, Harvard University Press, Cambridge, Massachusetts, ISBN 011281, 1968.

[3.16] Endrenyi. J, Analysis of Transmission Tower Potentials During Ground Faults, IEEE Transactions on Power Apparatus and Systems, Vol.PAS-86, No.10, p.1274-1283, October 1967.

[3.17] Griffiths. H, 'Aspects of Earthing System under Variable and Impulse Conditions', PhD thesis, Cardiff University 2008.

[3.18] Lorentzou. M. I., Hatziargriou. N. D: "Modelling of long grounding conductors using EMTP", In: IPST'99, International Conference on Power System Transients, Budapest, 20–24, June, 1999.

[3.19] Griffiths. H, Zedan. B, Haddad. A: 'Frequency Response O Earthing Systems', 28th International Universities Power Engineering Conference', Vol. 2, pp. 717-720, Thessaloniki (Greece), 2003.

[3.20] Grcev. L. D, Heimbach. M: “Frequency dependent and transient characteristics of substation grounding system”, IEEE Trans. Power Delivery 12 (1997) 172–178.

[3.21] Golde R.H. (Editor), Lightning Vol.1: Physics of Lightning, Academic Press, London, ISBN 0-12-287801-9, 1977.

[3.22] Bellaschi. P. L, Armington. R. E: "Impulse and 60-cycle characteristics of driven gounds - III: Effect of lead in ground installation", AIEE Transactions on Electrical Engineering, 1943, Vol. 62, pp. 335–345

[3.23] Geri, A: "Practical design criteria of grounding systems under surge conditions", 25rd ICLP, Rhodes, Greece, 18-22 September, 2000, pp. 458–463

[3.24] Grcev, LD: "Computer analysis of transient voltages in large grounding systems", IEEE Transactions on Power Delivery, Vol. 11, No. 2, April 1996, pp. 815–823

[3.25] Heimbach, M, Grcev, LD: "Grounding system analysis in transient programs applying electromagnetic field approach", IEEE Transactions on Power Delivery, Vol. 12, No. 1, January 1997, pp. 186–193

[3.26] Liu, Y, Zitnik, M & Thottappillil, R: “A time domain transmission line model of grounding system”, 12th ISH, Bangalore, India, 20 – 24 August 2001, vol. 1, pp. 154–157

[3.27] Nixon. K. J, Jandrell. I. R, Geldenhuys. H. J: "Sensitivity analysis of parameters influencing the lightning impulse current behaviour of earth

electrode components.", 25rd ICLP, Rhodes, Greece, 18-22 September, 2000, pp. 484–489

[3.28] Bellaschi. P. L: "Impulse and 60-cycle characteristics of driven gounds", AIEE Transactions on Electrical Engineering, March 1941, Vol. 60, pp. 123–128

[3.29] Bellaschi. P. L, Armington. R. E, Snowden, AE: "Impulse and 60-cycle characteristics of driven gounds - II", AIEE Transactions on Electrical Engineering, 1942, Vol. 61, pp. 349–363

[3.30] Bewley. L. V: "Theory and tests of the counterpoise", AIEE Transactions on Electrical Engineering, 12632, pp. 1163–1172

[3.31] BS 7430, Code of Practice for Earthing, British Standards Institution, 1991.

[3.32] Technical Specification 41-24, Guidelines for the Design, Testing and Maintenance of Main Earthing Systems in Substations, Electricity Association, 1992.

[3.33] Griffiths, H & Davies, AM, Frequency performance of concentrated earthing systems, 12th ISH, Bangalore, India, 20 – 24 August 2001, vol. 1, pp.142–145, 2001.

[3.34] Griffiths. H, Davies. A. M: "Effective length of earth electrodes under high frequency and transient conditions", 25th ICLP, Rhodes, Greece, 18-22 September, 2000, pp. 469–473

[3.35] Papalexopoulos, AD, Meliopoulos, AP: ‘Frequency dependent

characteristics of grounding systems', IEEE Transactions on Power Delivery, Vol. PWRD-2, No. 4, October 1987, pp. 1073–1081.

[3.36] Grcev. L. D, Heimbach. M: "On High-Frequency Circuit Equivalents of a Vertical Ground Rod", IEEE Transactions on Power Delivery, Vol. 20, No. 2, April 2005.

Chapter Four

[4.1] Cotton. I, "Windfarm Earthing", Proc. International Symposium on High Voltage Engineering, Vol.2, pp. 288-291, London, UK, 1999

[4.2] Hatziargyrious. N, Lorentzou. M, Cotton. I, Jenkins. N: "Transferred Overvoltages by Windfarm Grounding Systems" Proceedings of ICHQP Conference, Athens, Greece, 1998.

[4.3 Lorentzou, M., Hatziargyrious, N., Papadias: "Analysis of Wind Turbine Grounding System", Proc. 10th Mediterranean Electrotechnical Conference (MELECON 2000), Vol. 3, pp. 936-939, 2000

[4.4] Kontargyri V. T, Gonos. I. F, Stathopulos. I. A:. "Stathopulos, Frequency Response of Grounding System of Wind Turbine Generators", Proceedings of the XIVth International Symposium on High Voltage Engineering, Tsinghua University, Beijing, China, August 25-29, 2005

[4.5] IEC International Standard "Protection of Structures against Lightning" IEC

61024 –1998

[4.6] IEC Technical Report, “Wind Turbine Generation System -24: Lightning Protection”, TR61400-24, 2002

[4.7] Safe Engineering Services, ‘Current distribution electromagnetic grounding analysis Software (CDEGS)’, Canada, 2010.

[4.8] Davies, A. M.: ‘High Frequency and Transient Performance of Earthing Systems’ PhD Thesis University of Cardiff, 1999.

[4.9] Griffiths, H., Davies, A. M.: ‘Frequency performance of concentrated earthing systems’, 12th International Symposium on High Voltage Engineering(ISH), Bangalore (India), 2001, Vol. 1, pp.142-146.

[4.10] Grcev. L. D, Heimbach. M:: ‘Frequency Dependent and Transient Characteristics of Substation Grounding System’, IEEE Transaction on Power Delivery. Vol. 12, No. 1, 1997

[4.11] http://www.bwea.com/offshore/how.html

[4.12] Houlsby, G.T. and Byrne, B.W., Suction Caisson Foundations for Offshore Wind Turbines and Anemometer Masts, Journal of Wind Engineering Volume 24 No 4,pp 249-255, 2000. UK, March 2006.

[4.13] Houlsby, G.T., Byrne, B.W., Martin, C. and Fish, P., Suction Caisson Foundations for Offshore Wind Turbines, Journal of Wind Engineering Volume 26 No. 3, pp 144-155, 2002

[4.14] Laque, F L &Environmental Factors in the Corrosion of Metals in &&ater and Sea Air,A Marine Corrosion. Cu9 John Wiley and Sons, New York, 19Xx.

[4.15] Mazzetti. C, Veca. G.M "Impulse Behaviour of Ground Electrodes", IEEE Transactions on Power Apparatus and Systems, Vol.PAS-102, No.9, p.3148 Sept 1983.

[4.16] IEEE guide for safety in AC substation grounding., ANSI/IEEE standard 80,2000.

[4.17] BS 7354, Code of Practice for Design of High-Voltage Open-Terminal Stations, British Standards Institution, 1990.

[4.18] Technical Specification 41-24, Guidelines for the Design, Testing and Maintenance of Main Earthing Systems in Substations, Electricity Association

[4.19] IEC 479-2, 'Guide to Effect of Current Passing Through The Human Body Part2: Special Aspects'

[4.20] Geri, A: "Practical design criteria of grounding systems under surge conditions", 25th ICLP, Rhodes, Greece, 18-22 September, 2000, pp. 458–463

[4.21] Liu, Y, Zitnik, M & Thottappillil, R: "A time domain transmission line model of grounding system", 12th ISH, Bangalore, India, 20 – 24 August 2001, vol. 1, pp. 154–157

Chapter Five

[5.1] RES2DINV Ver. 3.4, Geoelectrical Imaging 2D & 3D, Geotomo Software, March 2001.

[5.3] LUND Imaging System, Instruction Manual, ABEM Instrument AB, Bromma, Sweden.

[5.3] ABEM Terrameter. Instruction manual and users guide. ABEM Instrument AB,

[5.4] IEEE: 'ANSI/IEEE Std 81-1983, IEEE Guide for Measuring Earth Resistivity, Ground Impedance, and Earth Surface Potential of a Ground System'. The Institute of Electrical and Electronic Engineers, New York, 1983.

[5.5] Thapar B, Gross E.T.B.: 'Grounding Grids for High-Voltage Stations IV_Resistance of grounding Grids in Non-Uniform Soils.' IEEE Transactions on Power Apparatus and Systems, October 1963 Vol. 82, pp.782-788

[5.6] Taylor, M.: 'Soil Resistivity Assessment for Electrical Application', PhD Thesis, Electrical Division, Cardiff University, 2001.

[5.7] Griffiths, D.H, and Barker, R.D.: 'two-dimensional Resistivity Imaging and Modelling in Areas of Complex Geology', Journal of Applied Geophysics, Vol. 29, pp. 211-226, 1993.

[5.8] Megger DET2/2. Auto earth tester specification. AVO.

[5.9] IEEE: ' IEEE 80, IEEE Guide for Safety in AC Substation Grounding'. The Institute of Electrical and Electronic Engineers, New York, 2000.

[5.10] Skioka. S, Funabashi. T: “Effective Length of Long Grounding in Windfarm” The International Conference on Power Systems Transients(IPST’07) in Lyon, France on June 4-7, 2007

[5.11] Farag. A. S, Cheng. T.C, Penn. D: “Grounding terminations of lightning protective systems”, IEEE Trans. Dielectics Elect. Insul. 5 (6) (1998) 869–877

[5.12] Lorentzou. M. I, Hatziargriou. N. D: “Modelling of long grounding conductors using EMTP”, In: IPST’99, International Conference on Power System Transients, Budapest, 20–24, June, 1999.

[5.13] He. J, Gao. J, Zeng. Y, Zou. R,. J, Liang. X, Zhang. B, Lee. J and Chang. S: “Effective length of Counterpoise Wire Under Lightning Current”, *IEEE Trans. on Power Delivery*, Vol. 20, No2, pp 1585-1591, April 2005.

[5.14] Mazetti. C and Veca. G. M: “Impulse Behaviour of .Grounding Electrodes”, *IEEE Trans. Power App. Syst*., Vol 102, no. PAS-9, 3148-3154, 1983.

[5.15] B. P. Gupta and B. Thapar, ‘Impulse characteristics of grounding electrodes’, *Journal of the Institution of Engineers India*, vol. 64, no. 4, pp. 178-182, February 1981.

[5.16] Mishra. A. K, Ametani. A, Nagaoka N. and. Okabe. S: “Non-Uniform Characteristics of a Horizontal Grounding Electrode”, *IEEE Trans. On Power Delivery*, Vol. 22, No4, pp 2327-2334, October 2007.

[5.17] Ghosh. S, Munshi. S, Biswas. J. R: “Computer aided analysis of surge behaviour of an earthing counterpoise discharging impulse current to ground,”

Journal of the Institution of Engineers India, vol. 77, pp. 128-132, November 1996.

[5.18] Jones, P.: 'Electrical Measurement of Large Area Substation Earth Grids', PhD Thesis, Electrical Division, Cardiff University, 2001.

[5.19] Safe Engineering Services, "Current distribution electromagnetic grounding analysis software (CDEGS)," Canada, 2006.

[5.20] Sunde E. D., Earth conduction Effects in Transmission line Systems, Dover Publications Inc., 1968.

[5.21] Grcev. L. D, Computer Analysis of Transient Voltages in Large Grounding Systems, IEEE Transactions on Power Delivery, Vol.11, No.2, p.815, April 1996.

[5.22] Gupta. B. R, Thapar. B: "Impulse Impedance of Grounding Grids", IEEE Transactions on Power Apparatus and Systems, Vol.PAS-99, No.6, p.2357 Nov/Dec 1980.

[5.23] Verma, R. and Mukhedkar, D,; 'Fundamental Consideration and Impulse of Ground Grids' IEEE Trns. PAS-100, Vol. No. 3. pp, 1023-1030, 1981.

Chapter Six

[1] Windfarm' the International Conference on Power Systems Transients (IPST'07) in Lyon, France on June 4-7, 2007

[6.2] Mazetti. C and Veca. G. M: "Impulse behavior of .grounding electrodes", *IEEE Trans. Power App. Syst.*, Vol 102, no. PAS-9, 3148-3154, 1983.

[6.3] Gupta. B. P, and Thapar. B: 'Impulse characteristics of grounding electrodes', *Journal of the Institution of Engineers India*, vol. 64, no. 4, pp. 178-182, February 1981.

[6.4] Mishra. A. K, Ametani. A, Nagaoka N. and. Okabe. S: "Non-Uniform Characteristics of a Horizontal Grounding Electrode", *IEEE Trans. On Power Delivery,* Vol. 22, No4, pp 2327-2334, October 2007.

[6.5] Ghosh. S, Munshi. S, and Biswas. J: "Computer aided analysis of surge behaviour of an earthing counterpoise discharging impulse current to ground," *Journal of the Institution of Engineers India*, vol. 77, pp. 128-132, November 1996.

[6.6] Farag. A. S, Cheng. T. S, Penn. D, "Grounding terminations of lightning protective systems", IEEE Trans. Dielectrics Elect. Insul. 5 (6) (1998) 869–877

[6.7] Griffiths. H: 'Aspects of Earthing System under Variable and Impulse Conditions', PhD thesis, Cardiff University 2008.

[6.8] Lorentzou, M. I, Hatziargriou. N. D: "Modelling of long grounding conductors using EMTP", In: IPST'99, International Conference on Power System Transients, Budapest, 20–24, June, 1999.

[6.9] He. J, Gao. Y, Zeng. R, Zou. J, Liang. X, Zhang. B, Lee. J and Chang. S: "Effective length of Counterpoise Wire Under Lightning Current", *IEEE Trans. on Power Delivery,* Vol. 20, No2, pp 1585-1591, April 2005.

[6.10] Safe Engineering Services, "Current distribution electromagnetic grounding analysis software (CDEGS)," Canada, 2006.

[6.11] Jones, P.: 'Electrical Measurement of Large Area Substation Earth Grids', PhD Thesis, Electrical Division, Cardiff University, 2001.

[6.12] IEC International Standard "Protection of Structures against Lightning" IEC 61024 –1998

[6.13] IEC Technical Report, "Wind Turbine Generation System -24: Lightning Protection", TR61400-24, 2002

[6.14] IEEE guide for safety in AC substation grounding., ANSI/IEEE standard 80,2000.

[6.15] BS 7354, Code of Practice for Design of High-Voltage Open-Terminal Stations, British Standards Institution, 1990.

[6.16] Technical Specification 41-24, Guidelines for the Design, Testing and Maintenance of Main Earthing Systems in Substations, Electricity Association

[6.17] IEC 479-2, (1987) 'Guide to Effect of Current Passing Through The Human Body Part2: Special Aspects'